THE UNIVERSITY
of EDINBURGH

NOVEL POSITRON EMISSION TOMOGRAPHY APPLICATIONS FOR IMAGING CARDIOVASCULAR DISEASE ACTIVITY

Dr Evangelos Tzolos

MBBS (Hons) MRCP

A thesis presented for the degree of Doctor of Philosophy at the University of Edinburgh April 2022

To Konstantinos, Evmorfia, Mum and Dad

Table of Contents

Figures Index

Tables Index

Declaration

This thesis represents research undertaken at the Clinical Research Facility, University of Edinburgh, Clinical Research Imaging Centre, University of Edinburgh, the Royal Infirmary of Edinburgh and Cedars-Sinai Medical Centre, Los Angeles between February 2019 and January 2022.

This thesis was supported by a grant ("Cardiac Imaging Research Initiative") from the Miriam & Sheldon G. Adelson Medical Research Foundation and then the British Heart Foundation Clinical PhD training fellowship FS/CRTF/20/24086. I was personally responsible for the setup, data analysis and statistical analysis of all studies featuring in Chapters 3 and 4. For Chapter 5 I came up with idea of the study, analysed 60% of the data, provided statistical analysis and co-authored the first draft. Dr Kwiecinski has completed 40% of the data analysis, designed the Central Illustration, helped with statistical analysis (multivariable models) and helped write the first draft of the paper. For Chapter 6 Dr Kwiecinski was responsible of setting up the study and running the machine learning models. I have provided the data analysis, tables, figures, co-authored first draft of the manuscript including results and discussion. For Chapter 7 I have recruited the patients in our centre, provided with 40% of the data analysis, completed all statistical analysis including tables and co-authored the first draft. Dr Kwiecinski helped with the rest of image analysis and co-authored the first draft of the manuscript. Data have also been contributed by the following investigators: Dr Timothy Cartlidge, Dr Nikhil Joshi and Dr Phil Adamson. These have been appropriately acknowledged throughout the thesis.

At the time of writing, Chapters 1, 3, 4, 5, 6 and 7 have been published in peer-reviewed journals, appropriate permissions have been obtained for reproduction. This thesis has not been accepted in any previous applications for a degree and all sources of information have been acknowledged. All studies were undertaken in accordance with the declaration of Helsinki of the World Medical Association and the regulations of the Southeast of Scotland Ethics Committee.

I have no personal disclosures.

26th January 2022

Acknowledgments

I would like to express my sincere gratitude to my supervisor and mentor Professor David Newby (Professor of cardiology and consultant cardiologist) at the University of Edinburgh for his continuous support, guidance and motivation and for always being there for me. I would also like to thank Professor Marc Dweck (Professor of cardiology and consultant cardiologist) who co-supervised this thesis and Dr Daniel Berman (director of cardiac imaging at Cedars-Sinai and professor of medicine at UCLA) for giving me the opportunity to perform research and get trained at computed tomography angiography under his supervision. All of these individuals have provided me with a huge number of skills, advice, encouragement and support for which I am obliged.

Dave and Marc were always there for me, and I couldn't ask for better companions in my research endeavours. Their generosity and friendship are hard to beat.

I am extremely grateful to the Miriam & Sheldon G. Adelson Medical Research Foundation and the British Heart Foundation for their generosity in supporting both myself and this research.

I would also like to thank all the staff at the Clinical Research Imaging who helped to organise and perform hundreds of research scans. I would like to acknowledge my friends in the barn who have been a huge support to me both professionally and

personally, with particular thanks to Jacek Kwiecinski who introduced me in image analysis and has been a great collaborator for most of my studies.

Finally, I would like to thank my family, without whose support, nothing would have been possible.

Lay summary

A heart attack is the commonest cause of death in the western world and is caused by damage to a diseased segment inside the heart artery. Diseased segments take years to build up inside the heart arteries and there are currently no tools to predict which diseased segments are going to rupture leading to a heart attack. Similarly, aortic stenosis is the commonest heart valve disease in the western world which leads to heart failure and death. Currently the only therapy for aortic stenosis is replacing the valve with an artificial one once the patients develop symptoms such as breathlessness or chest pain. Unfortunately, these valves also fail with time.

Microcalcification (actively forming calcium) is the main process underlying disease segment progression, heart valve narrowing and artificial valve failure. The overarching aim of this thesis was to explore whether advances in heart imaging could be harnessed to measure microcalcfication and subsequently improve patient care.

Positron emission tomography (PET) is an imaging technique used to study microcalcification processes at a molecular level. We have recently shown that PET can be used to measure the amount of calcium actively forming within the aortic valve and the coronaries.

In this thesis we aimed to answer current controversies surrounding PET. These include among others: 1) Which is the best way for quantifying calcification activity 2) Can we further improve the method? 3) Can PET predict heart attack in patients

with advanced heart vessel disease? 4) Can automated computed methods improve the risk prediction offered by PET? 5) Can PET predict degeneration of artificial valves?

The following body of work explores these key questions. First, we developed a technique that can reliably measure the calcification activity. The method was accurate at measuring the disease activity and it was better and more reproducible than the current golden standard. Second, we aimed to refine the current method further using the breathing tracing of the individual patient and correcting for heart motion caused by the lungs. PET collects data over 30 minutes hence patient's breathing can affect the measurement of calcium activity. Third, we showed that calcification activity can be used to predict heart attacks and that is the strongest predictor over current clinical risk scores. Fourth, we used complex computer technology to improve the prediction model offered by PET. Finally, we showed that calcification activity underlies the failing of artificial valves and PET can be used to accurately predict the failure of the valves in the long term.

The studies presented here have resulted useful findings and are results of great teamwork.

Abstract

Background

Calcification is one of the body's primary responses to injury and a key pathological feature of cardiovascular disease. Calcification activity can now be imaged using 18F-sodium-fluoride positron emission tomography and computed tomography which targets microcalcification (diameter <50 μm), providing different information to established macroscopic calcification (minimum diameter 200 to 500 μm) imaged with computed tomography. Indeed 18F-sodium fluoride PET has now been explored in a wide range of conditions including coronary atherosclerosis, aortic stenosis and bioprosthetic valve disease, offering a marker of vascular injury and disease activity in each condition studied. At the moment, we lack reliable and reproducible methods for predicting myocardial infarction in patients with established coronary artery disease. Moreover, there remain major uncertainties regarding disease activity within the retained native aortic valve as well as bioprosthetic valve durability following transcatheter aortic valve implantation.

In this thesis, I will address the following questions: 1) What is the optimal method for quantifying microcalcification activity and how reproducible is it? 2) Can we further refine it? 3) Can 18F-sodium fluoride PET/CT predict myocardial infarction in patients with advanced atherosclerosis? 4) Can machine learning improve the ability of 18F-sodium fluoride PET/CT to predict events? 5) Can 18F-sodium fluoride PET/CT predict native aortic valve disease progression and bioprosthetic valve degeneration in patients with transcatheter aortic valve implantation?

Methods and Results

Study one: 18F-sodium fluoride reproducibility

We aimed to establish the observer repeatability and interscan reproducibility of coronary 18F-sodium fluoride positron emission tomography (PET) uptake using a novel semi-automated approach, coronary microcalcification activity (CMA). Nineteen patients with established coronary artery disease were included for analysis. CMA was assessed twice in 43 coronary vessels on two PET/CT scans performed 12±5 days apart. We demonstrated that CMA is a repeatable and reproducible global measure of coronary atherosclerotic activity. There was excellent intraclass correlation for intraobserver and interobserver repeatability as well as interscan reproducibility (all ≥0.991). There was 100% intraobserver, interobserver and interscan agreement for the presence (CMA>0) or absence (CMA=0) of coronary18F-sodium fluoride uptake. Mean CMA was 3.12± 0.62 with coefficients of repeatability of 0.24 and 0.22 for intraobserver, 0.30 and 0.29 for interobserver and 0.33 and 0.32 for interscan analysis at a per-vessel and per-patient level respectively.

Study two: Refining 18F-sodium fluoride uptake

We aimed to evaluate the impact of respiratory-averaged computed tomography attenuation correction (RACTAC) compared to standard single-phase computed tomography attenuation correction (CTAC) map, on the quantitative measures of coronary atherosclerotic lesions of 18F-sodium fluoride in PET/CT. Twenty-three patients with calcified plaques in the coronary arteries were included. We evaluated 34 coronary lesions using CTAC and RACTAC reconstructions. We demonstrated that

respiratory-averaged and standard single-phase attenuation correction maps provide similar and reproducible methods of quantifying coronary 18F-sodium fluoride uptake on PET/CT. Assessments of the individual vessel microcalcification burden (CMA) revealed no major differences between PET images reconstructed using CTAC and RACTAC scans (median [IQR] CMA: CTAC = 0.10 [0-1.0], RACTAC = 0.15 [0-1.03], p=0.19). Bland-Altman plots of the CMA values revealed a high degree of agreement when comparing the per vessel burden, with coefficient of reproducibility of 0.17.

Study three: Coronary 18F-sodium fluoride PET/CT

In a multicentre study, we investigated whether coronary 18F-sodium fluoride PET uptake predicts future myocardial infarction in patients with established coronary artery disease, and whether it can provide additional prognostic information over and above current methods of risk stratification including clinical risk scores, coronary calcium scoring and the severity of obstructive coronary artery disease. We studied 293 participants (65±9 years; 84% male) with established coronary artery disease. Patients underwent 18F-sodium fluoride PET/CT and were followed-up for fatal or non-fatal myocardial infarction over 42 [31-49] months. Total coronary 18F-sodium fluoride uptake was determined using coronary microcalcification activity (CMA). Fatal or non-fatal myocardial infarction occurred only in patients with increased coronary 18F-sodium fluoride activity (20/203 CMA>0 versus 0/90 CMA=0; p<0.001). On receiver operator-curve analysis, fatal or non-fatal myocardial infarction prediction was highest for 18F-sodium fluoride CMA, outperforming coronary calcium scoring, modified Duke coronary artery disease index, cardiac risk scores

(areas under curve: 0.76 versus 0.54, 0.62, 0.52 and 0.54; p<0.001 for all). Patients with CMA>1.56 had >7-fold increase in fatal or non-fatal myocardial infarction (hazard ratio 7.1, 95% confidence interval 2.2 to 25.1; p=0.003) independent of age, gender, risk factors, segment involvement and coronary calcium scores, presence of coronary stents, coronary stenosis, cardiac risk scores, the Duke coronary artery disease index and recent myocardial infarction.

Study four: Artificial intelligence in 18F-sodium fluoride PET/CT

We undertook a post-hoc analysis of the population of patients from study three. Coronary 18F-sodium fluoride PET/CT and CT angiography-based quantitative plaque analysis have shown promise in refining risk stratification in patients with coronary artery disease. We combined both novel imaging approaches to develop an optimal machine-learning model for the future risk of myocardial infarction in patients with stable coronary disease. We demonstrated that our machine learning approach has overcome the challenges posed by co-linearity of these variables and, for the first time, demonstrated that this information is complementary and additive with the combination of both providing the most robust outcome prediction. On univariable receiver-operator-curve analysis, only 18F-sodium fluoride coronary uptake emerged as a predictor of myocardial infarction (c- statistic 0.76, 95% confidence interval [CI] 0.68-0.83). When incorporated into machine-learning models, clinical characteristics showed limited predictive performance (c-statistic 0.64, 95% CI 0.53-0.76;) and were outperformed by a quantitative plaque analysis-based machine-learning model (c-statistic 0.72, 95% CI 0.60-0.84). After inclusion of all available data (clinical, quantitative plaque and 18F-sodium fluoride PET), we achieved a substantial

improvement (p=0.008 versus 18F-sodium fluoride PET alone) in the model performance (c-statistic 0.85, 95% CI 0.79-0.91).

Study five: 18F-sodium fluoride in transcatheter aortic valves

We undertook a multicentre cross-sectional observational cohort study to determine whether the retained native aortic valves in patients undergoing transcatheter aortic valve implantation (TAVI) demonstrate evidence of ongoing disease progression. Additionally, since long-term durability of transcatheter aortic valves is yet to be established, we aimed to establish whether bioprosthetic valve durability or degeneration was appreciably different from patients with surgical aortic valve replacement (SAVR). Patients with TAVI or bioprosthetic SAVR underwent baseline echocardiography, CT angiography and 18F-sodium fluoride PET/CT. Subsequently patients underwent serial echocardiography to assess for changes in valve hemodynamic performance (change in peak aortic velocity) and evidence of structural valve dysfunction. Comparisons were made to matched patients with bioprosthetic SAVR who had undergone the same imaging protocol. We enrolled 47 patients (81±6 years old, 79% male) with TAVI from 3 high volume centres. We demonstrated that 18F-sodium fluoride uptake within the native aortic valve is higher with longer duration of implantation suggesting disease activity continues despite immobilisation of the valve leaflet. We have further shown using 3 complementary and distinct imaging modalities that the prevalence of valve degeneration within TAVI bioprostheses are similar to that of bioprosthetic SAVR valves for up to 7 years after valve replacement. Finally, we have confirmed that 18F-sodium fluoride PET of the bioprosthetic valve provides a powerful independent predictor of subsequent

hemodynamic bioprosthetic valve degeneration that is applicable to both TAVI and SAVR and outperforms all other traditional risk factors. In patients with TAVI, native aortic valves demonstrated 18F-sodium fluoride uptake around the outside of the bioprostheses which showed a modest correlation with the time from TAVI (r=0.36, p=0.023). 18F-sodium fluoride uptake in the bioprosthetic leaflets was comparable between the SAVR and TAVI groups (target-to-background ratio 1.3 [1.2-1.7] versus 1.3 [1.2-1.5] respectively, p=0.27). The frequencies of imaging evidence of bioprosthetic valve degeneration at baseline were similar on echocardiography (6% versus 8% respectively, p=0.78), CT (15% versus 14% respectively, p=0.87) and PET (15% versus 29% respectively, p=0.09). Baseline 18F-sodium fluoride uptake was associated with subsequent change in peak aortic velocity for both TAVI (r=0.7, p<0.001) and SAVR (r=0.7, p<0.001). On multivariable analysis, 18F-sodium fluoride uptake was the only predictor of peak velocity progression (p<0.001).

Conclusions

We have demonstrated that CMA is a repeatable and reproducible global measure of coronary atherosclerotic activity. Respiratory-averaged and standard single-phase attenuation correction maps provide similar and reproducible methods of quantifying coronary 18F-sodium fluoride uptake on PET/CT. In patients with established coronary artery disease, 18F-sodium fluoride PET provides powerful independent prediction of fatal or non-fatal myocardial infarction. Both 18F-sodium fluoride uptake and quantitative plaque analysis measures are additive and strong predictors of outcome in patients with established coronary artery disease. Optimal risk stratification can be achieved by combining clinical data with these approaches in a

machine-learning model. Finally, in patients with TAVI, native aortic valves demonstrate evidence of ongoing active disease. Across imaging modalities, TAVI degeneration appears to be of similar magnitude to bioprosthetic SAVR suggesting comparable mid-term durability.

Abbreviations

^{18}F-fluorodeoxyglucose	^{18}F-FDG
^{18}F-sodium fluoride	^{18}F-NaF
AVR	Aortic valve replacement
CMA	Coronary microcalcification activity
CT	Computed Tomography
CTAC	Computed tomography attenuation correction
LDL	Low-density lipoproteins
PET	Positron emission tomography
RACTAC	Respiratory-averaged computed tomography attenuation correction
TAVI	Trans-catheter aortic valve implantation
TBRmax	Maximum target to background ratio

Chapter 1 18F-sodium fluoride PET/CT for imaging cardiovascular disease activity

Extracts of this chapter have been published in the following review articles and book chapters:

Tzolos E, Andrews JP, Dweck MR. Aortic valve stenosis-multimodality assessment with PET/CT and PET/MRI. Br J Radiol. 2020 Sep 1;93(1113):20190688. doi: 10.1259/bjr.20190688.

Tzolos E, Dweck MR Imaging Cardiovascular Calcification Activity with 18F-sodium fluoride PET, Cardiovascular Calcification and Bone Mineralisation, Springer 2020

Tzolos E, McElhinney P, Williams MC, et al. Repeatability of quantitative pericoronary adipose tissue attenuation and coronary plaque burden from coronary CT angiography. J Cardiovasc Comput Tomogr. 2021 Jan-Feb;15(1):81-84. doi: 10.1016/j.jcct.2020.03.007.

Tzolos E, Dweck MR. ^{18}F-Sodium Fluoride (^{18}F-NaF) for Imaging Microcalcification Activity in the Cardiovascular System. Arterioscler Thromb Vasc Biol. 2020 Jul;40(7):1620-1626. doi: 10.1161/ATVBAHA.120.313785.

Kwiecinski J*, **Tzolos E*,** Berman D, et al. Imaging Coronary Atherosclerotic Plaque. European Heart Journal (In progress), *joint first co-authors

Tzolos E, Newby DE, Dweck MR. Aortic Stenosis & Bioprosthetic Valve Degeneration, Nuclear Cardiology and Multimodal Cardiovascular Imaging, E-Book: A Companion to Braunwald's Heart Disease, Elsevier 2022

1.1 Overview

Coronary artery disease is the leading cause of mortality and morbidity worldwide (1). According to statistical modelling and data on incidence, prevalence, case fatality, excess mortality and cause-specific mortality in 204 countries globally, it is estimated that almost 200 million people were living with ischemic heart disease in 2019. The disease remains more prevalent in males than in females (113.7 and 83.6 million people, respectively) and its prevalence has increased by 103.5% from 1990 to 2019 (1).

Despite remarkable advances in the management of coronary artery disease, prediction of adverse coronary events remains challenging. Current methods for identifying patients at risk of acute myocardial infarction rely on integrating risk factors using clinical scoring algorithms (2-4). These methods are not precise in estimating individual risk, and current strategies misclassify a large proportion of individuals who subsequently develop adverse events as being low risk (5-9). Indeed, patients who experience myocardial infarctions often have similar clinical risk profiles to those who do not (10).

Aside from risk profiles, non-invasive assessments of inducible ischaemia play a central role in the work up of patients with coronary artery disease (11). While identification of individuals with haemodynamically significant coronary stenoses is feasible by means of ischaemia imaging, studies evaluating ischaemia-based revascularisation have failed to reduce the subsequent rates of myocardial infarction

(11). In the landmark ISCHEMIA trial (12) among patients with chronic coronary syndromes and moderate or severe ischaemia, an initial invasive strategy, as compared with an initial conservative strategy, did not reduce the risk of ischaemic cardiovascular events or death from any cause over a median of 3.2 years. Given the lack of outcome benefit from ischaemia-guided revascularisation, a greater focus on factors and mechanisms leading to plaque rupture – which is responsible for the vast majority of myocardial infarctions – is warranted.

1.2 Back to Pathology

James Muller introduced the concept of the vulnerable plaque in 1989 when he described 'hemodynamically insignificant, albeit dangerous lesions' (13) at high risk of rupturing and causing myocardial infarction. Subsequently, multiple observational studies have confirmed that most of the plaques causing myocardial infarction are non-flow limiting at the time of antecedent angiography. Cardiovascular research of the last two decades has now established that ruptured plaques exhibit common key histopathological features including: a thin fibrous cap (<65 μm), large necrotic core, a positively remodelled vessel, macrophage infiltration resulting in plaque inflammation, hypoxia leading to neovascularisation and finally early stage microcalcification. (14-18) Figures 1.1 and 1.2.

The initiation phase of atherosclerosis begins with low-density lipoprotein (LDL) cholesterol that infiltrates into the intima of the vessel wall (19, 20). Subsequent oxidation of LDL cholesterol leads to an inflammatory response (progression phase) with infiltration of T-lymphocytes and macrophages. The latter consume LDL cholesterol and form foam cells. While this process is initially protective, with further LDL cholesterol accumulation, macrophage cell death is triggered, resulting in further inflammation and the development of a necrotic core. Plaque inflammation also has a detrimental effect on fibrous cap as it triggers the production of matrix metalloproteinases which weaken the fibrous cap, predisposing it to plaque rupture (16, 19).

Figure 1.1 Pathological characteristics of the vulnerable plaques.

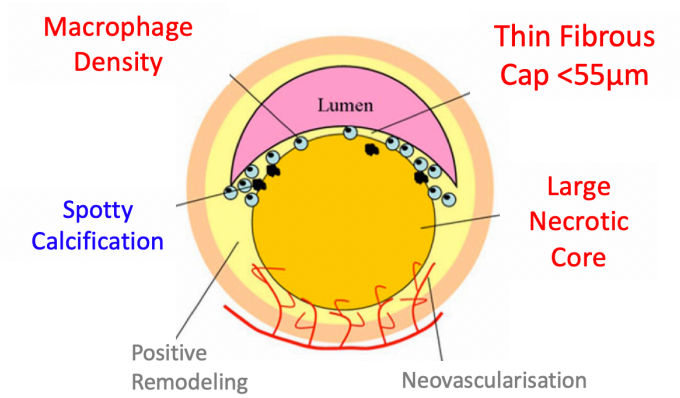

Figure 1.2 Molecular and structural targets for imaging. Cross section of a coronary artery containing plaque assumed to be rupture prone. Potential targets for imaging are highlighted. They comprise: 1) the large lipid-rich necrotic core (orange asterisk), 2) thin fibrous cap (blue arrows), 3) expansive remodelling (green arrow), and 4) vasa vasorum and neovascularisation (red open circles). (Reprinted from Falk et al. 2006) (19).

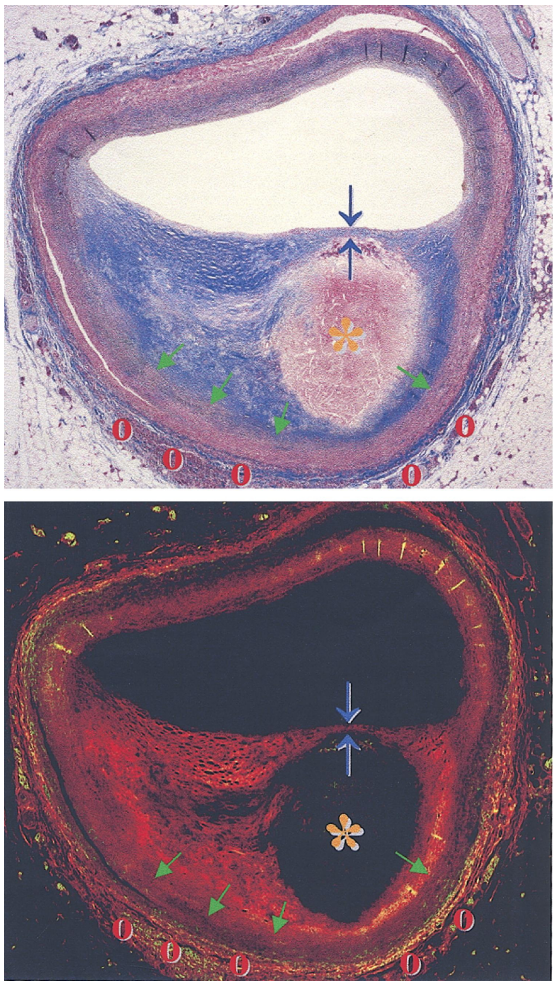

The role of calcification in atherosclerosis is two-fold. While it often acts as a healing response to intense necrotic plaque inflammation, the early stage of microcalcification is a common feature of ruptured and unstable plaques where healing is incomplete, inflammation remains active and the fibrous cap weakened by the tiny calcific deposits (21, 22).

The current dogma focused on high-grade stenosis and ischaemia does not make allowance for detection of these plaque characteristics. As shown nearly three decades ago by Falk et al (23) and recently confirmed by Chang et al (24), over two thirds of myocardial infarctions are caused by rupture of non-obstructive coronary lesions. This finding remains consistent regardless of whether the assessment of coronary stenosis is conducted with invasive angiography or non-invasive computed tomography angiography. The meaning of this observation is two-fold. It explains why the ischaemia-guided management of patients does not reduce the incidence of myocardial infarction and simultaneously it highlights the need for disease assessment beyond just focusing on coronary stenosis. Of note, the fact that rupture of non-obstructive lesions is responsible for the majority of myocardial infarctions does not per se mean that low-grade stenoses are more dangerous than high-grade stenosis. This statistic simply reflects the fact that non-obstructive lesions are more prevalent in the coronary vasculature and hence the likelihood that one of them shall rupture causing an adverse event is high. Similarly, high-grade lesions should not be neglected as aside from causing symptoms depending on the plaque morphology and activity, they may represent either burned-out stable disease or truly vulnerable plaques.

1.3 Imaging of atherosclerosis

The uncoupling of coronary luminal stenosis and the risk of myocardial infarction is perhaps most evident in the COURAGE (25), BARI-2D (26) and ISCHEMIA (12) trials in which coronary revascularisation failed to reduce the risk of coronary events despite effective relief of ischaemia. This highlights the need for a shift in the management of coronary artery disease. Considering the available evidence, 3 disease factors emerge as key players contributing to the overall risk of myocardial infarction: plaque type (often referred to as adverse plaque features or high-risk plaque), atherosclerotic disease burden and atherosclerotic disease activity.

1.3.1 Imaging Plaque Type

Given the well-defined characteristics of ruptured atherosclerotic plaques on histological ex vivo analysis, there is great interest in identifying such high-risk plaque features in patients with clinically stable coronary artery disease. Initial efforts were based around invasive imaging strategies, predominantly intravascular ultrasound (IVUS) (27) and optical coherence tomography (OCT) (28). The utility of invasive coronary plaque imaging for prediction of adverse events was comprehensively evaluated in the landmark PROSPECT (A Prospective Natural-History Study of Coronary Atherosclerosis) study (27). In 697 patients who presented with an acute coronary syndrome and underwent percutaneous coronary intervention, Stone et al performed 3-vessel IVUS in search of lesions with an unfavourable morphology. Despite a grand total of 595 thin-cap fibroatheromas identified on radiofrequency intravascular ultrasonography, only 21 myocardial infarctions were observed after 3 years' follow-up, suggesting that the majority of plaques with an adverse phenotype heal or rupture without causing a clinical event. These findings led to a shift in the understanding of the value of imaging individual plaque morphology. It was proposed that rather than being lesion centred, high-risk plaques should be assessed at a patient level as such an approach can help identify those who develop unstable patterns of disease and therefore are at higher risk of adverse outcomes.

Recent non-invasive high-risk plaque imaging with contrast-enhanced computed tomography angiography supports assessing lesion morphology on a per patient level. Motoyama et al. (29) have demonstrated that high-risk plaque on computed tomography angiography is an independent predictor of acute coronary syndromes

over a mid-term follow-up of 3.9±2.4 years. Similar findings were reported in a meta-analysis considering findings from a grand total of 13,977 patients (30). Adverse plaque features were confirmed as an independent predictor of major cardiovascular adverse events. It has however been postulated that these studies claiming independent risk prediction of certain plaque features share the fundamental limitation that the atherosclerotic disease burden was not considered as a potential confounder.

Most recently, these findings were supported by post-hoc analysis from the Prospective Multicentre Imaging Study for Evaluation of Chest Pain (PROMISE) (31) and Scottish COmputed Tomography of the HEART (SCOT-HEART) (32) trials. The latter study showed particularly compelling results as the associations in plaque morphology and future myocardial infarctions were not independent of coronary artery calcium score, a surrogate measure of coronary plaque burden. These results suggest that although plaque composition and its haemodynamic consequences are associated with future myocardial infarction, the predominant factor governing patient outcomes is the burden of coronary atherosclerosis.

1.3.2 Imaging Plaque Burden

Irrespective of the method used, plaque burden assessments provide powerful risk prediction. Since most acute coronary events occur as a result of plaque rupture, the presence of coronary atherosclerosis is a pre-requisite for type 1 myocardial infarction. It is therefore logical that the greater the extent of atherosclerosis, the greater the likelihood of an acute event (33). This observation is supported not only by studies demonstrating that the risk increases gradually with the extent of coronary artery disease, but also by the fact that in the absence of coronary atherosclerosis, the risk of myocardial infarction is very low even in the presence of symptoms suggestive of angina (34).

Studies further support the prognostic utility of simple cheap coronary artery calcium imaging across the spectrum of disease severity and clinical scenarios (35-37). The coronary artery calcium score was highly predictive of coronary events in both young and elderly patients suggesting that once disease is present, age has less importance. Compared with a coronary calcium score of 0, a score >100 was associated with an increased multivariable-adjusted risk of coronary events in younger individuals (45–54 years of age) with a hazard ratio of 12.4 (95% CI, 5.1–30.0) (38). This risk was similar even in the very elderly (75–84 years of age) with a hazard ratio of 12.1 (95% CI, 2.9–50.2). Likewise, in patients with a low risk of adverse cardiovascular events, coronary artery calcium was the strongest predictor of myocardial infarction. In multicentre registry data (39), inclusion of coronary artery calcium in multivariable models for prediction of myocardial infarction consistently improved model performance and in a recent study employing machine-learning, coronary artery

calcium score was the most important predictor of all atherosclerotic cardiovascular disease combined outcomes (37, 39).

Although coronary calcium scoring provides a surrogate of the atherosclerotic plaque burden at relatively low radiation doses (~1 mSv) and cost, it quantifies calcified plaques that are relatively unlikely to cause clinical events. There is therefore increasing interest in quantifying the burden of plaques with unfavourable morphology. This can be accomplished by means of quantitative plaque analysis derived from coronary computed tomography angiography. Quantitative assessment of plaque can provide standardised assessment with good observer variability and correlation with intravascular ultrasound (40). On CCTA, a lipid rich necrotic core can be detected as low-attenuation non-calcified plaque and this represents a strong independent predictor of myocardial infarction (24, 41). In a post-hoc analysis of the SCOT-HEART trial, Williams et al. (32) showed that low-attenuation plaque burden was the strongest predictor of outcome, with patients with a low-attenuation plaque burden >4% 5-times more likely to suffer a fatal or nonfatal myocardial infarction. Despite collinearity and strong correlations, this association remained irrespective of cardiovascular risk score, Agatston coronary artery calcium score or the presence of obstructive coronary artery disease.

Studies which assessed the interplay between plaque burden and ischaemia provide evidence that myocardial ischaemia is closely correlated with the extent of coronary atherosclerosis (42-44). While the associations in coronary artery calcium and myocardial ischaemia were only modest, coronary atherosclerosis is not limited to

calcified lesions. Indeed, studies employing quantitative plaque analysis have demonstrated that when more comprehensive plaque volume measures are employed, it is feasible to predict ischaemia from non-invasive CT angiography imaging with superior accuracy compared to lesion severity assessments. Driessen et al. (43) have shown that the noncalcified plaque volume is associated with detrimental downstream hyperaemic myocardial perfusion on positron emission tomography and fractional flow research measured invasively. In a substudy of the NXT trial (Analysis of Coronary Blood Flow Using CT Angiography: Next Steps), low-density non-calcified plaque (low-attenuation plaque) volumes predicted ischaemia independent of other plaque characteristics (45, 46). Most recently, a comprehensive machine-learning approach considering a wide range of correlated plaque volume measures improved the prediction of lesion-specific ischaemia by invasive fractional flow reserve, over stenosis, plaque measures and pre-test likelihood of coronary artery disease (47). These observations suggest that myocardial ischaemia is to some degree a function of atherosclerotic plaque burden and therefore ischaemia can be considered as a surrogate measure of the disease burden.

1.3.3 Assessing Disease Activity with molecular imaging

Imaging targets that include ischaemia, adverse plaque features and disease burden, do not make allowance for assessing disease activity. While plaque morphology has been linked to a poor prognosis, the propensity to developing an adverse event largely depends on the atherosclerotic activity. A thin-capped fibroatheroma might heal without rupture in a patient with low disease activity, but in a different individual with high disease activity, it might manifest clinically with an acute myocardial infarction.

The importance of plaque progression, which is a key manifestation of disease activity, has been elegantly highlighted in the analysis of 449 patients who underwent serial computed tomography angiography (29). While adverse events occurred in 8 (14.3%) of 56 patients with plaque progression, among those without plaque progression on serial imaging only 1 (0.27%) of 367 subjects experienced an acute coronary syndrome over a 4-year follow-up (29). Importantly, while plaque progression remained an independent predictor of adverse events, such predictive capacity was not shown for plaque morphology (adverse plaque features). These compelling observations have important implications. Aside from highlighting the necessity for assessment of atherosclerotic activity, the analysis by Motoyama et al. (29) demonstrates that such assessment can be performed with dual time point imaging. This is however suboptimal for clinical practice as it delays the decision regarding modification of therapy until a second imaging session is conducted.

Fortunately, non-invasive evaluation of disease activity can be accomplished with molecular imaging. Advances in hybrid scanners now allow combined non-invasive assessment of disease activity using hybrid PET imaging alongside the anatomic information provided by CT or MRI. While multiple PET tracers co-localise to coronary atherosclerotic lesions, to date, only ^{18}F-sodium fluoride (^{18}F-NaF) has been shown to act as an independent predictor of myocardial infarction (48, 49).

1.4 ^{18}F-sodium fluoride for imaging microcalcification activity in the cardiovascular system

Calcification is a key feature of atherosclerosis, heart valve disease and peripheral vascular disease, and is governed in a highly regulated manner with similarities to skeletal bone formation. Computed tomography (CT), which detects large macroscopic deposits of calcium, has until recently been the only available non-invasive imaging modality allowing visualisation of this process (50). However, imaging of this late stage means that the processes leading to calcium formation have often resolved. There is therefore interest in imaging the earlier stages of microcalcification where the disease process is active and therapeutic intervention may be more effective.

Over the last 10 years, ^{18}F-sodium fluoride PET has emerged as a non-invasive quantitative imaging modality capable of imaging calcification activity in the vasculature. This has provided major insights into the underlying pathophysiology of multiple different cardiovascular disease states and unique information regarding disease activity that may prove clinically useful in the future.

1.4.1 How does ^{18}F-sodium fluoride PET work?

Advanced hybrid PET/CT scanners now provide detailed molecular information about the activity of specific disease processes occurring in the body. In principle, the activity of any biological process can be a subject to study the availability of a targeted PET radiotracer. After manufacture, these radiotracers are injected into the body and accumulate in areas where that disease process is active, emitting radiation that can be detected by the PET scanner to create an image. Since the PET images lack spatial resolution, they are fused with an anatomical dataset provided by CT acquired simultaneously with the patient remaining in the same position on a single gantry. These anatomical scans also provide attenuation correction allowing precise quantification of tracer accumulation in different tissues. Indeed, modern hybrid PET/CT now effectively combine functional information from PET with fine anatomical detail from CT such that the activity of a range of pathological processes can be visualised within very small structures in the body (51).

Computed tomography (CT) is currently only able to identify macroscopic deposits of calcium with a diameter between 200 to 500 μm (CT calcium scoring) (52, 53), whereas ^{18}F-sodium fluoride uptake can identify areas of microcalcification (<50 μm). Newly developing calcium will pass through this microcalcification stage, so that ^{18}F-sodium fluoride uptake effectively provides a marker of calcification activity, detecting new calcium formation beyond the resolution of CT (50, 51).

Initially used as bone tracer with increased uptake observed in conditions associated with high bone turnover and new bone formation (54-56), ^{18}F-sodium fluoride has

demonstrated favourable pharmacokinetic properties and has an established and excellent safety profile. Following intravenous injection, roughly 70 % of ^{18}F-sodium fluoride is plasma based with the remaining 30 % found in erythrocytes. Because of its small size and negligible protein binding, only ~10% of the injected ^{18}F-sodium fluoride dose remains in the blood one hour after administration (57-59). The mechanism of ^{18}F-sodium fluoride uptake in bone is well understood. First it diffuses via the capillary network into the bone extracellular fluid and then it exchanges with hydroxyl groups on exposed regions of hydroxyapatite crystals on the bone surface, to form fluoroapatite (50). The intensity of the tracer uptake depends mainly on two factors: the bone blood flow and the surface area of exposed hydroxyapatite (50).

Hydroxyapatite is also a key feature of vascular calcification, with a growing literature demonstrating that similar mechanisms govern ^{18}F-sodium fluoride PET binding in the cardiovascular system. However, blood flow is likely to be constant, so the surface area of hydroxyapatite appears to be the major factor affecting ^{18}F-sodium fluoride uptake in the cardiovascular system. ^{18}F-Sodium fluoride uptake is highest in areas of microcalcification compared to large macroscopic deposits, due to the very high surface area of hydroxyapatite in these regions of powdery microcalcification (50, 54, 55, 60). Unlike other PET tracers, ^{18}F-sodium fluoride also demonstrates very low uptake in the myocardium, well below that observed even in the blood pool. This important characteristic facilitates clear visualisation of regions of increased ^{18}F-sodium fluoride uptake in areas of active calcification in the heart but also mediates precise co-registration via alignment of the ventricular blood pools on PET and contrast CT (59, 61-63).

Validation of cardiovascular ^{18}F-sodium fluoride uptake has now been provided in multiple independent studies. Using excised atherosclerotic plaque, Cocker et al. (64) demonstrated the association between cardiovascular ^{18}F-sodium fluoride PET uptake and the histological staining of hydroxyapatite with Goldner's trichome. Aikawa et al confirmed that ^{18}F-sodium fluoride binds predominantly to hydroxyapatite (65), whilst in the aortic valve, ^{18}F-sodium fluoride has demonstrated a close association with areas of tissue with positive histochemical staining for alkaline phosphatase ($r = 0.65$; $p = 0.04$) and areas with positive immunohistochemical reactivity for osteocalcin (r=0.68; P=0.03) (66, 67). Irkle et al. (68) demonstrated that ^{18}F-sodium fluoride uptake is increased in regions of microcalcification, rather than large macroscopic deposits. This is predominantly due to surface area effects and because much of the hydroxyapatite crystal is internalised in the centre of macroscopic deposit and therefore, not available for ^{18}F-sodium fluoride binding. Creager et al. (50) confirmed that ^{18}F-sodium fluoride binds to areas of microcalcification beyond the resolution of x-ray computed tomography and that this binding was proportional to the surface area of hydroxyapatite in a controlled *ex vivo* model. Recently, Youn et al. confirmed ^{18}F-sodium fluoride binding to microcalcifications in the coronary arteries as well as the carotids (69).

In effect, ^{18}F-sodium fluoride-PET detects the surface area of hydroxyapatite crystal and therefore provides different information to CT which detects tissue density. Put another way, ^{18}F-sodium fluoride detects microcalcification and areas of calcification activity, whilst CT detects establish macroscopic deposits of calcium. The difference

information provided by ^{18}F-sodium fluoride PET compared to CT has now been demonstrated in multiple human studies *in vivo* across a range of different conditions. However, this observation was perhaps first described by Derlin et al in a retrospective study of 75 patients undergoing whole-body ^{18}F-sodium fluoride PET/CT (70). They demonstrated that increased ^{18}F-sodium fluoride uptake was detected in only 12% of all calcified plaques of the aorta, carotid and femoral arteries while 75% of patients demonstrated increased ^{18}F-sodium fluoride uptake remote from CT-defined calcified plaques.

1.4.2. Microcalcification and imaging coronary disease activity with ^{18}F-sodium fluoride PET/CT

PET/CT has been extensively used in the clinical assessment of patients with cancer for many years, resulting in the widespread accessibility of scanners (71). Recent technological innovations including motion correction, improved PET resolution and fusion with detailed CT angiographic images has allowed the use of this technology to image the heart and cardiovascular system. To date, most studies have made use of established tracer already widely available for oncology imaging. These include ^{18}F-fluorodeoxyglucose (^{18}F-FDG) as a marker of vascular inflammation, but more recently ^{18}F-sodium fluoride to investigate calcification activity.

^{18}F-FDG is an excellent tracer for identifying inflammation in large arteries such as the aorta and carotids (72-75). However, due to its limited specificity and its strong uptake in the left ventricular myocardium, imaging of the coronary arteries is impaired. By contrast, ^{18}F-sodium fluoride demonstrates an excellent signal to noise ratio in the coronary arteries with very low uptake in the adjacent myocardium. Moreover, as a marker of developing microcalcification, this tracer appears capable of providing important clinical information with respect to disease activity and as a hallmark of vulnerable (or high-risk) plaques (76, 77).

Dweck et al first described ^{18}F-sodium fluoride uptake in the coronary arteries as a novel marker of plaque biology in subjects with and without aortic valve disease (78), with excellent reproducibility and feasibility. Furthermore, increased uptake of this

tracer localised to individual coronary plaques and importantly identified patients with increased Framingham risk scores and a history of prior MACE. This study again confirmed that ^{18}F-sodium fluoride provides different information to the presence of coronary calcium on CT. Indeed, >40 % of patients with coronary artery calcium scores >1000 Agatston Units did not demonstrate increased ^{18}F-sodium fluoride uptake, suggesting that ^{18}F-sodium fluoride might be able to differentiate between dormant and active atherosclerotic disease states in patients with advanced plaque burden.

Intense ^{18}F-sodium fluoride uptake localises to recent plaque rupture in patients with acute myocardial infarction (48) (Figure 1.3). Joshi et al. (48) examined 40 patients with stable angina and 40 patients presenting with type 1 myocardial infarction, referred for invasive angiography, who all underwent ^{18}F-sodium fluoride PET/CT imaging alongside CT coronary angiography, invasive coronary angiography and intravascular ultrasound. In the stable cohort, increased tracer activity localised to individual coronary plaques in approximately 40 % of patients. Using intravascular ultrasound (IVUS) and CT they have demonstrated that these plaques had multiple high-risk features, including microcalcification, positive remodelling and a large necrotic core. It was impossible, however, to undertake histological analysis of the ^{18}F-sodium fluoride signal in these patients. Instead, the authors confirmed that increased ^{18}F-sodium fluoride activity co-localises to carotid plaques (removed at the time of endarterectomy) with histological evidence of increased macrophage accumulation, cell death and calcification. Finally, in the myocardial infarction cohort, 37 out of 40 patients demonstrated increased ^{18}F-sodium fluoride uptake at in

the culprit territory responsible for the event. By comparison, ^{18}F-FDG was unable to provide similar discrimination of culprit coronary plaques.

In a similar study Li et al. (79) demonstrated that increased ^{18}F-sodium fluoride uptake in the coronary arteries was observed in patients at increased cardiovascular risk. Similarly, Oliveira-Santos M. et al. showed that patients with ≥ 5 risk factors (60%) had increased overall ^{18}F-sodium fluoride uptake (1.1 ± 0.3 vs. 0.7 ± 0.3, $p < 0.01$), and that a positive correlation was observed between ^{18}F-sodium fluoride uptake and the predicted fatal cardiovascular risk - SCORE ($r = 0.49$, $p = 0.01$) (80).

Finally, other studies have confirmed the localisation of increased ^{18}F-sodium fluoride to plaques with adverse characteristics including positive remodelling, low-attenuation plaque (<30 HU), spotty calcification, obstructive coronary stenosis, and plaque volumes >100 mm^3 determined by a range of different approaches, including CT, intravascular ultrasound, optical coherent tomography, and histology (69, 81-83). More recently, ^{18}F-sodium fluoride activity has been associated with increased pericoronary adipose tissue density: an emerging marking of coronary plaque inflammation (84).

Figure 1.3 Focal ^{18}F-sodium fluoride uptake in patients with myocardial infarction.

Patient with acute ST-segment elevation myocardial infarction with (A) proximal occlusion (red arrow) of the left anterior descending artery on invasive coronary angiography and (B) intense focal ^{18}F-sodium fluoride uptake (yellow-red) at the site of the culprit plaque (red arrow) on the combined positron emission and computed tomogram.

Patient with anterior non-ST-segment elevation myocardial infarction with (C) culprit (red arrow; left anterior descending artery) and bystander non-culprit (white arrow; circumflex artery) lesions on invasive coronary angiography that were both stented during the index admission. Only the culprit lesion had increased 18F-sodium fluoride uptake on combined positron emission and computed tomography (D) following percutaneous coronary intervention. (Adapted from Joshi et al.; Lancet, 2013 (48))

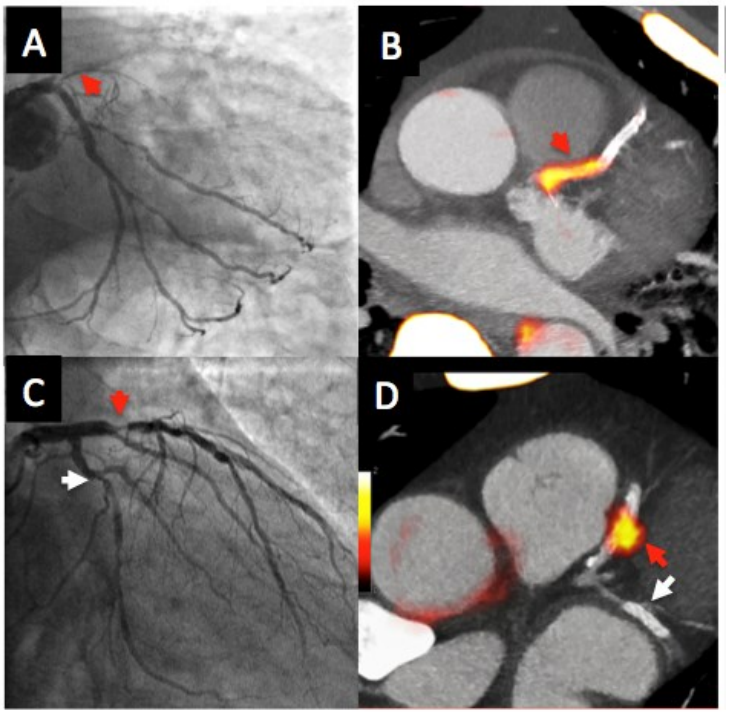

1.4.3 Valvular applications - Aortic stenosis and bioprosthetic valves

Aortic stenosis

Calcific aortic stenosis is the most common form of valve disease in the Western world and is set to become an increasing health burden with no available effective medical therapy (85). The only available treatment for patients that progress to severe symptomatic aortic stenosis remains surgical or transcatheter aortic valve implantation. There is therefore a pressing need to improve our pathophysiological understanding of the disease and to develop effective medical therapies capable of slowing disease progression (86, 87).

Dweck et al. (88) recruited 121 patients with a range of calcific aortic valve disease who underwent both ^{18}F-fluorodeoxyglucose (^{18}F-FDG - a marker of inflammation) and ^{18}F-sodium fluoride PET/CT imaging. ^{18}F-Sodium fluoride uptake was higher in patients with aortic stenosis than control subjects and increased progressively with more advanced stages of aortic stenosis. Interestingly, increased ^{18}F-FDG activity was also detected, but uptake values were lower than ^{18}F-sodium fluoride and had a more modest association with disease severity. Particularly, in the more advanced stages of the disease, calcification rather than inflammation, had a more predominant role in the disease progression (89). On this basis, we believe it should be the target of future therapeutic interventions, although we acknowledge that other processes such as fibrosis also determine valve stiffening and progression. Once again in aortic stenosis, ^{18}F-sodium fluoride uptake was observed in a different distribution to the presence of calcium on CT. Moreover, ^{18}F-sodium fluoride PET predicted where new areas of calcium on CT would develop on repeat scans performed 2 years later,

consistent with it acting as a marker of calcification activity, and therefore providing powerful prediction of disease progression and future aortic valve replacement or cardiovascular mortality (90, 91).

Bioprosthetic and Transcatheter Aortic Valve Degeneration

The increasing prevalence of valve disease in an ageing population and the emergence of transcatheter aortic valve implantation (TAVI) has led to a marked rise in the implantation of bioprosthetic heart valves (87, 92, 93). In the United States, there were more than 65,000 surgical bioprosthetic valves implanted and more than 80,000 TAVI procedures in 2011 alone (86, 87, 94). Bioprosthetic valve degeneration remains a major issue and is poorly understood. Calcification appears to be a major pathologic contributor leading to both progressive valve narrowing and regurgitation secondary to leaflet tears (95, 96).

Non-invasive methods for detecting this degenerative process have been lacking. Leaflet visualisation with both echocardiography and CT is made challenging because of blooming artifact and acoustic shadowing of the valve stent struts. Indeed, the detection of valve degeneration relies on echocardiographic identification of overt hemodynamic valve dysfunction when the valve has become overtly regurgitant or stenotic. Consequently, even with meticulous clinical follow-up and serial echocardiography, many patients present with unheralded valve failure because of rapid-onset valvular obstruction or regurgitation, requiring emergent repeat operation. This is suboptimal, especially given that emergency repeat aortic valve

replacement surgery is associated with a mortality of 22.6%, compared with 1.4% for elective repeat surgery (97).

The early detection of bioprosthetic valve degeneration is highly desirable, potentially permitting at-risk patients to be recognised early and thereby avoiding potentially catastrophic valve failure. Calcification appears to have an important role in bioprosthetic valve degeneration, acting as a major pathological contributor to both progressive bioprosthetic valve narrowing and leaflet tears (98). Cartlidge et al. (99) hypothesised that increased ^{18}F-sodium fluoride uptake would identify the early stages of prosthetic valve degeneration and predict subsequent deterioration in bioprosthetic valve function. 18F-Fluoride Assessment of Aortic Bioprosthesis Durability and Outcome (18F-FAABULOUS) was a longitudinal PET/CT study of subjects with surgically implanted bioprosthetic aortic valves. All explanted valves demonstrated ^{18}F-sodium fluoride leaflet uptake that correlated with micro- and macrocalcific deposits within the valve leaflets and co-localised with regions of tissue degradation, pannus and thrombus on histology. Moreover, they examined seventy-one patients without known bioprosthetic valve dysfunction. Similar to the ex vivo findings, increased ^{18}F-sodium fluoride uptake co-localised with areas of spotty calcification, non-calcific leaflet thickening (suggestive of thrombus), and pannus observed on the CT. Twenty-four patients with increased ^{18}F-sodium fluoride uptake at baseline demonstrated clear evidence of deteriorating bioprosthesis function after 2 years, while patients without uptake displayed no change in valve function. Ten patients developed new bioprosthetic valve failure: all 10 patients had increased ^{18}F-sodium fluoride uptake at baseline (99).

These data require confirmation in other cohorts but suggest that ^{18}F-sodium fluoride allows for the detection of bioprosthetic valve degeneration before it is evident on either echocardiography or CT and that, importantly, this can help identify patients at risk for imminent valve failure. ^{18}F-Sodium fluoride PET may well develop an important clinical role for this expanding clinical problem.

1.5 Aims and objectives

The overarching aim of this thesis was to evaluate and to optimise the use of ^{18}F-sodium fluoride PET/CT imaging techniques for the study and management of patients with coronary artery disease or transcatheter aortic valve implantation.

In particular, I sought to:

1. Determine the observer repeatability and scan reproducibility of coronary microcalcification activity (CMA) on ^{18}F-sodium fluoride PET/CT.
   Chapter 3
2. Refine current methods of coronary ^{18}F-sodium fluoride PET-CT image acquisition and analysis in the study of CMA to improve image quality and scan reproducibility.
   Chapter 4
3. Determine the ability of coronary ^{18}F-sodium fluoride PET/CT to predict myocardial infarction in patients with advanced atherosclerosis.
   Chapters 5 and 6
4. Determine the ability of machine learning to improve the ability of ^{18}F-sodium fluoride PET/CT to predict future myocardial infarction.
   Chapter 6
5. Determine the ability of aortic valve ^{18}F-sodium fluoride PET/CT to predict transcatheter aortic valve degeneration.
   Chapter 7

1.6 Hypotheses

I sought to address the following hypotheses

1. The observer repeatability and interscan reproducibility of ^{18}F- sodium fluoride PET/CT will be within acceptable limits for clinical application.
2. Current techniques of ^{18}F-sodium fluoride PET/CT imaging of the coronaries can be modified to enhance image quality whilst improving scan reproducibility.
3. In patients with advanced atherosclerosis, baseline ^{18}F-sodium fluoride PET/CT will predict coronary future myocardial infarction.
4. Machine learning will improve the ability of baseline ^{18}F-sodium fluoride PET/CT to predict myocardial infarction.
5. In patients with transcatheter aortic valves (TAVI), ^{18}F-sodium fluoride PET/CT can predict TAVI degeneration and future valve disease progression.

Chapter 2 Materials and methods

2.1 Overview

The design and methodology of each study is described in detail within the relevant chapters. The following section provides an overview of the study populations and investigations employed in the course of these studies.

2. 2 Study and populations

2.2.1 Patients with coronary atherosclerosis

Study populations are described in detail in their respective chapters but predominantly consisted of patients with established coronary artery disease undergoing hybrid coronary ^{18}F-sodium fluoride PET and contrast CT angiography as part of the following studies:

Novel Imaging Approaches to Identify Unstable Coronary Plaques study (NCT01749254; Chapters 5 and 6). In this prospective observational study, we recruited patients with acute ST-segment or non- ST-segment elevation myocardial infarction (100) and patients with stable angina pectoris undergoing elective invasive coronary angiography. Chapters 5 and 6 are based on post-hoc studies using imaging studies from the trial cohort. For these chapters, I undertook image analysis, outcome data collection, statistical analysis, data interpretation, drafting and revision of the manuscripts.

Dual Antiplatelet Therapy to Reduce Myocardial Injury study (DIAMOND) (NCT02110303; Chapters 3, 5 and 6). This investigator-initiated double-blind randomised parallel-group placebo-controlled trial was conducted at a single centre in Edinburgh, United Kingdom (101). Patients with angiographically proven multivessel coronary artery disease, defined as at least 2 major epicardial vessels with any combination of either: 1) >50% luminal stenosis; or 2) previous revascularisation

(percutaneous coronary intervention or coronary artery bypass graft surgery) were recruited. Chapter 3 is a reproducibility study of 20 patients with repeat imaging studies (^{18}F-sodium fluoride PET/CT) performed within 3 weeks of each other from the trial cohort. For this chapter, I undertook image analysis, statistical analysis, data interpretation, drafting and revision of the manuscript. Chapters 5 and 6 are based on post-hoc studies using baseline imaging studies from the trial cohort. For these chapters, I undertook image analysis, outcome data collection, statistical analysis, data interpretation, drafting and revision of the manuscripts.

^{18}F-Sodium fluoride PET for Identifying Coronary Atherosclerotic Plaques study (NCT02607748; Chapters 5 &6) In this prospective observational study, patients were recruited from a single centre (Cedars-Sinai Medical Center, Los Angeles)(49). Patients with angiographic evidence of at least a 50% stenosis in one or more coronary arteries, were recruited following type 1 myocardial infarction (100). Only patients undergoing percutaneous coronary intervention were included in the study. Chapters 5 and 6 are based on post-hoc studies using baseline imaging studies from the trial cohort. For these chapters, I undertook image analysis, outcome data collection, statistical analysis, data interpretation, drafting and revision of the manuscripts.

Effect of Evolocumab on Coronary Artery Plaque Volume and Composition by CCTA and Microcalcification by ^{18}F-sodium fluoride PET study (NCT03689946; Chapter 4). This is an ongoing single-arm, prospective, open-label study evaluating the effect of evolocumab injection in patients with calcified plaque in the coronary

arteries detected by computed coronary tomography angiography (CCTA). Patients with evidence by CCTA of noncalcified coronary artery plaque volume (>440 mm3) documented were recruited from a single centre (Cedars-Sinai Medical Center, Los Angeles). Chapter 4 is an image reconstruction optimisation study, utilising 23 patients with ^{18}F-sodium fluoride PET/CT studies and simultaneous CT attenuation maps obtained during both free-breathing and post 4D cine-CT scanning, from the trial cohort. For this chapter, I undertook recruitment, image analysis, statistical analysis, data interpretation, drafting and revision of the manuscript.

2.1.2 Patients with Transcatheter Aortic Valve Implantation

The patient population is described in detail in Chapter 7 but predominantly consisted of patients with transcatheter aortic valve implantation undergoing hybrid coronary ^{18}F-sodium fluoride PET and contrast CT angiography as part of the following study:

18F-Fluoride Assessment of Aortic Bioprosthesis Durability and Outcome (18F-FAABULOUS) (NCT02304276; Chapter 7). This longitudinal, cross-sectional study examined subjects with surgical or transcatheter implanted bioprostheses from 3 medical centres. Patients undertook a baseline ^{18}F-sodium fluoride PET/CT scan and patients were offered annual echocardiography to look for subsequent bioprosthetic valve degeneration. The results on surgical bioprosthetic valve degeneration have been previously reported (99) and in Chapter 7 we report the results of the transcatheter aortic valve degeneration. For this chapter, I recruited patients at Cedars-Sinai Medical Center and undertook image analysis, outcome data collection, statistical analysis, data interpretation, drafting and revision of the manuscript

The conduct of the baseline visits for the above studies (2.1.1 and 2.1.2) are identical and detailed below.

2.1.3 Ethical Considerations

All studies were conducted with the approval of the local research ethics committee, in accordance with the Declaration of Helsinki, and with the written informed consent of each participant. All studies were approved by the Research and Development Office at the University of Edinburgh, the South-East Scotland Research Ethics Committee and the Administration of Radioactive Substances Advisory Committee (ARSAC). Study conduct was overseen by the sponsors at the University of Edinburgh.

2.1.4 Recruitment

Patients under the care of cardiology teams at participating centres were firstly identified as potentially suitable study participants and approached by their usual care team. Those who agreed to be contacted by the research team were provided with an approved participant information sheet prior to attending for the first visit.

2.1.5 Study Visits

Study visits were primarily undertaken at Edinburgh Clinical Research facility in Edinburgh.

At the first visit, the process of obtaining written informed consent was performed, and the study inclusion and exclusion criteria were confirmed prior to further study involvement. The criteria for each study are detailed in the respective chapters.

2.1.6 Clinical History

Anonymised patient data were entered into case record forms and study visits were documented in the clinical notes. Demographics, specifically the date of birth, sex and ethnicity were recorded. Patients were then asked about symptoms of breathlessness, exertional chest pains and syncope. Breathlessness and angina were graded using the New York Heart Association (NYHA) and Canadian Cardiovascular Society scores respectively. The past medical history was documented using a combination of patient interview, electronic health records and clinical notes. Co-morbidities of particular interest included a confirmed diagnosis of hypertension, hypercholesterolaemia, diabetes, renal disease, angina, previous coronary artery bypass grafting, previous percutaneous coronary intervention, smoking status, cerebrovascular disease and current or past malignancies. All current medications including indication, dose, method of administration and start dates were recorded.

2.1.7 Clinical Examination

The height and weight were recorded for each patient, from which the body-mass index and body-surface area were calculated. Sphygmomanometry was used to determine the blood pressure and heart rate. All patients underwent a standardised cardiovascular examination in a semi-recumbent position, with the torso at 45 degrees. Specific examination was made of the pulse rate and rhythm, the jugular venous pressure and fluid status. The heart sounds were auscultated for murmurs and lung fields for inspiratory crackles.

2.1.8 Electrocardiogram

All patients underwent a 12-lead electrocardiogram (ECG) which was examined immediately for features of ischaemia, arrhythmia, conduction disease, left ventricular hypertrophy and strain. Left ventricular hypertrophy was diagnosed using two criteria: the Sokolow-Lyon criteria (the sum of the S wave in V1 and R wave in V5 or V6 ≥35mm) or the Modified Cornell Criteria (R wave in aVL ≥12 mm). Left ventricular strain was defined as asymmetric T wave inversion and ST segment depression in the anterolateral leads (102).

2.1.9 Venesection

At each visit, a cannula was inserted if required and up to 40 mL of blood was subsequently withdrawn. These were routinely tested for full blood count, renal and liver function, electrolytes, glucose and cholesterol. Serum and plasma samples were also spun and stored for future use.

2.2 Image acquisition and analysis

2.2.1 Echocardiography

Echocardiography employs ultrasound technology to obtain detailed information about cardiac structure and function. It remains the first-line imaging assessment and the gold-standard clinical tool for the diagnosis, grading and monitoring for aortic stenosis, providing haemodynamic assessment of aortic stenosis severity as well as aortic valve morphology (tricuspid vs bicuspid) and left ventricular function ((103-105).

Echocardiography was performed by experienced echocardiographers using a pre-specified protocol according to American Society of Echocardiography guidelines (104). Patients were asked to undress from the waist up and issued with a gown if necessary. Scans were performed with patients in the left lateral and supine positions.

For each patient, images were acquired in the parasternal long and short-axis views, apical 4 and 5-chamber views, subcostal and suprasternal views. Measurements were made of left and right ventricular dimensions, atrial size, left ventricular outflow tract diameter and aortic root dimensions. Right ventricular size was assessed visually in respect to the left ventricle and function was assessed using tricuspid annular plane systolic excursion (TAPSE). Left ventricular function was estimated using a combination of visual assessment and where possible confirmed using Simpson's biplane measurements. Detailed diastolic assessments were also performed using mitral valve pulsed wave and tissue doppler. All valves were examined by using a

combination of visual assessment, colour flow, continuous wave and pulsed wave Doppler. If possible, an assessment was made of pulmonary artery systolic pressure and any additional abnormalities including pericardial effusions.

Aortic stenosis severity was assessed based on the European Society of Echocardiography Guidelines (105). A semi-quantitative calcification score was assigned as previously published by Rosenhek et al; 1, no calcification; 2, mildly calcified with small isolated spots; 3, moderate calcified with multiple larger spots and 4, heavily calcified with extensive thickening and calcification of all cusps (106). Pulsed wave and continuous wave Doppler were used to determine aortic stenosis severity with measurements taken of the peak transvalvular velocity and mean gradient. The aortic valve area was calculated using the continuity equation. The continuous wave Doppler measurements were then subsequently repeated using the pencil probe at the apex, suprasternal notch and right sternal edge. For patients in sinus rhythm, the average of 3 measurements were used. This was increased to 5 measurements for those in atrial fibrillation.

With respect to discerning aortic valve severity, we have shown that echocardiography has good scan-rescan reproducibility (107) in 20 patients (mean peak velocity 3.47±0.78 m/s) who underwent repeated echocardiography within 3 weeks (mean difference = 0±0.28 m/s, reproducibility coefficient = 0.56) (107). Bioprosthetic valve regurgitation was graded as mild, moderate or severe according to guideline recommendations on the basis of visual appraisal of colour Doppler images,

measurement of pressure half-time (milliseconds) and assessment for aortic flow reversal in diastole (108).

2.2.2 18F-Sodium Fluoride Positron Emission Tomography-Computed Tomography Imaging

The radiotracer ^{18}F-sodium fluoride was synthesised by the radiochemistry department at the participating centres on the morning of scan days and underwent immediate quality assurance checks. Patients were transferred to lead-lined uptake rooms and given 25-50 mg of oral metoprolol if their resting heart rate was >65 beats/min provided there were no contra-indications. Patients were administered 250 MBq of ^{18}F-sodium fluoride (coronary study) or 125 MBq (aortic valve study), flushed with 10 mL of normal saline intravenously, before being required to rest for 60 min. Dynamic imaging has previously confirmed that 60 min after injection is time point at which optimal contrast between plasma and vascular tissues is observed (68). Prior to the scan all patients were requested to empty their bladder.

Image acquisition and reconstruction

All patients underwent ^{18}F-sodium fluoride PET on hybrid PET/CT scanners (128-slice Biograph mCT, Siemens Medical Systems, Knoxville, USA or Discovery 710 GE Healthcare, Milwaukee, WI, USA) using harmonised and validated imaging protocols 60 min following intravenous ^{18}F-sodium fluoride administration (88).

The detailed scanning protocol has been described in the relevant Chapter sections. Briefly, during a single imaging session, we acquired a non-contrast CT attenuation

correction scan followed by a 30-min PET emission scan in list mode. The electrocardiogram (ECG)-gated list mode dataset was reconstructed using a standard ordered expectation maximisation algorithm with time-of-flight, and point-spread-function correction. Using 4 cardiac gates, the data were reconstructed on a 256x256 matrix (with 75 or 47 slices using 2 iterations, 21 subsets and 5-mm Gaussian smoothing or 4 iterations, 24 subsets and 5-mm gaussian smoothing for Biograph and Discovery respectively). Immediately after the PET scan, a low dose non-contrast ECG-gated CT for calculation of the coronary calcium score was performed. Subsequently, a contrast-enhanced, ECG-gated coronary CT angiogram was obtained in mid-diastole on the same PET/CT system without repositioning the patient. To compensate for coronary motion associated with heart contraction, we performed cardiac motion correction of the PET/CT images; Figure 2.1 (109, 110).

Figure 2.1. Overview of the motion correction method.

(1) Coronary artery centrelines are extracted from CCTA in end-diastolic phase using CCTA analysis software. (2) Volumes of interest surrounding coronary arteries are extracted from 4- and 10-bin PET data using previously extracted CCTA centrelines. (3) All bins of data are registered to the common end-diastolic reference bin (bins 3 and 7 for 4- and 10-bin data, respectively) by nonlinear level-set registration restricted to coronary regions. Then, registered VOIs are inserted back into their original PET volumes, and all registered PET images are summed into a single volume to obtain motion-corrected 4- and 10-bin data. MC = motion-corrected; VOI = volume of interest (Reprinted from Rubeaux et al. 2016) (109)

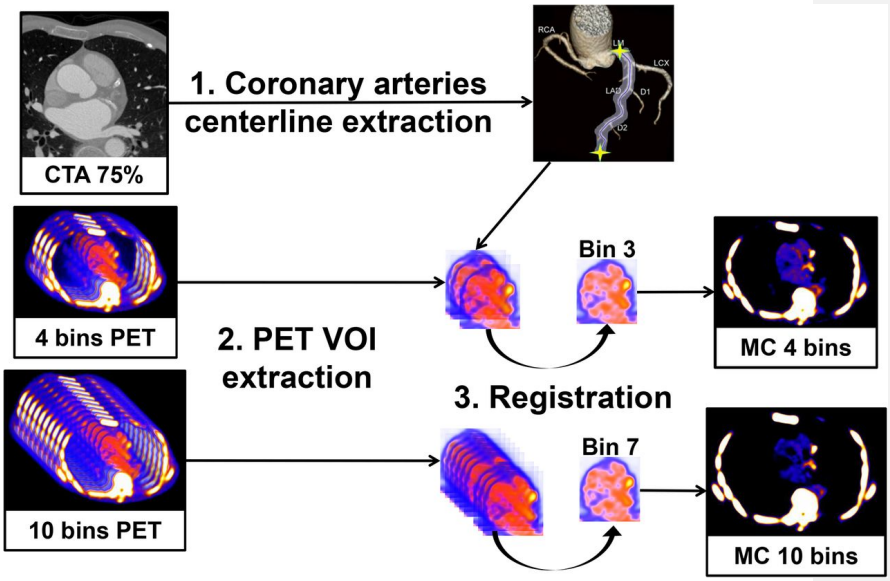

Image analysis - coronaries

We used a dedicated software package for coronary PET image analysis (FusionQuant, Cedars-Sinai Medical Center, Los Angeles). PET and CT angiography reconstructions were reoriented, fused and systematically co-registered in 3 orthogonal planes (111). We used two methods to evaluate coronary ^{18}F-sodium fluoride activity: the maximum target to background (TBRmax) approach (standard quantification) which relies on visual detection of lesions with increased tracer uptake; and the newly developed whole-coronary total microcalcification activity method (novel quantification) (Figure 2.2) (48, 112).

Figure 2.2 Methodology for co-registration of positron emission tomography and contrast computed tomography of coronary arteries.

Careful alignment of the positron emission tomography (PET) activity in the cardiac blood pool with the contrast-enhanced computed tomography (CT) images is performed in 3 planes (left). This is possible because of the high ^{18}F-sodium fluoride activity in the blood pool compared to the myocardium. TBRmax is then calculated using the SUVmax activity of lesions with visible uptake and SUVmax of blood pool (right atrium) (middle). Finally, using the coronary artery centrelines that are extracted from CCTA in end-diastolic phase using CCTA analysis software, we can calculate the whole coronary microcalcification activity (CMA).

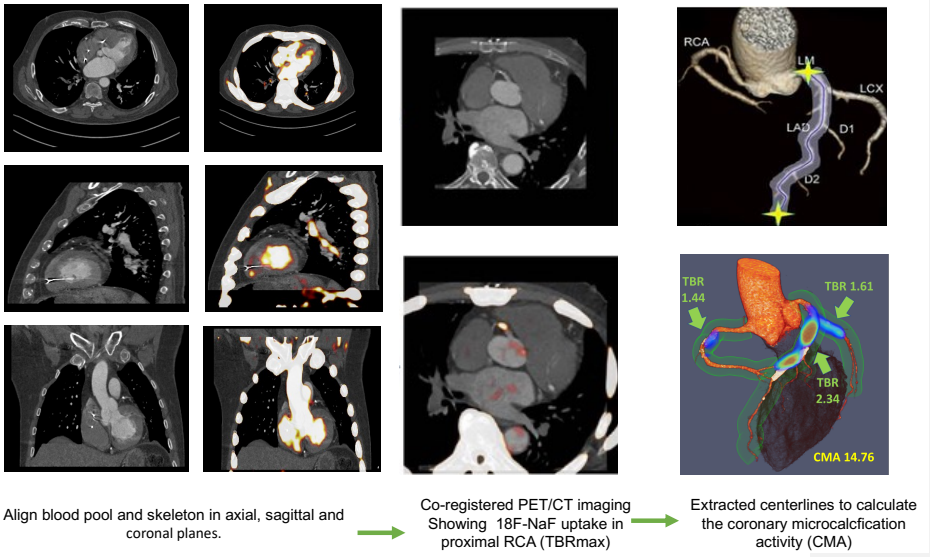

Image analysis – Transcatheter aortic valves

Reconstructed ECG-gated PET and contrast-enhanced CT images were reoriented, co-registered in orthogonal planes and cardiac motion corrected with automatic algorithm preserving counts from all cardiac phases (Figure 2.3) (109, 113-115).

Using en face images of the bioprosthetic valves, the maximum standard uptake values (SUV) in the native aortic valve was measured between the perimeter of the TAVI bioprostheses and the aorta. Care was taken to avoid regions of activity originating from the TAVI leaflets and nearby coronary arteries. Target to background ratio (TBR) values were derived from maximum SUV values corrected for blood-pool activity (mean SUV) measured in the right atrium (1-cm radius 9-mm high cylinder drawn on axial slices, at the level of the right coronary ostium).

With respect to ^{18}F-sodium fluoride uptake in the TAVI bioprosthetic valves, PET scans were adjudicated to be abnormal if discernible ^{18}F-sodium fluoride uptake originating from the valve leaflets was observed on 3 orthogonal planes. We quantified ^{18}F-sodium fluoride uptake according to a previously proposed methodology where a circular (area 1 cm^2) region of interest (ROI) was drawn around the area of maximal uptake originating in the valve cusps (63, 99). ROIs were carefully drawn to avoid any uptake originating from outside of the bioprosthetic valve leaflets, in particular uptake related to surrounding native aortic valve tissue. In subjects with no visible (exceeding blood-pool activity) uptake in the valve leaflets, a 1-cm^2 circular ROI was drawn in the centre of the valve (66, 88, 99). Maximum SUV values were extracted from these ROIs and divided by the blood-pool activity measured in the right atrium to calculate

the TBR values as described above. A similar approach was taken to the analysis of SAVR valves (99).

Figure 2.3 Methodology for co-registration of positron emission tomography and contrast computed tomography in bioprosthetic aortic valves.

Careful alignment of the positron emission tomography (PET) activity in the cardiac blood pool with the contrast-enhanced computed tomography (CT) images is performed in 3 planes (left). This is possible because of the high ^{18}F-sodium fluoride activity in the blood pool compared to the myocardium. Subsequently PET activity in the ascending aorta and aortic arch (centre) is aligned with the CT and final refinement of co-registration is performed according to landmarks around the bioprosthetic aortic valve such as the coronary arteries and mitral valve annulus. Hybrid images are then re-orientated to provide en face images of the bioprosthetic valve with corresponding perpendicular long-axis images. Finally, the PET windowing is adjusted to the point below which blood pool activity in the aorta is visible to assess uptake in the valve leaflets. (Reprinted from Cartlidge et al. 2019) (99)

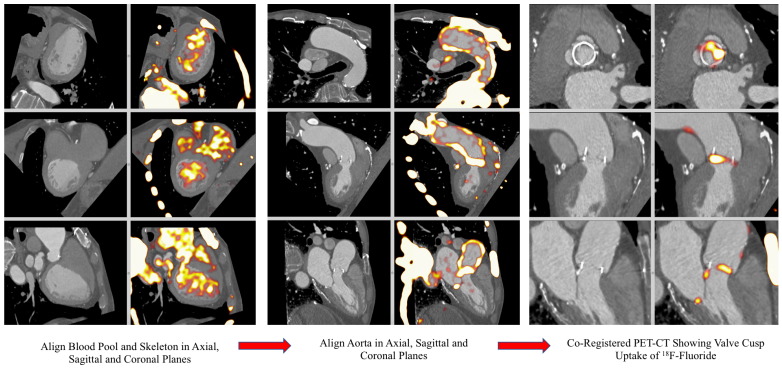

2.2.3. Reproducibility of PET-CT imaging

Several studies have demonstrated the excellent interobserver and intraobserver repeatability as well as interscan reproducibility of the coronary ^{18}F-sodium fluoride PET/CT (59, 116, 117), expressed as the maximum target to background ratio (TBRmax) metric. The reproducibility of the new metric, coronary microcalcification activity (CMA) is the subject of chapter 3.

Similarly, several studies have assessed the aortic valve ^{18}F-sodium fluoride reproducibility (99, 113, 114) showing excellent results.

2.2.4 Computed Tomography

CT creates cross-sectional images of the body and works on the principle that different tissues can be distinguished by their relative ability to absorb photons (attenuation coefficients). Typical CT images are composed of 512 rows, each of 512 pixels, which are multiplied by the slice width to create voxels. Calculating the attenuation coefficient for each voxel facilitates the creation of digital images. Attenuation coefficients are converted to the Hounsfield scale, expressed in Hounsfield units (HU).

Image acquisition

For anatomical localisation of PET uptake, coronary computed tomography angiography (CCTA) was performed immediately after the PET acquisition. The CCTA was performed using prospective gating, 330 ms rotation time, body-mass index (BMI) dependent voltage (<25 kg/m^2, 100 kV, ≥25 kg/m^2, 120 kV), and tube-current time product of 160–245 mAs. Patients were administered oral or intravenous beta-blocker therapy to achieve a target heartrate of <60 beats/min. A body-mass

index-dependent bolus-injection of contrast media (400 mg/mL) was administered to the patients with a flow of 5–6 mL/s after determining the appropriate trigger delay defined by a test bolus of 20 mL of contrast material.

Image analysis

The coronary artery calcium score was measured in Agatston units (AU) using clinical software (NetraMD, ScImage, Los Altos, CA, USA) on non-contrast CT scans. The presence, extent and severity of coronary artery disease were evaluated on contrast-enhanced CT angiography by defining the segment involvement score, DUKE coronary artery disease index and the number of vessels with >50% luminal stenosis ***(118)***. Multivessel coronary artery disease was defined as at least 2 major epicardial vessels with any combination of either >50% stenosis, or previous revascularisation.

We performed quantitative plaque analysis of all coronary segments with a lumen diameter greater than 2 mm using semi-automated software (AutoPlaque version 2.0, Cedars-Sinai Medical Center, Los Angeles, USA) (32, 41). Proximal and distal limits of lesions were manually marked by an experienced reader (physicians with several years of experience in clinical coronary CT image analysis) after examination of coronary CT angiography images in multiplanar format. Subsequent plaque quantification was fully automated using adaptive scan- specific thresholds. Total, calcified, non-calcified as well as low attenuation plaque volumes were calculated. The plaque burden was calculated according to the following equation (plaque volume x 100%/vessel volume). The contrast density difference was the maximal difference

in contrast density (mean Hounsfield unit / cross-sectional area) in the plaque and the reference proximal vessel cross section.

2.2.5 Safety issues

All CT scans were supervised by a medical practitioner. Where possible, CT angiography images were acquired with retrospective gating to minimise radiation exposure. The total dose received by a patient for a given scan (including injected doses, and dose-length product) were recorded and reviewed periodically by the medical physics department. All scans were reported by a consultant radiologist and incidental findings were acted upon as appropriate.

2.3. Histological analysis

Ex Vivo Analysis

To assess calcification activity in native aortic valves, tissue samples were selected from TAVI valves that had been harvested en bloc along with the aortic root and the surrounding native valve tissue. Immunohistochemistry was then performed on all native aortic valve explants: 4-µm paraffin sections of the native valve tissue were cut and stained for Runx2 and Osteopontin. Dilutions of 1:100 and 1:200 were used for Runx2 (Abcam, Ab76956) and osteopontin (Sigma-Aldrick Cat. No. 07264) respectively. For both Runx2 and osteopontin, staining was performed using the automated Leica Bond Rx system, Bond Epitope Retrieval Solution 1 (pH=6, Catalog No: AR9961) and Bond Polymer Refine Red Detection (Catalog No: DS9390).

To assess whether ^{18}F-sodium fluoride is providing an assessment of calcification activity in TAVI valve leaflets, TAVI valves of different implant durations were selected for evaluation. Haematoxylin and eosin (H&E) and Movat's pentachrome staining was performed on 4-µm paraffin sections of TAVI leaflets. Slides were imaged on a high-resolution Aperio Slide Scanner with images generated using ImageScope software (Leica Biosystems, Germany).

For ^{18}F-sodium fluoride autoradiography experiments, slide-mounted paraffin-embedded sections were rehydrated bathed in phosphate buffered saline and placed in 100 KBq/mL of ^{18}F-sodium fluoride for 1 hour, before being washed in phosphate

buffered saline again. The slides were then placed in the phosphor-images Amesham Typhoon (GE) at 4000 x 10 µm scale, the Fuji film high resolution film applied and left overnight for exposure. Autoradiography analysis was performed in the open-source software ImageJ (v2.0.0).

2.4 Statistical analysis

The majority of the statistical analyses within this thesis was performed by myself, using MedCalc Statistical Software version 16.4.3 (MedCalc Software, Ostend, Belgium), SPSS version 24 (IBM SPSS Statistics for Windows, Version 24.0. Armonk, NY: IBM Corp) and R studio and R software version 4.01 (R Foundation for Statistical Computing, Vienna, Austria). Continuous variables were expressed as mean ± standard deviation or median [interquartile range (IQR)] as appropriate. Categorical data were presented as number and percentage. Correlations between continuous variables were assessed with linear regression analysis and either Pearson's r or Spearman's Rho subject to the normality of the variables tested. Parametric (unpaired Student's *t*-test) and non-parametric (Mann-Whitney U) tests were used as appropriate. Reproducibility studies were performed using Bland-Altman analyses. Outcome variables were assessed using Kaplan-Meier curves and cox proportional hazards regression analyses. Two-sided significance was taken as $p<0.05$.

Chapter 3 Observer repeatability and interscan reproducibility of 18F-sodium fluoride coronary microcalcification activity

Published by **Tzolos E**, Kwiecinski J, Lassen ML et al. Observer repeatability and interscan reproducibility of 18F-sodium fluoride coronary microcalcification activity. *Journal of Nuclear Cardiology*. 2020 Jun 11;10.1007/s12350-020-02221-1.

Objective

We aimed to establish the observer repeatability and interscan reproducibility of coronary ^{18}F-sodium-fluoride positron emission tomography (PET) uptake using, a novel semi-automated approach, coronary microcalcification activity (CMA).

Methods

Patients with multivessel coronary artery disease underwent repeated hybrid PET and computed tomography angiography (CTA) imaging (PET/CTA). CMA was defined as the integrated standardised uptake values (SUV) in the entire coronary tree exceeding 2 standard deviations above the background SUV. The background activity was measured in the right atrium. Coefficients of repeatability between the same observer (intraobserver repeatability), between 2 observers (interobserver repeatability) and coefficient of reproducibility between 2 scans (interscan reproducibility), were determined at vessel and patient level.

Results

In 19 patients, CMA was assessed twice in 43 coronary vessels on two PET/CT scans performed 12±5 days apart. There was excellent intraclass correlation for intraobserver and interobserver repeatability as well as interscan reproducibility (all ≥0.991). There was 100% intraobserver, interobserver and interscan agreement for the presence (CMA>0) or absence (CMA=0) of coronary^{18}F-sodium fluoride uptake. Mean CMA was 3.12±0.62 with coefficients of repeatability of ≤10% for all measures: intraobserver 0.24 and 0.22, interobserver 0.30 and 0.29 and interscan 0.33 and 0.32 at a per-vessel and per-patient level respectively.

Conclusion

CMA is a repeatable and reproducible global measure of coronary atherosclerotic activity.

3.1 Introduction

Hybrid positron emission tomography and computed tomography (PET/CT) imaging with ^{18}F-sodium fluoride (^{18}F-NaF) can be used as a marker of developing microcalcification across multiple different vascular and valvular disease states (50, 66, 68, 78, 99, 119). It has been used to assess atherosclerotic disease activity in the coronary arteries, with the potential to identify high-risk plaques (48, 68, 81, 120, 121). To date, most studies have reported coronary ^{18}F-sodium fluoride PET uptake using maximum target to background ratio (TBR_{MAX}) (48, 59, 78, 81, 82). While TBR_{MAX} has been used as the primary measure for individual lesions (59, 117), its measurement can vary depending on plaque activity, the anatomical location of the background activity measured, and the partial volume effects of such small structures (122, 123).

We have developed a novel semi-automated approach to measure ^{18}F-sodium fluoride uptake throughout the entire coronary vasculature. This method uses centrelines defined by coronary CT angiography to build 3-dimensional tubular volumes of interest around each of the main epicardial coronary arteries (120) and thereby derive a single summary measure of total coronary microcalcification activity (CMA). This method allows evaluation of coronary ^{18}F-sodium fluoride activity on a per-vessel and per-patient basis, providing a global assessment of disease activity in the coronary arteries that is akin to the Agatston coronary artery calcium score for CT-defined coronary macrocalcification (120). CMA appears to correlate more closely with established CT-derived markers of plaque vulnerability than TBR_{MAX} (81). However, the observer repeatability and interscan reproducibility of CMA has yet to be established. In this study, we aimed to evaluate the intra- and interobserver repeatability and interscan reproducibility of CMA.

3.2 Methods

3.2.1 Study Population

Twenty patients were recruited from the Edinburgh Heart Centre outpatient cardiology clinics, as a part of the Dual Antiplatelet Therapy to Inhibit Coronary Atherosclerosis and Myocardial Injury in Patients with Necrotic High-risk Coronary Plaque Disease (DIAMOND) Study (NCT02110303) (101). Since this is a sub-study of the DIAMOND trial, patients were required to fulfil the same inclusion and exclusion criteria as those entering the main trial. These included renal failure and women of childbearing potential (full list in Appendix 1).

3.2.3 Image acquisition Protocol

Each patient underwent two ^{18}F-sodium fluoride positron emission tomography (PET) and computed tomography (CT) scans of the coronary arteries, within three weeks of each other.

3.2.4 PET acquisition

Patients underwent a 30-min list-mode PET-emission acquisitions approximately 1 h after injection of 250 MBq of ^{18}F-sodium fluoride. All patients were scanned with arms positioned above the head in a 128-slice Biograph mCT system (Siemens Healthineers, Knoxville, TN, USA). A low-dose CT for attenuation correction was acquired immediately before the PET acquisition (120 kV, 50 mAs, 3-mm slice thickness). All patients were imaged with 3-lead electrocardiogram cardiac gating.

3.2.5 Coronary computed tomography angiography acquisition

For anatomical localisation of PET uptake, coronary computed tomography angiography (CCTA) was performed immediately after the PET acquisition. The CCTA was performed using prospective gating, 330 ms rotation time, body-mass index (BMI) dependent voltage (<25 kg/m^2, 100 kV; ≥25 kg/m^2, 120 kV), and tube-current time product of 160–245 mAs. Patients were administered oral or intravenous beta-blocker therapy to achieve a target heartrate of <60 beats/min. A BMI-dependent bolus-injection of contrast media (400 mg/mL) was administered to the patients with a flow of 5–6 mL/s after determining the appropriate trigger delay defined by a test bolus of 20 mL of contrast material.

3.2.6 PET image reconstruction

PET images were reconstructed into 4 cardiac phases using a vendor provided software (JS-Recon12, Siemens, Knoxville, TN, USA). All PET image reconstructions were performed with corrections for time-of-flight and point-spread function. Using 4 cardiac gates, we reconstructed the data on a 256 × 256 matrix (109 slices, slice thickness 2.027 mm) using 2 iterations, 21 subsets and 5-mm Gaussian filter.

3.2.7 Cardiac Motion correction

Cardiac motion corrected images were obtained from the gated PET reconstructions through PET-PET image co-registration using a diffeomorphic registration and dedicated software (FusionQuant version 1.19.2.7, Cedars-Sinai Medical Center) (109).

3.2.8 Image registration

Prior to image analysis, the PET reconstructions were registered to the CCTA images, using a rigid translation of the PET images. The PET to CCTA registration was ensured using five key points of reference: sternum, vertebrae, blood pool in the left and right ventricle (based upon high ^{18}F-sodium fluoride activity in the blood pool in comparison to the surrounding myocardium), and the great vessels (111).

3.2.9 Blood clearance correction

To minimise the impact of variations in background blood pool activity introduced by the injection-to-scan delays (62, 117), we standardised the background blood pool activity to an injection-to-scan delay of 60 minutes using a previously described correction factor (117) (Equation 1):

$$SUVBackground\ corrected = SUVBackground * e^{(-0.004*(60-t))} \quad \text{(Equation 1)}$$

where t represents the injection-to-scan delay in minutes.

3.2.10 ^{18}F-sodium fluoride quantification: Coronary Microcalcification Activity (CMA) and maximum target to background ratio (TBR_{MAX})

Based upon PET image analysis techniques widely used in oncology and cardiac sarcoidosis (124-126) as well as the Agatston method for quantifying coronary CT calcium scores, we developed a novel measure to assess whole vessel activity in the coronary tree (120). To obtain the CMA values, two distinct steps were performed. First, we selected the proximal and distal end of the vessel (>2 mm) and applied a vessel tracking algorithm to extract whole-vessel tubular 3D volumes of interest from CCTA using dedicated semi-automated Autoplaque software (version 2, Cedars-Sinai Medical Center, Los Angeles, CA)(127) (Figure 3.1). These encompass all the main

epicardial coronary vessels and their immediate surroundings (4-mm radius) facilitating per-vessel and per-patient uptake quantification. In a tubular VOI, along the extracted centerlines, with 4-mm radius, we measured the CMA on the PET/CCTA co-registered images. For this study, we evaluated ^{18}F-sodium fluoride activity along the entire course of coronary arteries regardless of the presence of coronary stents, and we included the left main in the left anterior descending artery VOI. To avoid overspill of aortic root activity (spill-over effects), we excluded coronary activity in the orifice of the left main stem of being incorporated in the analysis. CMA was defined as the average SUV within the activity volume above threshold of background SUV mean +2 standard deviations. The background activity was measured in the right atrium. We have ensured that activity was co-localising with atherosclerotic plaque on CCTA and avoided potential areas of overspill activity (aortic valve, macular annular calcification). By using a threshold of background SUV mean +2 standard deviations we have excluded activity representing noise and made sure that windowing will not affect our results.

CCTA studies were assessed visually for percent stenosis according to the Society of Cardiovascular Computed Tomography guidelines (118). For a signal to be co-localised to a coronary artery, an atherosclerotic plaque had to be present on CT angiography, and the increased pattern of radiotracer had to arise from the coronary artery and follow its course over >5 mm in three dimensions on orthogonal views (128). On the co-registered PET and CTA images, ^{18}F-sodium fluoride PET uptake was measured in all coronary segments with a vessel diameter ≥2 mm and >25% stenosis as defined by CTA. The ^{18}F-sodium fluoride uptake in these lesions was

evaluated in a 3D spherical volume of interest (VOI) (radius 5 mm). In all plaques meeting these criteria, the maximum standardised uptake values (SUV_{MAX}) were measured within manually drawn regions of interest. TBR_{MAX} values were calculated by dividing the coronary SUV_{MAX} by the blood pool activity measured in the right atrium (cylindrical volume of interest radius 10 mm and thickness 5 mm) at the level of the right coronary artery ostium.

Figure 3.1 Three-dimensional rendering of coronary computed tomography (CT) angiography with superimposed tubular whole vessel volumes of interest (light green) employed for evaluation of ^{18}F-sodium fluoride (^{18}F-NaF) positron emission tomography (PET) uptake (blue and red). Despite the relatively low maximum target-to-background ratio (TBR_{MAX}) due to multiple foci of increased ^{18}F-NaF activity, the coronary microcalcification activity (CMA) in the right coronary artery (RCA) is higher than in the left anterior descending (LAD) coronary artery which presented with a higher TBR_{MAX} (LCx= Left circumflex artery).

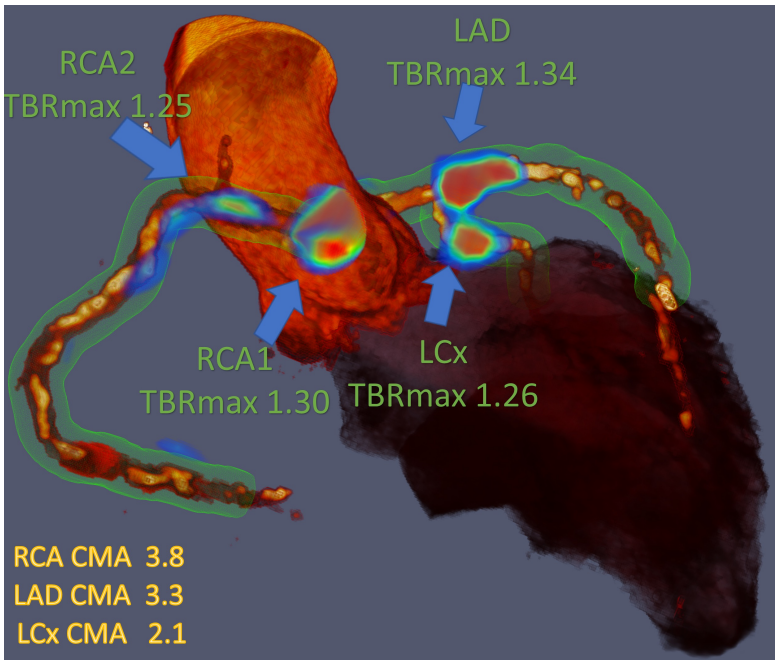

3.2.11 Diagnostic Evaluation of CMA and TBRMAX

Using CMA, the individual coronary arteries were marked as ^{18}F-sodium fluoride positive if CMA>0 and negative if CMA =0 (120). We also assessed the burden of activity on a per-vessel and per-patient level. To allow a per-patient analysis, we added the CMA activity of all major epicardial vessels (CMA_{total}). For TBR, PET uptake was quantified based on the CCTA lesion position, with lesions categorised as ^{18}F-sodium fluoride-positive (TBR_{MAX} ≥1.25) or ^{18}F-sodium fluoride-negative (TBR_{MAX} <1.25) (48, 78, 129). In order to compare TBR_{MAX} with CMA, we plotted the percentage differences in Bland-Altman plots.

3.2.12 Observer Repeatability and Interscan Reproducibility

Two anonymised scans for each of the 20 patients were presented to 2 experienced observers in random order. First, repeat assessments (observations 1 & 2) were performed by observer 1 at least 12 weeks apart in random order to prevent recall bias (intraobserver repeatability). Secondly, a second observer (observer 2) performed analysis for both scans and we compared them with measurements performed by the first observer (interobserver repeatability). Lastly, we compared the measurements between baseline scan (scan1) and repeat scan 2-3 weeks later (scan 2) in order to compute the interscan reproducibility.

3.2.13 Statistical Analysis

Data were tested for normality using the Shapiro–Wilk test. Statistical analysis was performed using MedCalc Statistical Software version 16.4.3 (MedCalc Software, Ostend, Belgium). Continuous, normally distributed variables were presented as mean ± standard deviation, whereas non-normally distributed continuous data were

presented as median [range]. Assessment of CMA and TBR_{MAX}, observer repeatability and interscan reproducibility were obtained using descriptive statistics with intraclass correlation coefficient (ICC) as well as Bland–Altman plots with mean bias and limits of agreement (LOA).

3.3 Results

3.3.1 Patient Characteristics

Twenty patients were recruited (Table 3.1), although one patient was excluded from the study due to incomplete list mode PET data. From the 57 coronary arteries included in the study, a total of 49 vessels fitted the size criterion (>2 mm in diameter). We excluded 6 vessels from the analysis: all vessels were the left circumflex coronary artery and were excluded due to spillover of ^{18}F-sodium fluoride activity from neighbouring mitral valve calcification (3 from scan 1 and 3 from scan 2), leaving a total of 43 vessels for the final analysis. A total of 47 lesions were identified on CCTA in these 43 vessels. The mean uptake values observed for the two readers and the repeated scans were 3.12± 0.62 for CMA and 1.62±0.49 for TBR_{MAX}.

Table 3.1 Patient Characteristics.

Age (years)	70 ± 8
Gender (males)	16 (84)
Body-mass index (kg/m^2)	27.6 ± 4.0
Cardiovascular risk factors	
- Diabetes mellitus (type II)	2 (11)
- Current smoker	2 (11)
- Hypertension	13 (68)
- Hyperlipidaemia	19 (100)
Agatston Calcium Score (AU)	1075 [0-1890]
Continuous variables reported as mean ± SD or median and interquartile range [IQR]; categorical variables reported as n (%).	

3.3.2 Presence or absence of ^{18}F-sodium fluoride activity.

There was 100% intraobserver, interobserver and interscan agreement for the presence of ^{18}F-sodium fluoride activity (CMA>0) or absence of ^{18}F-sodium fluoride activity (CMA=0) (Table 3.2). In addition, there were excellent intraclass correlations between the same observer, different observers and between scans (all intraclass correlation coefficient (ICC) >0.99, Table 3.3).

Table 3.2. Intraobserver (A), interobserver (B) and interscan (C) variability for the presence or the absence of ^{18}F-sodium fluoride uptake (coronary microcalcification activity) at a vessel level (n=43).

		Observation* 2			Observation* 2	
A Observation 1		CMA>0	CMA=0		TBR_{MAX}≥1.25	TBR_{MAX}<1.25
	CMA>0	34	0	TBR_{MAX}≥1.25	35	2
	CMA=0	0	9	TBR_{MAX}<1.25	1	12
B Observer 1		**Observer 2**			**Observer 2**	
	CMA>0	34	0	TBR_{MAX}≥1.25	35	1
	CMA=0	0	9	TBR_{MAX}<1.25	2	12
C Scan 1		**Scan 2**			**Scan 2**	
	CMA>0	34	0	TBR_{MAX}≥1.25	34	2
	CMA=0	0	9	TBR_{MAX}<1.25	2	13

Table 3.3 Intraclass correlation coefficient (ICC) for intraobserver and interobserver repeatability and interscan reproducibility for coronary microcalcification activity.

	Per-vessel (95% confidence interval)	**Per-patient** (95% confidence interval)
Intraobserver	**0.997 (0.995-0.998)**	**0.999 (0.998-0.999)**
Interobserver	**0.994 (0.991 – 0.997)**	**0.995 (0.992 – 0.997)**
Interscan	**0.991 (0.986 – 0.994)**	**0.993 (0.992 – 0.996)**

3.3.3 Intraobserver analysis.

There was excellent intraobserver repeatability for CMA measurement on a per-vessel level, with a coefficient of repeatability of 0.24, mean bias of −0.02 (p=0.39) and narrow limits of agreement (95% LOA −0.25 to 0.22; Figure 3.2). Similarly, at a patient level, CMA_{total} repeatability coefficient was 0.22 with a mean bias of −0.03 (p=0.12) and narrow limits of agreement (95% LOA −0.25 to 0.18; Figure 3.2).

Figure 3.2 Intraobserver repeatability of coronary microcalcification activity. Bland-Altman plots for intraobserver repeatability of coronary microcalcification activity at vessel.

(A) and patient (B) level. [CMA: coronary microcalcification activity, SD: standard deviation, CR: Coefficient of repeatability].

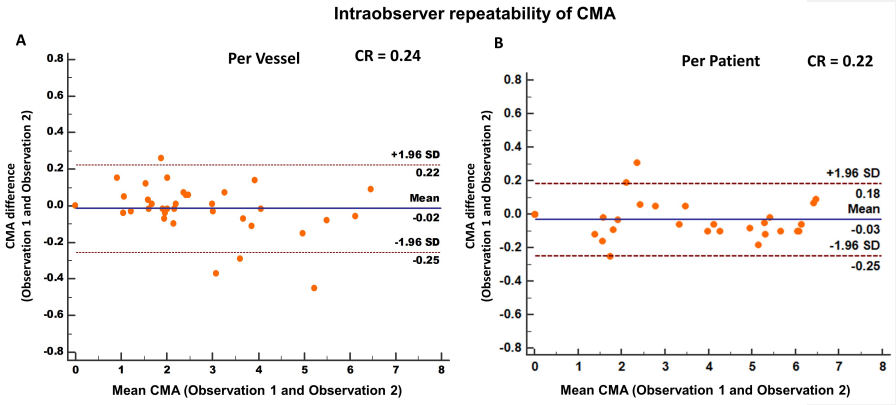

3.3.4 Interobserver analysis

Comparable to the intraobserver analysis, there was also excellent interobserver repeatability for CMA measurement on a per-vessel level, with a coefficient of repeatability of 0.30, mean bias of −0.01 (p=0.79) and narrow limits of agreement (95% LOA −0.31 to 0.29; Figure 3.3). At a patient level, CMA_{total} repeatability coefficient was 0.29 with a mean bias of −0.04 (p=0.17) and narrow limits of agreement (95% LOA −0.33 to 0.25; Figure 3.3).

Figure 3.3 Interobserver repeatability of coronary microcalcification activity. Bland-Altman plots at vessel (A) and patient (B) level.

[CMA: coronary microcalcification activity, SD: standard deviation, CR: Coefficient of repeatability].

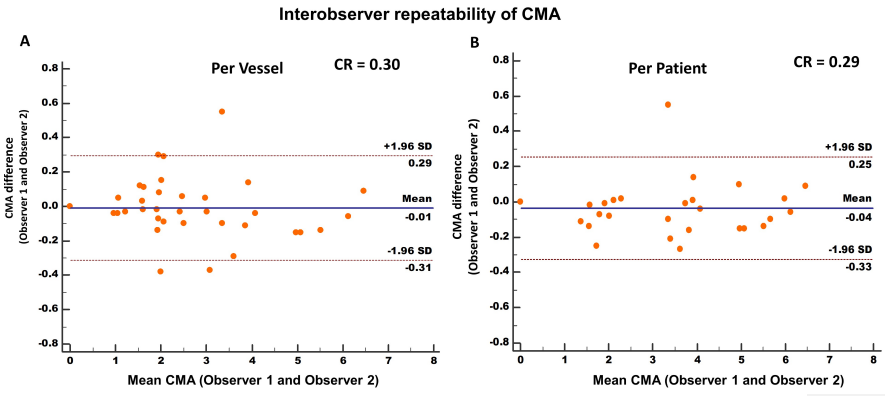

3.3.5 Interscan analysis

Similar to the interobserver analysis, interscan analysis of CMA showed very good reproducibility. At a vessel level, there was excellent interscan reproducibility with a coefficient of reproducibility of 0.33, mean bias of 0.02 (p=0.89) and narrow limits of agreement (95% LOA −0.31 to 0.35; Figure 3.4). Likewise, at a patient level, CMA_{total} reproducibility coefficient was 0.32 with a mean bias of −0.02 (p=0.30) and narrow limits of agreement (95% LOA −0.34 to 0.28; Figure 3.4).

Figure 3.4 Interscan repeatability of coronary microcalcification activity. Bland-Altman plots at vessel (A) and patient (B) level.

[CMA: coronary microcalcification activity, SD: standard deviation, CR: Coefficient of reproducibility.

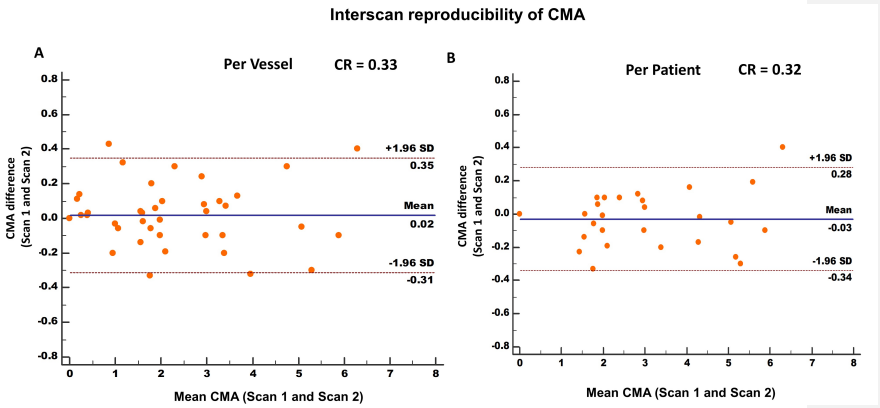

3.3.6 CMA and TBR_{MAX}

The activity of separate lesions (n=47) was assessed using maximum target-to-background ratio (TBR_{MAX}). Compared to TBR_{MAX}, CMA showed superior limits of agreement and smaller coefficients of repeatability for intraobserver and interobserver analysis, as well as smaller coefficient of reproducibility for interscan analysis. Between the same observer, CMA showed a mean bias and limits of agreement of 0.2% (95% LOA -10.6 to 11.1%) and TBR_{MAX} showed a bias of -2.4% (95% LOA -20.7 to 15.9%) with coefficients of repeatability of 10.8% and 18.3% respectively (Figure 3.5). Similarly, between different observers, CMA was more reproducible than TBR_{MAX} with a mean bias and limits of agreement of -0.1% (95% LOA -14.1 to 4.0) and -3.75% (95% LOA -25.2% to 17.8%) respectively and coefficients of repeatability of 14.0% and 19.5% (Figure 3.6). Finally, between scans, CMA showed a mean bias and limits of agreement of 0.1% (95% LOA -17.4 to 17.2%) and TBR_{MAX} showed a bias of 0.3% (95% LOA -24.0% to 24.6%) with coefficients of reproducibility of 17.2% and 24.3% respectively (Figure 3.6).

Figure 3.5 Intraobserver repeatability of TBRmax (A) and CMA (B) presented as % difference.

[CMA: coronary microcalcification activity, TBR_{MAX}: maximum target to background ratio SD: standard deviation].

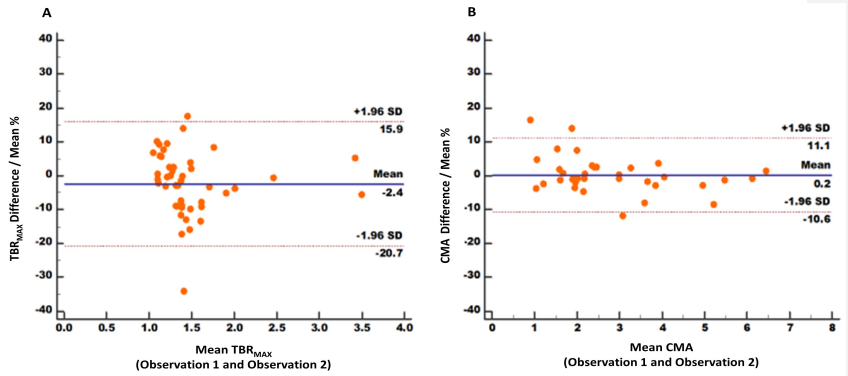

Figure 3.6 Interobserver repeatability of TBRmax (A) and CMA (B) presented as % difference.

[CMA: coronary microcalcification activity, TBR_{MAX}: maximum target to background ratio SD: standard deviation].

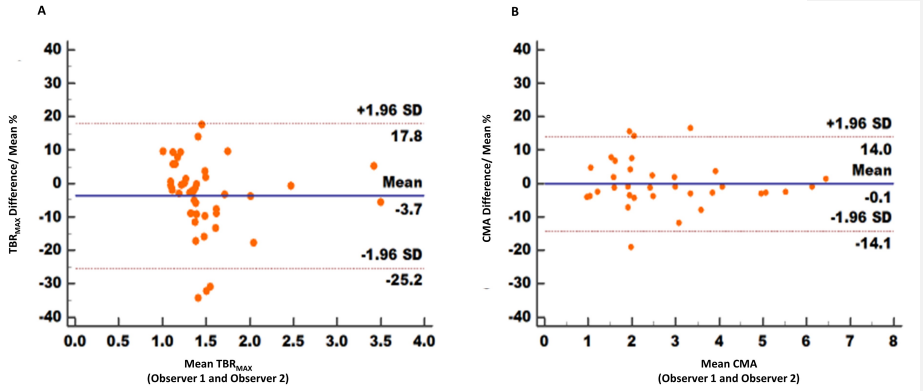

Figure 3.7 Interscan repeatability of TBRmax (A) and CMA (B) presented as % difference.

[CMA: coronary microcalcification activity, TBR_{MAX}: maximum target to background ratio SD: standard deviation].

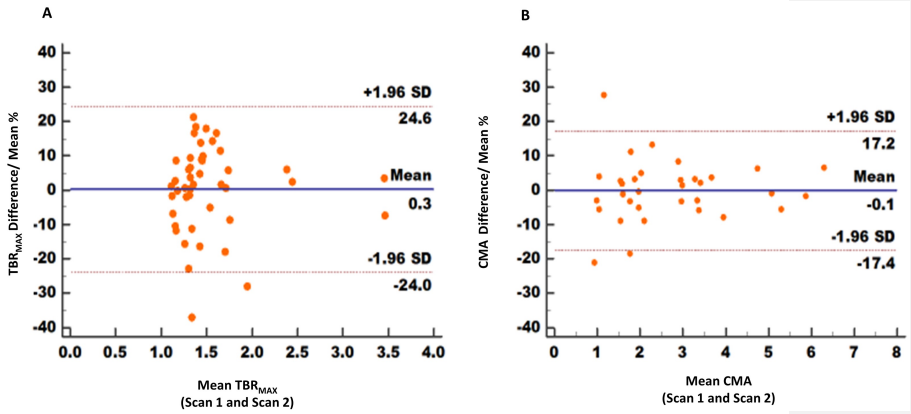

3.4 Discussion

Coronary ^{18}F-sodium fluoride PET is a non-invasive tool for imaging vulnerable atherosclerotic plaques (48, 120). We evaluated the repeatability and reproducibility of a novel methodology (CMA) for assessing whole vessel coronary ^{18}F-sodium fluoride uptake on PET/CT as a single measure of patient risk (120). We showed that CMA has excellent intra- and interobserver repeatability and interscan reproducibility and narrow limits of agreements within and between scans. This suggests that CMA is sufficiently robust to be used as single measure of coronary atherosclerotic activity and has the potential to provide a summary score of coronary risk similar to that described by the Agatston coronary artery calcium score (130).

It is now widely accepted that the anatomic assessment of the whole-coronary disease burden (vulnerable patient) is of greater importance than the identification of a single vulnerable plaque (131-133). We have shown that both TBR_{MAX} and CMA assessments were repeatable and reproducible, albeit CMA had the best repeatability and reproducibility. This has important implications for serial scanning and monitoring disease progression with coronary PET. Furthermore, there was no diagnostic discordance between observers or scans for CMA, something that is not always true for TBR_{MAX}. For the presence of ^{18}F-sodium fluoride activity (CMA>0) or absence of activity (CMA=0), there was 100% agreement in the categorisation between observers or scans with no crossover of cases observed (Table 3.2). On the other hand, there were 3 discordant values for TBR_{MAX} between observers and 4 discordant values between scans. This is of high importance in populations without known coronary artery disease if ^{18}F-sodium fluoride is to be used as a screening tool

where little or no activity is expected. In such population the fact that CMA=0 is reproducible between observers and scans is of extreme importance as it could reassure the physician.

This is the first study investigating the repeatability and interscan reproducibility of both CMA and TBR_{MAX}. In a previous study (59), we showed that TBR_{MAX} displayed good observer repeatability and interscan reproducibility when employing mid-diastolic PET images. This can be further improved using cardiac motion-corrected reconstructions (13). However, we have here reported narrower limits of agreement for observer repeatability and interscan reproducibility, both at a vessel as well as at a patient level.

Another strength of CMA is that it integrates the total activity of all 3 vessels in a score that resembles the well-established calcium score; i.e., a patient with CMA= 0 has no active microcalcification like a patient with zero calcium score. Unlike TBR, CMA measures patient-level total ^{18}F-sodium fluoride activity burden assessment and hence does not rely on a single hot pixel-value leading to better reproducibility. Furthermore, by identifying the coronary artery borders from CTA and limiting the assessment of ^{18}F-sodium fluoride uptake within these borders, the CMA approach has the strength to reduce the subjectivity and the time required to perform image analysis.

Despite the broad application of the individual lesion assessments using TBR_{MAX} (48, 59, 78, 81, 82, 117, 128, 133), this technique can only provide an estimation of activity at an individual plaque level, and as a result, the overall coronary disease burden of active macrocalcification cannot be appreciated. Indeed, this approach bears the risk

of underestimating the ^{18}F-sodium fluoride activity in patients with multiple plaques with increased tracer activity across the coronary tree (Figure 3.8). Using CMA, and computing the total activity burden, we were able to translate ^{18}F-sodium fluoride PET tracer uptake into the total coronary macrocalcification activity mirroring an approach successfully applied in the field of oncology and cardiac sarcoidosis (metabolic activity volume) (124-126). Thus, CMA provides a measure of the overall burden of disease activity for the patient.

Finally, despite the excellent prognostic information that coronary calcium scoring provides in asymptomatic individuals (35, 134) and those presenting with chest pain (135), its prognostic capability has been suboptimal in studies involving patients with established advanced coronary artery disease (136, 137). While coronary calcium visualises advanced and potentially healed disease (macrocalcification), it lacks the ability to visualise active disease (microcalcification) or predict future calcification progression. On the other hand, ^{18}F-sodium fluoride uptake is associated with culprit coronary plaques in patients with myocardial infarction (48), adverse plaque features in patients with apparently stable disease (81) and predicts the future progression of coronary calcium scores, confirming its status as a marker of disease activity (138). In addition, in a small study involving 32 patients, Kitagawa et al (82) showed that higher ^{18}F-Sodium fluoride uptake in established coronary atherosclerotic lesions on PET has a predictive value for future cardiac events (acute coronary syndrome or late coronary revascularisation) that was superior to the predictive value of the findings on CCTA, including coronary artery stenosis, high risk plaques and calcification. Moreover our group has recently shown, in a large multicohort study involving 293

patients with established multivessel coronary artery disease, that CMA outperforms coronary calcium score in prediction of myocardial infarction and major adverse cardiovascular events (MACE) (139).

Figure 3.8. Paired coronary tomography images (CT) and fused positron emission tomography (PET) /CT images of a representative patient with multiple lesions across the coronary tree assessed by two observers and with repeated scans.

Panel (A) shows the right coronary artery (RCA) with multiple plaques across the length of the artery and respective ^{18}F-sodium fluoride PET uptake. Tubular whole vessel volumes of interest (light green) employed for evaluation of ^{18}F-sodium fluoride (PET) uptake (bright yellow to red), B) Left main stem and left anterior descending artery (LMS/LAD) with multiple plaques and ^{18}F-sodium fluoride PET uptake and C) left circumflex (LCx) with a calcified proximal plaque and uptake.

[CMA: coronary microcalcification activity, TRB_{MAX}: maximum target to background ratio]

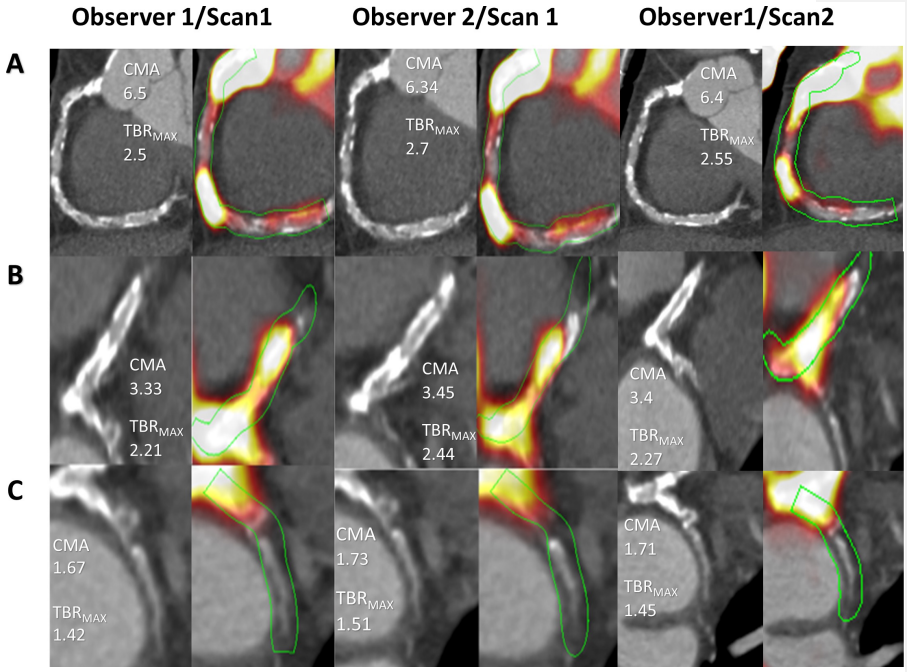

3.4.1 Limitations.

This study has several additional limitations; first is the number of patients included in the study (19). Despite the low number of participants, we were able to identify 47 separate lesions and we have evaluated each patient both at a per-vessel level and per-patient level. Another limitation was that we used only cardiac motion corrected images and did not apply gross patient motion and respiratory motion corrections (triple motion corrections) (117). The third limitation of this study was that all lesions were manually delineated by only two expert readers which may affect its broader generalisability. Finally, this study was obtained in a single centre using a PET/CT system from one vendor only. A bigger multicentre study including systems from multiple vendors would be required to confirm our findings.

3.5 Conclusion

In conclusion, we have shown CMA provides a novel metric of the per-vessel and per-patient coronary ^{18}F-sodium fluoride PET activity that has excellent intraobserver, and interobserver repeatability and interscan reproducibility. We suggest that CMA could be used as a global patient level measure of ^{18}F-sodium fluoride uptake with potential application to clinical trials and clinical practice.

Chapter 4 Respiration-averaged CT versus standard CT attenuation map for correction of 18F-Sodium Fluoride uptake in coronary atherosclerotic lesions on hybrid PET/CT

Published by **Tzolos E,** Lassen ML, Tinsu P et al. Respiration-averaged CT versus standard CT attenuation map for correction of 18F-sodium fluoride uptake in coronary atherosclerotic lesions on hybrid PET/CT

Journal of Nuclear Cardiology 2020 Jul 2;10.1007/s12350-020-02245-7.

Objective

To evaluate the impact of respiratory-averaged computed tomography attenuation correction (RACTAC) compared to standard single-phase computed tomography attenuation correction (CTAC) map, on the quantitative measures of coronary atherosclerotic lesions of ^{18}F-sodium fluoride uptake in hybrid positron emission tomography and computed tomography (PET/CT).

Methods

This study comprised 23 patients who underwent ^{18}F-sodium fluoride coronary PET in a hybrid PET/CT system. All patients had a standard single-phase CTAC obtained during free-breathing and a 4D cine-CT scan. From the cine-CT acquisition, RACTAC maps were obtained by averaging all images acquired over 5 seconds. PET reconstructions using either CTAC or RACTAC were compared. The quantitative impact of employing RACTAC was assessed using maximum target-to-background (TBR_{MAX}) and coronary microcalcification activity (CMA). Statistical differences were analysed using reproducibility coefficients and Bland-Altman plots.

Results

In 23 patients, we evaluated 34 coronary lesions using CTAC and RACTAC reconstructions. There was good agreement between CTAC and RACTAC for TBR_{MAX} (median [Interquartile range]): CTAC= 1.65[1.23-2.38], RACTAC= 1.63[1.23-2.33], p=0.55), with coefficient of reproducibility of 0.18, and CMA: CTAC= 0.10 [0-1.0], RACTAC= 0.15[0-1.03], p=0.55 with coefficient of reproducibility of 0.17.

Conclusion

Respiratory-averaged and standard single-phase attenuation correction maps provide similar and reproducible methods of quantifying coronary ^{18}F-sodium fluoride uptake on PET/CT.

4.1 Introduction

Hybrid positron emission tomography and computed tomography (PET/CT) imaging with ^{18}F-sodium fluoride (^{18}F-NaF) has been successfully employed for the assessment of atherosclerotic disease activity in the coronary arteries and can potentially identify high-risk plaques (48, 81, 120, 121). Currently, hybrid ^{18}F-sodium fluoride PET/CT scans are obtained utilizing a 30-min PET acquisition in listmode format, followed by PET image reconstructions employing four or ten cardiac phases with either breath-hold or free-breathing CT attenuation correction (CTAC) maps (62, 117, 128).

Previous studies on myocardial perfusion and viability have shown that misalignment of the PET emission data and the CTAC maps pose risks of false-positive findings in the clinical setting (140, 141), with loss in the predictive value if not corrected for motion (142). To ameliorate this problem, realignment of the CTAC maps and PET emission data before PET image reconstruction is sometimes required to obtain optimal predictive value (143). However, single-phase CTAC maps affect the quantitative accuracy of myocardial viability studies owing to the continuous respiratory translations during the PET emission acquisitions(144-147). Previous studies showed that employing respiratory averaged CTAC maps (RACTAC), obtained from cine-CT scans can improve the quantitative accuracy in myocardial perfusion and viability studies(148, 149).

Recently, ^{18}F-sodium fluoride PET has been established as a non-invasive imaging modality to identify high-risk and ruptured coronary atherosclerotic plaques(48, 78, 81, 111). Quantitative accuracy and reproducibility of imaging this tracer will be critical to establish its clinical value. However, the quantitative accuracy of lesion

micro-calcification activity assessed with ^{18}F-sodium fluoride PET and RACTAC for attenuation correction has not yet been evaluated.

In this study, we aimed to evaluate the quantitative impact of using RACTAC on ^{18}F-sodium fluoride uptake measurements, and to compare RACTAC and CTAC maps for the reconstruction of PET images (Figure 4.1). To this end, we aimed to compare the quantification of individual lesions using maximum target-to-background ratios (TBR_{MAX}) and whole-vessel and entire coronary tree microcalcification burden using coronary microcalcification activity (CMA) assessments (120, 139, 150).

Figure 4.1 Standard attenuation map-CTAC (left) vs respiratory average CT attenuation maps-RACTAC (right). Coronal (top) and transverse (bottom) images.

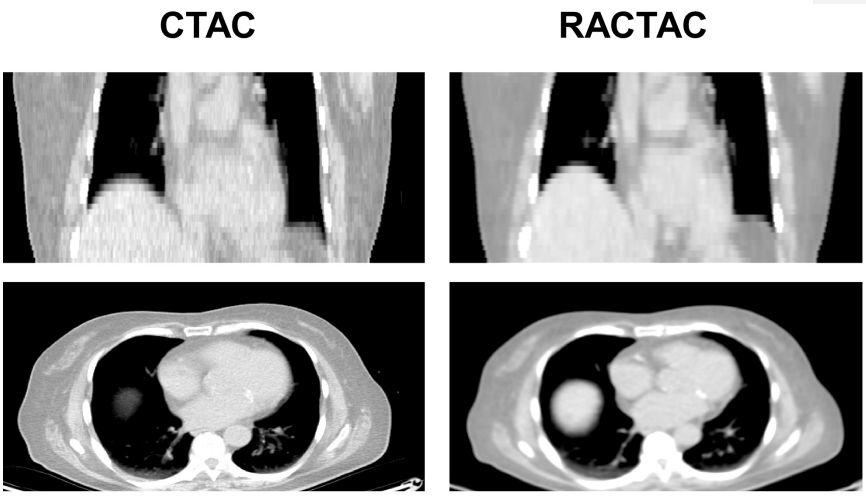

4.2 Methods

4.2.1 Study Population

Twenty-three patients underwent hybrid ^{18}F-sodium fluoride PET/CT examinations of the coronary arteries as part of the ongoing Effect of Evolocumab on Coronary Artery Plaque Volume and Composition by CCTA and Microcalcification by ^{18}F-sodium fluoride PET study (NCT03689946)***(151)***. Inclusion in the study required a Coronary Computed Tomography Angiography (CCTA) defined high non-calcified coronary artery plaque volume (>440 mm^3). Exclusion criteria were as follows: renal dysfunction (serum creatinine > 1.5 mg/dL) prior to imaging, history of allergy to iodine contrast agents, allergy to evolocumab, women who are pregnant or breastfeeding, active atrial fibrillation, history of coronary artery bypass graft surgery , inability to lie flat, inability or unwilling to give informed consent, major illness or life expectancy <1 year, planned coronary revascularisation or major non-cardiac surgery in the next 12 months, previous or current evolocumab use.

4.2.2 CCTA acquisition

The. The CCTA was acquired the same day as the PET scan for 13 patients, while the remaining cases (n=10) had the CCTA within 21 days (range=2-21 days). All patients were scanned with arms positioned above the head in a 192-slice Somatom Force Dual Source mCT system (Siemens Healthineers, Knoxville, TN, USA). The CCTA imaging parameters included prospective gating, 250 ms rotation time, body-mass index (BMI) dependent voltage (<25 kg/m^2, 100 kV; ≥25 kg/m^2, 120 kV), and tube-current time product of 160–245 mAs. Patients were administered beta-blockers (orally or intravenously) to achieve a target heart rate of <60 beats/min, followed by a BMI-dependent bolus-injection of contrast media (400 mg/mL) with a flow of 5–6 mL/s after determining the appropriate trigger delay defined by a test bolus of 20 mL of contrast material.

4.2.3 PET acquisition

Following the CCTA acquisition (at the same day or different day within a 21 days period as described above), all patients underwent ^{18}F-sodium fluoride positron emission tomography (PET), with arms positioned above the head on a hybrid PET-CT scanner (Discovery 710, GE Healthcare, Milwaukee, WI, USA). Prior to imaging, subjects were administered with a target dose of 250 MBq of ^{18}F-sodium fluoride and rested in a quiet environment for 180 min (Figure 4.2). All patients underwent 30 min PET emission acquisitions, using a standard 3-lead electrocardiogram using a free-breathing protocol, where the patients were advised to relax.

Figure 4.2 Imaging protocol for PET acquisition. All patients were scanned with arms positioned above the head.

AP: anteroposterior, CTAC: coronary tomography attenuation correction, PET: positron emission tomography

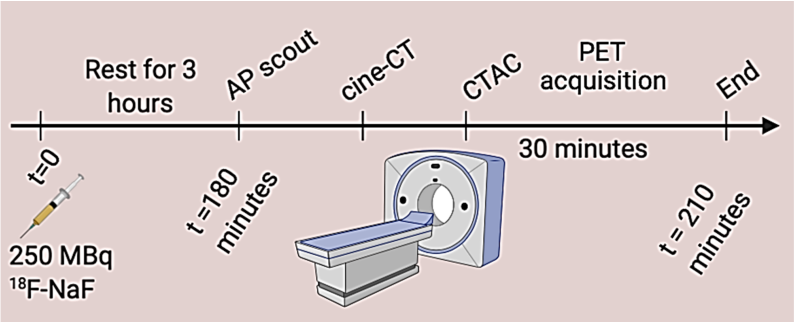

4.2.4 Cine-CT and standard CT attenuation correction acquisitions

Prior to the PET scans, an anteroposterior scout at 100 kV and 10 mA was obtained starting from the pulmonary artery bifurcation and extending to the diaphragm. Using the anatomical information, 4D cine-CT data were acquired with the following settings: 120 kV, 10 mA, slice thickness 2.5 mm, 0.8 sec/rotation, axial coverage of 14 cm, 7 cine acquisitions, and cine duration of 5 sec. Simultaneously with the cine-CT scan, we acquired information on the respiratory signal and its periodicity to perform quality-checks on the respiratory averaged CTAC maps using the Varian RPM system (Varian Medical Systems). In addition to the cine-CT scan, a standard AC map was acquired at the following settings: 100 kV, 40 mA, 0.5 second/rotation, 1.375 pitch factor, 5-mm slice thickness with an axial field of view of 15.4 cm, and acquisition time of 1.5 sec. The total radiation doses of 4D cine-CT and standard AC maps were 1.4 mSv and 0.8 mSv, respectively.

RACTAC map

From the CINE CT acquisition, we created RACTAC maps from averaging the CT images acquired over 5 seconds (Figure 4.1). To compensate for the reduced field-of-view, the RACTAC (axial coverage = 14 cm) was patched with the standard CT AC map (axial coverage = 15.4cm) for the missing 1.4 cm. In addition, the RACTAC maps were interpolated to obtain the same resolution in the axial direction as the standard CTAC map to preserve accurate attenuation correction of the PET images. Both the CTAC and the RACTAC maps were used for attenuation correction using a vendor-provided reconstruction toolbox.

4.2.5 PET quantification

Background blood pool clearance correction

To minimise the impact of variations in background blood pool activity introduced by variations in the injection-to-scan delays (117), we standardised the background blood pool activity to an injection-to-scan delay of 180 minutes using a previously described correction factor (117) (Eq. 1)

SUVBackground corrected = SUVBackground*e(−0.004*(180−t)) (1)

where t represents the injection-to-scan delay in minutes.

TBR_{MAX} quantification

TBR_{MAX} was obtained using a previously described protocol (120). In brief, for individual atherosclerotic lesions, the ^{18}F-sodium fluoride uptake was evaluated employing maximum standardised uptake values (SUV_{max}) obtained within 3D spherical volumes of interest (VOI) (radius 5 mm) placed on the lesions with ^{18}F-sodium fluoride focal uptake. TBR_{MAX} values were calculated by normalizing the atherosclerotic SUV_{MAX} values by the injection-to-scan delay corrected blood pool activity measured in the right atrium (cylindrical volume of interest radius 10 mm and thickness 5 mm) at the level of the right coronary artery ostium. Lesion SUVmax and TBRmax were evaluated using the same VOIs for both reconstructions, using VOIs inserted on PET images reconstructed using CTAC as reference.

CMA quantification

To obtain the CMA(120) values, two distinct steps were performed. First, we selected the proximal and distal end of the vessel (>2 mm) and applied a vessel tracking algorithm to extract whole-vessel tubular 3D volumes of interest from CCTA using dedicated semi-automated Autoplaque software (Cedars-Sinai Medical Center, Los Angeles, CA)(127). In a tubular VOI, along the extracted centrelines, with 4-mm diameter, we measured the coronary microcalcification activity (CMA) on the PET/CT co-registered images. CMA was defined as the average SUV within the activity volume above a threshold established as the mean background SUV +2 standard deviations. The background activity was measured in the right atrium. In order to evaluate the total uptake, we added the CMA activity of all epicardial vessels (CMAtotal).

4.2.6 Offset calculation between CTAC and RACTAC

The acquired electrocardiography-gated raw data (list mode dataset) were reconstructed using a standard ordered expectation-maximisation algorithm with time of flight, and resolution recovery using 4 cardiac bins. All images were reconstructed using a 256 × 256 matrix (47 slices) employing 4 iterations and 24 subsets, followed by a 5-mm Gaussian post-filtering.

Two series of PET images, one employing CTAC and another with RACTAC, were reconstructed into using a vendor-provided software (REGRECON-REL5, General Electric, Wisconsin, USA).

4.2.7 Statistical Methods

The data were tested for normality using the Shapiro–Wilk test. Statistical analysis was performed using MedCalc Statistical Software version 19.1.7 (MedCalc Software, Ostend, Belgium). Continuous, normally distributed variables were presented as mean ±SD (standard deviation), whereas non-normally distributed continuous data were presented as median [range]. We assessed CMA and TBR_{MAX}, using descriptive statistics and Bland–Altman plots, as well as coefficients of reproducibility. Boxplots were designed using R 3.5.0 and statistical significance of the difference between the correlated variances was calculated using the Pitman Morgan test; a two-sided p value <0.05 was considered significant.

4.3 Results

4.3.1 Patient Characteristics

Twenty-three patients (66±10 years, 78% male) underwent hybrid ^{18}F-sodium fluoride PET/CT examinations of the coronary arteries. Patient demographics are shown in Table 4.1. A total of 34 coronary lesions were identified on reconstructions on both PET corrected with CTAC and RACTAC maps (Figure 4.3). Across all patients, the median (IQR) offset for the CTAC and RACTAC maps were calculated to be 5.4 mm (2.2 mm – 9.9mm).

Table 4.1. Baseline Patient Characteristics.

Age (SD)	66±10
Sex (Males)	21 (78%)
BMI (SD)	27±4
Hyperlipidaemia	24 (89%)
Hypertension	14 (52%)
Diabetes	5 (18%)
Smoker/ex-smoker	7 (26%)
Total Plaque Volume (mm3)	837 [620-1066]
Total NCP Volume (mm3)	711 [55—859]
Total Calcified Volume (mm3)	103 [43-205]

Figure 4.3 Left anterior descending artery ^{18}F-sodium fluoride uptake. Left panel shows fused CTA and PET images reconstructed using the CTAC maps, whereas right shows the same CTA fused with PET an image reconstructed using RACTAC. There is good agreement between the measurements.

CTA = computed tomography angiography, CTAC = Computed Tomography Attenuation Correction and RACTAC = Respiratory averaged computed tomography attenuation correction.

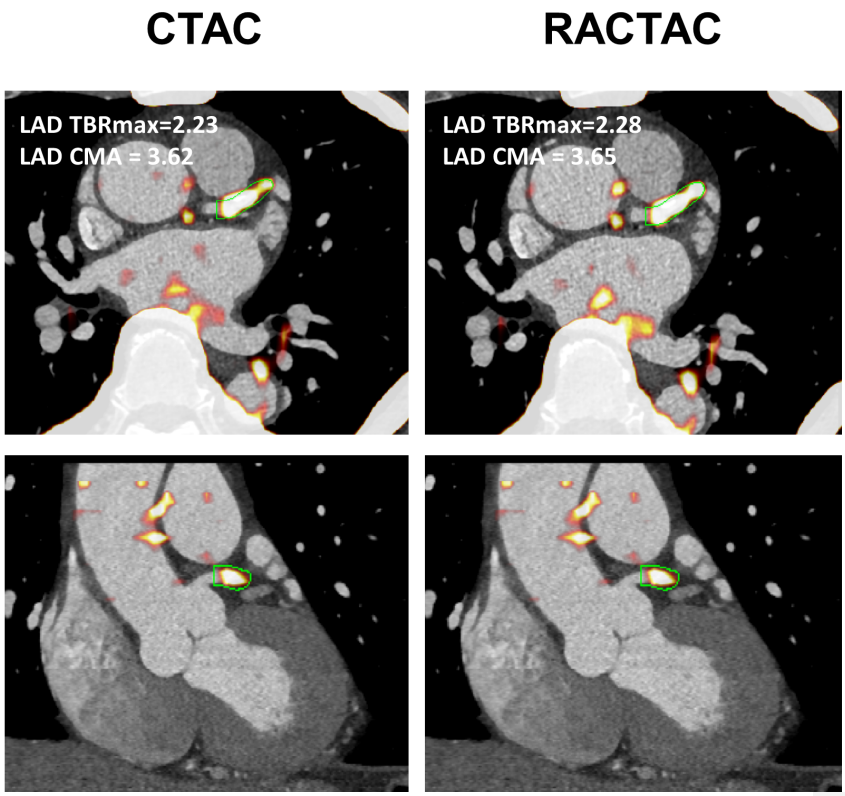

4.3.2 Per-lesion analysis (TBR_{MAX})

TBR values obtained using the same delineation of the lesions for reconstructions employing CTAC and RACTAC were similar (median TBR_{MAX} [Interquartile range; IQR]: CTAC = 1.65 [1.23-2.38], RACTAC = 1.63 [1.23-2.33], p =0.55). (Figure 4.4). Good agreement of the TBR measures obtained using the two different attenuation correction techniques was observed with coefficient of reproducibility of 0.18 (Figure 4.4).

Figure 4.4 A) Boxplot with connecting lines between the TBRmax measurements using the RACTAC maps vs CTAC maps (blue and red boxes represent interquartile range, with a thick solid line inside represents the median), B) Bland-Altman plot of the differences between the TBRmax measured using RACTAC maps vs CTAC maps. TBR_{max} = maximum Target to background ratio, CTAC = Computed Tomography Attenuation Correction and RACTAC = Respiratory averaged computed tomography attenuation correction, CR = coefficient of reproducibility

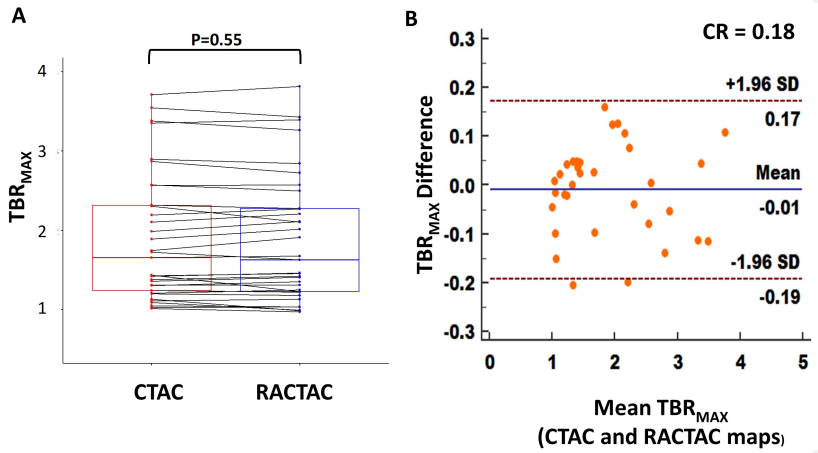

4.3.3 Per vessel analysis (CMA)

Assessments of the individual vessel microcalcification burden (CMA) revealed no major differences between PET images reconstructed using CTAC and RACTAC scans (median [IQR] CMA: CTAC = 0.10 [0-1.0], RACTAC = 0.15 [0-1.03], p=0.19) (Figure 4.5). Bland-Altman plots of the CMA values revealed a high degree of agreement when comparing the per vessel burden (Figure 4.5), with coefficient of reproducibility of 0.17.

Figure 4.5 A) Boxplot with connecting lines between the CMA measurements using the RACTAC maps vs CTAC maps (blue and red boxes represent interquartile range, with thick solid line inside represents the median), B) Bland-Altman plot of the differences between the CMA measured using RACTAC maps vs CTAC maps.

CMA = coronary microcalcification activity, CTAC = Computed Tomography Attenuation Correction and RACTAC = Respiratory averaged computed tomography attenuation correction, CR = coefficient of reproducibility

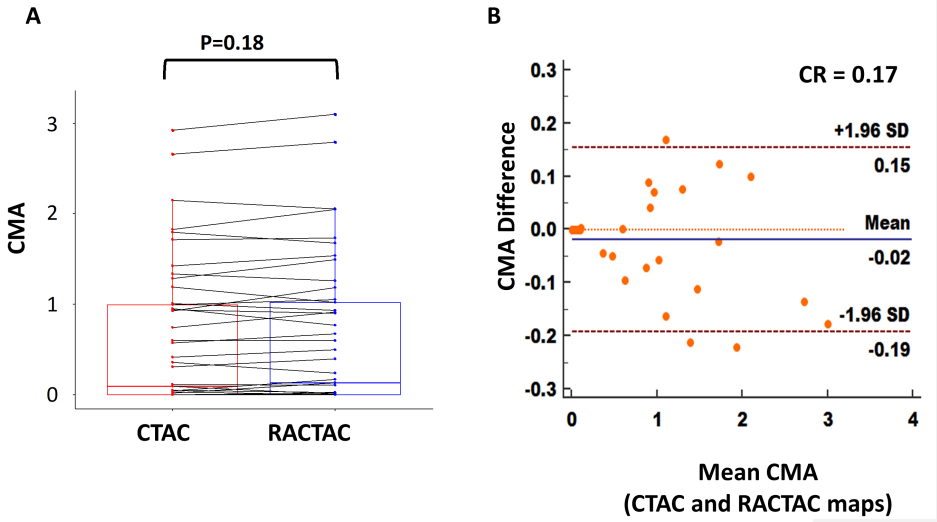

4.3.4 Coronary tree analysis (CMA)

Whole-coronary tree microcalcification burden (CMA for all three vessels combined), was comparable for the two series of reconstructions (CMAtotal: median [IQR]: CTAC = 1.01 [0-1.83], RACTAC = 1.05 [0-1.95], p=0.42) (Figure 4.6). In concordance with the single-vessel CMA burden, the data reconstructed using the two attenuation correction protocols were in agreement (Figure 4.6), with a coefficient of reproducibility of 0.17.

Figure 4.6 A) Boxplot with connecting lines between the CMA total measurements using the RACTAC maps vs CTAC maps (blue and red boxes represent interquartile range, with thick solid line inside represents the median), B) Bland-Altman plot of the differences between the CMAtotal measured using RACTAC maps vs CTAC maps. CMAtotal = whole coronary tree microcalcification activity, CTAC = Computed Tomography Attenuation Correction and RACTAC = Respiratory averaged computed tomography attenuation correction, CR = coefficient of reproducibility

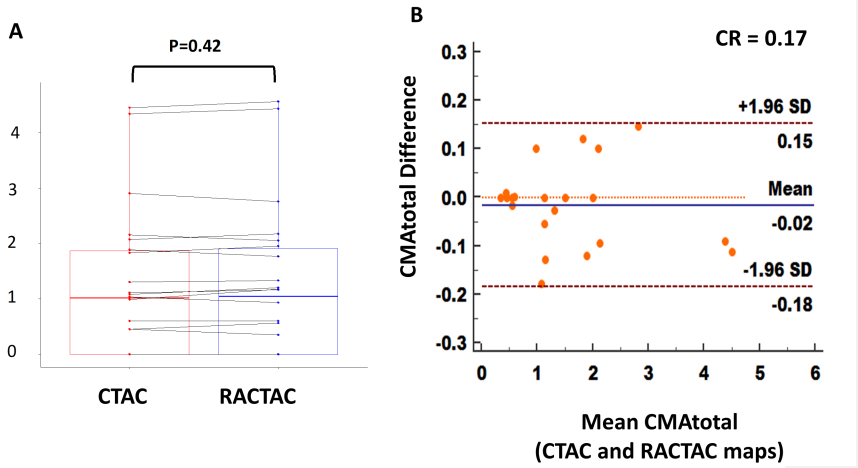

4.3.5 Correlation of lesion activity according to their location

Of the 34 coronary lesions, 2 were recognised in the left main stem (LMS), 15 in the left anterior descending artery, 8 in the right coronary artery and 9 in the left circumflex artery. There was excellent correlation among all lesions (R^2=0.97) and there was no difference between different vessels (Figure 4.7).

Figure 4.7 Correlation plot of SUVmax across the different lesion location. Excellent correlation (R^2) shown independent of the coronary artery involved.

LMS= left main stem, LAD= left anterior descending artery, RCA= right coronary artery and LCx= left circumflex artery, SUVmax= maximum standardised uptake value, CTAC = Computed Tomography Attenuation Correction and RACTAC = Respiratory averaged computed tomography attenuation correction

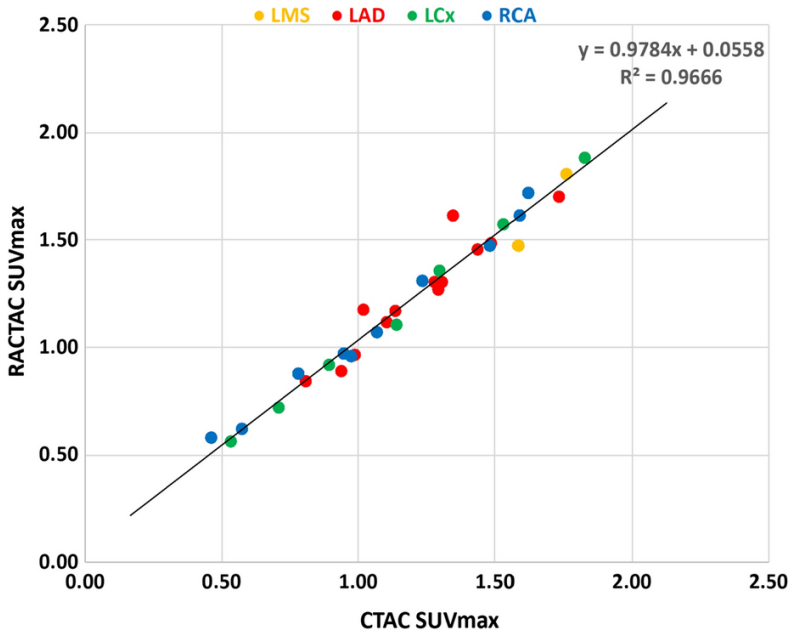

4.5 Discussion

In this study, we evaluated the impact of using standard CTAC maps and RACTAC maps obtained from cine-CT maps through respiratory averaging of CT data obtained in 4D on coronary PET. Our main finding was that using RACTAC did not introduce any significant changes in the quantitative comparisons, both when comparing single lesion activities and vessel and the whole coronary tree microcalcification burden. To our knowledge, this is the first study evaluating RACTAC maps in the assessment of coronary PET/CT.

Quantitative accuracy is of high importance in the assessment of both the singular vulnerable plaque and in the overall assessment of the coronary tree microcalcification burden (120). Previous studies have shown that both inter-reader and inter-scan variabilities are within acceptable ranges(59, 117). However, the quantitative accuracy can be impaired by significant respiratory and patient motion shifts during the acquisition (117, 129). Despite improvements in the test-retest reproducibility and reclassification of singular lesions following the introduction of sophisticated motion correction techniques, the quantitative accuracy might still be impaired by respiratory translations of the PET images during the 30-min long PET acquisitions. Current attenuation correction protocols employ a single-phase CT scan (free breathing, or end-expiratory breathing) (128, 144-147). The use of single-phase CTAC maps may change the observed uptake patterns in the heart, with deviations between 6% in canine models (152), and as much as 35% in human studies (153). In addition to the impact of the respiratory averaged CTAC maps, we also need to account for potential

problems between co-registered PET and CTAC maps which have shown to affect myocardial perfusion assessments (8, 9, 11). The impact of misregistration of PET emission data and transmission scans (CTAC maps) have not been evaluated in-depth yet. However, as many CTAC maps are acquired using free breathing protocols, the CTAC maps are likely acquired in an expiratory breathing phase, which is similar to the averaged respiratory position during the PET acquisitions. Several efforts to minimise potential mismatches have been proposed, hereunder the feasibility of scanning at the optimal time during respiration (154-156). Additionally, the sizes of coronary lesions are often of the same magnitude as the PET system resolution, which leaves the attenuation correction issues less dominant than partial volume effects.

Unfortunately, even with perfect breath instructions, it is challenging to state the optimal breath protocol applicable for all patients and even if the CT scan was obtained at the optimal breathing state. Pan et al.(149, 157) demonstrated that potential misalignment caused by different breathing phases during helical CT and PET affects both the quantitative and qualitative accuracy. By utilizing RACTAC for attenuation correction instead of the commonly employed CTAC, the frequency and impact of breathing artefacts were reduced, with improved tumor quantification as a result (148). It was argued that by utilizing, fast-scan cine CT acquisition of 5 seconds it is possible to bring together the temporal resolutions of CT and PET (148, 149, 157).

In this study, we did not observe any significant changes in PET uptake values between the reconstructions obtained using CTAC and RACTAC. This finding contrasts with previous reports (140, 149, 152), in which up to 40% of the false-positive results

normalised with the use of respiratory averaged CTAC maps (140). Several reasons could explain this. First, the investigators were measuring the activity of the myocardium and because of the higher diaphragmatic position at end-expiration they observed more misregistration artefacts resulting in decreased emission activity in inferior, inferoseptal, and inferolateral walls and compromised quantitative accuracy and the interpretation of myocardial viability. These artifacts were corrected by using respiratory-gated average attenuation maps. In our study, we concentrated on a focal activity away from the diaphragm and did not observe a difference in coronary ^{18}F-sodium fluoride uptake between the single-phase CTAC and respiratory averaged CTAC. Second, in these studies, the investigators measured the average activity, while we measured maximum activity (TBR_{MAX}) or activity above a specific threshold (CMA). By measuring maximum activity, we have encountered less variability by potential motion-driven misregistration as our volume of interest had a diameter of 5 mm. Gould et al. (140) showed that it was the transaxial misregistration of >6 mm that frequently caused artefactual defects and therefore by applying a volume of interest of 5 mm and measuring maximal activity we encountered less variability in our measurements. Third, the median offset of the CTAC and RACTAC images were of magnitude of 5.4mm (3D), with only 5 patients having translations of more than 10mm between the CTAC and RACTAC maps. These minor offsets combined with the averaging of the attenuation correction maps result in a relatively small impact of RACTAC images when compared to the CTAC maps. Finally, we used cardiac motion-corrected reconstructions(128) improving our ability to discriminate activity coming from the corresponding plaque lesion and improving our co-registration. We have previously shown that cardiac motion causes attenuation artifact and therefore

correcting for cardiac motion improves our ability to detect coronary artery disease on myocardial perfusion scans (158). Such cardiac motion correction was not used in previous RACTAC work with myocardial perfusion scans (159). In particular, the effects of cardiac contraction exceed that of respiration with regards to the displacement of the coronaries (cardiac contraction displaces the coronary arteries 8–26mm during the cardiac cycle, while normal respiration leads to movement of the heart of approximately 6–13mm (160).

The coefficient of reproducibility reported in this study is similar to findings reported in test-retest reproducibility studies where both similar interscan variations (117), and inter-reader variations we observed(59). While these results have focused on the test-retest and inter-reader variability for two different studies, our current study reports variations occurring as a result of the attenuation correction. The main finding of this study is that the variations added to the quantitative assessments of the per-lesion and whole coronary tree microcalcification burden are within the range of the reported variations. Therefore, RACTAC applied to the coronary plaque assessments does not seem to change the quantitative ^{18}F-sodium fluoride PET results when compared to the standard CTAC technique.

One concern in terms of employing the cine-CT in the routine clinical assessment is the added radiation dose, which conflicts with the as low as reasonably achievable (ALARA) principle. The ALARA principle might be compromised in studies of ^{18}F-sodium fluoride studies, as we in this study did not find any diagnostic relevant changes in the lesion assessment using the RACTAC corrected reconstructions. Based

on the calculations, the dose-burden given to a standard 70kg man equals 9.1mSv. This dose can be divided into the dose of the PET emission data (6.7mSv) and corresponding low-dose CTAC map (1mSv) and an additional 1.4mSv (15.2% extra dose) obtained for the cine-CT scan. While the difference between RACTAC and the regular CTAC is relatively low, the findings of this study indicate that the increased dose does not improve the quantification of coronary plaque scans using ^{18}F-sodium fluoride and, thus, should be omitted in future studies to comply with ALARA.

4.5.1 Study Limitations

Our study has limitations. First, our sample is small (23 patients). Despite that, we showed that our reproducibility coefficient is below the previously reported interobserver and interscan variation (59). Second, we report results obtained using cardiac motion correction which have less noise and lower TBR values than the commonly presented end-diastolic imaging reconstruction (48, 78). However, previous studies from our group have shown that both end-diastolic and cardiac motion corrected images can be used for ^{18}F-sodium fluoride coronary uptake assessments (117, 128). Third, a correlation between the volume with active microcalcification and the SUVmax or TBR measurements as the volume of activity is unknown. This limitation, although of clinical importance, is not affected by the attenuation correction, as shown in Figure 4.7 and thus, not considered to affect the results of this paper. Fourth, it is a single-centre study and we used only scanners from one vendor, thus, vendor-specific variations cannot be ruled out. A bigger study involving multiple centres and readers would be required to confirm our findings. Finally, the results presented in this study apply to the coronary PET imaging only, the effect of using RACTAC maps in other studies relying on absolute SUV measurements such as sarcoid PET/CT will need to be evaluated in future studies.

4.6 CONCLUSION

Applying respiration-averaged CT attenuation correction (RACTAC) maps do not affect the quantification of the coronary lesions as read in fusion PET/CT images. Current protocols utilizing single-shot CTAC maps provide equivalent corrections for the clinical reading of the patients.

Chapter 5 ^{18}F-Sodium Fluoride Coronary Uptake Predicts Outcome in Patients with Coronary Artery Disease

Published by **Kwiecinski J*, Tzolos E*,** Adamson P et al. ^{18}F-Sodium Fluoride Coronary Uptake Predicts Outcome in Patients with Coronary Artery Disease

Journal of American College of Cardiology 2020 Jun 23;75(24):3061-3074.

*Joint first co-authors

Objective

We lack reliable methods for predicting myocardial infarction in patients with established coronary artery disease. Coronary ^{18}F-sodium fluoride positron emission tomography (PET) provides an assessment of atherosclerosis activity. We assessed whether ^{18}F-sodium fluoride PET predicts myocardial infarction and provides additional prognostic information to current methods of risk stratification.

Methods

Patients with known coronary artery disease underwent ^{18}F-sodium fluoride PET computed tomography and were followed-up for fatal or non-fatal myocardial infarction over 42 [31-49] months. Total coronary ^{18}F-sodium fluoride uptake was determined using coronary microcalcification activity (CMA).

Results

In a post-hoc analysis of data collected for prospective observational studies we studied 293 study participants (65±9 years; 84% male), of whom 203 (69%) showed increased coronary ^{18}F-sodium fluoride activity (CMA>0). Fatal or non-fatal myocardial infarction occurred only in patients with increased coronary ^{18}F-sodium fluoride activity (20/203 CMA>0 versus 0/90 CMA=0; $p<0.001$). On receiver operator-curve analysis, fatal or non-fatal myocardial infarction prediction was highest for ^{18}F-sodium fluoride CMA, outperforming coronary calcium scoring, modified Duke coronary artery disease index, REACH and SMART risk scores (areas under curve: 0.76 versus 0.54, 0.62, 0.52 and 0.54; $p<0.001$ for all). Patients with CMA>1.56 had >7-fold increase in fatal or non-fatal myocardial infarction (hazard ratio 7.1, 95%

confidence interval 2.2 to 25.1; p=0.003) independent of age, gender, risk factors, segment involvement and coronary calcium scores, presence of coronary stents, coronary stenosis, REACH and SMART scores, the Duke coronary artery disease index and recent myocardial infarction.

Conclusions

In patients with established coronary artery disease, ^{18}F-sodium fluoride PET provides powerful independent prediction of fatal or non-fatal myocardial infarction.

5.1 Introduction

Despite improvements in therapies for atherosclerotic disease, myocardial infarction remains a leading cause of death worldwide. Robust tools to identify patients at risk of myocardial infarction would be extremely valuable as they could facilitate the targeted application of novel or intensive therapies to patients at the highest risk of events or down escalation of therapy in patients at low risk. However, to date, risk prediction in patients with established coronary artery disease has proven challenging. Current approaches are based around clinical risk scores, anatomic assessments of coronary artery calcification and the severity of obstructive coronary stenoses (161). These approaches have shown limited predictive value in patients with established coronary artery disease and there is growing interest in novel risk stratification methods, including assessments of atherosclerotic disease activity (132), that might be used to target expensive yet effective new treatments to patients at highest risk.

Advanced positron emission tomography (PET) imaging can provide assessment of disease activity in the coronary arteries to complement the anatomic plaque imaging provided by computed tomography (CT). The PET tracer ^{18}F-sodium fluoride is a marker of developing microcalcification and calcification activity across multiple different cardiovascular disease states (78). In coronary and carotid atherosclerosis, ^{18}F-sodium fluoride localises to culprit plaques following myocardial infarction and stroke as well as to plaques with multiple adverse characteristics in patients with stable disease (48, 82, 83). Moreover, coronary ^{18}F-sodium fluoride uptake has demonstrated its ability to predict disease progression and change in coronary calcium score, similar to results in other cardiovascular conditions (66, 162, 163). While coronary ^{18}F-sodium

fluoride uptake appears to provide a marker of atherosclerosis disease activity, the prognostic significance of increased coronary ^{18}F-sodium fluoride activity is unknown.

In this study, we investigated whether coronary ^{18}F-sodium fluoride PET uptake predicts future myocardial infarction and MACE in patients with established coronary artery disease, and whether it can provide additional prognostic information over and above current methods of risk stratification including clinical risk scores, coronary calcium scoring and the severity of obstructive coronary artery disease.

5.2 Methods

5.2.1 Study Design and Participants

Patients with established coronary artery disease undergoing hybrid coronary ^{18}F-sodium fluoride PET and contrast CT angiography at the Edinburgh Heart Centre and Cedars-Sinai Medical Center within prospective observational research studies were included in the current post-hoc analysis (NCT01749254, NCT02110303, NCT02607748) (48, 101). The study cohort comprised patients with recent myocardial infarction or established stable angina pectoris undergoing elective invasive coronary angiography (inclusion and exclusion criteria have been presented in Appendix 1). All patients underwent a comprehensive baseline clinical assessment including evaluation of their cardiovascular risk factor profile. In particular, REACH [Reduction of Atherothrombosis for Continued Health] and SMART [Secondary Manifestations of Arterial Disease] risk scores were calculated (Appendix 1). Both these scores were created specifically to predict risk in patients with established coronary artery disease (2, 161). Patients also underwent hybrid ^{18}F-sodium fluoride PET imaging alongside coronary CT calcium scoring and coronary CT angiography. Studies were conducted with the approval of the local research ethics committee, in accordance with the Declaration of Helsinki, and with the written informed consent of each participant.

5.2.2 ^{18}F-sodium fluoride and CT imaging acquisition and reconstruction

All patients underwent ^{18}F-sodium fluoride PET on hybrid PET/CT scanners (128-slice Biograph mCT, Siemens Medical Systems, Knoxville, USA or Discovery 710 GE Healthcare, Milwaukee, WI, USA) using harmonised imaging protocols 60 min following intravenous ^{18}F-sodium fluoride administration. During a single imaging session, we acquired a non-contrast CT attenuation correction scan followed by a 30-min PET emission scan in list mode. The electrocardiogram (ECG)-gated list mode dataset was reconstructed using a standard ordered expectation maximisation algorithm with time-of-flight, and point-spread-function correction. Using 4 cardiac gates, the data were reconstructed on a 256x256 matrix (with 75 or 47 slices using 2 iterations, 21 subsets and 5-mm Gaussian smoothing or 4 iterations, 24 subsets and 5-mm gaussian smoothing for Biograph and Discovery respectively). Immediately after the PET scan, a low dose non-contrast ECG-gated CT for calculation of the coronary calcium score was performed. Subsequently, a contrast-enhanced, ECG-gated coronary CT angiogram was obtained in mid-diastole on the same PET/CT system without repositioning the patient. To compensate for coronary motion associated with heart contraction, we performed cardiac motion correction of the PET/CT images (Described in detail in Chapter 2) (109, 110).

5.2.3 Image analysis

Computed Tomography

The coronary artery calcium score was measured in Agatston units (AU) using clinical software (NetraMD, ScImage, Los Altos, CA, USA). The presence of coronary atherosclerosis, and the extent and severity of obstructive coronary artery disease, was evaluated on contrast-enhanced CT angiography by defining the segment involvement score; the number of vessels with >50% luminal stenosis; and the modified Duke coronary artery disease index (combining the extent, severity, and location of coronary stenoses) (164). Multivessel coronary artery disease was defined as at least 2 major epicardial vessels with any combination of either >50% stenosis, or previous revascularisation.

^{18}F-Sodium Fluoride PET

We used a dedicated software package for coronary PET image analysis (FusionQuant, Cedars-Sinai Medical Center, Los Angeles). PET and CT angiography reconstructions were reoriented, fused and systematically co-registered in 3 orthogonal planes (111). We used two methods to evaluate coronary ^{18}F-sodium fluoride activity: the maximum target to background (TBR) approach (standard quantification) which relies on visual detection of lesions with increased tracer uptake; and the newly developed whole-coronary total microcalcification activity method (novel quantification) (48, 112).

Target to Background Ratio quantification

On co-registered PET and CT angiography images, for a signal to be co-localised to a coronary artery, an atherosclerotic plaque had to be present on the CT angiogram and the increased pattern of radiotracer had to arise from the coronary artery and follow its

course in three dimensions on 3-orthogonal views (78). In all plaques meeting these criteria, maximum standardised uptake values (SUVmax) were measured within manually drawn regions of interest. TBR values were calculated by dividing the coronary SUVmax by the blood pool activity measured in the right atrium (mean SUV in cylindrical volumes of interest at the level of the right coronary artery ostium: radius 10 mm and thickness 5 mm).

Blood clearance correction

To offset for variation in the delay between tracer injection and scanning, which has a major impact on blood pool activity, we used a recently validated correction factor to harmonise the background activity to a reference 60-minute injection-to-acquisition interval (Appendix 1) (117):

$$SUV_{Background\ corrected} = SUV_{Background} * e^{-0.004*(60-t)}$$

where t represents the injection-to-scan delay in minutes (103).

Coronary microcalcification activity (CMA) quantification

We used a recently described measure of coronary ^{18}F-sodium fluoride uptake, that quantifies PET activity across the entire coronary vasculature based upon analysis widely employed in oncology and cardiac sarcoidosis (125, 126). First, we automatically extracted whole-vessel tubular and tortuous 3D volumes of interest from CT angiography datasets (Figure 5.1). These encompass all the main epicardial coronary vessels and their immediate surroundings (4-mm radius) facilitating per-vessel and per-patient uptake quantification. Within such volumes of interest, we measured the coronary microcalcification activity (CMA) — representing the overall disease activity in the vessel and based upon both the volume and intensity of ^{18}F-

sodium fluoride PET activity within it (similar in principle to the Agatston score used for CT calcium scoring). CMA was defined as the integrated activity in SUV units exceeding the corrected background blood-pool mean SUV + 2 standard deviations (right atrium activity). The per-patient CMA was defined as the sum of the per-vessel CMA values.

Figure 5.1 Measuring disease activity across the coronary vasculature with ^{18}F-Sodium fluoride coronary microcalcification activity (CMA). 3-Dimensional rendering of coronary CT angiography with superimposed tubular whole vessel volumes of interest (light green) employed for evaluation of ^{18}F-sodium fluoride uptake (blue and red). Compared to target to background ratio (TBR) measurements (which depend on single pixel tracer uptake), the coronary microcalcification activity (CMA) is a summary measure of ^{18}F-sodium fluoride activity across the entire coronary vasculature as it includes all counts originating from the coronary arteries (uptake exceeding the threshold of background blood pool activity + 2 standard deviations).

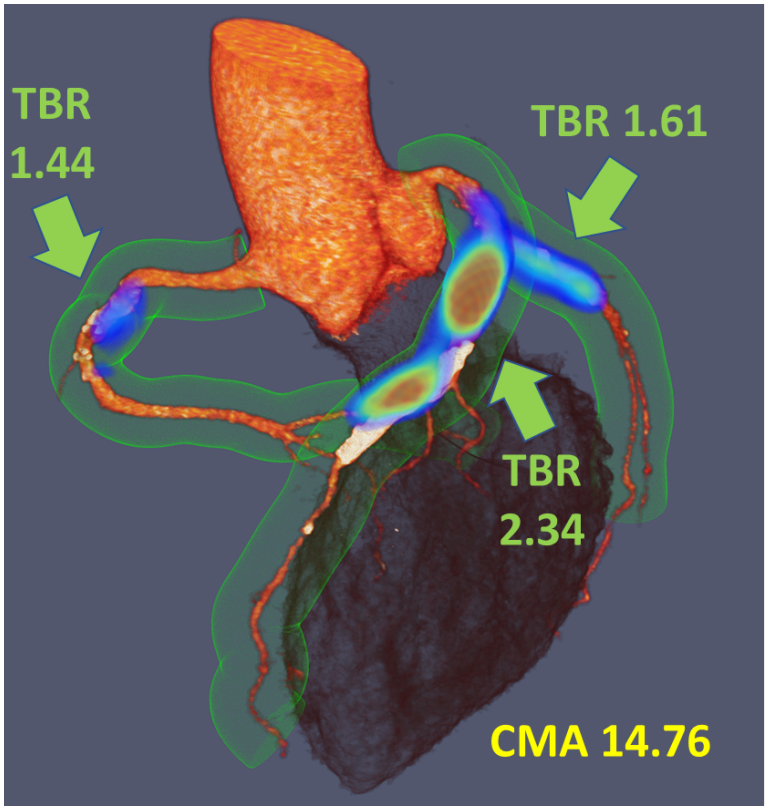

5.2.4 Clinical Follow-up

The primary endpoint of the study was fatal or non-fatal myocardial infarction. The secondary endpoint was major adverse cardiovascular events (MACE), defined as myocardial infarction, stroke, delayed revascularisation (more than 6 months after PET/CT) and cardiovascular death. Outcome information including invasive coronary angiography and coronary revascularisation (percutaneous coronary intervention or coronary artery bypass graft surgery) were obtained from the local and national healthcare record systems that integrates primary and secondary health care records. Categorisation of these outcomes was performed blinded to the coronary PET or other study data. Outcome data were collected in July 2019.

5.2.4 Statistical Analysis

We assessed the distribution of data with the Shapiro-Wilk test. Continuous parametric variables were expressed as mean (SD) and compared using Student's t tests. Non-parametric data were presented as median [Q1-Q3] and compared using Mann-Whitney U test. Fisher's exact test or chi-squared test was used for analysis of categorical variables. We used the receiver-operating characteristic (ROC) analysis and pairwise comparisons according to DeLong *et al* to compare areas under the curves. Kaplan-Meier curves were used to elucidate the survival distributions with regard to myocardial infarction and MACE. Differences in the outcome of patients with and without ^{18}F-sodium fluoride coronary activity exceeding the threshold derived from the ROC using Youden's index were assessed using the log-rank test. A Cox proportional hazard regression with adjustment for potential confounders was performed to determine the predictors of worse outcome. Statistical analysis was performed with SPSS version 24 (IBM SPSS Statistics for Windows, Version 24.0. Armonk, NY: IBM Corp). A two-sided $p<0.05$ was considered statistically significant.

5.3 Results

5.3.1 Patients

The study population comprised 293 patients (84% males, mean age: 65±9 years). All participants had established coronary artery disease, the majority (n=232) had stable disease and the remaining 61 individuals were recruited and imaged (14 [10-19)] days) following recent myocardial infarction (Appendix 1). Patients had advanced coronary atherosclerosis with a high burden of cardiovascular risk factors (hypertension 60%, hyperlipidaemia 88%, tobacco use 67%, REACH clinical risk scores of 13 [11-15], SMART clinical risk scores of 18 [13-26]), widespread utilisation of secondary preventative therapies (statin 90%, anti-platelet therapy 92%, ACE inhibitor or angiotensin receptor blockers 67%) and high rates of prior revascularisation (n=237, 81%). None of the patients were taking PCSK9 inhibitor or interleukin 1-beta inhibitor therapy. On invasive angiography, 87 (30%) individuals had single vessel obstructive disease, 191 (65%) had multi-vessel obstructive coronary artery disease, and 18 (6%) had left main stem involvement.

5.3.2 Computed Tomography

Patients had advanced coronary artery disease on CT. The median CT calcium score was 334 [76-804], 59 (20%) subjects had a calcium score > 1000, 133 (45%) patients had a score > 400, and only 84 (29%) presented with a score <100. On coronary CT angiography, the overall median segment involvement score was 5 [3-7] with three-quarters of patients (n=218, 74%) having at least 4 segments involved (Table 5.1). The median modified Duke index was 4 [3-5].

Table 5.1. **Baseline Characteristics of Study Participants.** Comparison of patients with (coronary microcalcification activity [CMA] > 0) and without (CMA = 0) increased coronary ^{18}F-sodium fluoride uptake.

	Entire Cohort	CMA=0 (n=90)	CMA>0 (n=203)	
Age in years, mean (SD)	65 (9)	63 (9)	65 (9)	P=0.0803
Men, n (%)	245 (84%)	71 (78.9%)	174 (86.1%)	p=0.1712
Body-mass index (kg/m^2), mean (SD)	29 (5)	29 (5)	29 (5)	P=1.0000
Systolic blood pressure (mm Hg), mean (SD)	141 (20)	137 (19)	144 (20)	**P=0.0054**
Diastolic blood pressure (mm Hg), mean (SD)	79 (11)	78 (9)	80 (12)	P=0.1584
Cardiovascular history, n (%)				
History of ACS	161 (55.1 %)	56 (62.2%)	105 (51.7%)	P=0.0749
History of PCI	237 (80.9 %)	57 (63.3%)	126 (62.1%)	P=0.8963
History of CABG	48 (16.4 %)	16 (17.8%)	32 (15.8%)	P=0.7326
History of angina	136 (46.6 %)	48 (53.3%)	88 (43.43%)	P=0.1283
CVA/TIA	9 (3.1 %)	2 (2.2%)	7 (3.4%)	P=0.7264
Comorbidities/risk factors, n (%)				
Hypertension	174 (59.6 %)	47 (52.2%)	128(63.1%)	P=0.0936
Hyperlipidaemia	257 (88 %)	81 (90.0 %)	177 (87.2%)	P=0.1571
Diabetes Mellitus	61 (20.8 %)	16 (17.8%)	35 (22.2%)	P=1.0000
Current smoking Ex-smoker	58 (19.9 %) 137 (46.9%)	26 (28.9%) 46 (51.1%)	32 (16.1%) 91 (45.7%)	p=0.0113 p=0.3745
Atrial fibrillation	10 (3.4 %)	5 (5.6 %)	5 (2.5%)	P=0.1827
Peripheral vascular disease	16 (5.5 %)	7 (7.8%)	9 (4.4%)	P=0.2698
Medications, n (%) *				
Aspirin	268 (91.8 %)	81 (90.0%)	187 (92.1%)	P=0.8185
P2Y12 antagonist	45 (15.4 %)	12 (13.3%)	33 (16.3%)	P=0.6005

Statin	262 (89.7 %)	80 (86.7%)	183 (90.1%)	P=0.8348
Beta Blocker	196 (67.1 %)	64 (71.1%)	133 (65.5%)	P=0.4184
ACEI/ARB	197 (67.4 %)	64 (71.1%)	134 (66.0%)	P=0.4194
Insulin	4 (1.4 %)	0 (0%)	4 (2.0%)	P=0.3161
Oral diabetic medications	48 (16.4 %)	17 (18.8%)	31 (15.2%)	P=0.4943
Calcium channel blockers	63 (21.6 %)	17 (18.9%)	46 (22.7%)	P=0.5388
Diuretics	38 (16.0 %)	12 (13.3%)	10 (4.9%)	0.0162
Biomarkers, median (IQR)				
Total Cholesterol (mmol/L)	4.1 (3.6-4.7)	4.1 (3.7-4.8)	4.1 (3.5-4.7)	P=0.81034
LDL (mmol/L)	1.9 (1.2-2.4)	1.9 (1.3-2.3)	1.9 (1.2- 2.5)	P=0.93624
HDL (mmol/L)	1.2 (1-1.7)	1.1 (0.9-1.6)	1.3 (1.0-1.7)	P=0.08186
TAG (mmol/L)	1.5 (1.1-2.3)	1.6 (1.1-2.4)	1.5 (1.1-2.3)	P=0.52218
Creatinine (µmol/L)	0.9 (0.8-1.0)	0.9 (0.8-1.0)	0.9 (0.8-1.0)	P=0.80258
CAD, n (%)				
Non-obstructive disease	15 (5.1 %)	7 (7.8%)	6 (3.0%)	P=0.1190
(<50%)	87 (29.8 %)	23 (25.6%)	67 (33.0%)	P=0.2191
- Single-vessel disease	110 (37.7 %)	39 (43.3%)	71 (35.0%)	P=0.1919
- Two-vessel disease	81 (27.6 %)	19 (23.3%)	59 (29.1%)	P=0.1970
- Three-vessel disease	18 (6.1 %)	2 (2.2%)	12 (5.9%)	P=0.2396
- LMS involvement				
Coronary Stent, n (%)	218 (73.4%)	61 (67.8%)	157 (77.3%)	P=0.1099
Segment involvement score. Median (IQR)	5 (3-7)	5 (3-7)	6 (4-7)	P=0.0562
SIS breakdown, n (%)				
0-1	20 (6.8%)	11 (12.2%)	9 (4.4%)	**P=0.0222**
2-3	55 (18.8%)	18 (20.0%)	37 (18.3%)	P=0.7468
4-5	73 (24.9%)	20 (22.2%)	53 (26.1%)	P=0.5587
>5	145 (49.4%)	41 (45.6%)	104 (51.2%)	P=0.3787

Modified Duke CAD index (IQR)	4 (3-5)	4 (3-5)	4 (3-5)	P=0.0574
Coronary Calcium Score, median (IQR)	334 (76-804)	179 (48-529)	378 (103-993)	**P=0.0027**
Coronary Calcium Score, n (%) 0-99 100-399 400-999 >1000	 84 (28.7%) 76 (25.9%) 74 (25.3%) 59 (20.1%)	 36 (40.0%) 22 (24.4%) 23 (25.6%) 9 (10.0%)	 48 (23.6%) 53 (26.6%) 52 (25.2%) 50 (24.6%)	 **P=0.0052** P=0.8847 P=1.0000 **P=0.0042**
TBR, median (IQR)	1.22 (1.1-1.42)	1.05 (0.99-1.11)	1.29 (1.19-1.48)	**P<0.0001**
TBR>1.28	113 (38.6%)	6 (6.7%)	107 (52.7%)	**P=0.0001**
CMA, median (IQR)	0.66 (0-2.84)	0	0.89 [0.47-3.10]	**P<0.0001**
Coronary Calcium Score>1000	59 (20.1%)	9 (10.0%)	50 (24.6%)	**P=0.0042**
Coronary Calcium Score>1199	46 (15.7%)	9 (10.0%)	37 (18.2%)	P=0.0831
REACH score CV event (IQR)	13 (11-15)	12 (10-14)	13 (11-15)	P=0.08012
SMART risk score % (IQR)	18 (13-26)	17 (13-23)	19 (13-27)	**P=0.0285**
MI during follow-up	20 (6.8%)	0 (0%)	20 (9.9%)	**P=0.0007**
MACE during follow-up	40 (13.6%)	7 (7.8%)	33 (16.3%)	P=0.0643

ACEI/ARB – angiotensin converting enzyme inhibitor/angiotensin receptor blocker, ACS – acute coronary syndrome, CABG – coronary artery bypass graft, CAD – coronary artery disease, CMA – coronary microcalcification activity, CVA - Cerebrovascular accident, MACE – major adverse cardiovascular event, PCI – percutaneous coronary intervention, REACH - Reduction of Atherothrombosis for Continued Health, SMART Secondary Manifestations of Arterial Disease, SIS – segment involvement score, TAG - triglycerides, TBR – target to background ratio, TIA - transient ischemic attack

*Medications at the time of scan

5.3.3 Positron Emission Tomography

On visual analysis of coronary PET, we identified increased tracer activity in 208 (70.9%) patients. Across the entire cohort, we found a median TBR of 1.22 [1.10-1.42]. Compared to those without uptake, patients with increased coronary ^{18}F-sodium fluoride uptake had higher SMART risk scores (17 [13-23] vs 19 [13-27], p=0.029), and higher coronary calcium scores (184 [50-528] vs 371 [102-974] AU, p=0.0031), but there was no difference in the presence or severity of obstructive coronary stenoses (all p>0.10).

Assessing whole vessel microcalcification activity, 203 (69.3%) patients presented with CMA>0. The median CMA value was 0.66 [0-2.84]. Again, we observed that patients with a CMA>0 had higher SMART risk scores (17 [13-23] vs 19 [13-27], p=0.028) and increased coronary calcium scores (378 [103-993] vs 179 [48-529], p=0.003) than subjects with CMA=0, but there was no difference in the presence or severity of obstructive coronary stenoses (all p>0.10; Table 5.1).

5.3.4 Clinical Outcomes

Over the 42 [31-49] months of follow-up, 20 subjects experienced a fatal (n=3) or non-fatal (n=17) myocardial infarction. Seven of these occurred in patients imaged following an acute coronary syndrome who had a median time from PET/CT to recurrent myocardial infarction of 12 (6-15) months. During follow-up a total of 40 patients suffered a MACE event (20 myocardial infarctions, 12 strokes, 3 cardiovascular deaths and 5 cases of delayed revascularisation).

5.3.5 Primary endpoint: fatal or non-fatal myocardial infarction

Patients who experienced myocardial infarction during follow-up had higher TBR values than those who did not (1.40 [1.28-1.77] versus 1.21 [1.09-1.40], p=0.006) and CMA (3.05 [1.62-5.25] versus 0.46 [0-2.47], p=0.002; Figure 5.2). Indeed, all the patients who had an infarct had increased coronary ^{18}F-sodium fluoride PET uptake at baseline (CMA > 0). Interestingly, patients who experienced a fatal or non-fatal myocardial infarction did not have increased clinical risk scores (REACH: 13 [11-15] versus 13 [11-15], p=0.79; SMART 20 [13-28] versus 18 [13-26], p=0.52) nor coronary calcium scores (397 [39-1456] versus 331 [76-775] AU, p=0.60) compared to patients who did not have an infarct. Moreover, they did not have an increased prevalence of obstructive coronary artery disease (segment involvement score 6 [4-8] versus 5 [3-7], p=0.25), multivessel coronary disease (70% versus 65%, p=0.64) nor previous coronary stents (75% versus 74%, p=1.00). In patients who had a fatal or non-fatal myocardial infarction, 30% had a coronary calcium score <100 AU, 20% were within the 100-399 AU range, 20% were within the 400-999 AU range and 30% had a coronary calcium score >1000 AU (Figures 5.3 & 5.4). Only 12% (7/59) of patients with coronary calcium score >1000 AU experienced myocardial infarction.

Figure 5.2 Coronary disease activity and plaque burden in patients with and without future myocardial infarction.

(A) CMA, **(B)** maximum TBR, and **(C)** CCS in patients with and without myocardial infarction during follow-up. For the Kaplan-Meier curves, patients were dichotomised according to thresholds derived from ROC curves using the Youden index: CMA: 1.56; TBR: 1.28; and CCS: 1,199 AU. AU = Agatston units; CCS = coronary calcium score; CMA = coronary microcalcification activity; ROC = receiver-operating characteristic; TBR = target to background ratio.

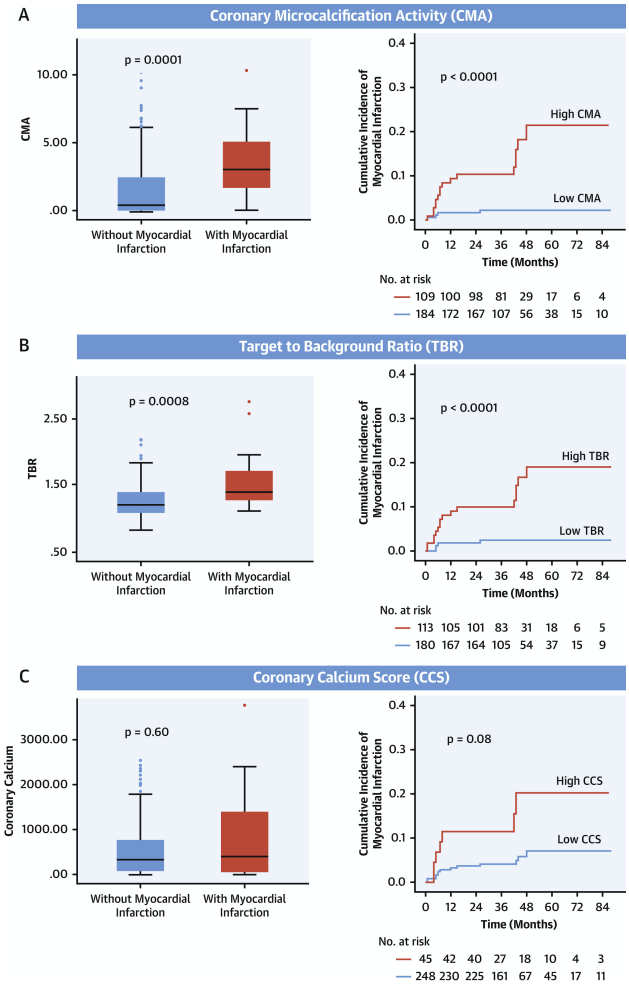

Figure 5.3 Case examples of ^{18}F-sodium fluoride positron emission tomography in patients with established coronary artery disease and myocardial infarction during follow-up. Hybrid CT angiography and ^{18}F-sodium fluoride positron emission tomography of coronary arteries in: **(A)** a 56-year-old male who demonstrated increased ^{18}F-sodium fluoride uptake in the RCA at baseline and presented with an inferior ST-segment elevation myocardial infarction and occlusion of the RCA during follow-up; **(B)** a 52-year-old male who demonstrated increased ^{18}F-sodium fluoride uptake in the LCx at baseline and presented with a lateral non-ST-segment elevation myocardial infarction during follow-up; **(C)** a 60-year-old female who showed increased ^{18}F-sodium fluoride uptake in the proximal RCA and presented with an inferior non-ST-segment elevation myocardial infarction during follow-up. LAD–left anterior descending, LCx–left circumflex, RCA–right coronary artery.

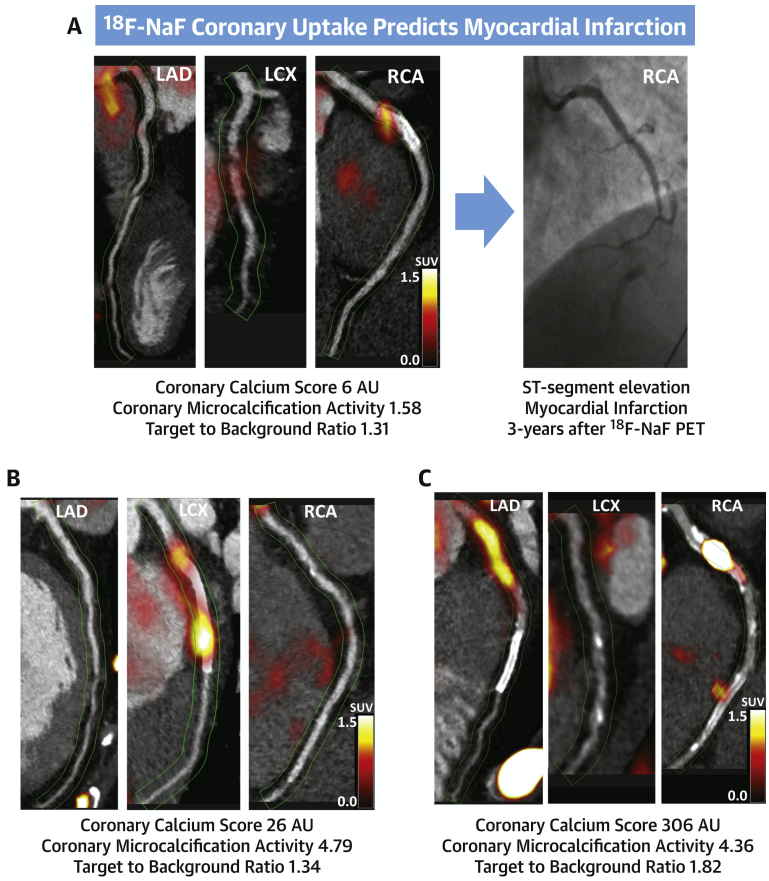

Figure 5.4 ^{18}F-sodium fluoride positron emission tomography in the prediction of myocardial infarction in patients with established coronary artery disease. In patients with established atherosclerosis the coronary microcalcification activity (as a marker of ^{18}F-sodium fluoride activity across the coronary vasculature) had a significantly larger area under the receiver operator curve than the coronary calcium score (non-contrast CT), the modified Duke index (contrast CT angiography) or the REACH score (patient clinical data).AU-Agatston units, CMA–coronary microcalcification activity, REACH-Reduction of Atherothrombosis for Continued Health

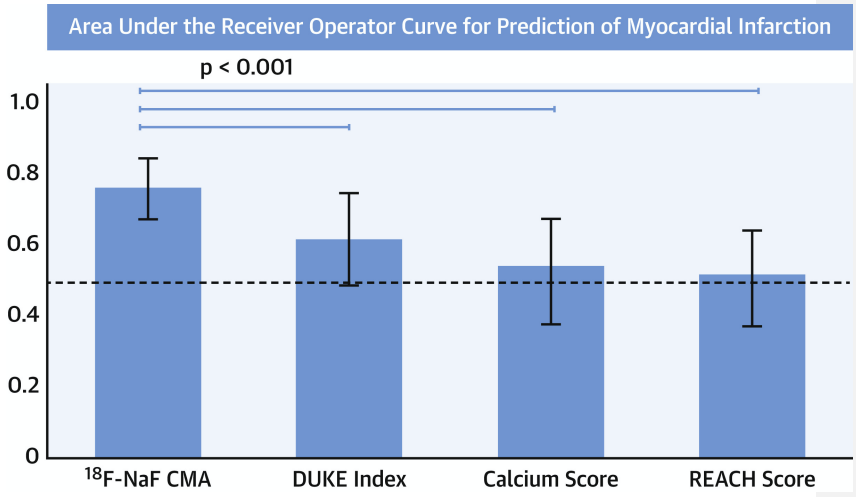

On ROC analysis, both CMA and TBR showed a greater area under the curve for the prediction of myocardial infarction than coronary calcium scores, or the REACH and SMART clinical risk scores (Figure 5.5). In order to generate distinct clinical risk groups, we dichotomised the population according to their coronary ^{18}F-sodium fluoride uptake and derived the optimal TBR and CMA cut-offs for event prediction using the Youden's index. A threshold of 1.56 for CMA achieved a specificity and sensitivity of 66% and 80% for the primary endpoint. A threshold of 1.28 for TBR achieved a specificity of 63% and sensitivity of 80% (Table 5.2). On univariable Cox proportional regression, both CMA >1.56 (hazard ratio (HR) 7.30, 95% confidence interval (CI) 2.44-21.84; p<0.001) and TBR >1.28 (HR 6.16, 95% CI 1.06-18.42; p=0.001) emerged as predictors of fatal or non-fatal myocardial infarction. Importantly, these associations persisted on multivariable analysis after adjustments for gender, comorbidities (presence of hypertension, hyperlipidaemia, diabetes, smoking), the segment involvement score, number of coronary stents, multivessel coronary artery disease, coronary calcium score, SMART and REACH risk scores, initial patients' presentation (acute coronary syndrome or stable coronary artery disease) and the study in which individuals were initially recruited (Figure 5.6).

Figure 5.5 Receiver operator curve analysis for the prediction of myocardial infarction in the study population (A), in patients with established stable coronary artery disease (B) and imaged shortly after myocardial infarction (C). Receiver operator curves for myocardial infarction prediction by coronary ^{18}F-sodium fluoride (^{18}F-NaF) PET (CMA), CT coronary calcium score, modified Duke index on CTCA and the REACH clinical risk scores.

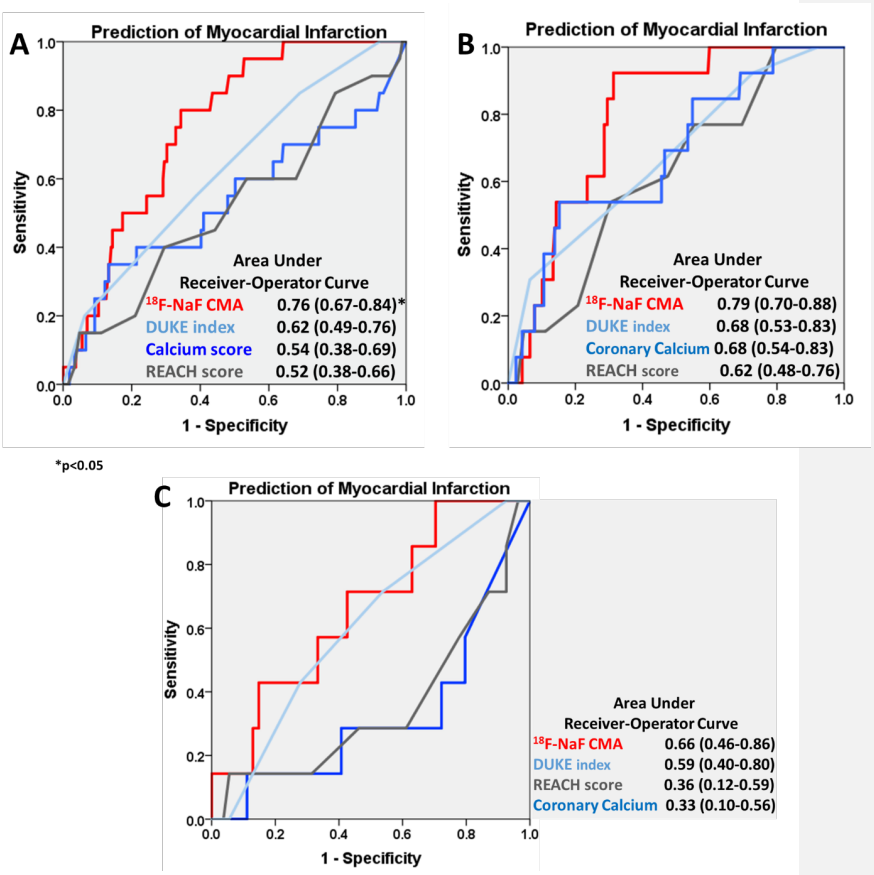

Table 5.2. Baseline Characteristics of Study Participants. Comparison of patients with coronary microcalcification activity (CMA) ≥1.56 vs <1.56, with Target to Background ratio (TBR) ≥1.28 vs <1.28 and coronary calcium score ≥1199 vs <1199.

	CMA			TBR			CCS		
	≥ 1.56 (n=109)	< 1.56 (n=184)	P	≥1.28 (n=113)	<1.28 (n=180)	P	≥1199 (n=45)	<1199 (n=248)	P
Age in years, mean (SD)	67 (8)	64 (9)	**0.0047**	67 (8)	63 (9)	**0.0001**	68 (8)	64 (9)	**0.006**
Men, n (%)	97 (89%)	148 (80%)	0.071	103 (91%)	142 (79%)	**0.006**	44 (98%)	201 (81%)	**0.004**
Body-mass index (kg/m2), mean (SD)	28 (5)	30 (5)	**0.024**	29 (6)	29 (5)	1.00	30 (5)	29 (5)	0.22
Systolic blood pressure (mm Hg), mean (SD)	142 (21)	141 (20)	0.68	142 (20)	141 (20)	0.68	143 (15)	141 (21)	0.54
Diastolic blood pressure (mm Hg), mean (SD)	79 (12)	80 (11)	0.46	78 (11)	80 (12)	0.15	78 (11)	80 (11)	0.26
Cardiovascular history, n (%)									
H of ACS	53 (48.6%)	108 (58.7%)	0.11	58 (51.3%)	103 (57.2%)	0.34	25 (55.6%)	136 (54.8%)	1.00
H of PCI	64 (58.7%)	119 (64.7%)	0.32	69 (61.1%)	114 (93.3%)	0.71	23 (51.1%)	160 (64.5%)	0.10
H of CABG	20 (18.3%)	28 (15.2%)	0.52	21 (18.6%)	27 (15.0%)	0.44	23 (51.1%)	25 (10.1%)	**0.0001**
H of angina	60 (55.0%)	76 (41.3%)	**0.029**	57 (50.4%)	79 (43.9%)	0.28	30 (66.7%)	106 (42.7%)	**0.003**
CVA/TIA	3 (2.8%)	6 (3.3%)	1.000	3 (2.7%)	6 (3.3%)	1.00	1 (2.2%)	8 (3.2%)	1.00
Comorbidities/risk factors, n (%)									
HTN	71 (65.1%)	103 (55.9%)	0.14	76 (67.3%)	98 (54.4%)	**0.038**	30 (66.7%)	144 (58.1%)	0.32
HPL	97 (89.0%)	160 (86.9%)	0.71	101 (89.3%)	156 (86.7%)	0.58	40 (88.9%)	217 (87.5%)	1.00
DM	26 (23.9%)	35 (19.0%)	0.37	26 (23.0%)	35 (19.4%)	0.46	13 (28.9%)	48 (19.4%)	0.16
Current smoking Ex-smoker	20 (18.3%) 44 (40.3%)	38 (21.1%) 93 (51.7%)	0.65 0.12	21 (18.6%) 51 (45.1%)	37 (20.6%) 86 (47.8%)	0.76 0.72	8 (17.8%) 19 (42.2%)	50 (20.2%) 118 (47.6%)	0.84 0.52
Atrial fibrillation	4 (3.7%)	6 (3.3%)	1.00	5 (4.4%)	5 (2.8%)	0.52	2 (4.4%)	8 (3.2%)	0.65
Peripheral vascular disease	4 (3.7%)	12 (6.5%)	0.43	4 (3.5%)	12 (6.7%)	0.30	8 (17.8%)	8 (3.2%)	**0.0008**
Medications, n (%) *									
Aspirin	101 (92.7%)	167 (90.7%)	0.67	107 (94.7%)	161 (89.4%)	0.14	41 (91.1%)	227 (91.5%)	1.00
PY12 antagonist	19 (17.4%)	26 (14.1%)	0.50	21 (18.6%)	24 (13.3%)	0.25	5 (11.1%)	40 (16.1%)	0.50
Statin	102 (93.6%)	160 (86.9%)	0.08	103 (91.2%)	159 (88.3%)	0.56	42 (93.3%)	220 (88.7%)	0.44
Beta Blocker	72 (66.1%)	124 (67.4%)	0.90	77 (68.1%)	119 (66.1%)	0.80	32 (71.1%)	164 (66.1%)	0.61
ACEI/ARB	76 (69.7%)	121 (65.7%)	0.61	81 (71.7%)	116 (64.4%)	0.20	38 (84.4%)	159 (64.1%)	**0.009**
Insulin	1 (0.9%)	3 (1.6%)	1.00	1 (0.9%)	3 (1.7%)	1.00	0	4 (1.4%)	1.00
Oral diabetic medications	17 (15.6%)	31 (16.8%)	0.87	19 (16.8%)	29 (1.6%)	0.87	8 (17.8%)	40 (16.1%)	0.83
CCB	23 (21.1%)	40 (21.7%)	1.00	27 (23.9%)	36 (20.0%)	0.47	12 (26.7%)	51 (20.6%)	0.43
Diuretics	7 (6.4%)	31 (16.8%)	**0.028**	7 (6.2%)	31 (17.2%)	**0.007**	7 (15.6%)	31 (12.5%)	0.63
Biomarkers, median (IQR)									
Total Cholesterol (mmol/L)	4.0 (3.5-4.7)	4.1 (3.6-4.8)	0.41	4.0 (3.5-4.8)	4.1 (3.6-4.7)	0.63	4.2 (3.5-4.9)	3.8 (4.1-4.7)	0.53
LDL (mmol/L)	1.9 (1.3-2.5)	1.9 (1.2-2.4)	0.75	1.7 (1.2-2.5)	2.1 (1.4-2.4)	0.21	2.2 (1.2-2.7)	1.9 (1.2-2.4)	0.12
HDL (mmol/L)	1.2 (1.0-1.7)	1.2 (1.0-1.8)	0.76	1.2(1.0-1.7)	1.2 (1.0-1.7)	0.69	1.2 (1.0-1.7)	1.2 (1.0 –1.7)	0.74
TAG (mmol/L)	1.5 (1.1-2.5)	1.6 (1.1-2.2)	0.87	1.5(1.0-2.5)	1.5 (1.1-2.2)	0.87	1.4 (1.2-2.0)	1.6 (1.1-2.4)	0.37
Creatinine (µmol/L)	80 (70-94)	77 (70-89)	0.42	78(70-88)	78(70-92)	0.95	80 (70-91)	77 (70-90)	0.48
CAD, n (%)									
Non-obstructive disease (<50%)	5 (4.6%)	10 (5.4%)	0.79	2 (1.8%)	13 (7.2%)	0.05	1 (2.2%)	14 (5.6%)	0.48
Single vessel disease	31 (28.4%)	56 (30.4%)	1.00	29 (25.7%)	58 (32.2%)	0.24	8 (17.8%)	79 (31.9%)	0.08
Two vessel disease	37 (33.9%)	73 (39.7%)	0.38	44 (38.9%)	66 (36.7%)	0.71	12 (26.7%)	98 (39.5%)	0.13
Three vessel disease	36 (33.0%)	45 (24.5%)	0.10	38 (33.6%)	43 (23.9%)	0.081	24 (53.3%)	57 (23.0%)	**0.0001**
LMS involvement	7 (6.4%)	7 (3.8%)	0.40	7 (6.2%)	7 (3.9%)	0.41	7 (15.6%)	7 (2.8%)	**0.002**
Coronary Stent, n (%)	83 (76.1%)	135 (73.4%)	0.68	85 (75.2%)	133 (73.9%)	0.89	24 (53.3%)	194 (78.2%)	**0.0013**
Segment involvement score. Median (IQR)	6 (4-8)	5 (3-7)	**0.008**	4 (6-8)	5(3-7)	**0.002**	7 (6-9)	5 (3-7)	**<0.0001**
SIS breakdown, n (%)									
0-1	4 (3.7%)	16 (8.7%)	0.15	3 (2.7%)	17 (9.4%)	**0.030**	1 (2.2%)	19 (7.7%)	0.33
2-3	19 (16.4%)	36 (19.6%)	0.76	14 (12.3%)	41 (22.8%)	**0.031**	0	55 (22.2%)	**0.0001**
4-5	23 (21.1%)	50 (27.2%)	0.27	29 (25.6%)	44 (24.4%)	0.89	5 (11.1%)	68 (27.4%)	**0.02**
>5	63 (57.8%)	82 (44.6%)	0.016	67 (59.3%)	78 (43.3%)	**0.009**	39 (86.7%)	106 (42.7%)	**0.0001**
CCS, median (IQR)	544 (184-1157)	201 (64-541)	**<0.0001**	498 (188-1089)	201 (59-558)	**<0.0001**	N/A	N/A	N/A
CCS, n (%)	21 (19.3%)	63 (34.2%)	**0.007**	20 (17.7%)	64 (35.6%)	**0.0009**			

0-99 100-399 400-999 >1000	24 (22.0%) 27 (24.8%) 37 (33.9%)	52 (28.3%) 47 (25.5%) 22 (12.0%)	0.27 1.00 **0.0001**	25 (22.1%) 33 (29.2%) 35 (31.0%)	51 (28.3%) 41 (22.8%) 24 (13.3%)	0.2742 0.2691 **0.0003**			
TBR, median (IQR)	1.45 (1.31-1.62)	1.13 (1.05-1.22)	**<0.001**	1.45 (1.35-1.62)	N/A	N/A	1.4 (1.23-1.62)	1.2 (1.1-1.4)	**<0.0001**
TBR≥1.28	86 (78.9%)	27 (14.7%)	**0.0001**	N/A	N/A	N/A	26 (57.8%)	87 (35.1%)	**0.005**
CCS>1199	27 (24.8%)	19 (10.3%)	**0.0015**	26 (23.0%)	20 (11.1%)	**0.0082**	N/A	N/A	N/A
Risk scores									
REACH score (IQR) CV event	13 (11-15)	13 (11-15)	0.075	14 (12-16)	12 (10-15)	**0.0039**	15 (13-17)	13 (11-15)	**<0.0001**
20-month risk of next CV event, % (IQR)	6.3 (4.7-8.5)	6.3 (4.7-8.5)	0.13	7.3 (4.7-9.2)	5.4 (4.0-8.5)	**0.0074**	8.5 (6.3-11.0)	5.4 (4.7-8.5)	**<0.0001**
REACH score (IQR) CV death	11 (10-13)	11 (9-13)	**0.015**	11 (10-13)	11 (9-12)	**0.0012**	12 (11-14)	11 (9-12)	**<0.0001**
20-month cardiovascular death, % (IQR)	1.8 (1.4-3.0)	1.8 (1.1-2.8)	**0.014**	1.8 (1.4-3.0)	1.5 (1.0-2.0)	**0.0011**	2.3 (1.8-3.8)	1.8 (1.1 -2.3)	**<0.0001**
Duke score	4 (3-5)	4 (3-5)	0.28	4 (3-5)	4 (3-5)	**0.0324**	5 (4-5)	4 (3-5)	**0.0024**
SMART risk score	21 (15-27)	17 (12-24)	**0.0050**	20 (14-28)	17 (13-24)	**0.0414**	24 (18-32)	17 (13-24)	**0.0002**
Outcomes									
Myocardial infarction	16 (14.7%)	4 (2.2%)	**0.0001**	16 (14.2%)	4 (2.2%)	**0.0002**	13 (15.6%)	7 (5.2%)	0.08
MACE	23 (21.1%)	17 (9.2%)	**0.008**	23 (20.4)	17 (9.4%)	**0.0078**	10 (22.2%)	30 (12.1%)	0.10
Stroke	3	9	**0.045**	3	9	**0.045**	1	11	**0.003**
Cardiovascular death	2	1	N/A	2	1	N/A	0	3	N/A
Delayed revascularisation	2	3	N/A	2	3	N/A	0	5	N/A

ACEI/ARB – angiotensin converting enzyme inhibitor/angiotensin receptor blocker, ACS – acute coronary syndrome, CABG – coronary artery bypass graft, CAD – coronary artery disease, CMA – coronary microcalcification activity, CVA - Cerebrovascular accident, MACE – major adverse cardiovascular event, PCI – percutaneous coronary intervention, REACH - Reduction of Atherothrombosis for Continued Health, SMART Secondary Manifestations of Arterial Disease, SIS – segment involvement score, TAG - triglycerides, TBR – target to background ratio, TIA - transient ischemic attack

*Medications at the time of scan

Figure 5.6 Predictors of myocardial infarction on Cox proportional hazards modelling. Forest plots of hazard ratios derived from multivariable modelling with 95% confidence intervals for the coronary microcalcification activity (CMA) (A) and the target to background ratio values (B) along with covariates: coronary calcium scores, SIS, REACH score, SMART score, total number of implanted coronary stents, presence of multivessel coronary artery disease, age, gender, hyperlipidaemia, hypertension, diabetes, smoking. CMA–coronary microcalcification activity, REACH-Reduction of Atherothrombosis for Continued Health, SMART - Secondary Manifestations of Arterial Disease, SIS–segment involvement score, TAG-triglycerides, TBR–target to background ratio

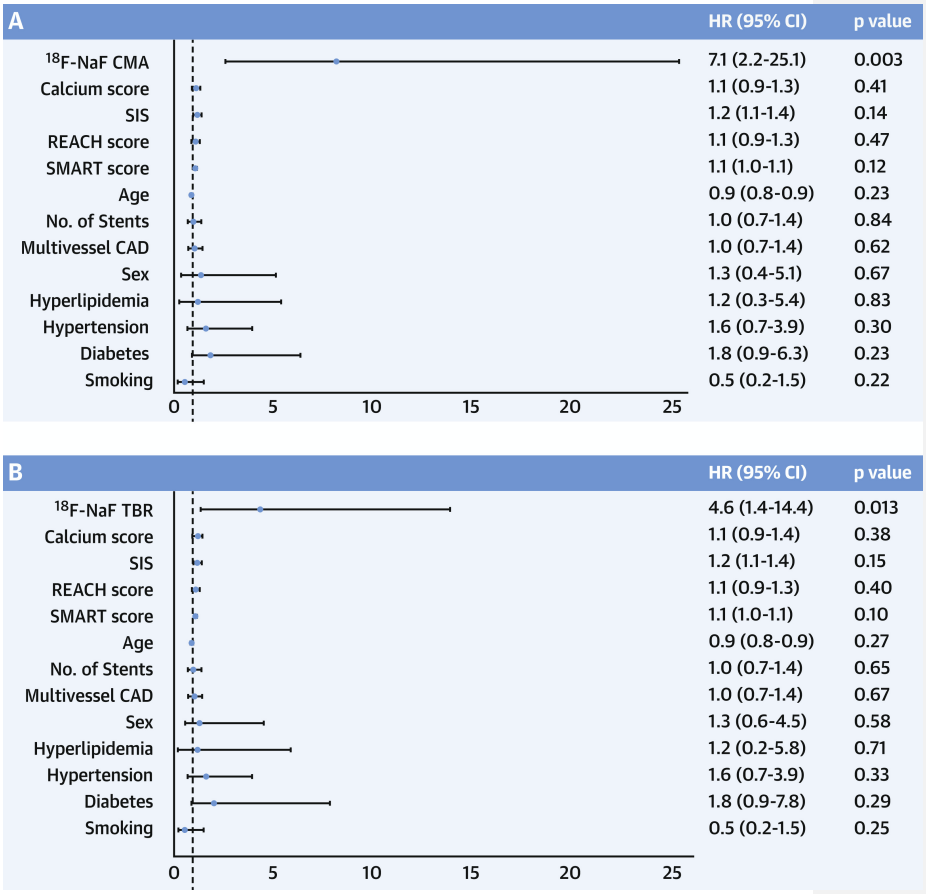

Indeed, patients with CMA>1.56 had an adjusted hazard ratio of 7.1 (95% CI 2.2 to 25.1; p=0.003) for the primary end point, whilst patients with a TBR >1.28 had an adjusted hazard ratio of 4.6 (95% CI 1.4 to 14.4, p=0.013; Table 5.3). Similar results were observed when both CMA and TBR were considered as continuous variables, with both again emerging as the only independent predictors of fatal or non-fatal myocardial infarction on Cox modelling (Table 5.4). In contrast, the number of stenosed vessels, the modified Duke index, age, and the SMART and REACH risk scores did not emerge as predictors of fatal non-fatal myocardial infarction on univariable Cox modelling (all p>0.1, Table 5.4). Coronary calcium score was a predictor of events on univariable but not multivariable analysis (Table 5.3). Despite low statistical power when patients with acute myocardial infarction and stable subjects were considered separately, the AUCs on receiver-operator-characteristic curve analyses remained numerically similar (Figure 5.7).

Table 5.3 Uni- and multivariable Cox proportional regression models for prediction of myocardial infarction during follow-up.

	Coronary Microcalcification Activity >1.56		Target to background ratio >1.28		Coronary Calcium Score > 1199	
	Hazard ratio (95% CI)	p-value	Hazard ratio (95% CI)	p-value	Hazard ratio (95% CI)	p-value
Model 1	7.30 (2.44-21.84)	<0.001	6.16 (1.06-18.42)	0.001	3.24 (1.29-8.11)	0.012
Model 2	7.20 (2.36-21.95)	0.001	5.94 (1.94-18.10)	0.002	-	
Model 3	6.66 (2.19-20.25)	0.001	5.57 (1.80-17.00)	0.003	2.65 (0.93-7.56)	0.069
Model 4	8.73 (2.44-31.29)	0.001	4.80 (1.54-14.93)	0.007	2.72 (0.90-8.21)	0.075
Model 5	8.91 (2.47-32.16)	0.001	4.83 (1.54-15.20)	0.007	-	
Model 6	8.12 (2.57-25.28)	p<0.001	4.30 (1.34-13.82)	0.014		
Model 7	7.10 (2.2-25.1)	0.003	4.6 (1.4-14.4)	0.013		

Model 1 – unadjusted; Model 2 – adjusted for Coronary Calcium Score; Model 3 – adjusted for segment involvement score, number of coronary stents, multivessel coronary artery disease; Model 4 – adjusted for segment involvement score, number of coronary stents, multivessel coronary artery disease, age, gender, hyperlipidaemia, hypertension, diabetes, smoking; Model 5 – similar to Model 4 and additionally adjusted for coronary calcium scoring; Model 6 – similar to Model 5 and additionally adjusted for REACH and SMART risk scores. Model 7 – similar to model 6 and additionally adjusted for initial patient's presentation (stable vs acute myocardial infarction) and the study into which the patient was initially recruited.

Table 5.4. Prediction of myocardial infarction and major adverse cardiovascular events (MACE) during follow-up. Univariable Cox proportional regression models with covariates as continuous variables.

	Myocardial Infarction		MACE	
	Hazard ratio (95% CI)	p-value	Hazard ratio (95% CI)	p-value
CMA	1.07 (1.03-1.12)	0.001	1.06 (1.01-1.10)	0.012
TBR	2.57 (1.66-3.98)	<0.001	2.08 (1.35-3.22)	0.001
Coronary Calcium Score	1.00 (1.00-1.01)	0.25	1.00 (1.00-1.00)	0.77
REACH	1.00 (0.86-1.16)	0.99	0.96 (0.86-1.07)	0.96
SMART	1.02 (0.98-1.06)	0.26	1.02 (0.99-1.05)	0.13
Duke index	1.59 (0.99-2.48)	0.07	1.23 (0.94-1.62)	0.14
Age	0.99 (0.94-1.04)	0.61	0.99 (0.95-1.03)	0.55

CMA – coronary microcalcification activity, TBR – target to background ratio, REACH -, CI-Confidence interval, Reduction of Atherothrombosis for Continued Health, SMART - Secondary Manifestations of Arterial Disease

Figure 5.7 Kaplan-Meier curve analysis for the prediction of myocardial infarction in patients imaged shortly after myocardial infarction (A) and in patients with established stable coronary artery disease (B).

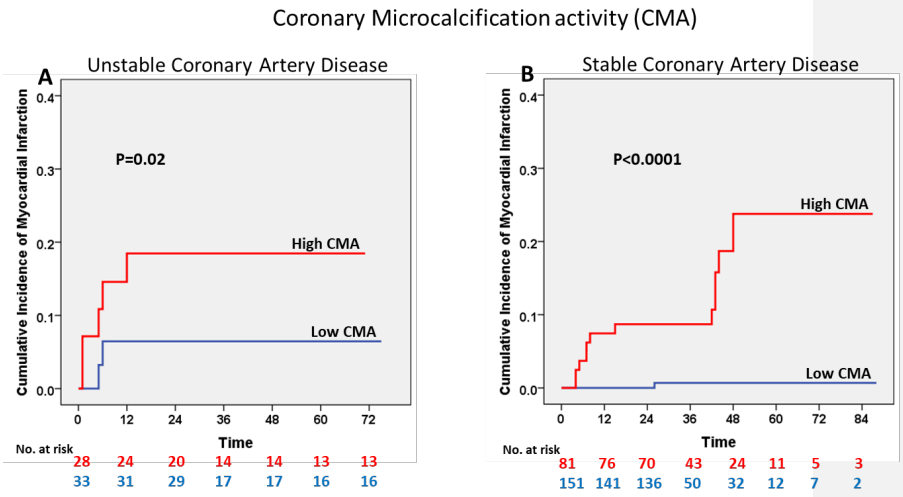

5.3.6 Secondary Endpoint: Major Adverse Cardiovascular Events

Patients with MACE had higher CMA (1.9 [1.65-4.76] versus 0.51 [0-2.42], p=0.0098) and an apparent trend for higher TBR values (1.34 [1.13-1.54] versus 1.22 [1.10-1.40], p=0.073) than patients without MACE. There were no differences in the extent of obstructive coronary artery disease on CT angiography (the segment involvement score, the modified Duke index, presence of multivessel disease or coronary stents) nor cardiovascular risk scores and co-morbidities in patients with and without MACE (Table 5.5). Similarly, there was no difference in coronary calcium scores 195 [50-1126] versus 344 [81-801] AU, p=0.50). Only 17% (10/59) of patients with a coronary calcium score >1000 AU experienced MACE.

On univariable Cox proportional regression, both CMA>1.56 and TBR>1.28 were predictors of MACE (HR 2.3, 95% CI 1.2-4.3, p=0.01 and HR 2.1, 95% CI 1.1-3.9, p=0.02). On multivariable analysis after adjustments for age, gender, comorbidities (presence of hypertension, hyperlipidaemia, diabetes, smoking), the segment involvement score, number of coronary stents multivessel coronary artery disease, coronary calcium score and the REACH and SMART risk scores, CMA remained the only independent predictor of MACE (HR 2.1, 95% CI 1.1-4.1, p= 0.030; Figure 5.6). When CMA and TBR were considered as continuous variables, these two measurements emerged as the only predictors of MACE on Cox modelling (Table 5.4).

In contrast, coronary calcium score exceeding 1199 AU (HR 1.9, 95% CI 0.9-4.0, p=0.07), the modified Duke index (HR 1.2, 95% CI 0.9-1.6, p=0.14), the REACH (HR

1.7, 95% CI 0.5-5.5, p=0.38) and SMART (HR 1.5, 95% CI 0.8-2.8, p=0.23) risk scores were not predictors of MACE on univariable analysis.

Table 5.5 Comparison of patients with and without major adverse cardiovascular events during follow-up.

	MACE (n= 40)	No MACE (n=253)	
Age in years, mean (SD)	64 (9)	65 (9)	P=0.5143
Men, n (%)	36 (90%)	209 (82.9%)	P=0.3567
Body-mass index (kg/m^2), mean (SD)	29 (5)	29 (5)	P=1.0000
Systolic blood pressure (mm Hg), mean (SD)	138 (21)	142 (20)	P=0.2440
Diastolic blood pressure (mm Hg), mean (SD)	76 (13)	79 (11)	P=0.1194
Cardiovascular history, n (%)			
H of ACS	16 (40.0%)	146 (57.7%)	**P=0.0409**
H of PCI	36 (90.0%)	201 (79.4%)	P=0.2836
H of CABG	6 (15.0%)	42 (16.6%)	P=1.0000
H of angina	24 (60.0%)	112 (44.3%)	P=0.1246
CVA/TIA	4 (10.0%)	5 (2.0%)	**P=0.0227**
Comorbidities/risk factors, n (%)			
HTN	27 (67.5%)	148 (58.5%)	P=0.3033
HPL	34 (85.0 %)	224 (88.5%)	P=0.5981
DM	11 (27.5 %)	50 (19.8%)	P=0.2947
Current smoking Ex-smoker	7 (17.5 %) 17 (42.5 %)	51 (20.4%) 120 (48.0%)	P=0.8322 P=0.6115
Atrial fibrillation	2 (5.0 %)	8 (3.2%)	P=0.6315
Peripheral vascular disease	6 (15.0%)	10 (4.0%)	**P=0.0126**
Medications, n (%) *			
Aspirin	36 (90.0%)	233 (92.1%)	P=0.7547
P2Y12 antagonist	18 (45.0%)	27 (10.7%)	**P<0.0001**

Statin	37 (92.5%)	226 (89.3%)	P=0.7792
Beta Blocker	26 (65.0%)	171 (67.6%)	P=0.7213
ACEI/ARB	23 (57.5%)	175 (69.1%)	P=0.0924
Insulin	1 (2.5%)	3 (1.2%)	P=0.4459
Oral diabetic medications	8 (20.0%)	40 (15.9%)	P=0.4944
CCB	13 (32.5%)	50 (19.8%)	P=0.0953
Diuretics	8 (20.0%)	30 (11.9%)	0=0.2012
Biomarkers, median (IQR)			
Total Cholesterol (mmol/L)	4.0 (3.4-4.6)	4.1 (3.6-4.8)	P=0.39532
LDL (mmol/L)	1.6 (0.9-2.3)	2.0 (1.4-2.5)	**P=0.0455**
HDL (mmol/L)	1.6 (1.0-2.0)	1.2 (1.0-1.7)	P=0.06432
TAG (mmol/L)	1.5 (1.1-2.3)	1.5 (1.1-2.3)	P=0.85716
Creatinine (µmol/L)	78 (69-94)	78 (70-90)	P=0.57548
CAD, n (%)			
Non-obstructive disease (<50%)	2 (5.0%)	13 (5.1%)	P=1.0000
- Single-vessel disease	14 (35.0%)	74 (29.2%)	P=0.4625
- Two-vessel disease	13 (32.5%)	97 (38.3%)	P=0.5986
- Three-vessel disease	11 (27.5%)	69 (27.2%)	P=1.000
- LMS involvement	4 (10.0%)	14 (5.5%)	P=0.2642
Coronary Stent, n (%)	29 (72.5%)	189 (74.7%)	P=0.8455
Segment involvement score. Median (IQR)	5 (4-8)	6 (3-7)	P=0.5485
SIS breakdown, n (%)			
0-1	1 (2.5%)	19 (7.5%)	P=0.3301
2-3	8 (20.0%)	47 (18.6%)	P=0.8286
4-5	14 (35.0%)	59 (23.3%)	P=0.1189
>5	17 (42.5%)	128 (50.6%)	P=0.4902

Duke index	4 (4-5)	4 (3-5)	P=0.16452
Coronary Calcium Score, median (IQR)	195 (50-1126)	344 (81-801)	P=0.4965
Coronary Calcium Score, n (%)			
0-99	14 (35.0%)	70 (27.7%)	P=0.3507
100-399	10 (25.0%)	66 (26.1%)	P=1.0000
400-999	6 (15.0%)	68 (26.8%)	P=0.1207
>1000	10 (25.0%)	49 (19.4%)	P=0.3999
TBR, median (IQR)	1.34 (1.13-1.54)	1.22 (1.10-1.40)	P=0.07346
CMA, median (IQR)	1.9 (1.65-4.76)	0.51 (0-2.42)	**P=0.00988**
TBR>1.28	23 (57.5%)	90 (35.6%)	**P=0.0135**
CMA>0	20 (50%)	170 (67%)	**P=0.0488**
CMA>1.56	23 (57.5%)	86 (34%)	**P=0.0076**
Coronary Calcium Score>1000	10 (25%)	49 (19.4%)	P=0.4012
REACH score CV event (IQR)	13 (11-15)	13 (11-15)	P=0.6672
SMART risk score %	19 (12-28)	18 (13-26)	P=0.76418

ACEI/ARB – angiotensin converting enzyme inhibitor/angiotensin receptor blocker, ACS – acute coronary syndrome, CABG – coronary artery bypass graft, CAD – coronary artery disease, CMA – coronary microcalcification activity, CVA - Cerebrovascular accident, MACE – major adverse cardiovascular event, PCI – percutaneous coronary intervention, REACH - Reduction of Atherothrombosis for Continued Health, SMART - Secondary Manifestations of Arterial Disease, SIS – segment involvement score, TAG - triglycerides, TBR – target to background ratio, TIA - transient ischemic attack

5.4 Discussion

In this two-centre multimodality imaging study, we have demonstrated for the first time that coronary ^{18}F-sodium fluoride PET is a powerful prognostic tool for predicting myocardial infarction in patients with advanced established coronary artery disease. In a comprehensive analysis, we show that both ^{18}F-sodium fluoride TBR values and whole vessel CMA emerge as powerful independent predictors of myocardial infarction outperforming all other established predictors including the presence of co-morbidities, the REACH and SMART risk scores, coronary calcium scoring and the presence, severity and extent of coronary artery disease. Our data therefore highlight the added prognostic value that assessments of disease activity can provide and confirm the potential of ^{18}F-sodium fluoride PET to improve the risk stratification of patients with established CAD, a group in whom prediction of events has previously proved challenging.

^{18}F-sodium fluoride PET provides an assessment of calcification activity across multiple different cardiovascular disease states including aortic stenosis, mitral annular calcification, abdominal aortic aneurysm, erectile dysfunction and bioprosthetic valve degeneration (66, 99). In each condition, it is associated with vascular injury, disease activity and future disease progression. This is also the case in coronary atherosclerosis. Increased ^{18}F-sodium fluoride uptake is associated with culprit coronary plaques in patients with myocardial infarction and adverse plaque features in patients with apparently stable disease (4). Moreover, similar to other cardiovascular conditions, baseline coronary ^{18}F-sodium fluoride activity predicts the future progression of coronary calcium scores, confirming its status as a marker of

disease activity (48, 82, 83). While there is major interest in using markers of atherosclerotic disease activity to improve patient assessment and risk stratification, this is the first study to demonstrate that increased ^{18}F-sodium fluoride activity provides powerful prediction of future myocardial infarction. Indeed, this technique outperformed all the other commonly used predictors of events in patients with established coronary artery disease including two established clinical risk scores designed for this patient population, co-morbidities, coronary calcium scoring, and the presence and severity of obstructive coronary artery disease. ^{18}F-sodium fluoride might therefore provide an important clinical tool in a patient population in whom risk stratification is currently suboptimal. A CMA >1.56 was associated with a >7-fold risk of myocardial infarction. This was despite almost universal prescription of aspirin, statins and other secondary preventative therapies. These patients might therefore be suitable for advanced medical therapies including PCSK9 or interleukin 1-beta inhibition, with ^{18}F-sodium fluoride PET providing the risk stratification tool that many have advocated for as a means of targeting these expensive drugs to those patients at greatest risk (Figure 5.8). In the wake of the ISCHEMIA trial this approach might also help select patients who would benefit from revascularisation (165). Of equal importance, patients without coronary ^{18}F-sodium fluoride uptake and a CMA=0 had an excellent prognosis with no myocardial infarctions observed in this group despite their advanced coronary artery disease. In these patients with dormant coronary artery disease (a third of the population studied), further intensification of medical therapy might not be warranted, nor might they benefit on prognostic grounds from complex revascularisation such as multivessel percutaneous intervention or coronary

artery bypass grafting. Further research is required to investigate these important clinical questions.

Figure 5.8. ^{18}F-sodium fluoride positron emission tomography as a marker of disease activity in the coronary arteries is a predictor of fatal or non-fatal myocardial infarction (MI) in patients with established coronary artery disease. ^{18}F-sodium fluoride PET can be used to measure disease activity across the coronary vasculature and to stratify patients into those with no, low and high disease activity. Patients with high disease activity (coronary microcalcification activity (CMA) >1.56) demonstrate a >7-fold risk of myocardial infarction. These patients might therefore be suitable for advanced medical therapies including PCSK9 or interleukin 1-beta inhibition, with ^{18}F-sodium fluoride PET used for targeting these expensive drugs to patients at greatest risk. Patients without coronary ^{18}F-sodium fluoride uptake (CMA=0) have an excellent prognosis with no myocardial infarctions observed during follow-up despite advanced coronary artery disease. In these patients with dormant coronary artery disease (a third of the population studied), further intensification of medical therapy might not be warranted, nor might they benefit on prognostic grounds from complex revascularisation such as multivessel percutaneous intervention or coronary artery bypass grafting.

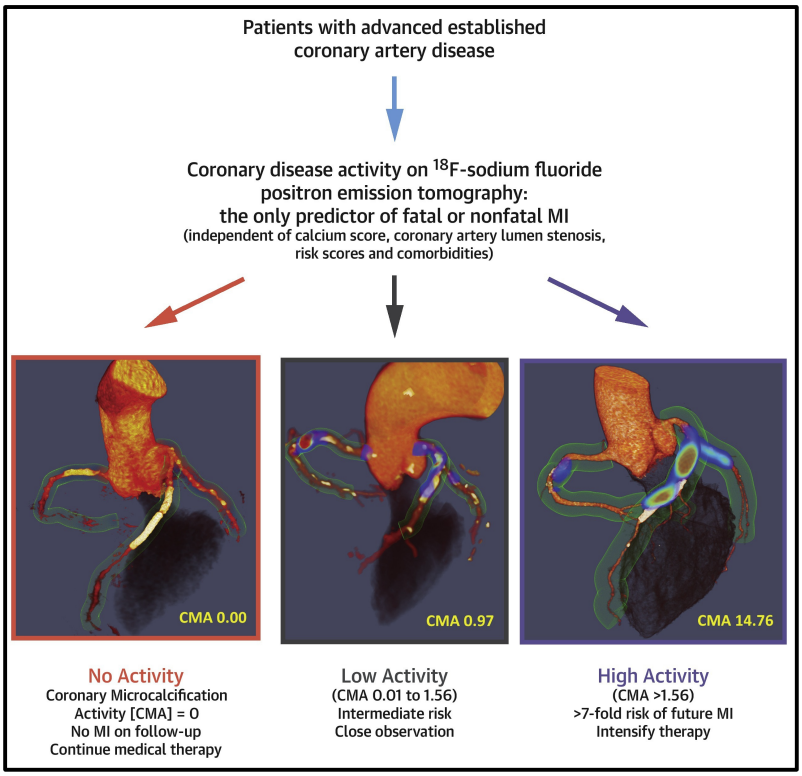

Our data demonstrating the modest predictive value of cardiovascular risk scores, coronary calcium scoring and obstructive coronary artery disease in patients with advanced established coronary artery disease is consistent with the recent literature. The diagnostic performance of the REACH and SMART risk scores was poor in several recent studies (C-statistic of 0.53 and 0.54 respectively (161, 166). While coronary calcium scoring provides powerful prognostic information in asymptomatic individuals and those presenting with chest pain, its prognostic capability has been disappointing in other studies of patients with established advanced coronary artery disease (134, 137). In line with recent literature, the presence and extent of obstructive coronary artery disease was also not a marker of adverse events in our study (24, 167).

Our study has notable strengths. We have focused our analysis on patients with advanced established coronary artery disease for whom we lack robust methods for risk stratification and showed that ^{18}F-sodium fluoride PET has the potential to fulfil this unmet clinical need. We utilised state-of-the-art ^{18}F-sodium fluoride PET imaging, employing the latest advances in image acquisition and motion correction (164). We also employed a novel quantification technique, CMA, that measures ^{18}F-sodium fluoride uptake along the course of the entire coronary vasculature and therefore provides a more complete summative assessment of disease activity than the TBR values derived from visually defined hot spot assessments (112). While both standard TBR values and CMA emerged as independent predictors of myocardial infarction, CMA demonstrated a superior hazard ratio for this endpoint, and was also the only independent predictor of MACE. CMA would therefore appear to hold advantages as

a method for quantifying overall coronary ^{18}F-sodium fluoride uptake and disease activity.

5.4.1 Limitations

Our study has some limitations. It is a post-hoc analysis of data collected for prospective observational studies. While all the subjects had advanced established coronary artery disease, we have included patients with both stable and unstable coronary artery disease thereby increasing the heterogeneity of the analysed cohort. Similar results were, however, observed when patients with unstable coronary artery disease were excluded from the analysis (Figure 5.6). Our data therefore require confirmation in large prospective studies. Indeed, we are currently completing recruitment for the Prediction of Recurrent Events With ^{18}F-Fluoride (PREFFIR) study which will prospectively investigate the ability of ^{18}F-sodium fluoride coronary PET to predict recurrent events in patients with multi-vessel disease and recent myocardial infarction. While performing a CT angiogram alongside the ^{18}F-sodium fluoride PET scan incurs a modest additional dose of radiation, this is currently essential for accurate image co-registration, interpretation and analysis (15). Although we have shown that delayed ^{18}F-sodium fluoride imaging may improve image quality, in this study participants underwent PET imaging 1 h after tracer injection (27). The potential prognostic benefits of delaying image acquisition therefore remain to be evaluated.

5.5 Conclusion

^{18}F-sodium fluoride PET is a determinant of disease activity in the coronary arteries and a powerful prognostic technique to predict myocardial infarction in patients with advanced established coronary artery disease. Further studies are required to confirm our findings and to investigate how best to use this technique to improve patient risk stratification and to guide the use of advanced therapeutic interventions.

Chapter 6 Machine-learning with 18F-sodium fluoride PET and quantitative plaque analysis on CT angiography for the future risk of myocardial infarction

Published by **Kwiecinski J, Tzolos E,** Meah M et al. Machine-learning with 18F-sodium fluoride PET and quantitative plaque analysis on CT angiography for the future risk of myocardial infarction *Journal of Nuclear Medicine* 2021 Apr 23; jnumed.121.262283.

Objectives

Coronary ^{18}F-sodium fluoride positron emission tomography (PET) and computed tomography (CT) angiography-based quantitative plaque analysis have shown promise in refining risk stratification in patients with coronary artery disease. We combined both novel imaging approaches to develop an optimal machine-learning model for the future risk of myocardial infarction in patients with stable coronary disease.

Methods

Patients with known coronary artery disease underwent coronary ^{18}F-sodium fluoride PET and CT angiography on a hybrid PET/CT scanner. Machine-learning by extreme gradient boosting was trained using clinical data, CT quantitative plaque analysis measures and ^{18}F-sodium fluoride PET, and it was tested using repeated 10-fold hold-out testing.

Results

Among 293 study participants (65±9 years; 84% male), 22 subjects experienced a myocardial infarction over the 53 [40-59] months of follow-up. On univariable receiver-operator-curve analysis, only ^{18}F-sodium fluoride coronary uptake emerged as a predictor of myocardial infarction (c- statistic 0.76, 95% confidence interval [CI] 0.68-0.83). When incorporated into machine-learning models, clinical characteristics showed limited predictive performance (c-statistic 0.64, 95% CI 0.53-0.76;) and were outperformed by a quantitative plaque analysis-based machine-learning model (c-statistic 0.72, 95% CI 0.60-0.84). After inclusion of all available data (clinical, quantitative plaque and ^{18}F-sodium fluoride PET), we achieved a substantial

improvement (p=0.008 versus ^{18}F-sodium fluoride PET alone) in the model performance (c-statistic 0.85, 95% CI 0.79-0.91).

Conclusions

Both ^{18}F-sodium fluoride uptake and quantitative plaque analysis measures are additive and strong predictors of outcome in patients with established coronary artery disease. Optimal risk stratification can be achieved by combining clinical data with these approaches in a machine- learning model.

6.1 Introduction

In every day clinical practice, prediction of myocardial infarction is challenging and is typically based on cardiovascular risk factors and scores, especially in subjects with suspected coronary artery disease (161). However, in patients with established coronary artery disease, the performance of risk scores is limited with c-statics ranging from 0.60 to 0.68 (161). Recently, advanced imaging techniques have demonstrated considerable promise in refining risk stratification in patients with established coronary artery disease. We have demonstrated that assessment of disease activity in the coronary arteries with ^{18}F-sodium fluoride positron emission tomography (PET) outperforms clinical variables and risk scores for the prediction of myocardial infarction in patients with a high burden of coronary artery disease (48, 49). Similarly, in observational studies and a sub-analysis of the SCOT-HEART trial, quantitative plaque analysis investigating both plaque type and burden on contrast enhanced CT angiography has emerged as a major predictor of adverse outcomes (32, 41). To date, no study has investigated whether these two promising methods (which can be obtained during a single imaging session on a hybrid PET/CT scanner) are interchangeable or can provide superior predictive performance when used in combination.

In this study, we employed machine-learning to investigate whether the prognostic information provided by quantitative CT plaque analysis and assessments of disease activity by ^{18}F-sodium fluoride PET are complementary, and to develop an optimised model to determine the future risk of myocardial infarction in patients with established coronary artery disease (168).

Commented [ET1]: Thank you. Reference was intented.

6.2 Methods

6.2.1 Study Population

The current study is based on a cohort of patients with established coronary artery disease on guideline recommended medical treatments which we assembled for our previous publication regarding the prognostic utility of ^{18}F-sodium fluoride PET (49). However, in the current study, we have included longer follow-up and utilised novel quantitative plaque analysis of coronary CT angiography. Our work is focused specifically upon whether machine learning methods can combine the prognostic information provided by clinical factors, quantitative CT plaque analysis and ^{18}F-sodium fluoride PET to improve the prediction of myocardial infarction. All participants underwent hybrid coronary ^{18}F-sodium fluoride PET and contrast CT coronary angiography within prospective observational research studies (NCT01749254, NCT02110303, NCT02607748) (48, 101, 116). All patients had established coronary artery disease and underwent a comprehensive baseline clinical assessment with evaluation of their cardiovascular risk factor profile including calculation of the Secondary Manifestations of ARTerial disease (SMART) risk score (Appendix 1) (161). Studies were conducted with the approval of the local research ethics committee, in accordance with the Declaration of Helsinki, and with written informed consent from each participant.

6.2.2 CT Angiography and ^{18}F-Sodium Fluoride PET

Patients underwent ^{18}F-sodium fluoride PET on hybrid PET/CT scanners (128-slice Biograph mCT, Siemens Medical Systems, Knoxville, USA or Discovery 710 GE Healthcare, Milwaukee, WI, USA) 60 min following intravenous administration of ^{18}F-sodium fluoride (250 MBq). We acquired a non-contrast CT attenuation correction scan followed by a 30-min PET emission scan in list mode, a low-dose non-contrast ECG-gated CT for calculation of the coronary calcium and a contrast-enhanced ECG-gated coronary CT angiogram (CTA) which was obtained in mid-diastole and end-expiration on the same PET/CT system without repositioning the patient. The ECG-gated PET list mode dataset was reconstructed using harmonised protocols as described previously (Appendix 1) (109, 116, 117).

6.2.3 Coronary microcalcification activity (CMA) quantification

Image analysis was performed in FusionQuant (Cedars-Sinai Medical Center, Los Angeles) (113). We used a recently described measure of coronary ^{18}F-sodium fluoride uptake, coronary microcalcification activity (CMA) that quantifies PET activity across the entire coronary vasculature (120). CMA is a highly reproducible and robust measure of disease activity predicting both disease progression and myocardial infarction (49, 150). We calculated the per vessel and per patient CMA (Figure 6.1), maximum coronary SUV and target to background ratio (TBR) as described previously (supplementary material) (48, 150).

6.2.4 Computed Tomography

The coronary artery calcium score was measured in Agatston units (AU) using clinical software (NetraMD, ScImage, Los Altos, CA, USA) on non-contrast CT scans. The presence, extent and severity of coronary artery disease were evaluated on contrast-enhanced CT angiography by defining the segment involvement score, DUKE coronary artery disease index and the number of vessels with >50% luminal stenosis (118). Multivessel coronary artery disease was defined as at least 2 major epicardial vessels with any combination of either >50% stenosis, or previous revascularisation.

6.2.5 Quantitative Plaque Analysis of CT angiography

We performed quantitative plaque analysis of all coronary segments with a lumen diameter greater than 2 mm using semi-automated software (AutoPlaque version 2.0, Cedars-Sinai Medical Center, Los Angeles, USA) (32, 41). Proximal and distal limits of lesions were manually marked by an experienced reader (physicians with several years of experience in clinical coronary CT image analysis) after examination of coronary CT angiography images in multiplanar format. Subsequent plaque quantification was fully automated using adaptive scan- specific thresholds. Total, calcified, non-calcified as well as low attenuation plaque volumes were calculated. The plaque burden was calculated according to the following equation (plaque volume x 100%/vessel volume). The contrast density difference was the maximal difference in contrast density (mean Hounsfield unit / cross-sectional area) in the plaque and the reference proximal vessel cross section.

Figure 6.1 Measuring disease activity across the coronary vasculature with ^{18}F-sodium fluoride coronary microcalcification activity (CMA) and the low attenuation plaque burden with quantitative plaque analysis. 3-Dimensional rendering of coronary CT angiography with superimposed tubular whole vessel volumes of interest (light green) employed for evaluation of ^{18}F-sodium fluoride uptake (blue and red; central panel). The coronary microcalcification activity (CMA) is a summary measure of ^{18}F-sodium fluoride activity across the entire coronary vasculature as it includes all counts originating from the coronary arteries (uptake exceeding the threshold of background blood pool activity + 2 standard deviations). 3-Dimensional rendering of CT angiography based quantitative plaque analysis with blue lumen, red noncalcified plaque, orange low attenuation plaque (LAP) and yellow calcified plaque. The low attenuation plaque burden was defined as the LAP volume x 100%/vessel volume.

LAD – left anterior descending, LCX – left circumflex, RCA – Right coronary artery

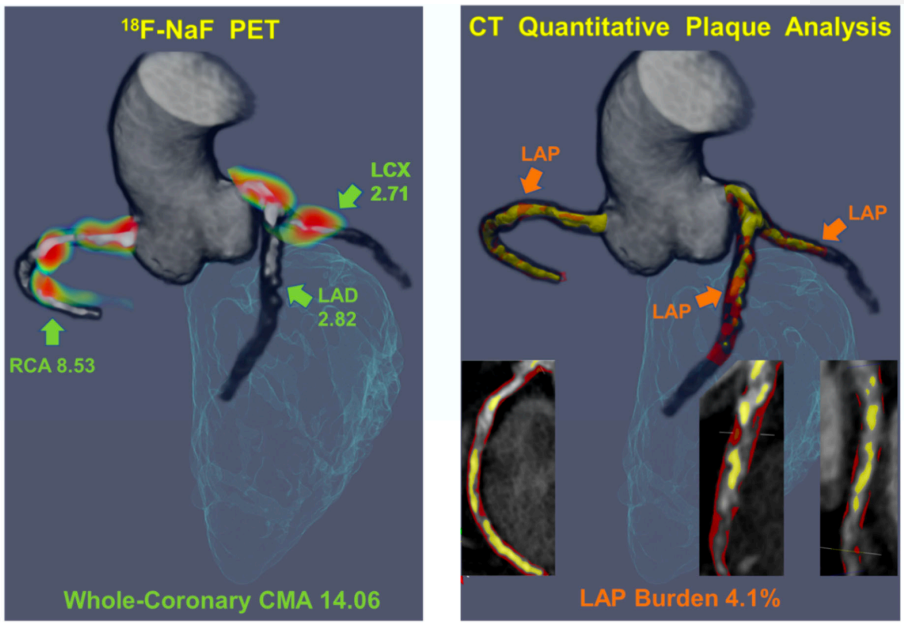

6.2.6 Machine-learning

Machine learning was used to derive a joint score for myocardial infarction by incorporating the key clinical variables, quantitative CT variables, and ^{18}F-sodium fluoride PET findings.

6.2.7 Model Building

XGBoost is a recent implementation of a gradient boosting algorithm, which iteratively trains a set of weak learners (simple decision trees) using a given set of patient data, to build a combined strong classifier to identify an outcome (169). For every patient, the XGBoost algorithm computes an individualised probability of outcome, considering all input variables.

We applied XGBoost for prediction of myocardial infarction by building 3 models. First, a clinical model with baseline clinical characteristics: age, gender, co-morbidities, medication, biomarkers, past medical history and coronary calcium score (model 1). The second model was

derived from quantitative plaque analysis variables (including low attenuation plaque burden and the contrast density difference). A final model incorporated clinical, CT and ^{18}F-sodium fluoride PET data in combination. All variables utilised in the machine-learning modelling are presented in Table 6.1.

Table 6.1 Variables used in machine-learning.

Category	No.	Variable name	Category	No.	Variable name
Clinical	1	abnormal rest ECG (0, 1)	Clinical	56	hsTnI ng/L
	2	age (years)		57	Total Cholesterol mmol/L
	3	body mass index (kg/m^2)		58	LDL mmol/L
	4	conduction disease (0, 1)		59	HDL mmol/L
	5	current smoker (0, 1)		60	Triglycerides mmol/L
	6	past smoker (0, 1)		61	SMART risk score (integer)
	7	diabetes mellitus (0, 1)		62	Recent acute coronary syndrome (0, 1)*
	8	dyslipidaemia (0, 1)	Computed Tomography – qualitative and non-contrast	63	Duke coronary artery disease score (integer)
	9	family history of premature coronary artery disease (0, 1)		64	Left Main Stenosis (0-5)
	10	height (cm)		65	pLAD Stenosis (0-5)
	11	hypertension (0, 1)		66	mLAD Stenosis (0-5)
	12	past cerebrovascular accident		67	dLAD Stenosis (0-5)
	13	past coronary artery bypass surgery (0, 1)		68	Diagonal Stenosis (0-5)
	14	past myocardial infarction (0, 1)		69	pLCx Stenosis (0-5)
	15	past open-heart surgery (0, 1)		70	AVCx Stenosis (0-5)
	16	past percutaneous coronary intervention (0, 1)		71	dLCx Stenosis (0-5)
	17	peripheral vascular disease (0, 1)		72	OM Stenosis (0-5)
	18	coronary stent (0, 1)		73	pRCA Stenosis (0-5)
	19	coronary stent in LM, LAD		74	mRCA Stenosis (0-5)
	20	coronary stent in LCX		75	dRCA Stenosis (0-5)
	21	coronary stent in RCA		76	PDA Stenosis (0-5)

	22	rest DBP (mmHg)		77	Multivessel Disease (0, 1)
	23	rest heart rate (bpm)		78	Maximum Stenosis Grade (0-5)
	24	rest SBP (mmHg)		79	Obstructive coronary artery disease (0, 1)
	25	sex (m, f)		80	Segment Involvement Score (0-16)
	26	atrial fibrillation (0, 1)		81	Coronary calcium score (integer)
	27	weight (kg)		82	Coronary calcium score <1000 (0, 1)
	28	Aspirin (0, 1)		83	Coronary calcium score <1199 (0, 1)
	29	PY12_anatagonist (0, 1)	Computed tomography - qualitative	84	Total plaque volume (continuous)
	30	Statin (0, 1)		85	Non-calcified plaque volume (continuous)
	31	ACE inhibitors (0, 1)		86	Calcified plaque volume (continuous)
	32	ARB (0, 1)		87	Low attenuation plaque volume (continuous)
	33	Diuretic (0, 1)		88	Total plaque burden (continuous)
	34	Beta blockers (0, 1)		89	Non-calcified plaque burden (continuous)
	35	Calcium channel blocker (0, 1)		90	Calcified plaque burden (continuous)
	36	Isosorbide mononitrate (0, 1)		91	Low attenuation plaque burden (continuous)
	37	Nicorandil (0, 1)		92	Area stenosis (continuous)
	38	Ivabradine (0, 1)		93	Contrast density difference (continuous)
	39	Warfarin/NOACS (0, 1)		94	Minimal lumen area (continuous)
	40	Nitrate Spray (0, 1)		95	Minimal lumen dimension (continuous)
	41	Metformin (0, 1)		96	Remodelling index (continuous)
	42	Gliclazide (0, 1)		97	Plaque length (continuous)
	43	insulin (0, 1)		98	Plaque composition LAP% (continuous)

	44	Proton pump inhibitors (0, 1)		99	Plaque composition non-calcified plaque (continuous)
	45	Alpha blockers (0, 1)		100	Plaque composition calcified plaque (continuous)
	46	Haemoglobin g/L		101	Ischemia score (continuous)
	47	WBC n/dL	^{18}F-NaF	102	CMA (continuous)
	48	Platelets n/dL		103	CMA LAD (continuous)
	49	Urea mmol/L		104	CMA RCA (continuous)
	50	Sodium mmol/L		105	CMA LCX (continuous)
	51	Potassium mmol/L		106	CMA > 1.56 (0, 1)
	52	Creatinine mmol/L		107	CMA < 0 (0, 1)
	53	eGFR ml/m2		108	Maximum TBR (continuous)
	54	Random Glucose mg/dL		109	Maximum SUV (continuous)
	55	HbA1c %			

^{18}F-NaF – ^{18}F- sodium fluoride, ACS – acute coronary syndrome, CMA – coronary microcalcfication activity, CCS – coronary calcium score, CVA – cardiovascular accident, DG – diagonal, eGFR – estimated glomerular filtration rate, HDL – High density lipoprotein, LAD – left anterior descending, LCX – left circumflex, LMN – left main, LDL – low density lipoprotein, RCA – right coronary artery, SD – standard deviation, SIS – segment involvement score, SUV – standard uptake value, TAG – Triglycerides, TBR – target to background ratio

*Because 61 patients in our study were subjects imaged shortly after an acute coronary syndrome for machine-learning we choose to differentiate them from subjects who had a percutaneous coronary intervention performed at a greater interval from PET imaging. These 61 patients were coded as recent ACS individuals and were considered positive for PCI only if an intervention was also conducted irrespective of the recent ACS.

6.2.8 Model Testing

Given the limited number of cases, we refrained from performing data-specific hypertuning and applied fixed XGBoost parameters established in our previous studies (169). Furthermore, to avoid biased results and limit overfitting, we tested all of our models using repeated 10-fold cross-testing, which separates training and testing data (170). The dataset was randomly split into 10 folds with similar myocardial infarction rates in each fold (stratified 10 folds). Ten models were created each from 90% of the data, and each tested in held-out test sample (10% of the data). These 10 held-out samples containing non-overlapping test results were subsequently concatenated to evaluate the average performance of XGBoost in unseen data.

6.2.9 Feature importance

To elucidate the influence of each of the variables included in the machine-learning model, we provided machine-learning feature importance scores. Importance is the relative amount that each attribute improves the XGBoost performance measure (similar to information gain). The variable importance was determined directly from the xgboost model separately in each fold and returned from the XGBoost model for each variable (171).

6.2.10 Clinical follow-up

The primary endpoint of the study was fatal or non-fatal myocardial infarction. Outcome information was obtained in June 2020 from the local and national healthcare record systems that integrates primary and secondary health care records. Categorisation of these outcomes was performed blinded to the coronary CT angiography and PET data.

6.2.11 Statistical analysis

We assessed the distribution of data with the Shapiro-Wilk test. Continuous parametric variables were expressed as mean ± standard deviation, and non-parametric data were presented as median [interquartile interval]. Fisher's exact test or chi-squared test was used for analysis of categorical variables. The performance of machine-learning models and single clinical characteristics in predicting myocardial infarction was assessed using receiver operator characteristic (ROC) analysis, and the area under the curve (c-statistic) values were compared with the DeLong test (172). Statistical analysis was performed with SPSS version 24 (IBM SPSS Statistics for Windows, Version 24.0. Armonk, NY: IBM Corp) and R studio and R software version 4.01 (R Foundation for Statistical Computing, Vienna, Austria). A two-sided $p<0.05$ was considered statistically significant.

6.3 Results

All 293 study participants (65±9 years; 84% male) had established coronary artery disease and were on guideline recommended medical treatments (Table 6.2). Two-hundred and thirty-seven (81%) patients had a history of revascularisation, 191 (65%) had multi-vessel obstructive coronary artery disease and the median coronary calcium score was 334 [76 to 804] AU. Over the 53 [40-59] months of follow-up, 22 subjects experienced a fatal (n=3) or non-fatal (n=19) myocardial infarction.

The high burden of atherosclerosis was reflected in the quantitative plaque analysis derived from coronary CT angiography. The median total plaque volume was 1174 [716 to 1772] mm3 and consisted largely of non-calcified plaque (1099 [647 to 1574] mm3) with a substantial volume of low-attenuation plaque (88 [44 to 167] mm3). Over half of the study population (166 [56%]) had a low-attenuation plaque burden exceeding 4%. On PET, 109 (37.2%) patients presented with a high ^{18}F-sodium fluoride coronary microcalcification activity (CMA>1.56; Figure 6.2).

Table 6.2 Baseline clinical characteristics.

Category	Variable	Mean± SD /median[Q1-Q3]/n
Baseline Clinical Characteristics	Age	65±9
	Men	245 (84%)
	Body-mass index (kg/m^2),	29±5
	Systolic blood pressure (mm Hg)	141±20
	Diastolic blood pressure (mm Hg)	79±11
Cardiovascular history	History of acute coronary syndrome	161 (55.1%)
	History of percutaneous coronary intervention	182 (62.3%)
	History of coronary artery bypass graft surgery	48 (16.4%)
	History of angina	136 (46.6%)
	Recent acute coronary syndrome*	61 (21%)
	Cerebrovascular accident or transient ischemic attack	9 (3.1%)
Comorbidities/risk factors	Hypertension	174 (59.6%)
	Hyperlipidaemia	257 (88%)
	Diabetes mellitus	61 (20.8%)
	Current smoking	58 (19.9%)
	Atrial fibrillation	10 (3.4%)
	Peripheral vascular disease	16 (5.5%)
Medications	Aspirin	268 (91.8%)
	Dual antiplatelet therapy	62 (21.2%)
	Statin	262 (89.7%)
	Beta Blocker	196 (67.1%)
	Angiotensin-converting enzyme inhibitor or	197 (67.4%)
	Insulin	4 (1.4 %)
	Oral diabetic medications	48 (16.4%)
	Calcium blockers	63 (21.6%)
	Diuretics	38 (16.0%)
Biomarkers	Total cholesterol (mg/dL)	159 [139-182]
	LDL cholesterol (mg/dL)	73 [46-93]
	HDL cholesterol (mg/dL)	46 [39-66]
	Triglycerides (mg/dL)	133 [97-204]
	Creatinine (mg/dL)	0.9 [0.8-1.0]

Risk Scores	SMART	18 (13-26)
Computed Tomography – qualitative & non-contrast	Single vessel disease	87 (29.8%)
	Coronary stent	218 (73.4%)
	Segment involvement score	5 [3-7]
	Segment involvement score >5	145 (73.5%)
	Coronary calcium score	334 (76-804)
Computed tomography - quantitative	Total plaque volume, mm^3	1174 [716, 1772]
	Non-calcified plaque volume, mm^3	1099 [647, 1574]
	Calcified plaque volume, mm^3	77 [23, 180]
	Low-attenuation plaque volume, mm^3	88 [44, 167]
	Total plaque burden, %	55 [49, 63]
	Non-calcified plaque burden, %	51 [45, 57]
	Calcified plaque burden, %	3.5 [1.4, 7.9]
	Low-attenuation plaque burden, %	4.4 [2.6, 7.0]
	Area stenosis, %	58 [47, 75]
	Contrast density difference, %	29 [24, 37]
	Ischemia score	31 [21, 47]
^{18}F-NaF PET	CMA	0.66 [0-2.84]
	TBRmax	1.22 [1.1-1.42]
	SUVmax	1.44 [1.19, 1.71]
Outcome	Myocardial infarction	22 (7.5%)

CMA – coronary microcalcification activity, PET – positron emission tomography, ^{18}F-NaF – ^{18}F-sodium fluoride, SMART - Secondary Manifestations of ARTerial disease risk score, SUVmax – maximum standard uptake value, TBRmax – maximum target to background ratio

* Recent acute coronary syndrome was defined as an event within less than 14 days prior to PET imaging

Figure 6.2 Case examples of quantitative plaque analysis on coronary CT angiography and ^{18}F-sodium fluoride positron emission tomography in patients with established coronary artery disease. Hybrid CT angiography and ^{18}F-sodium fluoride positron emission tomography of coronary arteries in: (A) a 70-year-old male who presented with diffused largely non-calcified disease (middle panel in red) in the LAD and demonstrated increased ^{18}F-sodium fluoride uptake in the LAD on positron emission tomography. (B) a 59-year-old male with mild LCX atherosclerosis, who presented with a high non-calcified plaque burden (middle panel in red) on CT angiography, significant. ^{18}F-sodium fluoride uptake and experienced a lateral non-ST-segment elevation myocardial infarction during follow-up. CMA – coronary microcalcification activity, LAP – low attenuation plaque

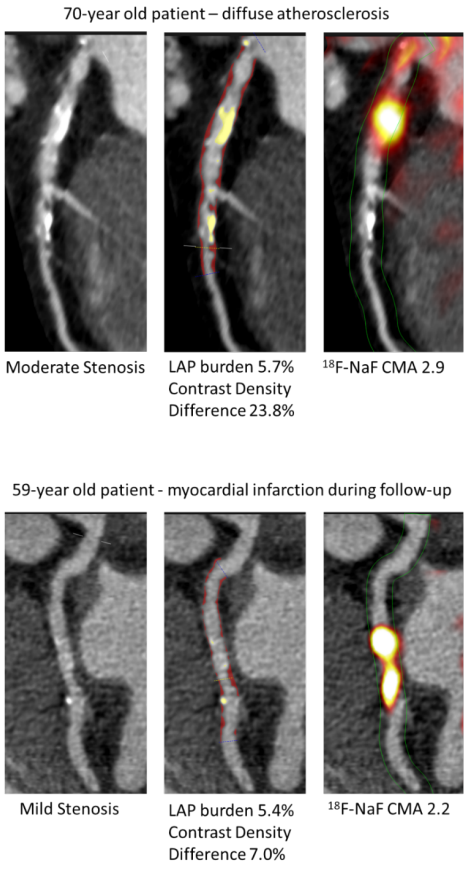

On receiver operator curve analysis, (CI) 0.68 to 0.83; p<0.001), maximum ^{18}F-sodium fluoride TBR (c-statistic 0.72, 95% CI 0.63 to 0.82; p<0.001) and maximum ^{18}F-sodium fluoride SUV (c-statistic 0.70, 95% CI 0.59 to 0.81; p=0.002) were the only statistically significant predictors of myocardial infarction. In contrast, baseline clinical characteristics, luminal stenosis severity, qualitative or quantitative CT-derived variables were not significant predictors of myocardial infarction on their own (Table 6.3). However, when incorporated into machine-learning models, the aforementioned variables emerged as predictors of adverse events. While a model based on clinical characteristics only showed limited predictive performance with a c-statistic of 0.64 (95% CI 0.53-0.76), an ^{18}F-sodium fluoride CMA alone model outperformed the former with an improved c-statistic of 0.72 (95% CI 0.60-0.84, p=0.02). The quantitative plaque analysis-based F-Sodium fluoride CMA machine-learning model was comparable to the latter (c-statistic 0.76, 95% CI 0.68-0.83, p=0.47). Inclusion of clinical data improved the ^{18}F-sodium fluoride CMA and quantitative plaque analysis-based models only slightly (0.77 [95% CI 0.69-0.84] and 0.74 [95% CI 0.64-0.83] respectively). Importantly, after inclusion of all available data (clinical, quantitative plaque and ^{18}F-sodium fluoride PET), we achieved an increase in model performance with a c-statistic of 0.85 (95% CI 0.79-0.91, p<0.001) which was higher than the quantitative CT plaque model (p=0.008) and the ^{18}F-sodium fluoride CMA (p=0.01; Figures 6.3 and 6.4) as well as the clinical characteristics model (p<0.001).

Table 6.3 Prediction of myocardial infarction in patients with advanced coronary artery disease. Receiver operator curve modelling for prediction of myocardial infarction.

Category	Variable	Area under the curve (95%	p value
Baseline Clinical Characteristics	Age	0.51 (0.35-0.67)	0.81
	Sex	0.51 (0.38-0.64)	0.84
	Body-mass index	0.58 (0.46-0.70)	0.23
	Systolic blood pressure	0.52 (0.37-0.67)	0.74
Past Medical History	Myocardial infarction	0.45 (0.33-0.58)	0.48
	Recent acute coronary syndrome	0.57 (0.43-0.71)	0.33
	Percutaneous coronary	0.53 (0.40-0.67)	0.66
	Coronary artery bypass graft	0.52 (0.39-0.65)	0.80
	Cerebrovascular accident	0.53 (0.40-0.67)	0.60
Comorbidities	Hypertension	0.47 (0.35-0.59)	0.57
	Hyperlipidaemia	0.48 (0.35-0.60)	0.61
	Diabetes	0.51 (0.37-0.65)	0.29
	Smoking	0.46 (0.32-0.60)	0.59
	Peripheral vascular disease	0.52 (0.39-0.66)	0.80
Biomarkers	Total cholesterol (mmol/L)	0.53 (0.38-0.68)	0.68
	LDL cholesterol (mmol/L)	0.59 (0.43-0.75)	0.18
	HDL cholesterol (mmol/L)	0.53 (0.38-0.67)	0.71
	Triglycerides (mmol/L)	0.57 (0.44-0.69)	0.33
	Creatinine (μmol/L)	0.54 (0.40-0.68)	0.54
Risk scores	SMART	0.57 (0.43-0.70)	0.35
Computed Tomography – qualitative & non-contrast	Multivessel disease	0.55 (0.42-0.68)	0.48
	Segment involvement score	0.56 (0.41-0.71)	0.40
	Coronary calcium score	0.51 (0.37-0.66)	0.87
	Modified Duke index	0.61 (0.48-0.74)	0.11
Computed tomography - quantitative	Total plaque volume	0.53 (0.39-0.67)	0.65
	Non-calcified plaque volume	0.54 (0.40-0.68)	0.53
	Calcified plaque volume	0.46 (0.33-0.58)	0.48
	Low-attenuation plaque volume	0.57 (0.41-0.72)	0.30
	Total plaque burden	0.45 (0.33-0.57)	0.42
	Non-calcified plaque burden	0.47 (0.35-0.59)	0.67
	Calcified plaque burden	0.41 (0.29-0.54)	0.16

	Low-attenuation plaque burden	0.61 (0.48-0.75)	0.071
	Area stenosis	0.48 (0.35-0.62)	0.79
	Contrast density difference	0.56 (0.40-0.71)	0.33
	Ischemia score	0.52 (0.38-0.65)	0.77
^{18}F-NaF PET	CMA total	0.76 (0.68-0.83)	<0.001
	TBRmax	0.72 (0.63-0.82)	<0.001
	SUVmax	0.70 (0.59-0.81)	0.002

CMA – coronary microcalcification activity, HDL – High density lipoprotein, LDL – low density lipoprotein, SD – standard deviation, PET – positron emission tomography, ^{18}F-NaF – ^{18}F-sodium fluoride, SMART - Secondary Manifestations of ARTerial disease risk score, SUVmax – maximum standard uptake value, TBRmax – maximum target to background ratio.

Figure 6.3 Prediction of myocardial infarction by machine-learning. A) Receiver operator curves for the risk of myocardial infarction: (1) ^{18}F-sodium fluoride (^{18}F-NaF) coronary microcalcification activity (CMA) alone; machine learning models based on (2) clinical data (3) quantitative plaque analysis, (4) clinical + quantitative plaque analysis + ^{18}F-NaF PET. The model based on both PET and quantitative CT-based plaque analysis data outperformed the clinical data and both unimodality models (p<0.01 for all). (B) Feature importance for the machine-learning model based on all variables. The solid bars and error bars represent the mean gain and standard deviation derived from the distribution of the importance within 10 folds of the cross testing, for each variable.

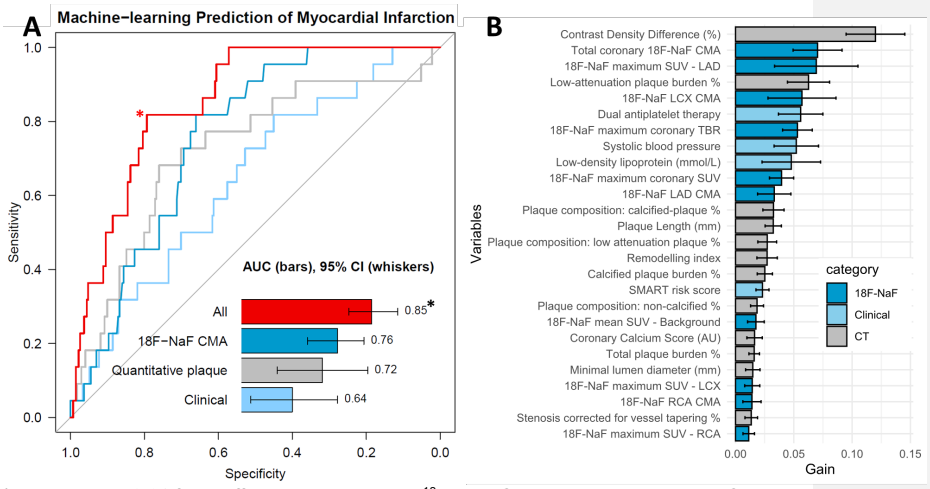

*Indicates a p<0.01 for a difference compared to ^{18}F-NAF CMA, quantitative plaque, Clinical and CT (DeLong test)

CMA – coronary microcalcification activity, SUV – standard uptake value, TBR – target to background ratio

Figure 6.4 Calibration plot for the clinical + quantitative plaque analysis + ^{18}F-sodium fluoride PET machine-learning XGBoost model. The calibration plot shows the relationship between the observed and predicted proportion of events, grouped by decile of risk. Our model showed very good calibration with the observed risk of myocardial infarction during follow-up.

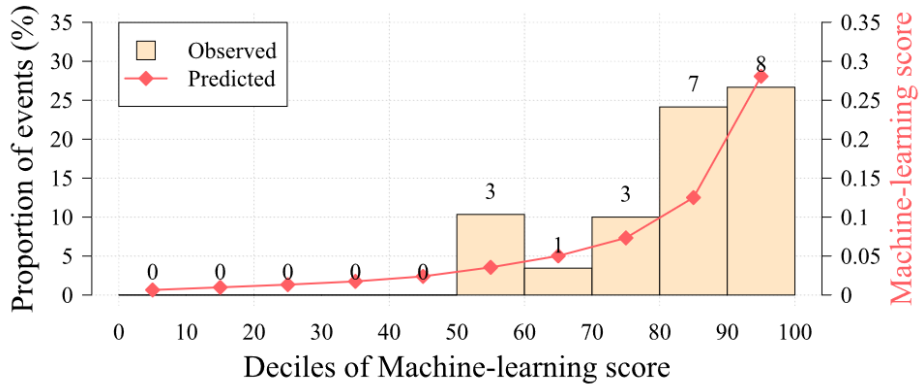

6.4 Discussion

We have built a machine-learning model for risk stratification in patients with established coronary artery disease. In our cohort of patients with advanced coronary atherosclerosis, we showed that risk prediction does not depend on cardiovascular risk scores, stenosis severity or CT calcium scoring. Rather the risk of myocardial infarction is primarily governed by the analysis of plaque type and plaque burden provided by coronary CT angiography and assessments of disease activity by ^{18}F-sodium fluoride PET. Importantly, our machine learning approach has overcome the challenges posed by co-linearity of these variables and, for the first time, has demonstrated that this information is complementary and additive with the combination of both providing the most robust outcome prediction. If confirmed in further studies this comprehensive approach holds major promise in refining risk stratification of patients with established coronary artery disease, a population where such prediction is currently challenging. Importantly, such stratification in these patients can be achieved objectively with quantitative variables obtained on a single hybrid PET/CT acquisition.

^{18}F-sodium fluoride PET provides an assessment of vascular injury and disease activity across a wide spectrum of cardiovascular conditions including aortic stenosis, mitral annular calcification, abdominal aortic aneurysm, erectile dysfunction, bioprosthetic valve degeneration and coronary artery disease (49, 66, 99, 173). Indeed, baseline ^{18}F-sodium fluoride PET is consistently associated with future disease progression and adverse events in each of these conditions. On the other hand, quantitative assessment of atherosclerotic plaque on contrast-enhanced CT angiography allows us to measure

the burden of different types of plaque across the coronary arteries (41). We recently demonstrated that the low-attenuation plaque burden provides powerful prediction of myocardial infarction, outperforming cardiovascular risk scores, Agatston coronary artery calcium scoring, or the presence and severity of obstructive coronary artery disease. Whether these two exciting developments can be used in combination to further advance risk prediction was previously unknown.

Using the information from these approaches and by leveraging machine-learning, we were able to build an integrated model for prediction of events in patients with established coronary artery disease, a group of patients where risk prediction is currently challenging. The XGBoost algorithm has been successfully implemented for risk prediction in a wide range of clinical scenarios(169, 174). It enables the incorporation of numerous predictors into the model even when these variables are correlated - a major limitation with conventional regression analyses. While we have previously shown that ^{18}F-sodium fluoride uptake is associated with quantitative plaque analysis indices, our current analysis highlights the complementary prognostic information that PET and quantitative CT plaque assessments provide together (81, 84). Indeed, our machine learning model incorporating the information from these two modalities alongside clinical factors outperformed the individual components analysed separately with a high c-statistic of 0.85. Importantly, our study also underscores that in patients with advanced coronary artery disease, markers of disease activity, plaque type and plaque burden provide superior risk prediction to clinical risk scores and conventional coronary calcium CT analyses.

According to societal guidelines, patients with clinically manifest atherosclerotic arterial disease are considered to be at very high risk of a recurrent cardiovascular events and cardiovascular mortality. However, in everyday clinical practice, it is apparent that there is a wide distribution of actual risk for recurrent vascular events in patients with clinically established arterial disease. While the population of subjects with manifested coronary artery disease is rapidly growing, accurate risk prediction in this important population remains challenging. The guideline recommended SMART risk score was shown to have only a moderate c-statistic (0.64-0.68), and there is a paucity of data regarding the role imaging could play in this cohort (1). In our study we have targeted this important high-risk population. We have demonstrated that quantitative plaque analysis measures and the coronary microcalcification activity considerably improve stratification of patients' risk (c-statistic 0.85). In a conservative 10-fold cross testing machine learning model, we showed that CT and PET data need to be employed together for optimal stratification.

6.4.1 Limitations

With the limited number of patients and events, our findings require confirmation in future studies. Machine-learning models can perform better when trained within bigger datasets and therefore further studies are needed to confirm our findings and allow further testing to refine and to calibrate the machine-learning models. External validation of our findings in other cohorts is needed. While this is currently challenging given that ^{18}F-sodium fluoride PET is an emerging technique, this will be possible in the future using outcome data from the Prediction of Recurrent Events With ^{18}F-Fluoride (PREFFIR) study which is prospectively investigating the ability of ^{18}F-sodium fluoride coronary PET and CT angiography to predict recurrent events in patients with multi-vessel disease and recent myocardial infarction. Since the majority of study participants had multivessel disease future studies should characterise the utility of ^{18}F-sodium fluoride PET in single vessel disease patients.

6.5 Conclusion

In conclusion, both ^{18}F-sodium fluoride uptake and quantitative plaque analysis measures from contrast CT are strong predictors of outcome in patients with established coronary artery disease. Optimal risk stratification can be achieved by combining these imaging assessments of plaque type, burden and activity with clinical variables in a machine-learning model.

Chapter 7 Native Aortic Valve Disease Progression and Bioprosthetic Valve Degeneration in Patients with Transcatheter Aortic Valve Implantation

Published by **Kwiecinski J*, Tzolos E*,** Cartlidge T et al. Native aortic valve disease progression and bioprosthetic valve degeneration in patients with transcatheter aortic valve implantation *Circulation* 2021 2021 Aug 29.

*Joint first co-authors

Objectives

There remain major uncertainties regarding disease activity within the retained native aortic valve as well as bioprosthetic valve durability following transcatheter aortic valve implantation (TAVI). We aimed to assess native aortic valve disease activity and bioprosthetic valve durability in patients with TAVI in comparison to subjects with bioprosthetic surgical aortic valve replacement (SAVR).

Methods

In a multicentre cross-sectional observational cohort study, patients with TAVI or bioprosthetic SAVR underwent baseline echocardiography, CT angiography and ^{18}F-sodium fluoride positron emission tomography (PET). Participants (n=47) were imaged once with ^{18}F-sodium fluoride PET/CT either at one-month (n=9, 19%), 2 years (n=22, 47%) or 5 years (16, 34%) after valve implantation. Subsequently patients underwent serial echocardiography to assess for changes in valve hemodynamic performance (change in peak aortic velocity) and evidence of structural valve dysfunction. Comparisons were made to matched patients with bioprosthetic SAVR (n=51) who had undergone the same imaging protocol.

Results

In patients with TAVI, native aortic valves demonstrated ^{18}F-sodium fluoride uptake around the outside of the bioprostheses that showed a modest correlation with the time from TAVI (r=0.36, p=0.023). ^{18}F-sodium fluoride uptake in the bioprosthetic leaflets was comparable between the SAVR and TAVI groups (target-to-background ratio 1.3 [1.2-1.7] versus 1.3 [1.2-1.5] respectively, p=0.27). The frequencies of imaging

evidence of bioprosthetic valve degeneration at baseline were similar on echocardiography (6% versus 8% respectively, p=0.78), CT (15% versus 14% respectively, p=0.87) and PET (15% versus 29% respectively, p=0.09). Baseline ^{18}F-sodium fluoride uptake was associated with subsequent change in peak aortic velocity for both TAVI (r=0.7, p<0.001) and SAVR (r=0.7, p<0.001). On multivariable analysis, ^{18}F-sodium fluoride uptake was the only predictor of peak velocity progression (p<0.001).

Conclusions

In patients with TAVI, native aortic valves demonstrate evidence of ongoing active disease. Across imaging modalities, TAVI degeneration is of similar magnitude to bioprosthetic SAVR suggesting comparable mid-term durability.

7.1 Introduction

Transcatheter aortic valve implantation (TAVI) has revolutionised intervention options in aortic valve stenosis (93, 96, 175, 176). Although the term TAVI and transcatheter aortic valve replacement (TAVR) are widely used interchangeably, TAVR is a misnomer since the native aortic valve is not replaced but rather displaced and splinted against the wall of the aorta at the time of bioprosthetic valve insertion. As a consequence, the native aortic valve is rendered immobile. Previously, it has been suggested that the impact of repeated valve closure and trauma is fundamental to aortic stenosis (177). Therefore, patients with TAVI present a unique opportunity to investigate the pathophysiology of aortic stenosis in the absence of the ongoing cyclical mechanical trauma of valve closure. Is aortic stenosis simply a disease of 'wear-and-tear' or is it an active regulated pathobiological process that continues despite valve immobilisation?

TAVI is rapidly gaining popularity as a treatment option in younger low-risk populations (96, 175, 176). With its more widespread use, questions regarding valve durability become increasingly important (178). All bioprosthetic valves are susceptible to degeneration, driven by similar processes to native aortic valve stenosis. Indeed, active calcification appears to be the final common pathway of such degeneration leading to bioprosthetic valve stenosis, leaflet tears and valvular regurgitation (95, 179). Whilst transcatheter bioprostheses are similar in structure to surgical valves, it has been suggested that the increased effective orifice area of TAVI will result in improved longevity. However, others have proposed that crimping of TAVI bioprostheses coupled with incomplete asymmetric frame expansion and suboptimal leaflet coaptation may lead to accelerated structural valve deterioration

(SVD) (180). Whilst long term hemodynamic valve data are lacking, there is interest in comparing earlier non-invasive markers of valve durability in patients with TAVI and those with bioprosthetic surgical aortic valve replacement (SAVR).

We have demonstrated that ^{18}F-sodium fluoride positron emission tomography (PET) provides a marker of calcification activity and vascular injury across a range of cardiovascular conditions (49, 66, 88, 99, 173, 181). In native aortic valve stenosis, ^{18}F-sodium fluoride uptake can assess valve calcification activity, providing important pathophysiological insights, a measure of disease severity and act as a predictor of subsequent disease progression and clinical events (66, 88). In bioprosthetic SAVR, ^{18}F-sodium fluoride PET uptake is an early and sensitive marker of leaflet degeneration, providing powerful prediction of subsequent valve dysfunction and valve failure (99).

In the present study, we sought to investigate whether the retained native aortic valves in patients undergoing TAVI demonstrate evidence of ongoing disease progression. Additionally, since long-term durability of transcatheter aortic valves is yet to be established, we aimed to establish whether bioprosthetic valve durability or degeneration was appreciably different between patients with TAVI or SAVR at mid-term follow-up.

7.2 Methods

7.2.1 Study Population

Patients with aortic stenosis who had undergone previous TAVI (1 month, 2 years or 5 years prior to study inclusion) using a balloon-expandable or self-expanding bioprosthesis were prospectively recruited into an observational cross-sectional cohort study at 3 high-volume TAVI centres between September 2016 and November 2019 (Edinburgh Heart Centre, Cedars Sinai Medical Center and Cambridge University Addenbrooke's Hospital; Figure 7.1). All participants were under routine clinical follow-up and did not have established clinical evidence of bioprosthetic valve degeneration (182). Each patient underwent clinical assessment, echocardiography, hybrid ^{18}F-sodium fluoride PET and computed tomography (CT) angiography at baseline with annual repeat echocardiography thereafter (Figure 7.1). We excluded patients unable to give informed consent, with claustrophobia, allergy to iodinated contrast, liver failure, chronic kidney disease (with estimated glomerular filtration rate <30 mL/min/1.73 m^2), Paget's disease, metastatic malignancy, or an inability to tolerate the supine position. Patients with TAVI were compared to patients with SAVR valves undergoing the same research protocol (including multi-modality imaging protocols, image analysis assessments and follow up) (NCT02304276). Patients were recruited prospectively, matching the age of SAVR and TAVI valves (time from valve implantation for aortic stenosis to imaging) in the two groups. Baseline and follow up data from the SAVR cohort in isolation have been reported previously (99). The study (NCT02304276) was conducted in accordance with the Declaration of Helsinki and was approved by NHS Scotland Research Ethics Committee (14/SS/1049), the Administration of Radioactive Substances Advisory Committee and Institutional

Review Boards at all sites. Recruitment was prematurely halted due to the onset of SARS-CoV-2 pandemic and the potential vulnerability of our target population. Additionally, we encountered difficulties in recruiting patients at 5 years following TAVI who were both alive and well enough to undergo study procedures. The data that support the findings of this study are available from the corresponding author upon reasonable request.

Figure 7.1 CONSORT flow diagram of study recruitment, allocation (assessments), follow-up, and analysis.

CT indicates computed tomography; and 18F-NaF PET, 18F-sodium fluoride positron emission tomography.

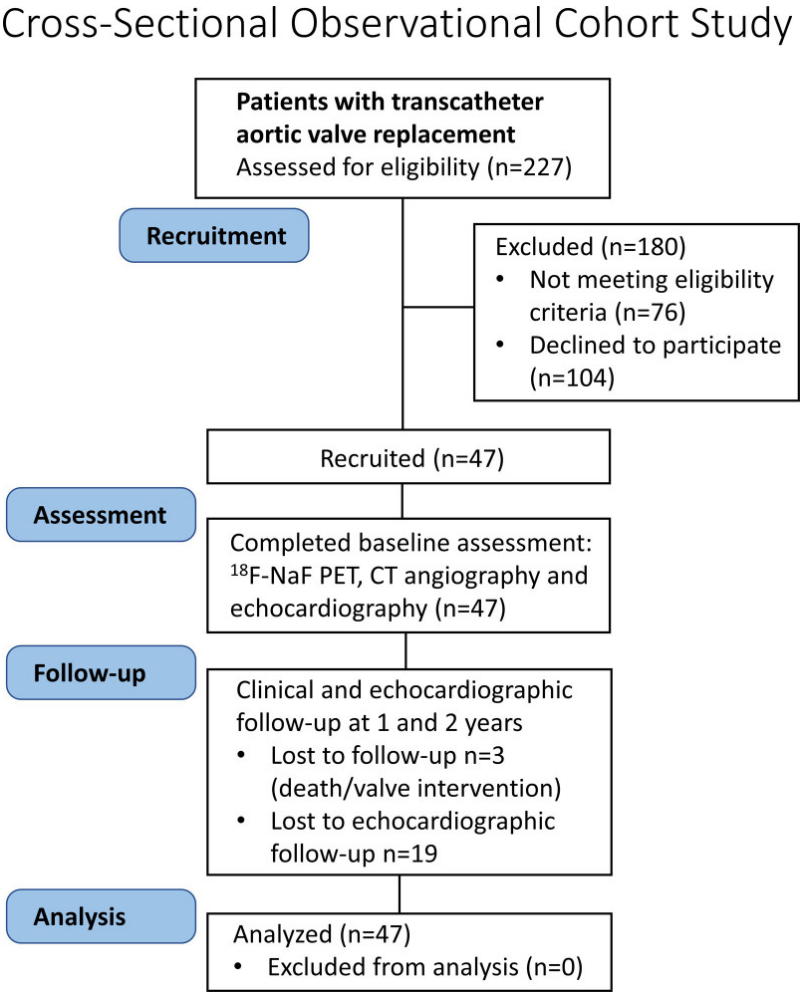

7.2.2 Aortic Valve Echocardiography

Two-dimensional and Doppler echocardiography was performed at baseline and annually thereafter according to American Society of Echocardiography guidelines (108). Aortic valve Doppler measurements were routinely assessed from the apex, suprasternal notch and right sternal edge to measure the peak aortic jet velocity, the mean gradient and the effective orifice area of the bioprosthesis. Mean values were taken from 3 measurements when subjects were in sinus rhythm and from 5 measurements if in atrial fibrillation. Bioprosthetic valve regurgitation was graded as mild, moderate or severe according to guideline recommendations based on visual appraisal of colour Doppler images, measurement of pressure half-time (milliseconds) and assessment for aortic flow reversal in diastole (108).

7.2.3 PET/CT Imaging

All patients underwent 18F-sodium fluoride PET at baseline on hybrid PET/CT scanners (128-slice Biograph mCT, Siemens Medical Systems, Knoxville, USA or Discovery 690/710 GE Healthcare, Milwaukee, WI, USA) using harmonised imaging protocols, 60 min after intravenous administration of 125 MBq of 18F-sodium fluoride (116) obtained in 3-dimensional mode in a single 30-min bed position centred on the valve. Attenuation-correction CT was performed before acquisition of PET data. Finally, electrocardiogram-gated contrast-enhanced CT angiography was performed on the same scanner with prospective gating in end-expiration. Patients were given beta-blockers if resting heart rate was >65 beats/min and in the absence of clinical contraindications. After co-registration with PET, the CT data served for anatomical reference and facilitated PET tracer uptake quantification (111).

7.2.4 Computed Tomography Analysis

Abnormalities on CT angiography were adjudicated using pre-specified criteria. Non-calcific leaflet thickening (hypoattenuated leaflet thickening - HALT) was defined as focal areas of low-attenuation [30 to 200 Hounsfield Units (HU)] leaflet thickening visualised in at least 2 planes typically thickest at its base and thinning to the tips in accordance with consensus guidelines (183, 184). Pannus was defined as circumferential low-attenuation (non-calcific) material with radial thickness ≥2 mm and encroachment on to the valve cusps (99). Leaflet calcification was defined as calcium >500 HU localised to a valve cusp in at least 2 planes and classified according to size as spotty calcification if maximum diameter was <3 mm, or large calcification if maximum diameter was ≥3 mm (185).

7.2.5 Positron Emission Tomography Analysis

Reconstructed ECG-gated PET and contrast-enhanced CT images were reoriented, co-registered in orthogonal planes and cardiac motion corrected with automatic algorithm preserving counts from all cardiac phases (Described in detail in Chapter 2) (109, 113-115). Using en face images of the bioprosthetic valves, the maximum standard uptake values (SUV) in the native aortic valve was measured between the perimeter of the TAVI bioprostheses and the aorta. Care was taken to avoid regions of activity originating from the TAVI leaflets and nearby coronary arteries. Target to background ratio (TBR) values were derived from maximum SUV values corrected for blood-pool activity (mean SUV) measured in the right atrium (1-cm radius 9-mm high cylinder drawn on axial slices, at the level of the right coronary ostium).

With respect to 18F-sodium fluoride uptake in the TAVI bioprosthetic valves, PET scans were adjudicated to be abnormal if discernible 18F-sodium fluoride uptake originating from the valve leaflets was observed on 3 orthogonal planes. We quantified 18F-sodium fluoride uptake according to a previously proposed methodology where a circular (area 1 cm2) region of interest (ROI) was drawn around the area of maximal uptake originating in the valve cusps (63, 99). ROIs were carefully drawn to avoid any uptake originating from outside of the bioprosthetic valve leaflets, in particular uptake related to surrounding native aortic valve tissue. In subjects with no visible (exceeding blood-pool activity) uptake in the valve leaflets, a 1-cm2 circular ROI was drawn in the centre of the valve (66, 88, 99). Maximum SUV values were extracted from these ROIs and divided by the blood-pool activity measured in the right atrium to calculate

the TBR values as described above. A similar approach was taken to the analysis of SAVR valves (99).

7.2.6 Clinical Follow up

Patients were invited to return annually for 2 years for repeat clinical assessment and echocardiography to assess for evidence of deterioration in hemodynamic bioprosthetic performance. In particular, change in peak velocity through the valve, change in mean pressure gradient and change in the effective orifice area were recorded. Changes in the grade of aortic regurgitation were documented.

Bioprosthetic valve deterioration was determined at baseline and after follow-up and was categorised as: stage 1 a morphological abnormality (detected on echocardiography or CT), including HALT, calcification or pannus, in the absence of hemodynamic changes; stage 2 either moderate valve obstruction, moderate regurgitation or both; stage 3 either severe valve obstruction or regurgitation (180, 182).

Patients were followed up for clinical events with outcome information obtained from local and national healthcare record systems that integrate primary and secondary health care records. The primary clinical endpoint of the study was a composite of bioprosthetic valve failure or repeat TAVI. Categorisation of these outcomes was performed blinded to the PET imaging or other study data. Outcome data were collected in September 2020.

7.2.7 Ex Vivo Assessment

To elucidate the pathology of aortic stenosis and TAVI degeneration and to validate our in vivo imaging findings, we studied surgically explanted native and bioprosthetic aortic valves obtained from patients with dysfunctional degenerated TAVI in the Cardiovascular Tissue Registry at St. Paul's Hospital. Ex vivo histological (hematoxylin and eosin; Movat's pentachrome), immunohistochemistry (runx2 and osteopontin) and 18F-sodium fluoride autoradiography assessments (179) were made on these samples in accordance with the approval of the Research Ethics Board of Providence Health Care (Described in detail in Chapter 2).

7.2.8 Statistical Analysis

We assessed the distribution of data with the Shapiro-Wilk test. Continuous parametric variables were expressed as mean (SD) and compared using Student's t tests. Non-parametric data were presented as median [interquartile interval], compared using Mann-Whitney U test and log transformed to achieve normality prior to inclusion in regression models and correlation. Fisher's exact test or chi-squared test was used for analysis of categorical variables. We assessed correlations with the Pearson's coefficient. Multivariable linear regression modelling was used to assess the change in echocardiographic measures of bioprosthesis performance, clinical characteristics, and 18F-sodium fluoride uptake. The multivariable model was constructed with annualised peak velocity change (m/sec) as the dependent variable and age, sex, time after aortic valve replacement, presence of HALT, valve TBR and baseline peak velocity and abnormalities on CT as independent variables, selected based on clinically relevant and plausible mechanisms that may relate to valvular degeneration. Model residuals were checked against fitted values and distributions confirmed with quantile-quantile plots. To assess imaging evidence of bioprosthetic valve degeneration in TAVI or SAVR, we compared the echocardiography, CT and 18F-sodium fluoride PET findings in our TAVI population with matched data from a previous study which characterised patients with bioprosthetic SAVR using the same clinical assessments, multi-modality imaging protocols and image analyses (12). Receiver operating characteristic (ROC) analysis was performed to identify the optimum cut-off for TBR to identify patients at increased risk of structural valve degeneration using Youden J statistic. Statistical analysis was performed with SPSS version 24 (IBM SPSS Statistics for Windows, Version 24.0. Armonk, NY: IBM

Corp), R studio and R software version 4.01 (R Foundation for Statistical Computing, Vienna, Austria). We used R packages: dlpyr, ggplot2, magrittr, QuantPsyc, Forestplot, cutpointr and ggpubr. A two-sided $p<0.05$ was considered statistically significant.

7.3 Results

7.3.1 Study Populations

We recruited 47 patients with TAVI from 3 high volume centres (81±6 years old, 79% male) who were compared with 51 patients with SAVR from the same institutions (Table 7.1). Like the SAVR cohort, patients with TAVI were imaged once with ^{18}F-sodium fluoride PET/CT at either one month (n=9, 19%), 2 years (n=22, 47%) or 5 years (16, 34%) after valve implantation. Twenty-five (53%) subjects were implanted with a balloon expanded bioprosthesis and 22 (47%) received a self-expanding valve.

Table 7.1. Comparison of patients following transcatheter aortic valve implantation versus patients following surgical aortic valve replacement.

	Patients with transcatheter bioprosthetic valves n=47	Patients with surgical bioprosthetic valves n=51	P value
Age (years)	82 [76-86]	72 [70-77]	<0.001
Men	29 (62%)	29 (57%)	0.63
Body-mass index (kg/m^2)	24 [20-26]	27 [24-32]	<0.001
Systolic blood pressure (mmHg)	132 [120-146]	156 [142-165]	<0.001
Diastolic blood pressure (mmHg)	68 [60-73]	80 [73-87]	<0.001
Heart rate	63 [59-74]	70 (63-82)	0.03
Bioprosthesis age			
Time since valve replacement (months)	24 [24-60]	24 [24-60]	0.91
5 years post valve replacement	16 (34%)	20 (39%)	0.65
2 years post valve replacement	22 (47%)	22 (43%)	0.68
1 month post valve replacement	9 (19%)	9 (18%)	0.79
Comorbidities			
Hypertension	38 (80%)	38 (75%)	0.45
Hyperlipidaemia	24 (51%)	39 (76%)	0.01
Diabetes	15 (31%)	3 (6%)	0.02
Smoking	28 (60%)	25 (49%)	0.31
Coronary Artery Disease	24 (51%)	18 (35%)	0.12
coronary artery bypass grafts	17 (31%)	14 (27%)	0.35
Medication			
Aspirin	27 (57%)	37 (73%)	0.12
P2Y12 antagonist	8 (17%)	7 (14%)	0.65
Warfarin	7 (14%)	4 (8%)	0.27
Direct Oral Anticoagulation	1 (2%)	1 (2%)	0.85
ACE inhibitor/angiotensin receptor blocker	30 (63%)	28 (55%)	0.37
Beta blocker	28 (60%)	24 (47%)	0.21
Statin	35 (74%)	35 (68%)	0.52
Electrocardiogram			
Sinus rhythm	27 (57%)	47 (92%)	<0.001
Paced rhythm	9 (20%)	0	<0.001
Atrial Fibrillation	7 (14%)	2 (4%)	0.06
Left ventricular hypertrophy	5 (11%)	20 (39%)	0.01
Left ventricular hypertrophy – with strain	3 (7%)	12 (24%)	0.02
Echocardiography			
Evidence of valve degeneration	3 (6%)	4 (8%)	0.78
Evidence of valve degeneration in 5-year-old valves	3 (19%)	4 (20%)	0.78
Reduced LV ejection fraction	9 (19%)	8 (16%)	0.65
Vmax (m/s)	2.4 [2.0-2.7]	2.7 [2.4-3.0]	0.03

Mean valve gradient (mm Hg)	12 [9-14]	15 [12-19]	0.18
Effective orifice area (cm^2)	1.5 [1.3-1.8]	1.1 [1.0-1.5]	0.02
Computed Tomography			
CT evidence of valve degeneration	7 (15%)	7 (14%)	0.87
CT evidence of valve degeneration in 5-year-old valves	6 (38%)	4 (20%)	0.42
Spotty calcification	1 (2%)	2 (4%)	0.61
Pannus	0	2 (4%)	0.07
Hypoattenuated leaflet thickening	6 (13%)	4 (8%)	0.42
^{18}F-Sodium Fluoride Positron Emission Tomography			
Increased leaflet ^{18}F-NaF	7 (15%)	15 (29%)	0.09
Increased leaflet ^{18}F-NaF in 5-year-old valves	7 (44%)	8 (40%)	0.79
Target to background ratio	1.3 [1.2-1.7]	1.3 [1.2-1.5]	0.27

Number (%); median [interquartile range]
ACE – angiotensin-converting enzyme; CT – computed tomography; ^{18}F-NaF - ^{18}F-sodium fluoride

7.3.2 Calcification Activity in Native Aortic Valve Tissue

Ex Vivo Validation

In five patients with TAVI for severe aortic stenosis, explanted TAVI valves and associated aortic roots were obtained 945 (range 3-2044) days after implantation (Tables 7.2 and 7.3). Calcified native aortic valve tissue was present around the perimeter of the TAVI bioprostheses (Figure 7.2) and histologically demonstrated evidence of ongoing calcification activity with increased staining for both osteopontin and Runx-2 (Figures 7.2, 7.3 and 7.4).

^{18}F-Sodium Fluoride Positron Emission Tomography

On contrast CT angiography at baseline, residual calcification from the native aortic valve was seen around the perimeter of the TAVI bioprosthesis in all cases. All subjects demonstrated ^{18}F-sodium fluoride uptake surrounding the TAVI bioprostheses that originated from the native aortic valve tissue (TBR range 1.6-5.8; Figure 7.2). Native valve ^{18}F-sodium fluoride uptake was highest in patients imaged 5 years after TAVI (TBR 3.3 [2.6-3.9] versus 2.2 [1.9-2.5] in those imaged one month after TAVI, p=0.023; Figure 7.2). Overall native valve uptake showed a modest positive correlation with the time from TAVI (r=0.36, p=0.023).

Table 7.2: Post transcatheter aortic valve implantation native valve explant cases

	Case 1	Case 2	Case 3	Case 4	Case 5
Time to Explant, months	52	81	1	31	2
Age at death, years	72	96	76	99	88
Sex, (0=female, 1=male)	0	1	1	0	0
Medical history					
Hypertension	-	-	+	+	+
Coronary artery disease	-	+	+	-	+
Coronary bypass surgery	-	+	+	-	-
Diabetes	-	+	-	-	-
Hypercholesterolemia	-	+	+	-	+
Smoking history	-	+	+	-	+
Medication					
Aspirin	-	+	+	+	+
Clopidogrel	-	+	-	-	-
Warfarin	-	-	-	-	-
Other anticoagulant	+	-	-	-	-
ACE inhibitor or Angiotensin receptor blocker	+	+	+	+	+
Beta-blocker	-	+	+	-	+
Statin	-	+	+	-	+
Pre-TAVI echocardiography					
LV ejection fraction, %	65	65	35	50	60
Mean valve gradient, mmHg	96	90	19*	76	24
Valve area, cm^2	0.47	0.48	0.8	0.4	0.7

* Mean gradient increased to 31 mmHg with dobutamine stress echo
ACE: angiotensin converting enzyme; LV: left ventricle; TAVI: transcatheter aortic valve implantation.

Table 7.3: Post transcatheter aortic valve implantation native valve explant cases demographics summary

	n=5
TAVI implant age (years)	31 [2-52]
Age at death (years)	88 [76-96]
Men	2 (40%)
Medical history	
Hypertension	3 (60%)
Coronary artery disease	3 (60%)
Coronary bypass surgery	2 (40%)
Diabetes	1 (20%)
Hypercholesterolemia	3 (60%)
Ex-smoker	3 (60%)
Medication	
Aspirin	4 (80%)
Clopidogrel	1 (20%)
Warfarin	0
Other anticoagulant	1 (20%)
ACE inhibitor or angiotensin receptor blocker	5 (100%)
Beta-blocker	3 (60%)
Statin	3 (60%)
Pre-TAVI echocardiography	
LV ejection fraction (%)	55 [50-60]
Mean valve gradient (mmHg)	76 [31-90]
Valve area (cm^2)	0.57 [0.47-0.70]

Number (%); median [interquartile range]
ACE - angiotensin converting enzyme; LV - left ventricle; TAVI - transcatheter aortic valve implantation.

Figure 7.2 Baseline assessment with ^{18}F-sodium fluoride activity in native aortic valve tissue following transcatheter aortic valve replacement.

A: Hybrid ^{18}F-sodium fluoride positron emission tomography and computed tomography (^{18}F-NaF PET/CT) *en face* and long axis images of native aortic valve tissue uptake. We observed intense tracer activity originating from the native valve tissue around the perimeter of the bioprosthesis in all patients with transcatheter aortic valve replacement (TAVI). **B:** Native aortic valve ^{18}F-NaF uptake in patients with TAVI was higher with longer duration since bioprosthesis implantation suggesting increased calcification activity following intervention. **C:** Representative macroscopic images of explanted TAVI valves (green arrow) surrounded by native aortic valve (red arrow) jailed between the bioprostheses and the aortic root (blue arrow): ventricular aspect (left), aortic aspect (middle) and view of the root with native valve tissue cut and opened out along its perimeter (right). **D:** Histology (Movat's pentachrome staining) and immunohistochemistry of native aortic valves showing morphology, high expression of Runx2 and osteopontin in the native aortic valves explanted a month, 32 and 53-months post-TAVI.

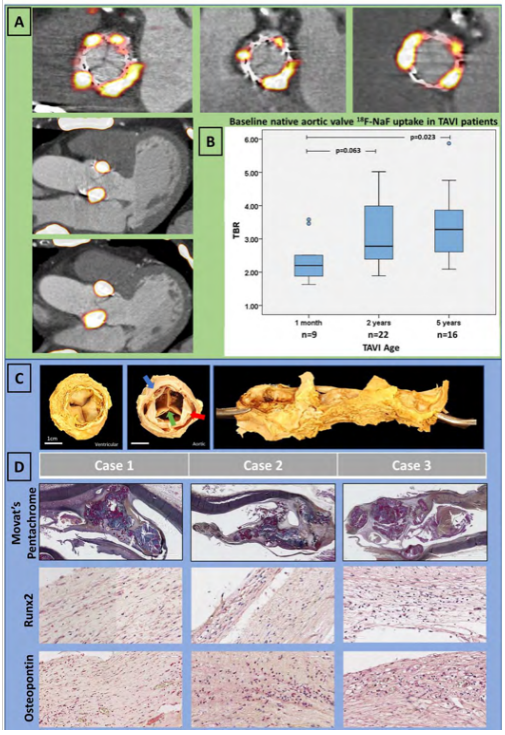

Figure 7.3 Further examples of native aortic valve ^{18}F-sodium fluoride uptake following transcatheter aortic valve implantation.

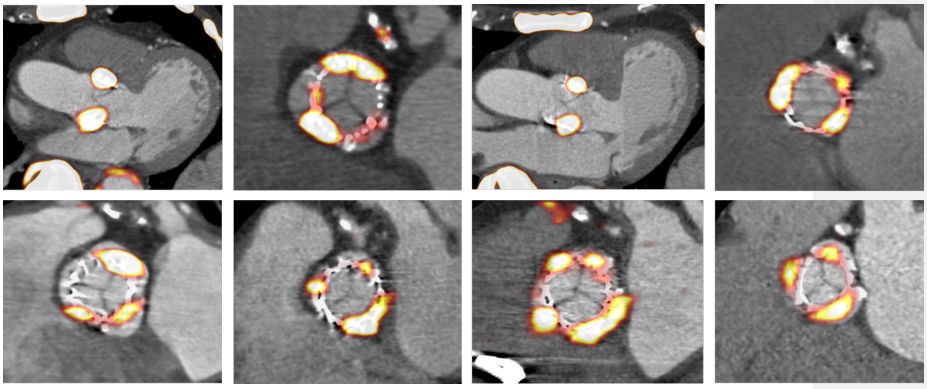

Figure 7.4 Histology of native aortic valves explanted post-transcatheter aortic valve implantation. Representative images of histological sections with Movat's pentachrome staining of left, right and non-coronary cusps (LCC, RCC, NCC) showing severely calcified valves at time of post-mortem explant in patients having undergone transcatheter aortic valve implantation. Histological images are shown at 1.7x.

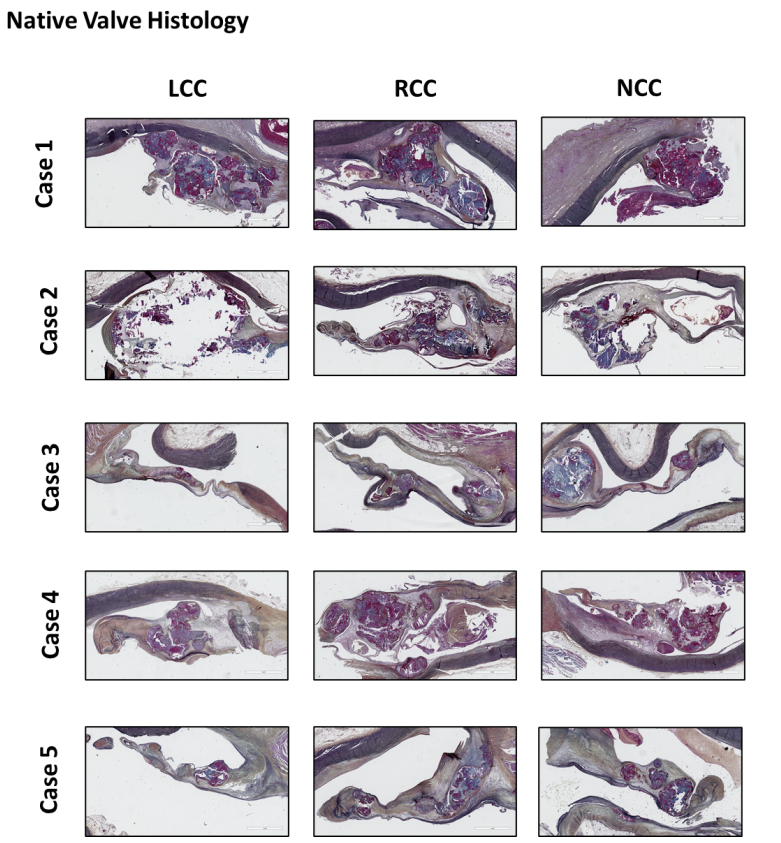

7.3.3 Assessments of Bioprosthetic Valve Degeneration

Ex Vivo Validation

In four explanted TAVI valves with evidence of valve leaflet degeneration, increased ^{18}F-sodium fluoride uptake was seen on autoradiography, with co-localisation of this signal to regions of calcification within the TAVI valve leaflets as observable on hematoxylin and eosin and Movat's pentachrome staining (Figure 7.5).

Baseline Echocardiography and Computed Tomography

On echocardiography during their baseline research visit, valve function was normal in all but 3 patients. These 3 patients had 5-year-old TAVI valves and demonstrated increased transvalvular gradients. This had not been appreciated on previous clinical echocardiograms or clinical follow up. No patient had clinically significant valvular regurgitation. Leaflet morphology was assessable in 77% of patients and no abnormalities were detected on baseline echocardiograms.

CT scans had image quality suitable for leaflet assessments in 87% of patients. Only one patient had evidence of TAVI leaflet calcification on CT, demonstrating spotty calcification that was just discernible from the valve struts (Figure 7.5). Pannus formation was not observed in any of our patients. HALT was found in 6 (13%) patients, 5 of whom were imaged 5 years after TAVI and one patient imaged 1 month after implantation. Four of these patients demonstrated minimal (<25%) leaflet involvement, while 2 patients had pronounced HALT (exceeding 50% of the leaflets) causing restricted single leaflet motion on 4-dimensional CT. One patient with HALT had evidence of hemodynamic valve deterioration on echocardiography (mean pressure gradient 24 mmHg).

Overall, 8 patients had imaging evidence of bioprosthetic TAVI valve degeneration on echocardiography or CT. Seven of these patients were in the cohort of patients imaged 5 years following TAVI, with no differences in their baseline clinical characteristics compared to patients with similar aged TAVI valves but normal imaging (Table 7.4).

Figure 7.5 ^{18}F-Sodium fluoride identifies early TAVI bioprosthetic valve degeneration. **A:** Top row: a 76-year-old female with hemodynamic valve deterioration on echocardiography imaged 5 years after transcatheter aortic valve replacement (TAVI) implantation. Computed tomography angiography revealed spotty calcification on the bioprosthetic leaflets. On ^{18}F-sodium fluoride positron emission tomography (^{18}F-NaF PET), we detected very high uptake in the leaflets (target-to-background [TBR] = 5.9). The patient developed bioprosthesis failure 18 months after baseline PET and underwent a successful TAVI-in-TAVI. Second row: an 88-year-old male with hemodynamic valve deterioration on echocardiography imaged 5 years after TAVI. Computed tomography angiography revealed hypoattenuated leaflet thickening. On ^{18}F-NaF PET we detected very high uptake in the leaflets (TBR = 3.8). **B:** There was a stepwise increase in TAVI ^{18}F-NaF uptake according to the presence and severity of valve dysfunction. ^{18}F-NaF uptake was highest in patients with hemodynamic dysfunction, and more pronounced in those with structural valve deterioration (SVD) than normal TAVI valves. **C:** Histological and autoradiography validation of ^{18}F-NaF avidity in an Edwards CE TAVI valve explanted after 86 months: Movat's pentachrome and hematoxylin and eosin staining, demonstrate that leaflet calcification corresponds closely with ^{18}F-NaF binding on autoradiography.

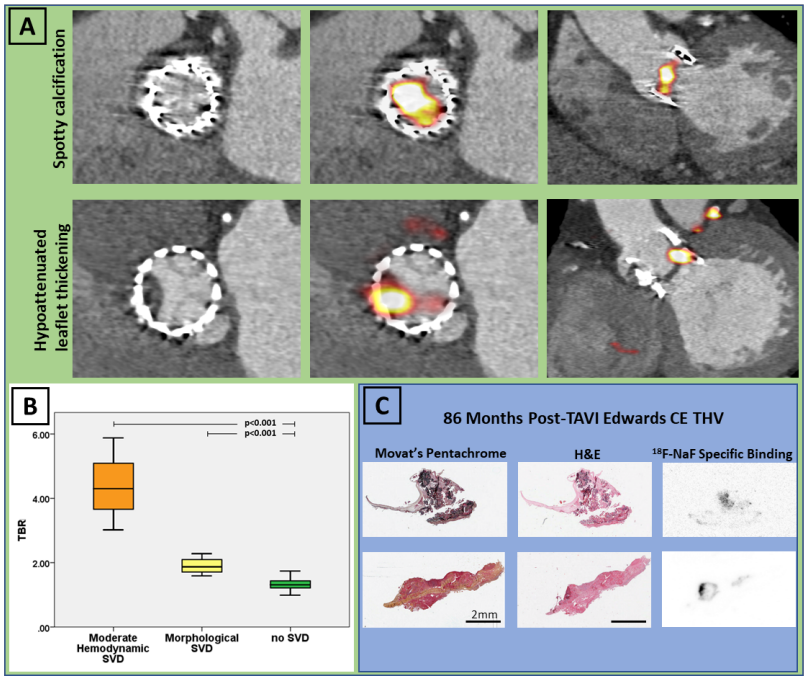

Table 7.4 Comparison of patients with and without ^{18}F-sodium fluoride transcatheter aortic valve leaflet uptake.

	Patients with ^{18}F-NaF transcatheter aortic valve leaflet uptake (n=7)	Patients without ^{18}F-NaF transcatheter aortic valve leaflet uptake (n=40)	**P value**
Age (years)	81 [75-86]	82 [76-87]	0.68
Men	5 (63%)	24 (62%)	0.74
Body-mass index (kg/m^2)	25 [21-27]	24 [20-26]	0.47
Systolic blood pressure (mmHg)	130 [118-137)	132 [120-146]	0.72
Diastolic blood pressure (mmHg)	62 [59-70)	68 [60-74]	0.56
Bioprosthesis age			
time since valve implantation (months)	59 [59-60]	24 [24-24]	<0.001
5 years post valve implantation	7 (100%)	9 (23%)	<0.001
2 years post valve implantation	0	22 (55%)	<0.001
1 month post valve	0	8 (20%)	<0.001
Comorbidities/risk factors, n (%)			
Hypertension	6 (86%)	32 (80%)	0.63
Hyperlipidaemia	6 (86%)	20 (50%)	0.40
Diabetes	2 (29%)	12 (30%)	0.54
Smoking	5 (71%)	23 (58%)	0.53
Coronary artery disease	4 (57%)	20 (50%)	N/A
Coronary artery bypass grafts	2 (29%)	15 (38%)	0.92
Medications			
Aspirin	4 (57%)	23 (58%)	0.39
P2Y12 antagonist	2 (29%)	6 (15%)	0.19
Warfarin	2 (29%)	5 (13%)	0.14
Direct oral anticoagulation	1 (14%)	0	N/A
ACE inhibitor/angiotensin receptor blocker	5 (71%)	25 (63%)	0.68
Beta blocker	5 (71%)	23 (58%)	0.52
Statin	6 (86%)	29 (73%)	0.71
Echocardiography			
Peak Valve Velocity (m/s)	2.9 [2.3-3.4]	2.0 [1.7-2.3]	<0.001
Effective orifice area (cm^2)	1.0 [0.8-1.3]	1.8 [1.6-2.2]	<0.001
Mean valve gradient (mmHg)	19 [17-22]	12 [10-15]	<0.001
LV ejection fraction (%)	60 [55-60]	58 [55-60]	0.46
Electrocardiogram			
Sinus rhythm	5 (71%)	22 (55%)	0.58
Paced rhythm	2 (29%)	7 (18%)	N/A
Atrial fibrillation	3 (43%)	4 (10%)	N/A
LV hypertrophy	1 (14%)	4 (10%)	0.35
Strain pattern	0	3 (8%)	N/A
^{18}F-NaF uptake			
Bioprosthetic uptake	7 (100%)	0	N/A
Target to background ratio	2.3 [1.7-4.3]	1.3 [1.1-1.5]	<0.001

Number (%); median [interquartile range]

ACE – angiotensin-converting enzyme; ^{18}F-NaF - ^{18}F-sodium fluoride

7.3.4 Baseline 18F-Sodium Fluoride Positron Emission Tomography

All patients had good image quality enabling assessment of ^{18}F-sodium fluoride uptake in the bioprosthetic leaflets. There was no difference in ^{18}F-sodium fluoride uptake in self-expandable versus balloon-expandable TAVI bioprostheses (TBR: 1.3 [1.2-1.6] versus 1.3 [1.2-1.7], p=0.74). We detected ^{18}F-sodium fluoride uptake localised to the TAVI leaflets in 7 patients (15%), all imaged 5 years after TAVI (TBR range 1.6 to 5.9). Valve TBR values were nearly double those in patients without visually apparent leaflet uptake (2.3 [1.7-4.3] versus 1.3 [1.2-1.4], p<0.001). The 3 highest TBR values (range 3.0-5.9) were observed in the patients with evidence of hemodynamic structural valve deterioration on echocardiography (Stage 2 SVD; mean transprosthetic pressure gradients > 20 mmHg). Increased uptake was also observed in patients with structural evidence of valve degeneration on CT (Stage 1 SVD) compared to valves with normal echocardiographic and CT appearances (Figure 7.5). One patient had evidence of increased ^{18}F-sodium fluoride leaflet uptake in the absence of any changes on CT or echocardiography. Of 6 patients presenting with HALT, 4 showed increased ^{18}F-sodium fluoride TAVI leaflet uptake (Figure 7.5 and Figure 7.6).

Figure 7.6 Further examples of increased ^{18}F-sodium fluoride uptake in the leaflets of transcatheter bioprosthesis.

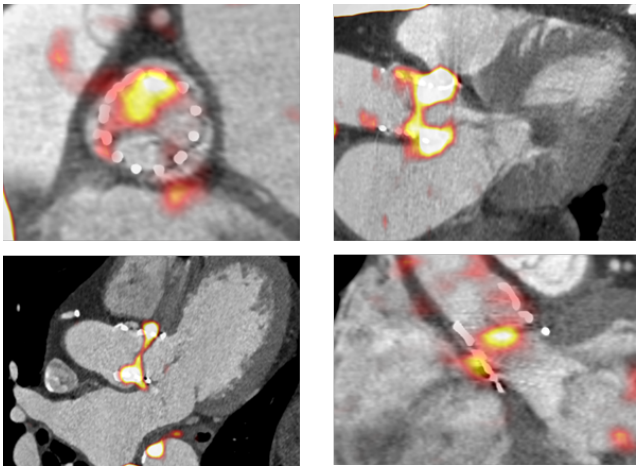

7.3.5 Disease Progression and Clinical Outcomes

Patients with TAVI underwent repeat echocardiographic evaluation at 15 [12-17] months to assess for evidence of progressive valve dysfunction. A strong correlation was observed between baseline ^{18}F-sodium fluoride TBR values in the TAVI leaflets and the subsequent annualised change in bioprosthetic valve peak velocity on echocardiography ($r=0.70$, $p<0.001$; Figure 7.7). Similar correlations were observed between ^{18}F-sodium fluoride leaflet uptake and the change in the mean pressure gradient ($r=0.55$, $p=0.01$) and the change in the effective orifice area ($r=-0.71$, $p=0.007$). On univariable analysis, the only predictors of the annualised change in peak velocity were valve age ($p=0.035$), abnormal CT findings ($p=0.006$) and ^{18}F-sodium fluoride leaflet uptake ($p<0.001$; Table 7.5). On multivariable analysis incorporating age, sex, duration of valve implantation, baseline peak prosthetic valve velocity and abnormal CT findings, ^{18}F-sodium fluoride uptake was the only predictor of the annualised change in peak velocity ($p<0.001$; Table 7.6).

Four patients developed clinical criteria for hemodynamic SVD during the follow up period, with each developing bioprosthetic valve stenosis (mean pressure gradient 27 [24-31] mmHg and peak velocity 3.6 [3.4-4.1] m/s). Three patients had increased ^{18}F-sodium fluoride TAVI leaflet uptake at baseline. In the single patient without increased ^{18}F-sodium fluoride uptake at baseline, the increased mean pressure gradient normalised after 3 months of anti-coagulation therapy and in retrospect was attributed to valve thrombosis rather than established irreversible structural valve disease. The patient with the highest leaflet ^{18}F-sodium fluoride uptake in the TAVI cohort developed bioprosthesis failure 18 months after baseline PET and underwent a successful TAVI-in-TAVI. Based on the Youden's index, the optimal cut-off TBR

value to identify patients at increased risk of structural valve degeneration was 1.59. In our study, the 1.59 TBR threshold had a sensitivity of 86%, specificity of 89%, positive predictive value of 86%, negative predictive value of 97% and accuracy of 89% for prediction of hemodynamic valve degeneration.

Figure 7.7 Baseline ^{18}F-sodium fluoride uptake predicts subsequent deterioration in TAVI function. A: Case example of an 84-year-old patient imaged 5 years following transcatheter aortic valve replacement (TAVI). We detected TAVI ^{18}F-sodium fluoride (^{18}F-NaF) leaflet uptake in the absence of abnormalities on echocardiography (mean pressure gradient 11 mmHg) and computed tomography (CT). At follow up, the patient developed moderate bioprosthesis stenosis with mean pressure gradient of 23 mmHg. **B:** A strong correlation was observed between baseline ^{18}F-NaF uptake in the TAVI valves (TBR) and subsequent progression in bioprosthetic valve peak velocity (r=0.7; p < 0.001). **C:** Forest plot of unstandardised coefficients (95% confidence intervals) from a multivariable linear regression analysis predicting change in TAVI valve function (annualised change in peak velocity) during follow-up. When examining all relevant baseline characteristics, ^{18}F-NaF uptake was the only independent predictor of hemodynamic TAVI deterioration.

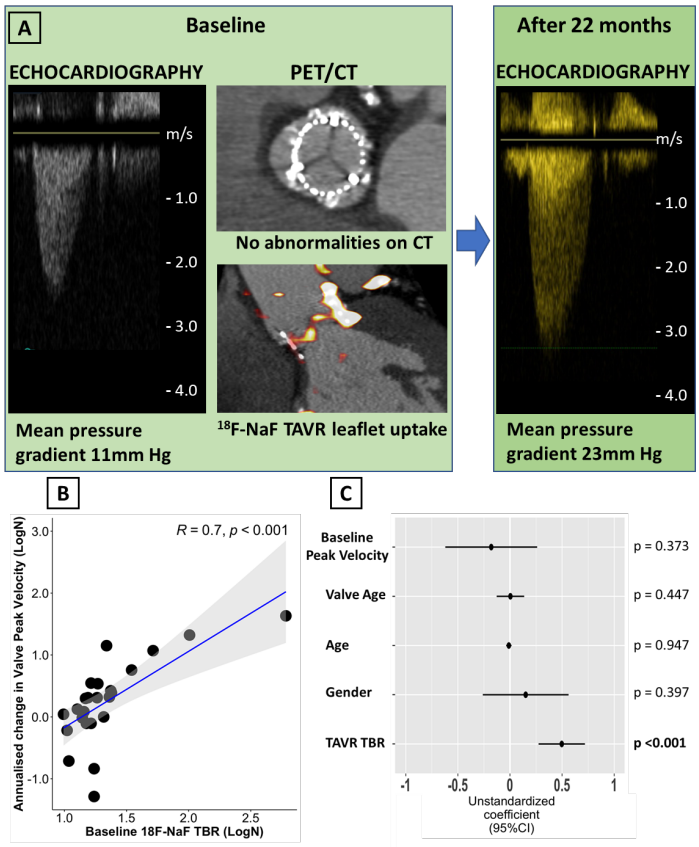

Table 7.5 Factors associated with future deterioration in TAVI function (annualised change in peak velocity after 2 years): univariable analysis.

UNIVARIABLE PREDICTORS OF PROGRESSION IN PEAK VELOCITY				
Variable	**Unstandardised Coefficient (95% Confidence Interval)**	**Standard Error**	**Standardised Coefficient**	**P value**
Sex	0.106 (-0.491 to 0.704)	0.298	0.083	0.72
Age	-0.006 (-0.040 to 0.027)	0.013	-0.086	0.70
Body-mass Index	-0.016 (-0.064 to 0.031)	0.023	-0.169	0.47
Valve Age	0.139 (0.011 to 0.268)	0.064	0.431	**0.035**
Valve Type	-0.021 (-0.050 to 0.010)	0.015	-0.085	0.54
Systolic blood pressure	-0.005 (-0.021 to 0.011)	0.013	-0.153	0.50
Hypertension	0.028 (-1.318 to 1.373)	0.6429	0.010	0.96
Diabetes	0.104 (-0.473 to 0.681)	0.276	0.086	0.71
Dyslipidaemia	0.255 (-0.713 to 1.224)	0.463	0.126	0.59
Smoking	-0.865 (-2.096 to 0.366)	0.479	-0.628	0.13
Baseline Peak Velocity	-0.2417 (-0.850 to 0.367)	0.294	-0.173	0.42
Hypoattenuated leaflet thickening on CT	0.4495 (-0.346 to 1.245)	0.383	0.242	0.25
Abnormal CT findings	0.889 (0.277 to 1.501)	0.295	0.540	**0.006**
Native valve TBR	0.032 (-0.218 to 0.282)	0.120	0.058	0.79
TAVI TBR	0.509 (0.348 to 0.669)	0.078	0.813	**<0.001**

CT: computed tomography; TAVI: transcatheter aortic valve implantation; TBR: target to background ratio.

Table 7.6 Factors associated with future deterioration in TAVI function (annualised change in peak velocity after 2 years): multivariable analysis.

MULTIVARIABLE ANALYSIS: PREDICTORS OF PROGRESSION IN PEAK VELOCITY				
SUMMARY:	**R = 0·760**		**R Square 0.580**	**p = 0.002**
Variable	**Unstandardised Coefficient (95% Confidence Interval)**	**Standard Error**	**Standardised Coefficient**	**P value**
Age	-0.013 (-0.039 to 0.012)	0.012	-0.176	0.287
Sex	0.109 (-0.303 to 0.520)	0.193	0.090	0.447
Valve Age	-0.029 (-0.171 to 0.113)	0.066	-0.088	0.663
Baseline Peak Velocity	-0.09 (-0.552 to 0.366)	0.214	-0.070	0.670
Abnormal CT findings	0.565	0.445	0.330	0.225
TAVI TBR	0.476 (0.244 to 0.727)	0.114	0.628	**<0.001**

TAVI: transcatheter aortic valve implantation; TBR: target to background ratio.

7.3.6 Comparison to Patients with Age-matched SAVR Valves

Fifty-one patients with SAVR who underwent the same research imaging protocol were compared to the 47 patients with TAVI. The latter were older (82 [76-86] versus 72 [70-77] years, p<0.001) and had more co-morbidity than patients with SAVR. The time from valve replacement to imaging was similar (24 [24-60] vs 24 [24-60] months, p=0.91) as were the number of SAVR and TAVI patients imaged 1 month, 2 years and 5 years after valve replacement (Table 1). Patients with TAVI had lower peak aortic jet velocity (2.4 [2.0-2.7] vs 2.7 [2.4-3.0] m/s, p=0.03) and larger effective orifice area (1.5 [1.3-1.8] vs 1.1 [1.0-1.5] cm^2, p=0.02, Table 7.1) than patients with SAVR.

Evidence of bioprosthetic degeneration was similar in TAVI and SAVR groups on echocardiography (6% vs 8% respectively, p=0.78) and CT (15% vs 14% respectively, p=0.87; Figure 7.8). While the overall prevalence of patients with increased leaflet ^{18}F-sodium fluoride uptake appeared to be nearly double in patients with SAVR (29% versus 15% in those with TAVI), this did not reach statistical significance (p=0.09) and in those studied at 5 years, there was no difference in the proportion of patients demonstrating bioprosthetic uptake (40% SAVR vs 44% TAVI patients, p=0.79). Overall ^{18}F-sodium fluoride uptake was similar in both TAVI and SAVR valves (TBR: 1.3 [1.2-1.7] vs 1.3 [1.2-1.5], p=0.27).

Figure 7.8 Comparison of imaging findings and valve deterioration in TAVI versus bioprosthetic SAVR.

We compared echocardiographic, computed tomography (CT) and ^{18}F-sodium fluoride (^{18}F-NaF) findings in 47 patients with transcatheter aortic valve replacement (TAVI) with 51 patients with surgical aortic valve replacement (SAVR) who underwent the same research imaging protocol. We observed ^{18}F-NaF uptake on the peripheral of all TAVI valves and none of the SAVR valves. While patients with TAVI showed lower peak velocity (2.4 [2.0-2.7] vs 2.7 [2.4-3.0] m/s, p=0.03) and larger effective orifice area (1.5 [1.3-1.8] vs 1.1 [1.0-1.5] cm^2, p=0.02) than patients with SAVR, we detected baseline echocardiographic (6 vs 8% p=0.78) and CT abnormalities (15 vs 14% p=0.87) suggestive of bioprosthetic degeneration in a similar proportion of patients with either TAVI or SAVR. The overall prevalence of patients with increased leaflet ^{18}F-NaF uptake was nearly double in patients with SAVR compared to those with TAVI (29% and 15%, p=0.09). In both patients with SAVR or TAVI, baseline ^{18}F-NaF leaflet uptake was predictive of the change in the peak transvalvular velocity on echocardiography.

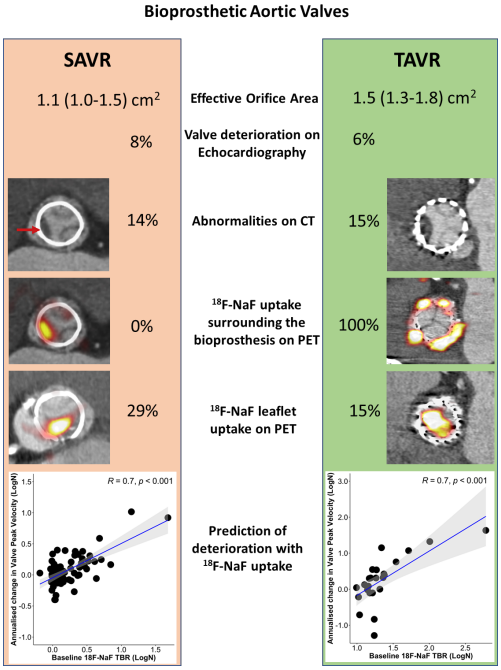

7.5 Discussion

In patients with TAVI, we have demonstrated that ^{18}F-sodium fluoride uptake within the native aortic valve is higher with longer duration of implantation suggesting disease activity continues despite immobilisation of the valve leaflet. This was further supported by our histological finding of continued activation of pro-calcific markers in explanted native valves after TAVI. We have further shown using 3 complementary and distinct imaging modalities that the prevalence of valve degeneration within TAVI bioprostheses is similar to that of bioprosthetic SAVR valves for up to 7 years after valve replacement. Finally, we have confirmed that ^{18}F-sodium fluoride PET of the bioprosthetic valve provides a powerful independent predictor of subsequent hemodynamic bioprosthetic valve degeneration that is applicable to both TAVI and SAVR and outperforms all other traditional risk factors. We conclude that aortic stenosis is an active regulated disease process rather than solely the result of simple wear and tear of the valve, and that TAVI appears to have similar durability to SAVR with comparable modest rates of mid-term bioprosthetic valve degeneration.

We have previously established ^{18}F-sodium fluoride PET as a tool for the *in vivo* assessment of calcification activity across multiple different cardiovascular disease states (49, 66, 88, 99, 173, 181). In patients with aortic stenosis, valvular ^{18}F-sodium fluoride uptake provides an assessment of disease activity and prediction of subsequent disease progression and clinical events (88, 186). We have here demonstrated that ^{18}F-sodium fluoride uptake continues to occur in the retained native aortic valve of all patients with TAVI. We had hypothesised that ^{18}F-sodium fluoride uptake might have transiently increased early following TAVI when native valve calcium has been

disrupted, thereby increasing the available surface area for ^{18}F-sodium fluoride binding. Thereafter, ^{18}F-sodium fluoride uptake would be anticipated to decline as the valve heals and the mechanical trauma of repeated valve closure ceased. However, we observed the opposite. Native aortic valve^{18}F-sodium fluoride uptake and calcification activity was higher with longer duration of implantation. We observed a modest correlation between native valve uptake and the time from TAVI. This finding was supported by our *ex vivo* data that demonstrated histological evidence of ongoing calcification activity in native aortic valve tissue many years following TAVI. These observations are consistent with the hypothesis that once established, calcification activity in the native aortic valve continues to accelerate in an ongoing pathobiological process with continuing mineralisation (the propagation phase) that is not halted even following TAVI (187). Indeed, the fact that it continues several years after TAVI, when mechanical stresses are no longer being exerted on the valve leaflets, confirms that aortic stenosis is an active regulated disease process and not simply the result of valve wear and tear. Therapies focused on slowing this cycle of calcification are required if we are going to develop the medical treatments for aortic stenosis that are so urgently needed. Medications interfering with tissue calcification and ectopic bone formation (alendronate and denosumab) have recently been tested in this context but unfortunately were unable to alter aortic valve calcification or disease progression (177, 188, 189).

In patients with bioprosthetic SAVR, ^{18}F-Sodium fluoride uptake provides a marker of bioprosthetic valve degeneration and a powerful predictor of subsequent valve dysfunction (99). Our current study extends these findings to patients with TAVI,

demonstrating that increased ^{18}F-sodium fluoride uptake in the bioprosthetic valve leaflets provides an early indication of valve degeneration and a more powerful predictor of subsequent valve dysfunction than valve age, cardiovascular co-morbidities and imaging assessments provided by echocardiography and computed tomography. Interestingly, the association between baseline bioprosthetic leaflet ^{18}F-sodium fluoride uptake and subsequent change in bioprosthetic valve peak velocity was identical in patients with TAVI ($r=0.7$, $p<0.001$) to that previously reported for bioprosthetic SAVR valves ($r=0.7$, $p<0.001$). Combined with the existing bioprosthetic SAVR data, this positions ^{18}F-sodium fluoride PET as a highly promising marker of early bioprosthetic valve degeneration that might provide important value in the prediction of bioprosthesis failure, particularly as other imaging modalities such as echocardiography and CT are currently limited in this regard. Future trials are now required to assess whether this molecular imaging technique can aid clinical decision making and risk stratify patients with bioprosthetic valves. Based on the findings of this study, one potential strategy would be to perform a 5-year ^{18}F-sodium fluoride PET scan after TAVI as a screening tool for identifying those at increased risk of rapid deterioration. This might help the planning of repeat intervention and differentiate patients who require close monitoring from those with no evidence of even early valve degeneration who can be assessed much less frequently.

Given the powerful prediction of valve dysfunction provided by ^{18}F-sodium fluoride in both bioprosthetic SAVR and TAVI valves, our dataset provides a unique opportunity to compare early valve degeneration in age-matched bioprosthetic SAVR

and TAVI valves, thereby helping address one of the most important current questions in heart valve disease. Are TAVI valves likely to last as long as surgical bioprostheses? In the present study, there were no differences in the proportion of patients with TAVI or SAVR bioprostheses who had echocardiographic or CT evidence of valve degeneration for up to 7 years after replacement. Very similar rates of increased ^{18}F-sodium fluoride uptake were observed in patients with SAVR and TAVI valves implanted 5 years previously (40 versus 44 %) despite patients with TAVI having a much higher burden of cardiovascular co-morbidities. Taken together, our data suggest that imaging assessments of valve degeneration are similar between these two types of valves, supporting similar mid-term durability of TAVI and SAVR bioprosthetic valves. If confirmed in larger studies, then this would help assuage one of the main lingering concerns about performing TAVI as the first line valve replacement method in patients with aortic stenosis.

7.5.1 Limitations

Our study has several strengths and weaknesses. We have employed a state-of-the-art multi-modality imaging study design and employed the same protocols to image patients with age matched SAVR and TAVI valves thereby providing a unique opportunity to compare imaging findings in these 2 valve types. Moreover, we provide longitudinal data confirming the predictive value of ^{18}F-sodium fluoride PET in both SAVR and TAVI valves. Whilst relatively large for a complex molecular imaging study, our overall sample size is modest (47 TAVI and 51 SAVR valves). Our observations therefore require confirmation in larger data sets with longer follow-up. Patients with bioprosthetic SAVR and TAVI were not matched for age nor co-morbidities however, given the different patient populations who currently received these two treatments, this is inevitable, and our results would suggest that these co-morbidities do not greatly influence valve degeneration nor durability. Given the cross-sectional nature of our study, we acknowledge the potential for survivor bias. This could be addressed in future longitudinal cohort studies to ensure prospective capture of all cases of valvular degeneration. Due to the outbreak of SARS-CoV-2 pandemic, we discontinued further recruitment before reaching our pre-defined number of study participants and therefore further studies are needed to confirm our findings. Finally, in our study, we focused on bioprosthetic valves, and our findings should not be extrapolated to mechanical aortic valve prostheses which have better durability than both forms of bioprosthetic valve.

7.6 Conclusions

In conclusion, we have demonstrated that native aortic valves after TAVI demonstrate evidence of ongoing disease activity, suggesting that aortic stenosis is an active disease process that is independent of motion and mechanical injury. Across three complementary and distinct imaging modalities, TAVI degeneration appears to be of similar magnitude to bioprosthetic SAVR suggesting comparable mid-term durability. ^{18}F-sodium fluoride PET appears to be a consistent method of detecting early bioprosthetic valve degeneration and predicting subsequent dysfunction for both TAVI and SAVR.

Chapter 8 Conclusions and Future Directions

Extracts of this chapter have been published in the following research papers:

Tzolos E, Bing R, Dweck R Marc, David E Newby, Categorising myocardial infarction with advanced cardiovascular imaging, Lancet, 2021 Aug 7;398(10299): e9

Kwiecinski J*, **Tzolos E***, Berman D, et al. Imaging Coronary Atherosclerotic Plaque, European Heart Journal (In progress), *joint first co-authors

Tzolos E, Kwiecinski J, Berman D, et al. Latest advances in multimodality imaging of aortic stenosis, Journal of Nuclear Medicine (In progress)

Kwiecinski J*, Tzolos E*, Adamson P et al. 18F-Sodium Fluoride Coronary Uptake Predicts Outcome in Patients with Coronary Artery Disease
Journal of American College of Cardiology 2020 Jun 23;75(24):3061-3074.

8.1 Coronary ^{18}F-sodium fluoride positron emission tomography and computed tomography

8.1.1 Coronary microcalcification activity (CMA) is reliable and is here to stay

Coronary ^{18}F-sodium fluoride imaging has proven to be an excellent non-invasive tool for imaging and identification of high-risk coronary artery plaques. The ^{18}F-sodium fluoride uptake quantification method should mirror our current dogma of assessing coronary atherosclerotic disease. The focus has shifted away from the "vulnerable plaque" and we are now interested in the vulnerable patient (132). The concept of the vulnerable patient has evolved, with the atheroma burden, its disease activity, and the disposition to vascular thrombosis building the triangle of risk. While maximum target to background ratio (TBRmax) can assess a vulnerable plaque (per lesion approach), it does not consider the global patient disease activity and can prove suboptimal. To adapt ^{18}F-sodium fluoride coronary uptake quantification to the novel per patient paradigm, we evaluated a novel semiautomated approach for image analysis. The coronary microcalcification activity (CMA) characterises ^{18}F-sodium fluoride uptake throughout the entire coronary vasculature using CT angiography-derived centrelines to build 3-dimensional tubular volumes of interest around each of the main epicardial coronary arteries. CMA allows the evaluation of coronary ^{18}F-sodium fluoride activity on a per vessel and per patient basis, offering a more global assessment of disease activity of the coronary arteries than the per lesion approach. CMA measure provides information regarding coronary disease activity in a similar fashion to the Agatston method for quantifying coronary CT calcium score. As a result, in patients and vessels

with multiple foci of uptake, CMA provides a measure of disease activity across the coronary vasculature.

We evaluated the repeatability and reproducibility of a novel methodology (CMA) for assessing whole vessel coronary ^{18}F-sodium fluoride uptake on PET/CT as a single measure of patient risk (120). We have shown that CMA provides a novel metric of the per-vessel and per-patient coronary ^{18}F-sodium fluoride PET activity that has excellent intraobserver, and interobserver repeatability and interscan reproducibility. There was 100% intraobserver, interobserver and interscan agreement for the presence (CMA>0) or absence (CMA=0) of coronary^{18}F-sodium fluoride uptake Compared to TBRmax CMA shows better repeatability and reproducibility. We suggest that CMA could be used as a global patient level measure of ^{18}F-sodium fluoride uptake with potential application to clinical trials and clinical practice.

8.1.2 Impact of motion on ^{18}F-sodium fluoride cardiovascular imaging and optimised methods

Quantitative accuracy and reproducibility of imaging will be critical to establish its clinical value. A major challenge facing PET/CT of the heart is the lengthy imaging sessions, with acquisition times reaching 30 minutes(48, 49, 99, 181). The impact of cardiac, respiratory, and gross patient movement on PET image quality has been the focus of several previous coronary and aortic valve ^{18}F-sodium fluoride PET/CT optimisation imaging studies (109, 114, 116, 117). Originally, cardiac PET/CT scans did not account for cardiac motion. Initial attempts to reduce cardiac motion exploited PET counts acquired during the end-diastolic phase when the heart is relatively still

(between 50%–75% of the R-R interval). This led to reduced blurring from cardiac motion, but increased noise because 75% of the counts were effectively disregarded (63). Moreover, respiratory motion seems and patient movement during the scans can have a detrimental effect in the quantification accuracy (117). Lassen et al. (117) reported significant improvements in the TBR test-retest reproducibility when employing the complex triple motion (cardiac, respiratory and patient) correction techniques. Despite that this remains a complex process requiring expertise and software not widely available and cannot be currently utilised. Moreover, the simplest and more widely available cardiac motion correction allows for similar reproducibility by improving the image quality and reducing the noise significantly (117). This has been shown in studies investigating coronary and aortic valve disease activity (109, 113).

We have tried to explore if we could further improve the current quantification method by reconstructing the PET data using a respiratory averaged CT attenuation map (RACTAC) as compared to the standard free breath or end-expiratory attenuation correction map (CTAC). Our main finding was that using RACTAC did not introduce any significant changes in the quantitative comparisons, both when comparing single lesion activities and vessel and the whole coronary tree microcalcification burden (CMA). This is a significant finding that simplifies the PET reconstruction. We do not need to utilise complex and time-consuming reconstruction methods and we can stick to the current cardiac motion correction who gives the best results for CMA. Our findings validate those of prior studies which showed that the effects of cardiac contraction exceed that of respiration with regards to the displacement of the

coronaries: cardiac contraction displaces the coronary arteries 8–26 mm during the cardiac cycle, while normal respiration leads to movement of the heart of approximately 6–13 mm (160). While the radiation difference between RACTAC and the regular CTAC is relatively low, the findings of this study indicate that the increased radiation dose does not improve the quantification of coronary plaque scans using ^{18}F-sodium fluoride and, thus, should be omitted in future studies to comply with as low as reasonably achievable principle (ALARA). Future studies that utilise artificial intelligence and automatic extraction of centrelines could streamline CMA quantification and improve its reproducibility further.

8.1.3 CMA is the strongest predictor of future myocardial infarction

In patients with established coronary artery disease, current approaches are based around clinical risk scores, anatomic assessments of coronary artery calcification and the severity of obstructive coronary stenoses (161). These approaches have shown limited predictive value in patients with established coronary artery disease and there is growing interest in novel risk stratification methods, including assessments of atherosclerotic disease activity (132), that might be used to target expensive yet effective new treatments to patients at highest risk.

In a comprehensive analysis (Chapter 5), ^{18}F-sodium fluoride uptake measured across the coronary vasculature (quantified using the coronary microcalcification activity [CMA]) emerged as the most powerful independent predictor of myocardial infarction outperforming all other established predictors, including the burden of comorbidities; cardiovascular risk scores; coronary calcium scoring; and the presence, severity, and extent of obstructive coronary artery disease. These data therefore confirmed the

potential of ^{18}F-sodium fluoride PET to improve risk stratification of patients with established coronary artery disease, a group in whom prediction of events has previously proven challenging.

Whilst patients with intense coronary ^{18}F-sodium fluoride activity (CMA>1.56) had an 8-fold risk of myocardial infarction, there were no subsequent myocardial infarctions in patients who had no coronary ^{18}F-sodium fluoride activity (CMA=0), despite their advanced disease. The former might potentially be targeted with aggressive treatments such as PCKSK9 (proprotein convertase subtilisin kexin type 9) inhibitors, anti-inflammatory agents and complex revascularisation, whilst these expensive and invasive treatments could be avoided in the latter. Further work is required to explore this concept further and indeed shall be tested in the ongoing PRE^{18}FFIR (Prediction of Recurrent Events With ^{18}F-Fluoride) trial (190). The central hypothesis of the PRE^{18}FFIR study is that coronary ^{18}F-sodium fluoride uptake can identify high-risk and ruptured atherosclerotic plaque in patients with recent myocardial infarction. This has the potential to assist in the diagnosis, risk stratification, investigation, management and treatment of patients with acute myocardial infarction.

Another potential assessment of disease activity and surrogate measure of plaque inflammation is the pericoronary adipose tissue (PCAT) density measured on CCTA. This new technique assesses the CT attenuation of adipose tissue lying immediately adjacent to the coronary arteries and has shown to be a sensitive and dynamic biomarker of coronary inflammation that provides strong and independent prediction

of adverse cardiac events (191). A major advantage is that it can be assessed retrospectively on any CCTA scan performed. Interestingly PCAT attenuation is associated with ^{18}F-sodium fluoride uptake supporting the link between these two assessments of disease activity and more generally between vascular inflammation and calcification activity (84). The added value of measuring PCAT density on top of ^{18}F-sodium fluoride uptake and quantitative plaque analysis remains to be addressed in future studies.

8.1.4 The future is here: Machine learning to enhance risk prediction

The SCOT-HEART (Scottish Computed Tomography of the Heart) trial indicated that treatment decisions based around coronary plaque assessments can improve clinical outcomes and reduce myocardial infarction. In this trial, aspirin and statin therapy was recommended in patients with non-obstructive as well as obstructive plaque, whereas patients with normal coronary arteries were advised to stop their medication. This resulted in the high targeted use of secondary preventative drugs in patients with CCTA-defined plaque: a major potential contributor to the 41% reduction in fatal or non-fatal myocardial infarction observed in patients randomised to CCTA in this trial (192). Further research is required to investigate this hypothesis and to understand how incorporation of plaque burden, plaque type, disease activity and blood thrombogenicity might further improve clinical decision making and the prescription of therapy.

Machine learning may make an important contribution in this regard, with the potential to harness and combine all the potential information on plaque burden, plaque type

and disease activity that is available with CT and PET imaging alongside traditional cardiovascular risk markers. To elucidate the potential of multimodality advanced coronary imaging for risk stratification by leveraging machine-learning, we developed a model based on both ^{18}F-sodium fluoride PET and quantitative plaque analysis derived from coronary CT angiography (193). In our recent study (Chapter 6), a machine learning model based on both quantitative CCTA plaque assessments and ^{18}F-sodium fluoride PET measurements of disease activity, confirmed the powerful and complementary risk prediction provided by these different techniques. By combining such multiparametric and multimodality data, we showed that the risk of myocardial infarction is primarily governed by the analysis of plaque type and plaque burden provided by coronary CT angiography and assessments of disease activity by ^{18}F-sodium fluoride PET. Our machine learning model incorporating the information from these two modalities alongside clinical factors outperformed the individual components analysed separately with a high c-statistic of 0.85. Importantly, our analysis underscored that in patients with advanced coronary artery disease, markers of disease activity, plaque type and plaque burden provide superior risk prediction to clinical risk scores and conventional coronary calcium CT analyses.

These promising findings shall be tested in the context of the large, multicentre, observational PREFFIR (NCT02278211) study of 700 patients with multivessel coronary artery disease who underwent baseline ^{18}F-sodium fluoride PET and coronary CT angiography and are being followed-up for recurrent myocardial infarction.

8.2 Vascular applications of 18F-sodium fluoride positron emission tomography and computed tomography

8.2.1 Native aortic valve disease is more than wear and tear

Aortic stenosis is considered a degenerative condition whereby 'wear and tear' results in initial progressive microcalcification and thereafter calcium deposition upon the valve which stiffens and becomes less mobile leading to haemodynamic obstruction. Currently there are no effective drug treatments as demonstrated by several medical therapy trials: Scottish Aortic Stenosis and Lipid Lowering Trial, Impact on Regression (SALTIRE) (194), the Aortic Stenosis Progression Observation: Measuring Effects of Rosuvastatin (ASTRONOMER) (195), Simvastatin and Ezetimibe in Aortic Stenosis (SEAS) (196) and SALTIRE 2 (188) trials.

Surgical aortic valve replacement or transcatheter aortic valve implantation are the only treatment options and work by alleviating the haemodynamic valve obstruction. In cases of surgical aortic valve replacement, the old native aortic valve is removed. In cases of transcatheter aortic valve implantation, the old native valve is pushed to the side by the transcatheter aortic valve struts. By removing the injury caused by repeated valve opening and closure, we would expect that native aortic valve disease activity would halt and that that ^{18}F-sodium fluoride activity would decrease. In our multicentre study (18F-Fluoride Assessment of Aortic Bioprosthesis Durability and Outcome – Chapter 7), we showed that in patients with transcatheter aortic valve implantation, native aortic valves demonstrate evidence of ongoing active disease. We

demonstrated that ^{18}F-sodium fluoride uptake within the native aortic valve is higher with longer durations of implantation suggesting disease activity continues despite immobilisation of the valve leaflet. This was further supported by our histological finding of continued activation of pro-calcific markers in explanted native valves after transcatheter aortic valve implantation.

We had hypothesised that ^{18}F-sodium fluoride uptake might have transiently increased early following transcatheter aortic valve implantation when native valve calcium has been disrupted, thereby increasing the available surface area for ^{18}F-sodium fluoride binding. Thereafter, ^{18}F-sodium fluoride uptake would be anticipated to decline as the valve heals and the mechanical trauma of repeated valve closure ceased. However, we observed the opposite. Native aortic valve ^{18}F-sodium fluoride uptake and calcification activity was higher with longer duration of implantation. We observed a modest correlation between native valve uptake and the time from transcatheter aortic valve implantation. This finding was supported by our *ex vivo* data that demonstrated histological evidence of ongoing calcification activity in native aortic valve tissue many years following transcatheter aortic valve implantation. These observations are consistent with the hypothesis that once established, calcification activity in the native aortic valve continues to accelerate in an ongoing pathobiological process with continuing mineralisation (the propagation phase) that is not halted even following transcatheter aortic valve implantation (187). Indeed, the fact that it continues several years after transcatheter aortic valve implantation, when mechanical stresses are no longer being exerted on the valve leaflets, confirms that aortic stenosis is an active regulated disease process and not simply the result of valve wear and tear. Therapies

focused on slowing this cycle of calcification are required if we are going to develop the medical treatments for aortic stenosis that are so urgently needed. Until a promising drug shows any potential in halting aortic stenosis progression patients are left only with the option of invasive aortic valve replacement.

8.2.2 18F-Sodium fluoride predicts transcatheter aortic valve degeneration

Cartlidge et al. (99) showed that ^{18}F-sodium fluoride PET-CT identifies subclinical surgical bioprosthetic aortic valve degeneration, providing powerful prediction of subsequent valvular dysfunction and highlighting patients at risk of valve failure. This technique holds major promise in the diagnosis of valvular degeneration and the surveillance of patients with bioprosthetic valves.

Our current study extends these findings to patients with transcatheter aortic valve implantation, demonstrating that increased ^{18}F-sodium fluoride uptake in the bioprosthetic valve leaflets provides an early indication of valve degeneration and a more powerful predictor of subsequent valve dysfunction than valve age, cardiovascular co-morbidities and imaging assessments provided by echocardiography and computed tomography. Interestingly, the association between baseline bioprosthetic leaflet ^{18}F-sodium fluoride uptake and subsequent change in bioprosthetic valve peak velocity was identical in patients with transcatheter aortic valve implantation ($r=0.7$, $p<0.001$) to that previously reported for bioprosthetic surgical aortic valves ($r=0.7$, $p<0.001$). Future trials are now required to assess whether this molecular imaging technique can aid clinical decision making and risk stratify patients with bioprosthetic valves.

8.2.3 Mechanistic insights and clinical trials

The initial ^{18}F-sodium fluoride PET studies highlighted the key pathological role that calcification plays in aortic stenosis, highlighting that any potential novel therapy would have to try and break the self-perpetuating cycle of valve calcification that drives the propagation phase of this disease. Other PET studies have also highlighted other potential targets most notably lipoprotein (a) (Lp[a]) (197-199). In a recent multicentre multi-cohort multimodality imaging study, Zheng et al. (200) investigated the importance of Lp(a) in determining disease activity, disease progression, and clinical events in patients with aortic stenosis. The study included 145 patients with available blood samples for Lp(a) and oxidised phospholipids on apolipoprotein B (apoB)-100 measurements. On baseline PET/CT, patients having the highest Lp(a) tertile had increased valve ^{18}F-sodium fluoride PET/CT uptake and therefore calcification activity compared with those in lower tertiles. After follow up, these PET data translated into accelerated disease progression (assessed by both echocardiography and CT aortic valve calcium score) and more clinical events in patients with the highest Lp(a) tertile. This effect appeared to be mediated by the pro-calcific, pro-osteoblastic effects of Lp(a) on valve interstitial cells via the actions of oxidised phospholipid. These findings therefore indicate that Lp(a) lowering or oxidised phospholipid inactivation may slow aortic stenosis progression, and alongside other observational data (201), provides a clear rationale for randomised controlled trials of this strategy.

The capacity of ^{18}F-sodium fluoride PET/CT to measure calcification activity in aortic stenosis, combined with its excellent scan-rescan reproducibility, makes it an attractive endpoint for clinical studies looking to establish the efficacy of novel therapies for this condition. Changes in valvular ^{18}F-sodium fluoride uptake may potentially be detectable earlier than standard assessments of disease progression made with echocardiography and CT aortic valve calcium scoring which require several years to demonstrate a treatment effect. Several recent studies used ^{18}F-sodium fluoride PET/CT to gain insights into the pathophysiology underlying aortic stenosis and as an endpoint of clinical interventional trials. Indeed, this hypothesis is being evaluated in numerous ongoing clinical trials of novel therapies and mechanistic insights in aortic stenosis where ^{18}F-sodium fluoride PET is being used as an exploratory endpoint (Table 8.1).

In a recently published double-blind randomised controlled trial (Scottish Aortic Stenosis and Lipid Lowering Trial, Impact on Regression - SALTIRE II; NCT02132026) (188), ^{18}F-sodium fluoride PET/CT was used as an exploratory secondary endpoint to establish whether alendronate or denosumab could reduce disease activity and slow disease progression in patients with aortic stenosis. Participants underwent serial assessments with Doppler echocardiography, computed tomography aortic valve calcium scoring (baseline and 24 months), ^{18}F-sodium fluoride positron emission tomography (baseline and after 1 year of therapy) and coronary computed tomography angiography. The study clearly demonstrated that denosumab and alendronic acid have no effect on calcification activity as assessed with ^{18}F-sodium fluoride PET nor disease progression as assessed with either

echocardiography or CT aortic valve calcium scoring. Despite that, baseline aortic valve ^{18}F-sodium fluoride maximum target to background ratio was once again associated with subsequent progression in the CT aortic valve calcium score and peak aortic jet velocity confirming previous observational data (202). The ongoing BASIK-2 trial (NCT02917525) seeks to influence calcification activity in aortic stenosis via an alternative pathway, investigating the effects of vitamin K2 on ^{18}F-sodium fluoride PET activity and CT aortic valve calcium scoring progression in patients with bicuspid aortic valve disease (203).

Table 8.1 Studies using PET radiotracers in patients with aortic stenosis

Study	NCT #	Intervention	Population	Follow-Up	Primary Efficacy Endpoints
Lp(a) and OxPL-apoB role in aortic stenosis[26-29]	NCT01358513	^{18}F-sodium fluoride PET/CT	Aortic stenosis (Vmax >2.5 m/s) (n=145)	2 years	Change in CT-AVC score and aortic valve ^{18}F-sodium fluoride uptake
PCSK9 inhibitors in the progression of aortic stenosis	NCT03051360	Biweekly injection of PCSK9 inhibitor vs. placebo	Mild-moderate aortic stenosis (n = 140)	2 years	Change in CT-AVC score and ^{18}F-sodium fluoride uptake
SALTIRE II - Study Investigating the Effect of Drugs Used to Treat Osteoporosis on the Progression of Calcific Aortic Stenosis[20]	NCT02132026	Alendronic acid (n = 50) vs Denosumab (n = 50) vs placebo injections (n = 50)	Aortic stenosis (Vmax >2.5 m/s)	2 years	Change in CT-AVC score and aortic valve ^{18}F-sodium fluoride uptake
BASIK2 - Bicuspid Aortic Valve Stenosis and the Effect of vitamin K2 on Calcium metabolism on ^{18}F-Fluoride PET/MR[31]	NCT02917525	Daily vitamin K2 360 µg (n = 22) vs. placebo (n = 22)	Bicuspid aortic valve and calcified mild to moderate aortic stenosis	18 months	Change in aortic valve ^{18}F-sodium fluoride uptake at 6 months; change in CT-AVC score at 6 and 18 months
^{18}F-Fluoride Assessment of Aortic Bioprosthesis Durability and Outcome [18F-FAABULOUS][34, 35]	NCT02304276	^{18}F-sodium fluoride PET/CT	Previous Bioprosthesis or TAVI	10 years	Aortic valve ^{18}F-sodium fluoride uptake at baseline
In-vivo Thrombus Imaging With ^{18}F-GP1, a Novel Platelet PET Radiotracer (BioThrombus)	NCT03943966	^{18}F-GP1 PET CT	Previous bioprosthesis or TAVI	5 years	Aortic valve ^{18}F-GP1 uptake at baseline

8.2.4 Future tracers

New radiotracers targeting thrombus formation, inflammation and fibrosis activity have become available with major potential for both aortic stenosis and bioprosthetic valve degeneration. ^{18}F-GP1 is a novel radiotracer that binds with high affinity to the glycoprotein IIb/IIIa receptor on activated platelets (204). It can detect *in vivo* venous and arterial thrombosis, and shows higher sensitivity compared to other current imaging modalities (204-207). In the "18F-GP1 PET-CT to Detect Bioprosthetic Aortic Valve Thrombosis" study (NCT04073875), we have used this tracer in a cross-sectional analysis involving seventy-two participants: 50 with bioprosthetic aortic valves and 22 normal native valves. We showed that all bioprosthetic valves but none of the native aortic valves demonstrated focal ^{18}F-GP1 uptake in the valve leaflets. Higher ^{18}F-GP1 uptake was independently associated with hypo-attenuated leaflet thickening and duration of valve implantation but not with valve type. This suggests widespread platelet activation on the surface of all bioprosthetic valves with further work now required to understand if and how this relates to subsequent bioprosthetic valve degeneration (208).

Gallium 68–labelled fibroblast-activation protein inhibitor (^{68}Ga-FAPI) is a novel tracer that is highly specific for activated fibroblasts and demonstrates intense signal in regions of developing fibrosis activity across multiple organ systems. Current imaging techniques detect the presence of established fibrosis or its functional surrogates, when the window to prevent or inhibit this pathological process may have elapsed. ^{68}Ga-FAPI therefore appears a promising agent for to investigate the timing and pattern of myocardial fibrosis activity following myocardial infarction and

therefore allow earlier detection of disease and more effective assessments of disease progression and response to new antifibrotics agents. We are currently exploring the utility of this tracer in patients post myocardial infarction and in patients with aortic stenosis.

Finally, ^{68}Ga-DOTATATE targets the somatostatin type 2 receptor expressed by activated macrophages and might therefore also prove of value in better understanding the role of inflammation in aortic stenosis and improving upon the data provided by ^{18}F-FDG, which has been limited by non-specific physiological tracer activity in the myocardium (209).

8.3 Future perspectives – the diamond of risk

Based on the underlying pathology and recent clinical trial data, 4 factors emerge as key players contributing to the overall risk of myocardial infarction. Our diamond of risk comprises four points: plaque burden, plaque type, atherosclerotic disease activity and blood thrombogenicity (Figure 8.1). It builds upon the triangle of risk proposed by Arbab-Zadeh and Fuster, but includes assessment of atherosclerotic plaque type on the basis of multiple recent observational studies (132).

Figure 8.1 The diamond of risk of myocardial infarction. Based on the underlying pathology and recent clinical trial data, 4 factors emerge as key players contributing to the overall risk of myocardial infarction: plaque burden, plaque type, atherosclerotic disease activity and blood thrombogenicity.

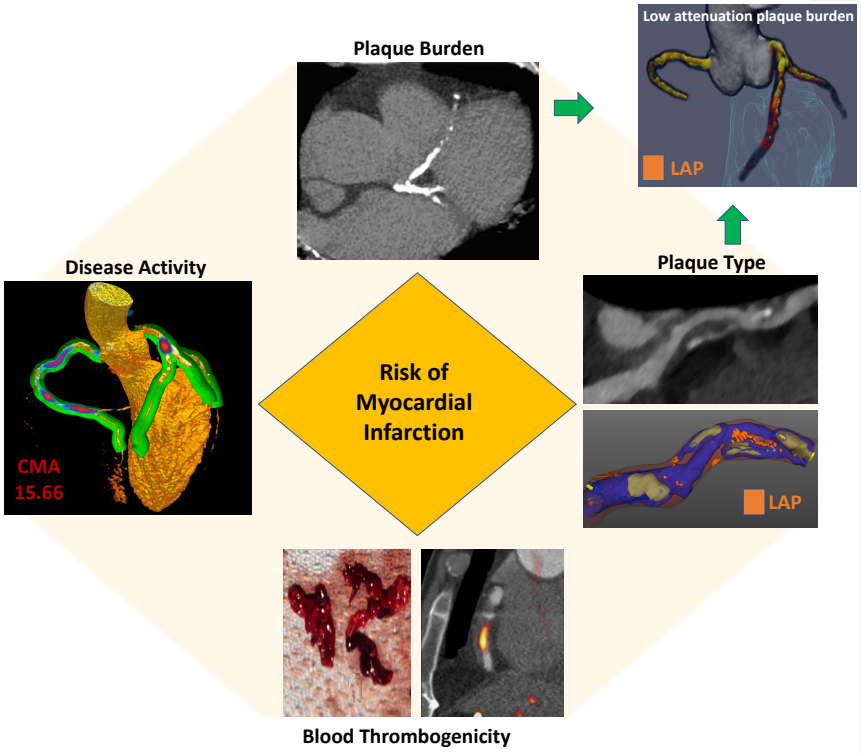

CMA – coronary microcalcification activity; LAP – low attenuation plaque

The final key component of the diamond of risk relates to the blood rather than atherosclerotic plaque and in particular the size of thrombus formed in response to plaque rupture. If the balance between prothrombotic and fibrinolytic factors means that blood thrombogenicity is low at the time of plaque rupture, then only a small clot will form, and the event will be subclinical resulting in plaque growth rather than infarction. However, if the blood is pro-thrombotic then a large thrombus is more likely to develop leading to vessel occlusion or distal embolisation and a type 1 myocardial infarction (132). Pro-thrombotic states, most notably smoking, are closely linked with the risk of myocardial infarction, and discontinuing smoking represents a key preventative strategy. In practice, it has proven challenging to go further and to derive accurate objective measures of blood thrombogenicity which demonstrate considerable daily fluctuation in individual patients. Blood biomarkers of thrombogenicity may be influenced by many processes that are non-specific to the cardiovascular system. There is therefore interest in imaging assessments that can target arterial thrombus formation more directly and help determine the culprit plaque post-myocardial infarction as well as detecting subclinical plaque rupture in apparently stable patients.

8.3.1 T1-weighted cardiovascular magnetic resonance imaging

T1-weighted cardiovascular magnetic resonance imaging allows assessment of met-haemoglobin, a component of acute thrombus and haemorrhage that has a very high signal on T1-weighted imaging. In a study of 568 stable patients, Noguchi et al identified 159 subjects with high-intensity coronary plaque on T1-weighted imaging

(210). During follow-up, 26% of these 159 patients had an adverse coronary event, compared with 3% of the 409 patients who did not present with such lesions.

8.3.2 ^{18}F-GP1 positron emission tomography and computed tomography imaging

Molecular PET imaging can also identify thrombus formation in both the arterial and venous systems. The glycoprotein IIb/IIIa (GPIIb/IIIa) receptor on activated platelets is a key player in thrombus formation and an attractive target for molecular imaging. ^{18}F-labeled elarofiban-class ligand called ^{18}F-GP1 is a novel radiotracer that binds with high affinity to the glycoprotein IIb/IIIa receptor on activated platelets (211). Early results from the "In-vivo Thrombus Imaging With ^{18}F-GP1, a Novel Platelet PET Radiotracer (iThrombus); NCT03943966", a retrospective study involving 51 patients with recent myocardial infarction, showed that ^{18}F-GP1 depicts activated platelets and in-vivo thrombus with high specificity. The tracer images intracoronary thrombus, beyond the resolution of CT, and can accurately identify culprit vessels. Furthermore, ^{18}F-GP1 can identify activated platelets outwith the coronary arteries, aiding in the identification of thrombus formation in both the left atrium and left ventricle and potentially facilitating the distinction between Type1 and Type2 myocardial infarction (207). Further ^{18}F-GP1 studies to explore the prevalence of subclinical plaque rupture in stable patients are now required, on the basis that patients with unstable atheroma undergoing plaque rupture events may also be more likely to have a clinically evident myocardial infarction in the near future.

8.3.3 Bedside applications of ^{18}F-Sodium Fluoride PET

In this thesis we have established that 18F-Sodium fluoride PET provides an assessment of calcification activity in patients with multivessel disease and aortic bioprosthetic valve degeneration. In both conditions, it is associated with disease activity and future disease progression. Could we use this tool in every day clinical practice anytime soon?

In Chapter 5 we have demonstrated for the first time that 18F-Sodium fluoride activity provides a powerful prediction of future myocardial infarction. Indeed, this technique outperformed all other commonly used predictors of events in patients with established coronary artery disease, including 2 established clinical risk scores designed for this patient population, comorbidities, coronary calcium scoring, and the presence and severity of obstructive coronary artery disease. This makes it an exciting tool in a patient population in whom risk stratification is currently suboptimal. A CMA of >1.56 was associated with a >7-fold risk of myocardial infarction. This was despite almost universal prescription of aspirin, statins, and other secondary preventative therapies. These patients might therefore be suitable for advanced medical therapies, including PCSK9 or interleukin 1-beta inhibition, providing the risk stratification tool that many have advocated for as a means of targeting these expensive drugs to those patients at greatest risk. Of equal importance, patients without coronary 18F-NaF uptake and a CMA of 0 had an excellent prognosis with no myocardial infarctions observed in this group despite their advanced coronary artery disease. In these patients with dormant coronary artery disease (one-third of the population studied), further intensification of medical therapy might not be warranted; neither might they benefit on prognostic

grounds from complex revascularization such as multivessel percutaneous intervention or coronary artery bypass grafting. Further research is required to investigate these important clinical questions.

In Chapter 7 we have demonstrated that ^{18}F-sodium fluoride PET is a highly promising marker of early bioprosthetic valve degeneration that might provide important value in the prediction of bioprosthesis failure, particularly as other imaging modalities such as echocardiography and CT are currently limited in this regard. Based on the findings of this study, one potential strategy would be to perform a 5-year ^{18}F-sodium fluoride PET scan after TAVI as a screening tool for identifying those at increased risk of rapid deterioration. This might help the planning of repeat intervention and differentiate patients who require close monitoring from those with no evidence of even early valve degeneration who can be assessed much less frequently. A negative scan at 5 years could potentially mean that no further follow-up is required.

Unfortunately, we need to overcome several limitations before this tool could be part of our daily routine. First of all, preparation of the tracer requires a specialised PET physicists team that will prepare the tracer the morning of the scanning. Even at the best centres the tracer can fail to pass quality control meaning that the scanning list get cancelled at very short notice. More centres are required across the country for this to become a mainstream procedure. Even if we overcome this hurdle remains the issue of injection to scan delays. Patients need to wait for an hour before we can acquire the images. Afterwards patients need to isolate for up to 6 hours which they can do at their house. Given this there is a limit of patients that we could scan and therefore the test

needs to be reserved for the patients that could benefit the most (multivessel coronary disease or an old bioprosthesis). Appropriate use criteria will need to be established.

Current clinical research has focused around improving the post acquisition image reconstruction and analysis (Chapter 4) and modern scanners have improved the image quality dramatically. Nevertheless, the issues of coronary motion, respiratory motion and patient motion remains, and expert readers are required in order to interpret the results appropriately. This hurdle can be resolved if we use central imaging laboratories that can provide with expert reading ana analysis. Moreover, as discussed in Chapter 6 machine learning could improve our reading. Ongoing research has focused on automatic reading of the scans, that will require minimal involvement by the imaging cardiologists, and I believe this will be feasible in the next few years. This approach is currently developed by our collaborators in L.A.

Moreover, different scanners provide different thresholds of activity and in order to harmonise them and have useful cut-off values for risk stratification we will need larger multicentre studies using different scanners (PREFFIR). Again, artificial intelligence will play a critical role in order to compare scans acquired in different scanners. Currently, we are in the process of analysing the results of a phantom study comparing ^{18}F-sodium fluoride PET activity acquired in a GE vs Siemens PET/CT scanner.

Finally, the scans remain expensive (around 1000£ per scan) and cost benefit analysis is required before being offered in a large scale. I believe that if utilised appropriately

they could actually save money for large organisations like the NHS; the cost of Evolocumab and other PCK-9 inhibitors is around 4.000£ per year and even more expensive in the USA. As CMA of zero is really protective of future events many patients that are otherwise meeting clinical criteria for these agents may not requiring them. Similarly, the number of patients with TAVI implants is increasing exponentially and require outpatient clinical resources (appointment, secretaries, nurse, doctors) and echocardiography resources. Patients with negative scans could be discharged from further follow up and potentially saving money and clinician time in the long-term.

Further larger prospective trials are required in order to establish the clinical utility and applicability of ^{18}F-sodium fluoride PET but it's future remains bright.

8.4 Conclusion

We stand at the threshold of new era in the assessment of coronary artery disease with an increasing focus on the pathological processes leading to myocardial infarction. In particular, the diamond of risk holds important promise whereby assessments of plaque burden, plaque type, disease activity and blood thrombogenicity might improve patient risk stratification and be used to direct a truly personalised medicine approach to treatment for our patients. ^{18}F-Sodium fluoride PET plays a central role in evaluating coronary disease activity offering better risk progression over clinical risk scores and plaque burden.

PET imaging with ^{18}F-sodium fluoride provides complementary information regarding disease activity in both native and bioprosthetic valves that has become an established and exciting research tool that has altered our understanding of the pathology of aortic stenosis and is advancing development of the effective medical therapies urgently required for this increasingly prevalent condition. There are a number of emerging tracers that promise to expand our ability to track a number of pathophysiological mechanisms and to help us understand, treat and perhaps prevent aortic stenosis and bioprosthetic valve degeneration.

REFERENCES

1. Diseases GBD, Injuries C. Global burden of 369 diseases and injuries in 204 countries and territories, 1990-2019: a systematic analysis for the Global Burden of Disease Study 2019. Lancet. 2020;396(10258):1204-22.
2. Wilson PW, D'Agostino R, Sr., Bhatt DL, Eagle K, Pencina MJ, Smith SC, et al. An international model to predict recurrent cardiovascular disease. Am J Med. 2012;125(7):695-703 e1.
3. Wilson PW. Assessing coronary heart disease risk with traditional and novel risk factors. Clin Cardiol. 2004;27(6 Suppl 3):III7-11.
4. Yusuf S, Hawken S, Ounpuu S, Dans T, Avezum A, Lanas F, et al. Effect of potentially modifiable risk factors associated with myocardial infarction in 52 countries (the INTERHEART study): case-control study. Lancet. 2004;364(9438):937-52.
5. Schlendorf KH, Nasir K, Blumenthal RS. Limitations of the Framingham risk score are now much clearer. Prev Med. 2009;48(2):115-6.
6. Shaw LJ, Lewis JF, Hlatky MA, Hsueh WA, Kelsey SF, Klein R, et al. Women's Ischemic Syndrome Evaluation: current status and future research directions: report of the National Heart, Lung and Blood Institute workshop: October 2-4, 2002: Section 5: gender-related risk factors for ischemic heart disease. Circulation. 2004;109(6):e56-8.
7. Karim R, Hodis HN, Detrano R, Liu CR, Liu CH, Mack WJ. Relation of Framingham risk score to subclinical atherosclerosis evaluated across three arterial sites. Am J Cardiol. 2008;102(7):825-30.
8. Akosah KO, Schaper A, Cogbill C, Schoenfeld P. Preventing myocardial infarction in the young adult in the first place: how do the National Cholesterol Education Panel III guidelines perform? J Am Coll Cardiol. 2003;41(9):1475-9.
9. Shaw LJ, Blumenthal RS, Raggi P. Screening asymptomatic low-risk individuals for coronary heart disease: issues and controversies. Journal of nuclear cardiology : official publication of the American Society of Nuclear Cardiology. 2004;11(4):382-7.
10. Wilson PW, Smith SC, Jr., Blumenthal RS, Burke GL, Wong ND. 34th Bethesda Conference: Task force #4--How do we select patients for atherosclerosis imaging? J Am Coll Cardiol. 2003;41(11):1898-906.
11. De Bruyne B, Fearon WF, Pijls NH, Barbato E, Tonino P, Piroth Z, et al. Fractional flow reserve-guided PCI for stable coronary artery disease. N Engl J Med. 2014;371(13):1208-17.
12. Maron DJ, Hochman JS, Reynolds HR, Bangalore S, O'Brien SM, Boden WE, et al. Initial Invasive or Conservative Strategy for Stable Coronary Disease. N Engl J Med. 2020;382(15):1395-407.
13. Muller JE, Tofler GH, Stone PH. Circadian variation and triggers of onset of acute cardiovascular disease. Circulation. 1989;79(4):733-43.
14. Burke AP, Farb A, Malcom GT, Liang YH, Smialek J, Virmani R. Coronary risk factors and plaque morphology in men with coronary disease who died suddenly. N Engl J Med. 1997;336(18):1276-82.

15. Burke AP, Kolodgie FD, Farb A, Weber DK, Malcom GT, Smialek J, et al. Healed plaque ruptures and sudden coronary death: evidence that subclinical rupture has a role in plaque progression. Circulation. 2001;103(7):934-40.
16. Falk E, Nakano M, Bentzon JF, Finn AV, Virmani R. Update on acute coronary syndromes: the pathologists' view. Eur Heart J. 2013;34(10):719-28.
17. Finn AV, Nakano M, Narula J, Kolodgie FD, Virmani R. Concept of vulnerable/unstable plaque. Arterioscler Thromb Vasc Biol. 2010;30(7):1282-92.
18. Virmani R, Burke AP, Farb A, Kolodgie FD. Pathology of the vulnerable plaque. J Am Coll Cardiol. 2006;47(8 Suppl):C13-8.
19. Falk E. Pathogenesis of atherosclerosis. J Am Coll Cardiol. 2006;47(8 Suppl):C7-12.
20. Williams KJ, Tabas I. The response-to-retention hypothesis of early atherogenesis. Arterioscler Thromb Vasc Biol. 1995;15(5):551-61.
21. Vengrenyuk Y, Carlier S, Xanthos S, Cardoso L, Ganatos P, Virmani R, et al. A hypothesis for vulnerable plaque rupture due to stress-induced debonding around cellular microcalcifications in thin fibrous caps. Proc Natl Acad Sci U S A. 2006;103(40):14678-83.
22. Vengrenyuk Y, Cardoso L, Weinbaum S. Micro-CT based analysis of a new paradigm for vulnerable plaque rupture: cellular microcalcifications in fibrous caps. Mol Cell Biomech. 2008;5(1):37-47.
23. Falk E, Shah PK, Fuster V. Coronary plaque disruption. Circulation. 1995;92(3):657-71.
24. Chang HJ, Lin FY, Lee SE, Andreini D, Bax J, Cademartiri F, et al. Coronary Atherosclerotic Precursors of Acute Coronary Syndromes. J Am Coll Cardiol. 2018;71(22):2511-22.
25. Boden WE, O'Rourke RA, Teo KK, Hartigan PM, Maron DJ, Kostuk WJ, et al. Optimal medical therapy with or without PCI for stable coronary disease. N Engl J Med. 2007;356(15):1503-16.
26. Group BDS, Frye RL, August P, Brooks MM, Hardison RM, Kelsey SF, et al. A randomized trial of therapies for type 2 diabetes and coronary artery disease. N Engl J Med. 2009;360(24):2503-15.
27. Stone GW, Maehara A, Lansky AJ, de Bruyne B, Cristea E, Mintz GS, et al. A Prospective Natural-History Study of Coronary Atherosclerosis. N Engl J Med. 2011;364(3):226-35.
28. Yabushita H, Bouma BE, Houser SL, Aretz HT, Jang IK, Schlendorf KH, et al. Characterization of human atherosclerosis by optical coherence tomography. Circulation. 2002;106(13):1640-5.
29. Motoyama S, Ito H, Sarai M, Kondo T, Kawai H, Nagahara Y, et al. Plaque Characterization by Coronary Computed Tomography Angiography and the Likelihood of Acute Coronary Events in Mid-Term Follow-Up. J Am Coll Cardiol. 2015;66(4):337-46.
30. Nerlekar N, Ha FJ, Cheshire C, Rashid H, Cameron JD, Wong DT, et al. Computed Tomographic Coronary Angiography-Derived Plaque Characteristics Predict Major Adverse Cardiovascular Events: A Systematic Review and Meta-Analysis. Circ Cardiovasc Imaging. 2018;11(1):e006973.

31. Douglas PS, Hoffmann U, Patel MR, Mark DB, Al-Khalidi HR, Cavanaugh B, et al. Outcomes of anatomical versus functional testing for coronary artery disease. New England Journal of Medicine. 2015;372(14):1291-300.
32. Williams MC, Kwiecinski J, Doris M, McElhinney P, D'Souza MS, Cadet S, et al. Low-Attenuation Noncalcified Plaque on Coronary Computed Tomography Angiography Predicts Myocardial Infarction. Circulation. 2020;141(18):1452-62.
33. Budoff MJ, Shaw LJ, Liu ST, Weinstein SR, Mosler TP, Tseng PH, et al. Long-term prognosis associated with coronary calcification: observations from a registry of 25,253 patients. J Am Coll Cardiol. 2007;49(18):1860-70.
34. Arrey-Mbi TB, Klusewitz SM, Villines TC. Long-Term Prognostic Value of Coronary Computed Tomography Angiography. Curr Treat Options Cardiovasc Med. 2017;19(12):90.
35. Greenland P, Blaha MJ, Budoff MJ, Erbel R, Watson KE. Coronary Calcium Score and Cardiovascular Risk. J Am Coll Cardiol. 2018;72(4):434-47.
36. Greenland P, LaBree L, Azen SP, Doherty TM, Detrano RC. Coronary artery calcium score combined with Framingham score for risk prediction in asymptomatic individuals. Jama. 2004;291(2):210-5.
37. Ambale-Venkatesh B, Yang X, Wu CO, Liu K, Hundley WG, McClelland R, et al. Cardiovascular Event Prediction by Machine Learning: The Multi-Ethnic Study of Atherosclerosis. Circ Res. 2017;121(9):1092-101.
38. Tota-Maharaj R, Blaha MJ, Blankstein R, Silverman MG, Eng J, Shaw LJ, et al. Association of coronary artery calcium and coronary heart disease events in young and elderly participants in the multi-ethnic study of atherosclerosis: a secondary analysis of a prospective, population-based cohort. Mayo Clin Proc. 2014;89(10):1350-9.
39. Dudum R, Dzaye O, Mirbolouk M, Dardari ZA, Orimoloye OA, Budoff MJ, et al. Coronary artery calcium scoring in low risk patients with family history of coronary heart disease: Validation of the SCCT guideline approach in the coronary artery calcium consortium. J Cardiovasc Comput Tomogr. 2019;13(3):21-5.
40. Matsumoto H, Watanabe S, Kyo E, Tsuji T, Ando Y, Otaki Y, et al. Standardized volumetric plaque quantification and characterization from coronary CT angiography: a head-to-head comparison with invasive intravascular ultrasound. Eur Radiol. 2019;26(10):019-06219.
41. Hell MM, Motwani, M, Otaki, Y, Cadet, S, Gransar, H, Miranda-Peats R, Valk J, Slomka PJ, Cheng V, Rozanski R, Tamarappoo BK, Hayes S, Achenbach S, Berman DS, Dey D. . Quantitative global plaque characteristics from coronary CT Angiography for the prediction of future cardiac death during 5 years of follow-up. European Heart Journal Cardiovascular Imaging. 2017;18(12):1331-9.
42. Naya M, Murthy VL, Foster CR, Gaber M, Klein J, Hainer J, et al. Prognostic interplay of coronary artery calcification and underlying vascular dysfunction in patients with suspected coronary artery disease. J Am Coll Cardiol. 2013;61(20):2098-106.
43. Driessen RS, Danad I, Stuijfzand WJ, Raijmakers PG, Schumacher SP, van Diemen PA, et al. Comparison of Coronary Computed Tomography Angiography,

Fractional Flow Reserve, and Perfusion Imaging for Ischemia Diagnosis. J Am Coll Cardiol. 2019;73(2):161-73.
44. Gaur S, Øvrehus KA, Dey D, Leipsic J, Bøtker HE, Jensen JM, et al. Coronary plaque quantification and fractional flow reserve by coronary computed tomography angiography identify ischaemia-causing lesions. European Heart Journal. 2016;37(15):1220-7.
45. Diaz Zamudio M, Dey D, Schuhbaeck A, Nakazato R. Slomka PJ, Bermand DS, Achenbach S, Min JK, Doh JH, Koo BK. Automated quantitative plaque burden from coronary CT Angiography noninvasively predicts hemodynamic significance by fractional flow reserve in intermediate coronary lesions Radiology. 2015:Aug;276(2):408-15. PubMed PMID: 25897475.
46. Diaz-Zamudio M FT, Slomka PJ, Arsanjani R, Gransar H, Germano G, Berman DS, Kaufmann P, Dey D. Quantitative plaque features from coronary computed tomography angiography to identify regional ischemia by myocardial perfusion imaging Eur Heart J Cardiovasc Imaging. 2017;18(5):499-507.
47. Dey D, Gaur S, Ovrehus KA, Slomka PJ, Betancur J, Goeller M, et al. Integrated prediction of lesion-specific ischaemia from quantitative coronary CT angiography using machine learning: a multicentre study. European Radiology. 2018;28:2655-64.
48. Joshi NV, Vesey AT, Williams MC, Shah AS, Calvert PA, Craighead FH, et al. 18F-fluoride positron emission tomography for identification of ruptured and high-risk coronary atherosclerotic plaques: a prospective clinical trial. Lancet. 2014;383(9918):705-13.
49. Kwiecinski J, Tzolos E, Adamson PD, Cadet S, Moss AJ, Joshi N, et al. Coronary (18)F-Sodium Fluoride Uptake Predicts Outcomes in Patients With Coronary Artery Disease. J Am Coll Cardiol. 2020;75(24):3061-74.
50. Creager MD, Hohl T, Hutcheson JD, Moss AJ, Schlotter F, Blaser MC, et al. (18)F-Fluoride Signal Amplification Identifies Microcalcifications Associated With Atherosclerotic Plaque Instability in Positron Emission Tomography/Computed Tomography Images. Circ Cardiovasc Imaging. 2019;12(1):e007835.
51. Bockisch A, Beyer T, Antoch G, Freudenberg LS, Kuhl H, Debatin JF, et al. Positron emission tomography/computed tomography--imaging protocols, artifacts, and pitfalls. Molecular imaging and biology : MIB : the official publication of the Academy of Molecular Imaging. 2004;6(4):188-99.
52. Ritman EL. Small-animal CT - Its Difference from, and Impact on, Clinical CT. Nucl Instrum Methods Phys Res A. 2007;580(2):968-70.
53. Baheza RA, Welch EB, Gochberg DF, Sanders M, Harvey S, Gore JC, et al. Detection of microcalcifications by characteristic magnetic susceptibility effects using MR phase image cross-correlation analysis. Med Phys. 2015;42(3):1436-52.
54. Blau M, Ganatra R, Bender MA. 18 F-fluoride for bone imaging. Seminars in nuclear medicine. 1972;2(1):31-7.
55. Hawkins RA, Choi Y, Huang SC, Hoh CK, Dahlbom M, Schiepers C, et al. Evaluation of the skeletal kinetics of fluorine-18-fluoride ion with PET. J Nucl Med. 1992;33(5):633-42.

56. Czernin J, Satyamurthy N, Schiepers C. Molecular mechanisms of bone 18F-NaF deposition. Journal of nuclear medicine : official publication, Society of Nuclear Medicine. 2010;51(12):1826-9.
57. Hoh CK, Hawkins RA, Dahlbom M, Glaspy JA, Seeger LL, Choi Y, et al. Whole body skeletal imaging with [18F]fluoride ion and PET. Journal of computer assisted tomography. 1993;17(1):34-41.
58. Blake GM, Park-Holohan SJ, Cook GJ, Fogelman I. Quantitative studies of bone with the use of 18F-fluoride and 99mTc-methylene diphosphonate. Seminars in nuclear medicine. 2001;31(1):28-49.
59. Moss AJ, Doris MK, Andrews JPM, Bing R, Daghem M, van Beek EJR, et al. Molecular Coronary Plaque Imaging Using (18)F-Fluoride. Circ Cardiovasc Imaging. 2019;12(8):e008574.
60. Blau M, Nagler W, Bender MA. Fluorine-18: a new isotope for bone scanning. J Nucl Med. 1962;3:332-4.
61. Andrews JPM, MacNaught G, Moss AJ, Doris MK, Pawade T, Adamson PD, et al. Cardiovascular (18)F-fluoride positron emission tomography-magnetic resonance imaging: A comparison study. J Nucl Cardiol. 2019.
62. Kwiecinski J, Berman DS, Lee SE, Dey D, Cadet S, Lassen ML, et al. Three-Hour Delayed Imaging Improves Assessment of Coronary (18)F-Sodium Fluoride PET. J Nucl Med. 2019;60(4):530-5.
63. Pawade TA, Cartlidge TR, Jenkins WS, Adamson PD, Robson P, Lucatelli C, et al. Optimization and Reproducibility of Aortic Valve 18F-Fluoride Positron Emission Tomography in Patients With Aortic Stenosis. Circ Cardiovasc Imaging. 2016;9(10).
64. Cocker MS, Spence JD, Hammond R, deKemp RA, Lum C, Wells G, et al. [18F]-Fluorodeoxyglucose PET/CT imaging as a marker of carotid plaque inflammation: Comparison to immunohistology and relationship to acuity of events. Int J Cardiol. 2018;271:378-86.
65. Aikawa E, Nahrendorf M, Sosnovik D, Lok VM, Jaffer FA, Aikawa M, et al. Multimodality molecular imaging identifies proteolytic and osteogenic activities in early aortic valve disease. Circulation. 2007;115(3):377-86.
66. Dweck MR, Jenkins WS, Vesey AT, Pringle MA, Chin CW, Malley TS, et al. 18F-sodium fluoride uptake is a marker of active calcification and disease progression in patients with aortic stenosis. Circ Cardiovasc Imaging. 2014;7(2):371-8.
67. Creager Michael D, Hohl T, Hutcheson Joshua D, Moss Alastair J, Schlotter F, Blaser Mark C, et al. 18F-Fluoride Signal Amplification Identifies Microcalcifications Associated With Atherosclerotic Plaque Instability in Positron Emission Tomography/Computed Tomography Images. Circulation: Cardiovascular Imaging. 2019;12(1):e007835.
68. Irkle A, Vesey AT, Lewis DY, Skepper JN, Bird JL, Dweck MR, et al. Identifying active vascular microcalcification by (18)F-sodium fluoride positron emission tomography. Nat Commun. 2015;6:7495.
69. Youn T, Al'Aref Subhi J, Narula N, Salvatore S, Pisapia D, Dweck Marc R, et al. 18F-Sodium Fluoride Positron Emission Tomography/Computed Tomography in Ex Vivo Human Coronary Arteries With Histological Correlation. Arteriosclerosis, Thrombosis, and Vascular Biology. 2020;40(2):404-11.

70. Derlin T, Richter U, Bannas P, Begemann P, Buchert R, Mester J, et al. Feasibility of 18F-sodium fluoride PET/CT for imaging of atherosclerotic plaque. J Nucl Med. 2010;51(6):862-5.
71. Lubbers M, Dedic A, Coenen A, Galema T, Akkerhuis J, Bruning T, et al. Calcium imaging and selective computed tomography angiography in comparison to functional testing for suspected coronary artery disease: the multicentre, randomized CRESCENT trial. Eur Heart J. 2016;37(15):1232-43.
72. Yun M, Yeh D, Araujo LI, Jang S, Newberg A, Alavi A. F-18 FDG uptake in the large arteries: a new observation. Clinical nuclear medicine. 2001;26(4):314-9.
73. Yun M, Jang S, Cucchiara A, Newberg AB, Alavi A. 18F FDG uptake in the large arteries: a correlation study with the atherogenic risk factors. Seminars in nuclear medicine. 2002;32(1):70-6.
74. Tatsumi M, Cohade C, Nakamoto Y, Wahl RL. Fluorodeoxyglucose uptake in the aortic wall at PET/CT: possible finding for active atherosclerosis. Radiology. 2003;229(3):831-7.
75. Tahara N, Kai H, Yamagishi S, Mizoguchi M, Nakaura H, Ishibashi M, et al. Vascular inflammation evaluated by [18F]-fluorodeoxyglucose positron emission tomography is associated with the metabolic syndrome. J Am Coll Cardiol. 2007;49(14):1533-9.
76. Joshi NV, Vesey A, Newby DE, Dweck MR. Will 18F-sodium fluoride PET-CT imaging be the magic bullet for identifying vulnerable coronary atherosclerotic plaques? Curr Cardiol Rep. 2014;16(9):521.
77. Adamson PD, Vesey AT, Joshi NV, Newby DE, Dweck MR. Salt in the wound: (18)F-fluoride positron emission tomography for identification of vulnerable coronary plaques. Cardiovasc Diagn Ther. 2015;5(2):150-5.
78. Dweck MR, Chow MW, Joshi NV, Williams MC, Jones C, Fletcher AM, et al. Coronary arterial 18F-sodium fluoride uptake: a novel marker of plaque biology. J Am Coll Cardiol. 2012;59(17):1539-48.
79. Li Y, Berenji GR, Shaba WF, Tafti B, Yevdayev E, Dadparvar S. Association of vascular fluoride uptake with vascular calcification and coronary artery disease. Nuclear medicine communications. 2012;33(1):14-20.
80. Oliveira-Santos M, Castelo-Branco M, Silva R, Gomes A, Chichorro N, Abrunhosa A, et al. Atherosclerotic plaque metabolism in high cardiovascular risk subjects - A subclinical atherosclerosis imaging study with (18)F-NaF PET-CT. Atherosclerosis. 2017;260:41-6.
81. Kwiecinski J, Dey D, Cadet S, Lee SE, Tamarappoo B, Otaki Y, et al. Predictors of 18F-sodium fluoride uptake in patients with stable coronary artery disease and adverse plaque features on computed tomography angiography. Eur Heart J Cardiovasc Imaging. 2019.
82. Kitagawa T, Yamamoto H, Nakamoto Y, Sasaki K, Toshimitsu S, Tatsugami F, et al. Predictive Value of (18)F-Sodium Fluoride Positron Emission Tomography in Detecting High-Risk Coronary Artery Disease in Combination With Computed Tomography. J Am Heart Assoc. 2018;7(20):e010224.
83. Lee JM, Bang JI, Koo BK, Hwang D, Park J, Zhang J, et al. Clinical Relevance of (18)F-Sodium Fluoride Positron-Emission Tomography in Noninvasive

Identification of High-Risk Plaque in Patients With Coronary Artery Disease. Circ Cardiovasc Imaging. 2017;10(11).
84. Kwiecinski J, Dey D, Cadet S, Lee SE, Otaki Y, Huynh PT, et al. Peri-Coronary Adipose Tissue Density Is Associated With (18)F-Sodium Fluoride Coronary Uptake in Stable Patients With High-Risk Plaques. JACC Cardiovascular imaging. 2019;11(19):30076-2.
85. Thaden JJ, Nkomo VT, Enriquez-Sarano M. The global burden of aortic stenosis. Prog Cardiovasc Dis. 2014;56(6):565-71.
86. Brown JM, O'Brien SM, Wu C, Sikora JA, Griffith BP, Gammie JS. Isolated aortic valve replacement in North America comprising 108,687 patients in 10 years: changes in risks, valve types, and outcomes in the Society of Thoracic Surgeons National Database. The Journal of thoracic and cardiovascular surgery. 2009;137(1):82-90.
87. Brennan JM, Thomas L, Cohen DJ, Shahian D, Wang A, Mack MJ, et al. Transcatheter Versus Surgical Aortic Valve Replacement: Propensity-Matched Comparison. J Am Coll Cardiol. 2017;70(4):439-50.
88. Dweck MR, Jones C, Joshi NV, Fletcher AM, Richardson H, White A, et al. Assessment of valvular calcification and inflammation by positron emission tomography in patients with aortic stenosis. Circulation. 2012;125(1):76-86.
89. Dweck MR, Khaw HJ, Sng GK, Luo EL, Baird A, Williams MC, et al. Aortic stenosis, atherosclerosis, and skeletal bone: is there a common link with calcification and inflammation? Eur Heart J. 2013;34(21):1567-74.
90. Baumgartner H, Falk V, Bax JJ, De Bonis M, Hamm C, Holm PJ, et al. 2017 ESC/EACTS Guidelines for the management of valvular heart disease. European Heart Journal. 2017;38(36):2739-91.
91. Clavel MA, Burwash IG, Pibarot P. Cardiac Imaging for Assessing Low-Gradient Severe Aortic Stenosis. JACC Cardiovasc Imaging. 2017;10(2):185-202.
92. Nkomo VT, Gardin JM, Skelton TN, Gottdiener JS, Scott CG, Enriquez-Sarano M. Burden of valvular heart diseases: a population-based study. Lancet. 2006;368(9540):1005-11.
93. Cribier A, Eltchaninoff H, Bash A, Borenstein N, Tron C, Bauer F, et al. Percutaneous transcatheter implantation of an aortic valve prosthesis for calcific aortic stenosis: first human case description. Circulation. 2002;106(24):3006-8.
94. Carroll JD, Mack MJ, Vemulapalli S, Herrmann HC, Gleason TG, Hanzel G, et al. STS-ACC TVT Registry of Transcatheter Aortic Valve Replacement. J Am Coll Cardiol. 2020;76(21):2492-516.
95. Rodriguez-Gabella T, Voisine P, Puri R, Pibarot P, Rodes-Cabau J. Aortic Bioprosthetic Valve Durability: Incidence, Mechanisms, Predictors, and Management of Surgical and Transcatheter Valve Degeneration. J Am Coll Cardiol. 2017;70(8):1013-28.
96. Sondergaard L, Ihlemann N, Capodanno D, Jorgensen TH, Nissen H, Kjeldsen BJ, et al. Durability of Transcatheter and Surgical Bioprosthetic Aortic Valves in Patients at Lower Surgical Risk. J Am Coll Cardiol. 2019;73(5):546-53.
97. Vogt PR, Brunner-LaRocca H, Sidler P, Zund G, Truniger K, Lachat M, et al. Reoperative surgery for degenerated aortic bioprostheses: predictors for emergency surgery and reoperative mortality. European journal of cardio-

thoracic surgery : official journal of the European Association for Cardio-thoracic Surgery. 2000;17(2):134-9.
98. Cartlidge TR, Pawade TA, Dweck MR. Aortic stenosis and CT calcium scoring: is it for everyone? Heart. 2017;103(1):8-9.
99. Cartlidge TRG, Doris MK, Sellers SL, Pawade TA, White AC, Pessotto R, et al. Detection and Prediction of Bioprosthetic Aortic Valve Degeneration. J Am Coll Cardiol. 2019;73(10):1107-19.
100. Thygesen K, Alpert JS, Jaffe AS, Chaitman BR, Bax JJ, Morrow DA, et al. Fourth Universal Definition of Myocardial Infarction (2018). Circulation. 2018;138(20):e618-e51.
101. Moss AJ, Dweck MR, Doris MK, Andrews JPM, Bing R, Forsythe RO, et al. Ticagrelor to Reduce Myocardial Injury in Patients With High-Risk Coronary Artery Plaque. JACC Cardiovasc Imaging. 2019.
102. Carter WA, Estes EH, Jr. Electrocardiographic Manifestations of Ventricular Hypertrophy; a Computer Study of Ecg-Anatomic Correlations in 319 Cases. Am Heart J. 1964;68:173-82.
103. Singh S, Goyal A. The origin of echocardiography: a tribute to Inge Edler. Texas Heart Institute journal. 2007;34(4):431-8.
104. Baumgartner H, Hung J, Bermejo J, Chambers JB, Edvardsen T, Goldstein S, et al. Recommendations on the Echocardiographic Assessment of Aortic Valve Stenosis: A Focused Update from the European Association of Cardiovascular Imaging and the American Society of Echocardiography. Journal of the American Society of Echocardiography : official publication of the American Society of Echocardiography. 2017;30(4):372-92.
105. Baumgartner H, Hung J, Bermejo J, Chambers JB, Edvardsen T, Goldstein S, et al. Recommendations on the Echocardiographic Assessment of Aortic Valve Stenosis: A Focused Update from the European Association of Cardiovascular Imaging and the American Society of Echocardiography. Journal Of The American Society Of Echocardiography: Official Publication Of The American Society Of Echocardiography. 2017;30(4):372-92.
106. Rosenhek R, Binder T, Porenta G, Lang I, Christ G, Schemper M, et al. Predictors of outcome in severe, asymptomatic aortic stenosis. The New England journal of medicine. 2000;343(9):611-7.
107. Smith LA, Cowell SJ, White AC, Boon NA, Newby DE, Northridge DB. Contrast agent increases Doppler velocities and improves reproducibility of aortic valve area measurements in patients with aortic stenosis. Journal of the American Society of Echocardiography : official publication of the American Society of Echocardiography. 2004;17(3):247-52.
108. Zoghbi WA, Chambers JB, Dumesnil JG, Foster E, Gottdiener JS, Grayburn PA, et al. Recommendations for evaluation of prosthetic valves with echocardiography and doppler ultrasound: a report From the American Society of Echocardiography's Guidelines and Standards Committee and the Task Force on Prosthetic Valves, developed in conjunction with the American College of Cardiology Cardiovascular Imaging Committee, Cardiac Imaging Committee of the American Heart Association, the European Association of Echocardiography, a registered branch of the European Society of Cardiology, the Japanese Society of Echocardiography and the Canadian Society of Echocardiography, endorsed

by the American College of Cardiology Foundation, American Heart Association, European Association of Echocardiography, a registered branch of the European Society of Cardiology, the Japanese Society of Echocardiography, and Canadian Society of Echocardiography. J Am Soc Echocardiogr. 2009;22(9):975-1014; quiz 82-4.
109. Rubeaux M, Joshi NV, Dweck MR, Fletcher A, Motwani M, Thomson LE, et al. Motion Correction of 18F-NaF PET for Imaging Coronary Atherosclerotic Plaques. J Nucl Med. 2016;57(1):54-9.
110. Massera D, Doris MK, Cadet S, Kwiecinski J, Pawade TA, Peeters F, et al. Analytical quantification of aortic valve 18F-sodium fluoride PET uptake. J Nucl Cardiol. 2018.
111. Kwiecinski J, Adamson PD, Lassen ML, Doris MK, Moss AJ, Cadet S, et al. Feasibility of Coronary (18)F-Sodium Fluoride Positron-Emission Tomography Assessment With the Utilization of Previously Acquired Computed Tomography Angiography. Circ Cardiovasc Imaging. 2018;11(12):e008325.
112. Kwiecinski J, Cadet S, Dey D, Daghem M, Lassen ML, Germano G, et al. 5966Whole-vessel coronary 18F-sodium fluoride coronary microcalfication activity is associated with Low density plaque. European Heart Journal. 2019;40(Supplement_1).
113. Massera D, Doris MK, Cadet S, Kwiecinski J, Pawade TA, Peeters F, et al. Analytical quantification of aortic valve 18F-sodium fluoride PET uptake. Journal of nuclear cardiology : official publication of the American Society of Nuclear Cardiology. 2020;27(3):962-72.
114. Doris MK, Rubeaux M, Pawade T, Otaki Y, Xie Y, Li D, et al. Motion-Corrected Imaging of the Aortic Valve with (18)F-NaF PET/CT and PET/MRI: A Feasibility Study. J Nucl Med. 2017;58(11):1811-4.
115. Rubeaux M, Joshi N, Dweck MR, Fletcher A, Motwani M, Thomson LE, et al. Demons versus Level-Set motion registration for coronary (18)F-sodium fluoride PET. Proc SPIE Int Soc Opt Eng. 2016;9784.
116. Doris MK, Otaki Y, Krishnan SK, Kwiecinski J, Rubeaux M, Alessio A, et al. Optimization of reconstruction and quantification of motion-corrected coronary PET-CT. Journal of nuclear cardiology : official publication of the American Society of Nuclear Cardiology. 2020;27(2):494-504.
117. Lassen ML, Kwiecinski J, Dey D, Cadet S, Germano G, Berman DS, et al. Triple-gated motion and blood pool clearance corrections improve reproducibility of coronary (18)F-NaF PET. Eur J Nucl Med Mol Imaging. 2019;46(12):2610-20.
118. Leipsic J, Abbara S, Achenbach S, Cury R, Earls JP, Mancini GJ, et al. SCCT guidelines for the interpretation and reporting of coronary CT angiography: a report of the Society of Cardiovascular Computed Tomography Guidelines Committee. J Cardiovasc Comput Tomogr. 2014;8(5):342-58.
119. Massera D, Trivieri MG, Andrews JPM, Sartori S, Abgral R, Chapman AR, et al. Disease Activity in Mitral Annular Calcification. Circ Cardiovasc Imaging. 2019;12(2):e008513.
120. Kwiecinski J, Cadet S, Daghem M, Lassen ML, Dey D, Dweck MR, et al. Whole-vessel coronary (18)F-sodium fluoride PET for assessment of the global coronary microcalcification burden. Eur J Nucl Med Mol Imaging. 2020.

121. Kwiecinski J, Slomka PJ, Dweck MR, Newby DE, Berman DS. Vulnerable plaque imaging using 18F-sodium fluoride positron emission tomography. The British Journal of Radiology. 2019:20190797.
122. Chen W, Dilsizian V. PET assessment of vascular inflammation and atherosclerotic plaques: SUV or TBR? J Nucl Med. 2015;56(4):503-4.
123. Blomberg BA, Bashyam A, Ramachandran A, Gholami S, Houshmand S, Salavati A, et al. Quantifying [18F]fluorodeoxyglucose uptake in the arterial wall: the effects of dual time-point imaging and partial volume effect correction. European Journal of Nuclear Medicine and Molecular Imaging. 2015;42(9):1414-22.
124. Rahim MK, Kim SE, So H, Kim HJ, Cheon GJ, Lee ES, et al. Recent Trends in PET Image Interpretations Using Volumetric and Texture-based Quantification Methods in Nuclear Oncology. Nucl Med Mol Imaging. 2014;48(1):1-15.
125. Larson SM, Erdi Y, Akhurst T, Mazumdar M, Macapinlac HA, Finn RD, et al. Tumor Treatment Response Based on Visual and Quantitative Changes in Global Tumor Glycolysis Using PET-FDG Imaging. The Visual Response Score and the Change in Total Lesion Glycolysis. Clin Positron Imaging. 1999;2(3):159-71.
126. Ahmadian A, Brogan A, Berman J, Sverdlov AL, Mercier G, Mazzini M, et al. Quantitative interpretation of FDG PET/CT with myocardial perfusion imaging increases diagnostic information in the evaluation of cardiac sarcoidosis. J Nucl Cardiol. 2014;21(5):925-39.
127. Dey D, Schepis T, Marwan M, Slomka PJ, Berman DS, Achenbach S. Automated Three-dimensional Quantification of Non-calcified Coronary Plaque from Coronary CT Angiography: comparison with Intravascular Ultrasound Radiology. 2010;257(2):516-22.
128. Doris MK, Otaki Y, Krishnan SK, Kwiecinski J, Rubeaux M, Alessio A, et al. Optimization of reconstruction and quantification of motion-corrected coronary PET-CT. J Nucl Cardiol. 2018.
129. Lassen ML, Kwiecinski J, Cadet S, Dey D, Wang C, Dweck MR, et al. Data-Driven Gross Patient Motion Detection and Compensation: Implications for Coronary (18)F-NaF PET Imaging. J Nucl Med. 2019;60(6):830-6.
130. Agatston AS, Janowitz WR, Hildner FJ, Zusmer NR, Viamonte M, Jr., Detrano R. Quantification of coronary artery calcium using ultrafast computed tomography. J Am Coll Cardiol. 1990;15(4):827-32.
131. Arbab-Zadeh A, Fuster V. The Myth of the "Vulnerable Plaque". Transitioning From a Focus on Individual Lesions to Atherosclerotic Disease Burden for Coronary Artery Disease Risk Assessment. 2015;65(8):846-55.
132. Arbab-Zadeh A, Fuster V. From Detecting the Vulnerable Plaque to Managing the Vulnerable Patient: JACC State-of-the-Art Review. J Am Coll Cardiol. 2019;74(12):1582-93.
133. Bellinge JW, Francis RJ, Majeed K, Watts GF, Schultz CJ. In search of the vulnerable patient or the vulnerable plaque: (18)F-sodium fluoride positron emission tomography for cardiovascular risk stratification. J Nucl Cardiol. 2018;25(5):1774-83.
134. Budoff MJ, Young R, Burke G, Jeffrey Carr J, Detrano RC, Folsom AR, et al. Ten-year association of coronary artery calcium with atherosclerotic

cardiovascular disease (ASCVD) events: the multi-ethnic study of atherosclerosis (MESA). Eur Heart J. 2018;39(25):2401-8.
135. Greenland P, Bonow RO, Brundage BH, Budoff MJ, Eisenberg MJ, Grundy SM, et al. ACCF/AHA 2007 clinical expert consensus document on coronary artery calcium scoring by computed tomography in global cardiovascular risk assessment and in evaluation of patients with chest pain: a report of the American College of Cardiology Foundation Clinical Expert Consensus Task Force (ACCF/AHA Writing Committee to Update the 2000 Expert Consensus Document on Electron Beam Computed Tomography) developed in collaboration with the Society of Atherosclerosis Imaging and Prevention and the Society of Cardiovascular Computed Tomography. J Am Coll Cardiol. 2007;49(3):378-402.
136. Budoff MJ, Mayrhofer T, Ferencik M, Bittner D, Lee KL, Lu MT, et al. Prognostic value of coronary artery calcium in the PROMISE study (Prospective Multicenter Imaging Study for Evaluation of Chest Pain). Circulation. 2017;136(21):1993-2005.
137. Erbel R, Mohlenkamp S, Moebus S, Schmermund A, Lehmann N, Stang A, et al. Coronary risk stratification, discrimination, and reclassification improvement based on quantification of subclinical coronary atherosclerosis: the Heinz Nixdorf Recall study. J Am Coll Cardiol. 2010;56(17):1397-406.
138. Doris M, Moss AJ, Andrews JPM, Williams M, Van Beek EJR, Forsyth L, et al. Coronary 18F-sodium fluoride uptake predicts progression of coronary arterial calcification. European Heart Journal. 2019;40:53-.
139. 18F-Sodium Fluoride Coronary Uptake Predicts Outcome in Patients with Coronary Artery Disease [press release]. JACC2020.
140. Gould KL, Pan T, Loghin C, Johnson NP, Guha A, Sdringola S. Frequent diagnostic errors in cardiac PET/CT due to misregistration of CT attenuation and emission PET images: a definitive analysis of causes, consequences, and corrections. J Nucl Med. 2007;48(7):1112-21.
141. Martinez-Moller A, Souvatzoglou M, Navab N, Schwaiger M, Nekolla SG. Artifacts from misaligned CT in cardiac perfusion PET/CT studies: frequency, effects, and potential solutions. J Nucl Med. 2007;48(2):188-93.
142. Slomka PJ, Rubeaux M, Le Meunier L, Dey D, Lazewatsky JL, Pan T, et al. Dual-Gated Motion-Frozen Cardiac PET with Flurpiridaz F 18. J Nucl Med. 2015;56(12):1876-81.
143. Slomka PJ, Diaz-Zamudio M, Dey D, Motwani M, Brodov Y, Choi D, et al. Automatic registration of misaligned CT attenuation correction maps in Rb-82 PET/CT improves detection of angiographically significant coronary artery disease. Journal of nuclear cardiology : official publication of the American Society of Nuclear Cardiology. 2015;22(6):1285-95.
144. Loghin C, Sdringola S, Gould KL. Common artifacts in PET myocardial perfusion images due to attenuation-emission misregistration: clinical significance, causes, and solutions. J Nucl Med. 2004;45(6):1029-39.
145. Koshino K, Fukushima K, Fukumoto M, Sasaki K, Moriguchi T, Hori Y, et al. Breath-hold CT attenuation correction for quantitative cardiac SPECT. EJNMMI Res. 2012;2(1):33.

146. Kovalski G, Israel O, Keidar Z, Frenkel A, Sachs J, Azhari H. Correction of heart motion due to respiration in clinical myocardial perfusion SPECT scans using respiratory gating. J Nucl Med. 2007;48(4):630-6.
147. Fricke H, Fricke E, Weise R, Kammeier A, Lindner O, Burchert W. A method to remove artifacts in attenuation-corrected myocardial perfusion SPECT Introduced by misalignment between emission scan and CT-derived attenuation maps. J Nucl Med. 2004;45(10):1619-25.
148. Pan T, Lee TY, Rietzel E, Chen GT. 4D-CT imaging of a volume influenced by respiratory motion on multi-slice CT. Medical physics. 2004;31(2):333-40.
149. Pan T, Mawlawi O, Luo D, Liu HH, Chi PC, Mar MV, et al. Attenuation correction of PET cardiac data with low-dose average CT in PET/CT. Medical physics. 2006;33(10):3931-8.
150. Tzolos E KJ, Lassen ML, Cadet S, Adamson P, Moss A et al. Observer repeatability and interscan reproducibility of 18F-sodium fluoride coronary microcalcification activity. JNC. 2020.
151. ClinicalTrials.gov. Effect of Evolocumab on Coronary Artery Plaque Volume and Composition by CCTA and Microcalcification by F18-NaF 2018 [Available from: https://clinicaltrials.gov/ct2/show/NCT03689946.
152. Chin BB, Nakamoto Y, Kraitchman DL, Marshall L, Wahl R. PET-CT evaluation of 2-deoxy-2-[18F]fluoro-D-glucose myocardial uptake: effect of respiratory motion. Molecular imaging and biology : MIB : the official publication of the Academy of Molecular Imaging. 2003;5(2):57-64.
153. Goerres GW, Burger C, Kamel E, Seifert B, Kaim AH, Buck A, et al. Respiration-induced attenuation artifact at PET/CT: technical considerations. Radiology. 2003;226(3):906-10.
154. Goerres GW, Kamel E, Heidelberg TN, Schwitter MR, Burger C, von Schulthess GK. PET-CT image co-registration in the thorax: influence of respiration. European journal of nuclear medicine and molecular imaging. 2002;29(3):351-60.
155. Beyer T, Antoch G, Blodgett T, Freudenberg LF, Akhurst T, Mueller S. Dual-modality PET/CT imaging: the effect of respiratory motion on combined image quality in clinical oncology. European journal of nuclear medicine and molecular imaging. 2003;30(4):588-96.
156. Nakamoto Y, Osman M, Cohade C, Marshall LT, Links JM, Kohlmyer S, et al. PET/CT: comparison of quantitative tracer uptake between germanium and CT transmission attenuation-corrected images. J Nucl Med. 2002;43(9):1137-43.
157. Chi PC, Mawlawi O, Luo D, Liao Z, Macapinlac HA, Pan T. Effects of respiration-averaged computed tomography on positron emission tomography/computed tomography quantification and its potential impact on gross tumor volume delineation. Int J Radiat Oncol Biol Phys. 2008;71(3):890-9.
158. Suzuki Y, Slomka PJ, Wolak A, Ohba M, Suzuki S, De Yang L, et al. Motion-frozen myocardial perfusion SPECT improves detection of coronary artery disease in obese patients. J Nucl Med. 2008;49(7):1075-9.
159. Dawood M, Buther F, Stegger L, Jiang X, Schober O, Schafers M, et al. Optimal number of respiratory gates in positron emission tomography: a cardiac patient study. Medical physics. 2009;36(5):1775-84.

160. Shechter G, Resar JR, McVeigh ER. Displacement and velocity of the coronary arteries: cardiac and respiratory motion. IEEE Trans Med Imaging. 2006;25(3):369-75.
161. Dorresteijn JA, Visseren FL, Wassink AM, Gondrie MJ, Steyerberg EW, Ridker PM, et al. Development and validation of a prediction rule for recurrent vascular events based on a cohort study of patients with arterial disease: the SMART risk score. Heart. 2013;99(12):866-72.
162. Delgado V, Saraste A, Dweck M, Bucciarelli-Ducci C, Bax JJ. Multimodality imaging: Bird's eye view from the European Society of Cardiology Congress 2019 Paris, August 31st-September 4th, 2019. J Nucl Cardiol. 2019.
163. Doris M, Moss AJ, Andrews JPM, Williams M, Van Beek EJR, Forsyth L, et al. 172Coronary 18F-sodium fluoride uptake predicts progression of coronary arterial calcification. European Heart Journal. 2019;40(Supplement_1).
164. Min JK, Shaw LJ, Devereux RB, Okin PM, Weinsaft JW, Russo DJ, et al. Prognostic value of multidetector coronary computed tomographic angiography for prediction of all-cause mortality. J Am Coll Cardiol. 2007;50(12):1161-70.
165. Maron DJ, Harrington RA, Hochman JS. Planning and Conducting the ISCHEMIA Trial. Circulation. 2018;138(14):1384-6.
166. Kaasenbrood L, Bhatt DL, Dorresteijn JAN, Wilson PWF, D'Agostino RB, Sr., Massaro JM, et al. Estimated Life Expectancy Without Recurrent Cardiovascular Events in Patients With Vascular Disease: The SMART-REACH Model. J Am Heart Assoc. 2018;7(16):e009217.
167. Hoffmann U, Ferencik M, Udelson JE, Picard MH, Truong QA, Patel MR, et al. Prognostic Value of Noninvasive Cardiovascular Testing in Patients With Stable Chest Pain: Insights From the PROMISE Trial (Prospective Multicenter Imaging Study for Evaluation of Chest Pain). Circulation. 2017;135(24):2320-32.
168. Motwani M, Dey D, Berman DS, Germano G, Achenbach S, Al-Mallah MH, et al. Machine learning for prediction of all-cause mortality in patients with suspected coronary artery disease: a 5-year multicentre prospective registry analysis. Eur Heart J. 2017;38(7):500-7.
169. Commandeur F, Slomka, P.J., Goeller M, Chen, X, Cadet, S, Razipour, A, McElhinney, P, Gransar, H, Cantu, S, Miller R.J.H, Rozanski A, Achenbach S, Tamarappoo B.K., Berman D.S., Dey D. Machine learning to predict the long-term risk of myocardial infarction and cardiac death based on clinical risk, coronary calcium score and epicardial adipose tissue: a prospective study. European Society Of Cardiology Annual Scientific Sessions; European Heart Journal (supplement). 2019:in press.
170. Kim J-H. Estimating classification error rate: Repeated cross-validation, repeated hold-out and bootstrap. Computational Statistics & Data Analysis. 2009;53(11):3735-45.
171. Hastie T TR, Friedman J. . The Elements of Statistical Learning Data Mining, Inference and Prediction. 2001.
172. DeLong ER, DeLong DM, Clarke-Pearson DL. Comparing the Areas under Two or More Correlated Receiver Operating Characteristic Curves: A Nonparametric Approach. Biometrics. 2007;44(3):837-45.

173. Forsythe RO, Dweck MR, McBride OMB, Vesey AT, Semple SI, Shah ASV, et al. (18)F-Sodium Fluoride Uptake in Abdominal Aortic Aneurysms: The SoFIA(3) Study. J Am Coll Cardiol. 2018;71(5):513-23.
174. van Rosendael AR, Maliakal G, Kolli KK, Beecy A, Al'Aref SJ, Dwivedi A, et al. Maximization of the usage of coronary CTA derived plaque information using a machine learning based algorithm to improve risk stratification; insights from the CONFIRM registry. J Cardiovasc Comput Tomogr. 2018;12(3):204-9.
175. Mack MJ, Leon MB, Thourani VH, Makkar R, Kodali SK, Russo M, et al. Transcatheter Aortic-Valve Replacement with a Balloon-Expandable Valve in Low-Risk Patients. N Engl J Med. 2019;380(18):1695-705.
176. Popma JJ, Deeb GM, Yakubov SJ, Mumtaz M, Gada H, O'Hair D, et al. Transcatheter Aortic-Valve Replacement with a Self-Expanding Valve in Low-Risk Patients. N Engl J Med. 2019;380(18):1706-15.
177. Rajamannan NM, Evans FJ, Aikawa E, Grande-Allen KJ, Demer LL, Heistad DD, et al. Calcific aortic valve disease: not simply a degenerative process: A review and agenda for research from the National Heart and Lung and Blood Institute Aortic Stenosis Working Group. Executive summary: Calcific aortic valve disease-2011 update. Circulation. 2011;124(16):1783-91.
178. Salaun E, Mahjoub H, Dahou A, Mathieu P, Larose E, Despres JP, et al. Hemodynamic Deterioration of Surgically Implanted Bioprosthetic Aortic Valves. J Am Coll Cardiol. 2018;72(3):241-51.
179. Sellers SL, Turner CT, Sathananthan J, Cartlidge TRG, Sin F, Bouchareb R, et al. Transcatheter Aortic Heart Valves: Histological Analysis Providing Insight to Leaflet Thickening and Structural Valve Degeneration. JACC Cardiovascular imaging. 2019;12(1):135-45.
180. Dvir D, Bourguignon T, Otto CM, Hahn RT, Rosenhek R, Webb JG, et al. Standardized Definition of Structural Valve Degeneration for Surgical and Transcatheter Bioprosthetic Aortic Valves. Circulation. 2018;137(4):388-99.
181. Kwiecinski J, Tzolos E, Cartlidge TRG, Fletcher A, Doris MK, Bing R, et al. Native Aortic Valve Disease Progression and Bioprosthetic Valve Degeneration in Patients with Transcatheter Aortic Valve Implantation. Circulation. 2021.
182. Varc-3 Writing C, Genereux P, Piazza N, Alu MC, Nazif T, Hahn RT, et al. Valve Academic Research Consortium 3: updated endpoint definitions for aortic valve clinical research. Eur Heart J. 2021;42(19):1825-57.
183. Makkar RR, Fontana G, Jilaihawi H, Chakravarty T, Kofoed KF, De Backer O, et al. Possible Subclinical Leaflet Thrombosis in Bioprosthetic Aortic Valves. N Engl J Med. 2015;373(21):2015-24.
184. Blanke P, Leipsic JA, Popma JJ, Yakubov SJ, Deeb GM, Gada H, et al. Bioprosthetic Aortic Valve Leaflet Thickening in the Evolut Low Risk Sub-Study. J Am Coll Cardiol. 2020;75(19):2430-42.
185. Fujita B, Kutting M, Seiffert M, Scholtz S, Egron S, Prashovikj E, et al. Calcium distribution patterns of the aortic valve as a risk factor for the need of permanent pacemaker implantation after transcatheter aortic valve implantation. Eur Heart J Cardiovasc Imaging. 2016;17(12):1385-93.
186. Dweck MR, Jenkins WS, Vesey AT, Pringle MA, Chin CW, Malley TS, et al. 18F-NaF Uptake Is a Marker of Active Calcification and Disease Progression in Patients with Aortic Stenosis. Circ Cardiovasc Imaging. 2014.

187. Chester AH, El-Hamamsy I, Butcher JT, Latif N, Bertazzo S, Yacoub MH. The living aortic valve: From molecules to function. Glob Cardiol Sci Pract. 2014;2014(1):52-77.
188. Pawade TA, Doris MK, Bing R, White AC, Forsyth L, Evans E, et al. Effect of Denosumab or Alendronic Acid on the Progression of Aortic Stenosis: A Double-Blind Randomized Controlled Trial. Circulation. 2021;143(25):2418-27.
189. Demer LL, Tintut Y. Hearts of Stone: Calcific Aortic Stenosis and Antiresorptive Agents for Osteoporosis. Circulation. 2021;143(25):2428-30.
190. ClinicalTrials.gov. National Library of Medicine (U.S.). Study Prediction of Recurrent Events With 18F-Fluoride. . Accessed 4th November 2021.
191. Oikonomou EK, Marwan M, Desai MY, Mancio J, Alashi A, Hutt Centeno E, et al. Non-invasive detection of coronary inflammation using computed tomography and prediction of residual cardiovascular risk (the CRISP CT study): a post-hoc analysis of prospective outcome data. The Lancet. 2018;392(10151):929-39.
192. Investigators S-H, Newby DE, Adamson PD, Berry C, Boon NA, Dweck MR, et al. Coronary CT Angiography and 5-Year Risk of Myocardial Infarction. N Engl J Med. 2018;379(10):924-33.
193. Kwiecinski J, Tzolos E, Meah M, Cadet S, Adamson PD, Grodecki K, et al. Machine-learning with (18)F-sodium fluoride PET and quantitative plaque analysis on CT angiography for the future risk of myocardial infarction. J Nucl Med. 2021.
194. Cowell SJ, Newby DE, Prescott RJ, Bloomfield P, Reid J, Northridge DB, et al. A randomized trial of intensive lipid-lowering therapy in calcific aortic stenosis. N Engl J Med. 2005;352(23):2389-97.
195. Chan KL, Teo K, Dumesnil JG, Ni A, Tam J, Investigators A. Effect of Lipid lowering with rosuvastatin on progression of aortic stenosis: results of the aortic stenosis progression observation: measuring effects of rosuvastatin (ASTRONOMER) trial. Circulation. 2010;121(2):306-14.
196. Rossebo AB, Pedersen TR, Boman K, Brudi P, Chambers JB, Egstrup K, et al. Intensive lipid lowering with simvastatin and ezetimibe in aortic stenosis. N Engl J Med. 2008;359(13):1343-56.
197. Zheng KH, Tzolos E, Dweck MR. Pathophysiology of Aortic Stenosis and Future Perspectives for Medical Therapy. Cardiol Clin. 2020;38(1):1-12.
198. Tzolos E, Dweck MR. Threshold effect for lipoprotein(a) in aortic stenosis. Heart. 2021;107(17):1367-8.
199. Capoulade R, Yeang C, Chan KL, Pibarot P, Tsimikas S. Association of Mild to Moderate Aortic Valve Stenosis Progression With Higher Lipoprotein(a) and Oxidized Phospholipid Levels: Secondary Analysis of a Randomized Clinical Trial. JAMA Cardiol. 2018.
200. Zheng KH, Tsimikas S, Pawade T, Kroon J, Jenkins WSA, Doris MK, et al. Lipoprotein(a) and Oxidized Phospholipids Promote Valve Calcification in Patients With Aortic Stenosis. J Am Coll Cardiol. 2019;73(17):2150-62.
201. Capoulade R, Chan KL, Yeang C, Mathieu P, Bosse Y, Dumesnil JG, et al. Oxidized Phospholipids, Lipoprotein(a), and Progression of Calcific Aortic Valve Stenosis. J Am Coll Cardiol. 2015;66(11):1236-46.

202. Jenkins WS, Vesey AT, Shah AS, Pawade TA, Chin CW, White AC, et al. Valvular (18)F-Fluoride and (18)F-Fluorodeoxyglucose Uptake Predict Disease Progression and Clinical Outcome in Patients With Aortic Stenosis. J Am Coll Cardiol. 2015;66(10):1200-1.
203. Peeters F, van Mourik MJW, Meex SJR, Bucerius J, Schalla SM, Gerretsen SC, et al. Bicuspid Aortic Valve Stenosis and the Effect of Vitamin K2 on Calcification Using (18)F-Sodium Fluoride Positron Emission Tomography/Magnetic Resonance: The BASIK2 Rationale and Trial Design. Nutrients. 2018;10(4).
204. Lohrke J, Siebeneicher H, Berger M, Reinhardt M, Berndt M, Mueller A, et al. (18)F-GP1, a Novel PET Tracer Designed for High-Sensitivity, Low-Background Detection of Thrombi. J Nucl Med. 2017;58(7):1094-9.
205. Kim C, Lee JS, Han Y, Chae SY, Jin S, Sung C, et al. Glycoprotein IIb/IIIa receptor imaging with (18)F-GP1 positron emission tomography for acute venous thromboembolism: an open-label, non-randomized, first-in-human phase 1 study. Journal of nuclear medicine : official publication, Society of Nuclear Medicine. 2018;60(2):244-9.
206. Chae SY, Kwon TW, Jin S, Kwon SU, Sung C, Oh SJ, et al. A phase 1, first-in-human study of (18)F-GP1 positron emission tomography for imaging acute arterial thrombosis. EJNMMI Res. 2019;9(1):3.
207. Tzolos E, Bing R, Newby DE, Dweck MR. Categorising myocardial infarction with advanced cardiovascular imaging. Lancet. 2021;398(10299):e9.
208. Bing R, Andrews J, Williams M, Clark T, Semple S, Van Beek E, et al. Thrombus formation on bioprosthetic aortic valves. European Heart Journal. 2020;41(Supplement_2).
209. Tarkin JM, Joshi FR, Evans NR, Chowdhury MM, Figg NL, Shah AV, et al. Detection of Atherosclerotic Inflammation by (68)Ga-DOTATATE PET Compared to [(18)F]FDG PET Imaging. J Am Coll Cardiol. 2017;69(14):1774-91.
210. Noguchi T, Kawasaki T, Tanaka A, Yasuda S, Goto Y, Ishihara M, et al. High-intensity signals in coronary plaques on noncontrast T1-weighted magnetic resonance imaging as a novel determinant of coronary events. J Am Coll Cardiol. 2014;63(10):989-99.
211. Tzolos E, Bing R, Andrews J, Macaskill M, Tavares A, MacNaught G, et al. In vivo coronary artery thrombus imaging with 18F-GP1 PET-CT. European Heart Journal. 2021;42(Supplement_1).

Appendix 1

Chapters 3, 5 and 6 Study Participants

Study	NCT02110303 DIAMOND Dual Antiplatelet Therapy to Reduce Myocardial Injury n=193	NCT01749254 Novel Imaging Approaches to Identify Unstable Coronary Plaques n=78	NCT02607748 ^{18}F-NaF PET for Identifying Coronary Atherosclerotic Plaques n=22	Total (n=293)
Stable angina	n=202(193) (9 excluded as no available baseline PET/CT)	n=40(39) (1 excluded as no available baseline PET/CT)	N/A	232
STEMI/NSTEMI	N/A	n=40 (39) (1 excluded as no available baseline PET/CT)	n= 22	61

Chapters 3, 5 and 6 Studies inclusion and exclusion criteria

Study / Exclusion criteria	NCT02110303 DIAMOND Dual Antiplatelet Therapy to Reduce Myocardial Injury	NCT01749254 Novel Imaging Approaches to Identify Unstable Coronary Plaques	NCT02607748 ^{18}F-NaF PET for Identifying Coronary Atherosclerotic Plaques
Age	<40	<50	<18
DM	N/A	insulin-dependent diabetes mellitus or pt with BG>11mmol/L were excluded	N/A
Pregnant/breast feeding women	Excluded	Excluded	Excluded
ACS within the last 12 months	Excluded	N/A	N/A
Dual anti-platelet therapy or warfarin or NOAC	Excluded	N/A	N/A

PCI/CABG within the last 3 months (or plan for PCI/CABG in the next 12 months)	Excluded	N/A	N/A
Bleeding diathesis	Excluded	N/A	N/A
Renal dysfunction	eGFR<30	Serum creatinine >250 μmol/L	Serum creatinine >132 μmol/L
Known contrast allergy	Excluded	Excluded	Excluded
Inability to provide informed consent	Excluded	Excluded	Excluded
Permanent atrial fibrillation/Multiple premature ventricular or atrial contractions	N/A	N/A	Excluded
EF<35% or Class III congestive heart failure	N/A	N/A	Excluded

REACH and SMART risk scores

REACH score. "REACH (REduction of Atherothrombosis for Continued Health) is an outpatient registry of patients with either stable symptomatic vascular disease (CAD, cerebrovascular disease, or peripheral artery disease) or with multiple atherosclerotic risk factors. The data collected from 3647 centres in 29 countries enabled establishing the REACH score which enables prediction of 20-month risk of a recurrent cardiovascular event (1). The REACH score calculator can be found at: https://www.u-prevent.com/en-GB/ReachCalculator/ReachCalculator

SMART Score. The SMART (Second manifestations of arterial disease) risk score estimates the 10-year risk for myocardial infarction, stroke or vascular death in individual patients with previous cardiovascular disease, including coronary artery disease, cerebrovascular disease, peripheral artery disease, abdominal aortic aneurysm and polyvascular disease. The SMART risk score was developed in a population of vascular patients in the Netherlands that were included in the Secondary Manifestations of Arterial Disease (SMART)-study (2). External validation and updating were performed in pooled trial cohorts of 18,436 vascular patients from W-Europe, S-Europe, Israel, USA, Canada, Mexico, S-Africa, Australia, and N-Zealand (3). The SMART score calculators can be found at: https://www.escardio.org/Education/ESC-Prevention-of-CVD-Programme/Risk-assessment/SMART-Risk-Score

Appendix 2

Publications arising from this thesis

- **Tzolos E**, Newby DE. Coronary Computed Tomography Angiography Improving Outcomes in Patients with Chest Pain. Curr Cardiovasc Imaging Rep. 2019 Mar 22; 12:15. doi: 10.1007/s12410-019-9492-6.

- **Tzolos E**, Andrews JP, Dweck MR. Aortic valve stenosis-multimodality assessment with PET/CT and PET/MRI. Br J Radiol. 2020 Sep 1;93(1113):20190688. doi: 10.1259/bjr.20190688.

- Zheng KH, **Tzolos E**, Dweck MR. Pathophysiology of Aortic Stenosis and Future Perspectives for Medical Therapy. Cardiol Clin. 2020 Feb;38(1):1-12. doi: 10.1016/j.ccl.2019.09.010.

- **Tzolos E**, McElhinney P, Williams MC, et al. Repeatability of quantitative pericoronary adipose tissue attenuation and coronary plaque burden from coronary CT angiography. J Cardiovasc Comput Tomogr. 2021 Jan-Feb;15(1):81-84. doi: 10.1016/j.jcct.2020.03.007.

- **Tzolos E**, Dweck MR. ^{18}F-Sodium Fluoride (^{18}F-NaF) for Imaging Microcalcification Activity in the Cardiovascular System. Arterioscler Thromb Vasc Biol. 2020 Jul;40(7):1620-1626. doi: 10.1161/ATVBAHA.120.313785.

- **Tzolos** E, Kwiecinski J, Lassen ML, et al. Observer repeatability and interscan reproducibility of 18F-sodium fluoride coronary microcalcification activity. J Nucl Cardiol. 2020 Jun 11:10.1007/s12350-020-02221-1. doi: 10.1007/s12350-020-02221-1.

- **Kwiecinski J*, Tzolos E***, Adamson PD, et al. Coronary ^{18}F-Sodium Fluoride Uptake Predicts Outcomes in Patients With Coronary Artery Disease. *J Am Coll Cardiol.* 2020;75(24):3061-3074. doi:10.1016/jacc.2020.04.046 ***joint first co-authors**

- **Tzolos E**, Lassen ML, Pan T, et al. Respiration-averaged CT versus standard CT attenuation map for correction of ^{18}F-sodium fluoride uptake in coronary atherosclerotic lesions on hybrid PET/CT [published

online ahead of print, 2020 Jul 2]. *J Nucl Cardiol*. 2020;10.1007/s12350-020-02245-7. doi:10.1007/s12350-020-02245-7

- Kwiecinski J, **Tzolos E**, Meah M, et al. Machine-learning with ^{18}F-sodium fluoride PET and quantitative plaque analysis on CT angiography for the future risk of myocardial infarction [published online ahead of print, 2021 Apr 23]. *J Nucl Med*. 2021; jnumed.121.262283. doi:10.2967/jnumed.121.262283

- **Tzolos E**, Bing R, Newby DE, Dweck MR. Categorising myocardial infarction with advanced cardiovascular imaging. *Lancet*. 2021;398(10299): e9. doi:10.1016/S0140-6736(21)01329-5

- **Kwiecinski J*, Tzolos E***, Cartlidge TRG, et al. Native Aortic Valve Disease Progression and Bioprosthetic Valve Degeneration in Patients with Transcatheter Aortic Valve Implantation [published online ahead of print, 2021 Aug 29]. *Circulation*. 2021;10.1161/CIRCULATIONAHA.121.056891. doi:10.1161/CIRCULATIONAHA.121.056891 ***joint first co-authors**

Grants relating to this thesis

- Dr. Miriam and Sheldon G. Adelson Medical Research Foundation

- British Heart Foundation Grants (FS/CRTF/20/24086, SS/CH/09/002, CH/09/002 and RE/18/5/34216)